Departamento de Estratigrafía y Paleontología
Facultad de Ciencias
Universidad de Granada

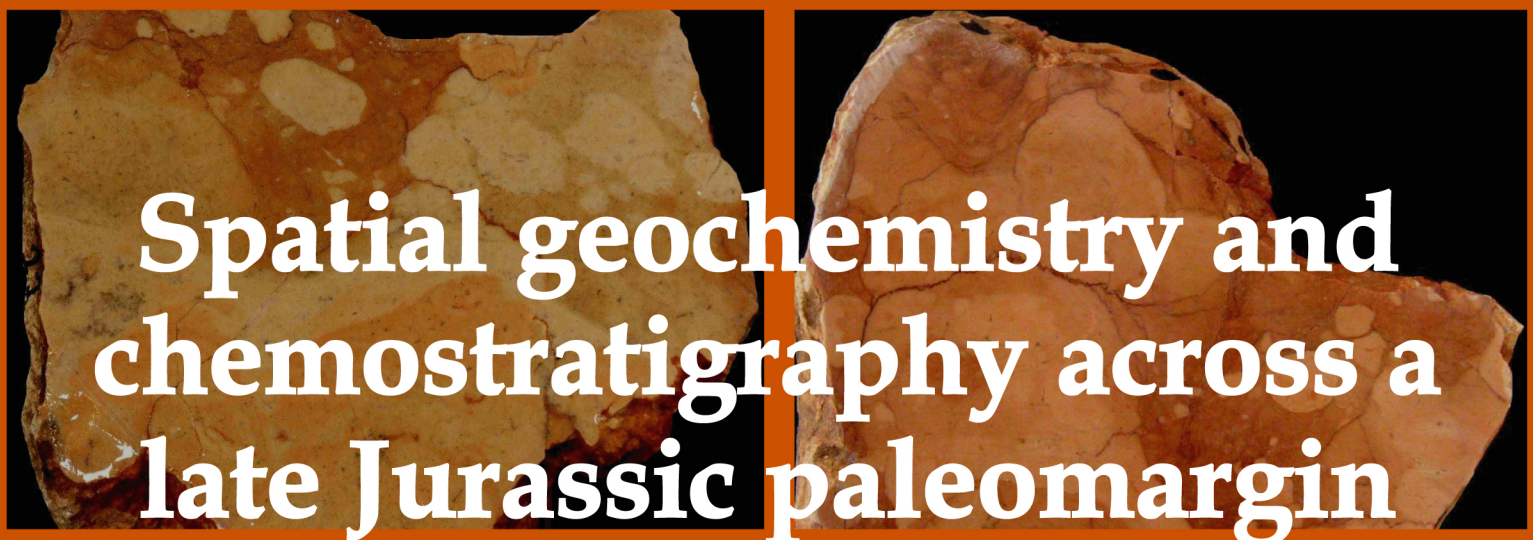

Spatial geochemistry and chemostratigraphy across a late Jurassic paleomargin -marine water masses in S-E Iberia

Rute Coimbra

Septiembre 2011

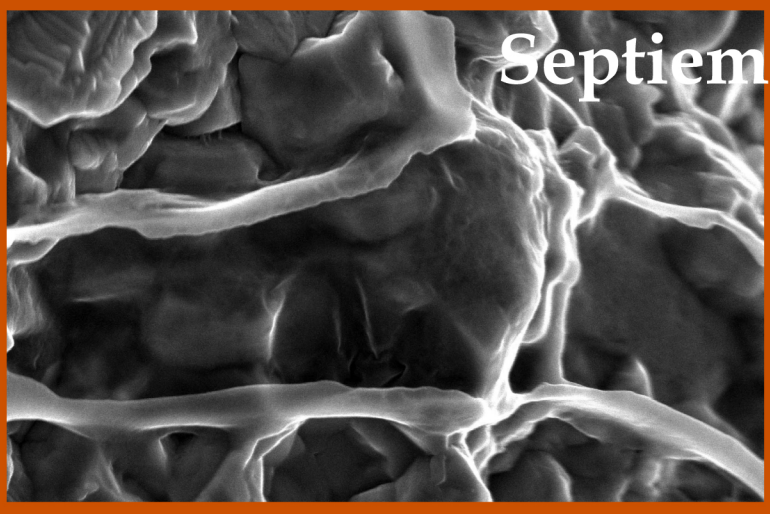

Editor: Editorial de la Universidad de Granada
Autor: Rute Coimbra
D.L.: GR 1074-2012
ISBN: 978-84-695-0821-3

Spatial geochemistry and chemostratigraphy across a late Jurassic paleomargin – marine water masses in S-E Iberia

Departamento de Estratigrafía y Paleontología
Universidad de Granada

Federico Olóriz Sáez, Profesor Catedrático del Departamento de Estratigrafía y Paleontología de la Universidad de Granada hace constar:

Que la presente memoria titulada "***Spatial geochemistry and chemostratigraphy across a late Jurassic paleomargin – marine water masses in S-E Iberia***" ha sido realizada bajo su dirección por la doctoranda Rute Lourenço Coimbra y cumple las suficientes condiciones para que su autor pueda optar al grado de Doctor en Ciencias Geológicas por la Universidad de Granada en la modalidad de *Doctor Europeus*.

Rute Lourenço Coimbra Federico Olóriz Sáez

Granada, septiembre 2011

TABLE OF CONTENTS

Agradecimientos/Acknowledgements

Mi recuerdo y agradecimiento a todos aquellos que acompañaron mis inicios en investigación en las Universidades de Coimbra y Vigo, en líneas de trabajo diferentes a la desarrollada en la Universidad de Granada.

Varias personas han contribuido para el desarrollo de esta tesis. Me gustaría agradecer a:

En primer lugar, a Federico: gracias por siempre disponer de un momento para que la geoquímica nunca se distanciara de la realidad Jurásica. Desde mini-reuniones casi a diario, a días de campo en lugares idílicos (Salcedo definitivamente excluido), la constancia nos permitió llegar más lejos. Adrian: it is hard to express the kindness and support that you dedicate to your PhDs and *ad latere*. From at the end of the hall (in Bochum), or thousands of kilometres away, you keep finding time and will to push our science.

A Alberto y Serafín Montes: tras una temporada ajustando dinámicas, todo el proceso de cortar, clasificar, fotografiar, volver a cortar, pulir y por fin, obtener láminas delgadas ha sido más eficiente de lo esperable en principio. Gracias por la disponibilidad y por entender que el trabajo bajo presión es como nuestra sombra.

To everyone at the Bochum lab: thank you for keeping up with our plans. Thousands of samples were processed, weighed and analysed under your caring watch. Dieter, Ulrike, Beate, Noushin, Barbara, the students that helped on this epic task, thank you. From the nice welcome chocolates on my desk, to the (very) early morning coffee at Dieters office, my time with you was a pleasure. To Rolf: regarding CL, the expectations are always high. Fortunately, you always had nice surprises for me. Blue and orange became more than colors.

A los compañeros de Granada: Lejos de casa es fundamental encontrar tu rincón, y me lo habéis regalado desde el primer día. Mil gracias por hacer que Granada sea también mi casa, donde siempre me sentí arropada por vuestro cariño. Ahora lo arriesgado de nombrar a cada uno…"las niñas": Vero (& Ca.), Pili, Marta, Silvia y Carmen (tanta afinidad era improbable, pero cierta); "geodinámicos": Pedro, Chema, Carlos, Vicente, Ana, Lourdes; del despacho de Mine: Aitor, Vanesa, Juan, Erwin; compañeros de despacho: Noel, Carmina, Antonio, Anja y Simone. Todo un privilegio poder contar con vosotros en todo momento. CUVIs, gracias por seguir ahí.

To the colleagues in Bochum: Despite the huge amount of work one always carries abroad, the need to feel at home and surrounded by friends is always there. And that's exactly where you guys come in. From daily lunch breaks, to gatherings in really nice places, I've become used to count on you and enjoy this unusual (3 months/year) friendship that lasts for the whole year and prevails despite the distance. To my office mates: Niels, Renee, Sylvia, thank you for not killing the invader; to Nico, Stephan, Stéphane and Violaine, Sabine, Jasper, Ariane, Suzanne, and to Mélanie (myself in another body), thank you for making me feel like one of you. Sabine (Sitter) and Cornelia, thank you for taking care of all of us. Bram, your help at the very beginning is still appreciated.

Aos amigos que já o eram antes: Manter amizades à distância não é uma tarefa fácil. Esta fase atribulada filtrou o meu mundo de antes, e ficaram vocês... Os que sempre têm estado comigo, servindo de ponte entre duas vidas paralelas. Mana, bemvinda. Obrigada por sempre me receberem com um sorriso do tamanho da saudade.

Marco: cá estamos, uma vida depois...Agradecer tamanha paciência e apoio ficaría sempre aquém. Escolher estar juntos, apesar das limitações, superou as expectativas. Sem questionar opções de vida, demos o nosso melhor. E temos mais para dar...

Ao meu Pai

Summary

1. Introduction

Unravelling paleoenvironmental conditions from carbonate archives is a complex task. From multiple settings where carbonate deposition takes place, the marine record is especially informative due to the strong dependence on oceanographic parameters. Hence the prolific research dealing with this issue, from modern to ancient settings. Nevertheless, from original differences (precipitation modes and environments, mineralogy) to differential preservation potentials widely recognized for the variety of carbonate materials, carbonate diagenesis investigations form a complementary discipline to those interested in retrieving paleoenvironmental information from ancient carbonates. Given the previous, general considerations are briefly addressed.

The aims and relevance of this research- are integrated on a description of previous works revealing a gap regarding paleoenvironmental approaches along a proximal to distal transect on ancient (Late Jurassic) carbonate settings from the S-E paleomargin of Iberia. In fact, such an approach, widely applied for the recent marine carbonate record, is uncommon for ancient examples.

The three studied areas are described in detail. Synthetic regional geology from Southern Portugal, Southern Spain and the Majorca Island is presented, as well comprehensive description of the seven stratigraphic sections under scope, along with their respective lithofacies under strict biostratigraphic control.

Details on the working approach are given for field and laboratory procedures, as well as a thorough description of the applied methods (optical under transmitted-light microscopy and pixel counting, cathodoluminescence, scanning electron microscopy, geochemical and statistical).

2. Matrix micrite $\delta^{13}C$ and $\delta^{18}O$ reveals synsedimentary marine lithification of Upper Jurassic Ammonitico Rosso limestones (Betic Cordillera, SE Spain)

Three Upper Jurassic Ammonitico Rosso sections from the Betic Cordillera are discussed in terms of their geochemical signature (carbon and oxygen isotopes) and respective paleoenvironmental regime. By comparison with modern and ancient analogues, valuable information is used to characterize the studied distal, epioceanic settings.

Optical analysis (ultrastructure and cathodoluminescence) agree with a good preservation degree of the studied Ammonitico Rosso materials (mainly nodules), also consistent with the obtained geochemical data obtained. This is true for the carbon isotope record that matches the well known pattern commonly described along Tethyan margins, but interestingly, also for oxygen isotope values. The latter are higher than expected for Upper Jurassic open marine carbonates, and are interpreted as corresponding to a close to original isotope signature, with fluctuations attributed to changes in relative seawater depth and/or temperature, considered within the context of potential marine currents.

Early diagenetic nodule formation is the mechanism responsible for such an exceptional geochemical preservation. The interplay between current velocity, sedimentary input and winnowing, burrowing and water pumping is discussed , and considered decisive for providing favorable conditions for the very early occurrence of nodules, which “freezed” the isotope signal registered. A relevant contribution is made towards a better understanding of Ammonitico Rosso facies.

3. Contrast comparison of differential diagenetic pathways of Lower Tithonian carbonate materials from the Betic Cordillera (S Spain): Evidence for physico-chemical paleo-seawater properties

Two sections showing successions deposited in epioceanic Tethyan areas and corresponding to the same Lower Tithonian ammonite biozone are debated: a condensed, pelagic and cephalopod-rich limestone intercalated in marls and mafic rocks, and a typical Ammonitico Rosso facies. A thorough comparison is made between the geochemical signature (C and O stable isotopes and major and trace elements) of different carbonate materials: matrix micrite, neomorphic ammonite shells, belemnite rostra and carbonate cements. Environmental, early burial and latter diagenetic conditions and processes are

discussed in the light of the obtained data and information about ammonite and belemnite ecology.

A fair preservation is demonstrated for matrix micrite from both studied sites (Cardador and Alamedilla) and also for neomorphic ammonite shells and belemnite rostra encased on Alamedilla matrix micrite. Latter carbonate cements provide the only record of more pervasive diagenetic overprint. Carbon isotope values fall within the typical Tethyan Late Jurassic range (*ca.* 2‰), except data from belemnite rostra which are depleted around -1‰, which is interpreted as resulting from metabolic fractionation (vital effect). Oxygen isotope values are more variable, but a rather conservative diagenesis agrees with the narrow range of values from -1 to 1‰. Warmer burial fluids explain lower values in later diagenetic carbonate cements.

Elemental abundances are coherent with rather well preserved carbonate materials. The recognition of hydrothermal contamination is depicted by increased abundance of Mg, Fe, and specially Mn. The vicinity of presumable hydrothermal sources (i.e., the Mid-Subbetic Volcanic Ridge) supports higher Mn concentration at the Alamedilla site. Interestingly, the timing of mineralogical stabilization of each carbonate material seems to reveal the potential record of a post-sedimentary geochemical event. A relative paragenetic succession for the mineralogical stabilization of the studied carbonate materials is proposed.

4. Spatial geochemistry of Upper Jurassic marine carbonates (Iberian Subplate)

The Upper Jurassic sections investigated are analysed for their sedimentologic, stratigraphic and geochemical records. These comprise a several-hundred-kilometer long geochemical transect, ranging from the neritic middle shelf to variable settings in the epioceanic fringe across the south and eastern paleomargins of the Iberian sub-plate. By comparing the isotopic and elemental composition of different carbonate materials, epioceanic (distal) matrix micrite geochemical signals are demonstrated as reasonable proxies for bottom paleo-seawater properties. In contrast, the geochemical approach to characterize the epicontinental (proximal) record shows a high level of complexity, with potential admixture of marine, continental and diagenetic geochemical signals.

The epioceanic record shows a carbon-isotope stratigraphy comparable to Upper Jurassic reference sections from northern Tethyan paleomargins. In contrast, oxygen isotope ratios are ^{18}O-enriched relative to those previously reported for equivalent deposits. This pattern is consistent with early diagenetic porewater stabilization. Oxygen isotope thermometry is applied to matrix micrite $\delta^{18}O$ values. Obtained results are coherent with increasing distance from shore, inferred depth variations and/or hydrodynamics with probability for reflecting local forcing factors.

Skeletal abundances and manganese concentrations are compared with the available isotope composition, in order to shed light into local deviation from an overall regional to global geochemical signal. Skeletal maxima values coincide with positive peak values in oxygen isotope ratio. This relation is discussed in terms of relative sea level fluctuations, related effects on the sedimentary record and their potential signature on the geochemical record. Other local features, such as silica-bearing intervals are attributed to increased nutrient levels potentially triggered by hydrothermal pulses, based on the comparison between oxygen isotope and manganese trends. Evidence for this comes from the anti-phase correlation of manganese elemental abundances and oxygen isotopic composition.

The presented data set hopes to be of relevance for further investigations concerning spatial chemostratigraphy in Mesozoic oceans.

5. Sediment provenance supported by geochemical evidence (Upper Jurassic, Majorca Island)

Typical Ammonitico Rosso carbonate deposits in the Cuber and Cala Fornells sections are compared to the atypical Aumedrá carbonates that disrupt background conditions for Tethyan open marine sedimentation and its geochemical record on epioceanic swells.

Very high accumulation rates, dark brown colour (in fresh samples) and scarce skeletals in Aumedrá limestones remained enigmatic until contrasted with the geochemical data presented in this research. The geochemical record obtained provided the first arguments that cleared the origin of this peculiar facies according its stratigraphic and paleogeographic contexts.

Higher than expected $\delta^{13}C$ and $\delta^{18}O$ values, high Sr and low Mn, Fe concentrations, support an atypically shallow open-sea sedimentary supply for Aumedrá sediments. An aragonite factory at a shallower, warmer setting dictated the mineralogy of the sediments. Remobilization and sorting during transport account for the observed macroscopic, microscopic and geochemical differences. Source areas to the NE of the Majorca Island are envisaged.

The notion that diagenetic overprint compromises the paleoenvironmental information retrieved from ancient carbonates is demonstrated to be an oversimplified hypothesis. The application of this approach to analogous cases of intercalation of atypical lithofacies in epioceanic swells is encouraged.

6. Statistical analysis of elemental chemostratigraphy in Upper Jurassic Ammonitico Rosso

The seven sections that comprising the proximal to distal transect presented in chapter 4, are discussed in terms of their elemental record (Mg, Sr, Fe and Mn). A complex statistics approach allowed to distinguish between primary (paleoenvironmental), very early (syn-depositional) and secondary (latter diagenesis) signals.

Elemental associations provided by principal component analysis (PCA) and hierarchical cluster analysis revealed a consistent relation between Mg, Fe and Sr. This elemental association is discussed in the light of early nodule formation on Ammonitico Rosso facies, and how each element contributes to this process. Manganese exhibits a behavior that clearly deviates from all other analyzed proxies. Local trigger factors are considered, and hydrothermal supply is envisaged and coherent with high rates of seafloor spreading during Late Jurassic times, added to the widespread synsedimentary faulting typical in the physiographic restructuring of the epioceanic fringe in the studied area.

Variogram computation applied to geochemical data of ancient carbonates is for the first time attempted. The obtained results revealed several patterns in time-fluctuations of geochemical behavior, not provided by any other attempted method. The obtained general trends are discussed in terms of their cyclicity and time recurrence and mechanisms that may account for recurrent patterns and trends.

7. Conclusions

The conclusion chapter shows that the complex working approach developed during this research is as a step forward regarding the cases and materials under scope, from field sampling, laboratory processing and data treatment.

The reliability of the obtained geochemical record provided by Ammonitico Rosso matrix micrite resulted from thorough comparisons between different settings, as well as different carbonate materials with variable preservation potentials. Regional to global trends were identified for the epioceanic record, with stratigraphic patterns in agreement with known relative sea level fluctuations, mainly at the short-term, for the Late Jurassic and spatial variation coherent with proposed paleogeographic differences along the studied proximal to distal transect.

Future research is proposed, as complementary information would be valuable for a better understanding of the complexity of factors that forced oceanographic and environmental dynamics during Mesozoic times and of the way in which they were registered in sedimentary packages.

8. Appendix: Pixel counting for percentage estimation: applications to sedimentary petrology

Relative abundance quantification of different types of materials identified in thin sections through pixel counting percentage estimation is presented as an alternative to the use of the visual comparison charts or to other time consuming quantitative estimations.

The proposed automated, objective method provides a new parameter comparable and compatible with other quantitative datasets. The use of the pixel counting percentage estimation procedure grants a fast and easy way to solve the quantification issue, and its application to several different lithofacies, shapes, sizes and particle colours is demonstrated.

Resumen

1. Introducción

Descifrar condiciones paleoambientales a partir de registros carbonatados no es una tarea simple. De las múltiples y variadas situaciones en las que se produce sedimentación carbonatada, el registro marino tiene una especial relevancia debido a su estrecha dependencia de parámetros oceanográficos. De ahí, la prolífica investigación realizada, tanto en casos actuales como en registros antiguos. No obstante, desde diferencias originales como en modalidades de precipitación, medio ambiente y mineralogía, a las ampliamente reconocidas diferencias en el potencial de preservación de un amplio espectro de materiales carbonatados, la investigación en la diagénesis de carbonatos constituye una complementaria y valiosa disciplina para los interesados en la interpretación de los paleoambientes correspondientes a carbonatos fósiles. De acuerdo con esto, se presentarán breves consideraciones generales.

Los objetivos y la relevancia de la investigación realizada se basan en la evaluación de trabajos previos, con la finalidad de reconocer su orientación temática. De esta manera se ha reconocido una laguna de conocimiento respecto al desarrollo de aproximaciones a la reconstrucción de paleoambientales en las que se afronten transectos proximal-distal. De hecho, este planteamiento ha sido ampliamente aplicado a ejemplos actuales. El caso seleccionado ha sido representado por registros rocosos correspondientes al Jurásico tardío en el palaeomargen S-E de Iberia.

Tres áreas han sido seleccionadas y se describen en detalle. De manera sintética se presenta el contexto geológico regional del sur de Portugal, Sur-sureste de España y de la isla de Mallorca en el archipiélago balear, que se acompaña de una descripción apropiada de los siete perfiles estratigráficos analizados, sometidos a un estricto control lito- y bioestratigráfico.

Se proporcionan detalles de los protocolos seguidos en análisis de campo y laboratorio, así como sobre la descripción de la metodología analítica aplicada (microscopía óptica de luz trasmitida y conteo automatizado del contenido de partículas/matriz, catodoluminiscencia, microscopía electrónica de barrido, geoquímica, y tratamiento estadístico).

2. $\delta^{13}C$ y $\delta^{18}O$ obtenidos en matriz micrítica de facies Ammonitico Rosso del Jurasico Superior (Cordillera Bética, SE España) revelan litificación marina sinsedimentaria.

Tres perfiles de la Cordillera Bética con facies ammonitic rosso se discuten en términos de las señales geoquímicas registradas (isótopos estables de carbono y oxígeno) y sus respectivos paleoambientes. Para caracterizar los correspondientes enclaves de depósito distales, epioceánicos, se usa valiosa información derivada de la comparación con análogos actuales y fósiles.

El análisis óptico (ultraestructura y catodoluminiscencia) concuerda con un buen grado de preservación de los materiales estudiados en las facies ammonitico rosso. La información obtenida es congruente con los datos geoquímicos. Este hecho se constata para el registro isotópico del carbono, que no distorsiona el patrón ya reconocido para márgenes del Tethys, e incluso también lo es para el registro isotópico del oxígeno, lo que resulta una información de sumo interés. Los valores isotópicos de oxígeno resultan algo más altos que los esperados para carbonatos marinos de mar abierto en el Jurásico tardío y se interpretan como relacionados con una señal isotópica original, cuyas fluctuaciones se atribuyen a cambios en la profundidad relativa y/o en la temperatura, consideradas ambas en el contexto de posibles patrones de corrientes marinas.

La formación de nódulos carbonatados durante la diagénesis temprana se considera el mecanismo responsable para esta excepcional preservación geoquímica. Se analiza la interacción de procesos como velocidad del flujo, tasa de sedimentación y frecuente aventamiento, bioturbación e irrigación de sedimento poco maduro. Dicha interacción se considera crucial para generar condiciones favorables a la generación muy temprana de estructuras nodulares que favorecieron la "congelación" de la señal isotópica registrada. Se aporta una contribución relevante para una mejor comprensión de las facies ammonitico rosso estudiadas.

3. Análisis comparativo de cursos diagenéticos diferenciales en materiales carbonatados del Tithoniense Inferior de la Cordillera Bética (Sur de

España): evidencia de propiedades físico-químicas de aguas marinas pretéritas.

Se analizan y comparan dos perfiles que muestran sucesiones depositadas en áreas epioceánicas del Tethys y que corresponden a la misma biozona de ammonites del Tithoniense Inferior: una de ellas muestra una caliza pelágica condensada y rica en cefalópodos, intercalada entre mafitas, y la otra corresponde a una típica facies ammonitico rosso. Se realiza una comparación detallada de los registros geoquímicos obtenidos (isótopos estables de carbono y oxigeno, de elementos mayores y de elementos traza) en diferentes materiales carbonatados –matriz micrítica, conchas neomórficas de ammonites, rostros de belemnites y cementos carbonatados. Sobre la base de la información obtenida y la consideración de aspectos ecológicos de ammonites y belemnites, se discuten procesos relacionados con las condiciones ambientales y las correspondientes fases tempranas y tardías de la diagénesis.

En ambos perfiles estudiados (Cardador y Alamedilla) se demuestra que la matriz micrítica está suficientemente bien preservada, así como las conchas neomórficas de ammonites y los rostros de belemnites englobados en la matriz micrítica en Alamedilla. Los cementos carbonatados tardíos proporcionan el único testimonio de una impronta diagenética más acentuada. Los valores isotópicos obtenidos para el carbono concuerdan con el rango típico para el Jurásico tardío en el Tethys (*ca*. 2‰), excepto los obtenidos en rostros de belemnites que resultan menores en torno a -1‰, hecho que se interpreta como derivado de fraccionamiento metabólico (efecto vital). Los registros isotópicos del oxígeno son más variables, pero una diagénesis no muy agresiva es coherente con el estrecho rango de valores entre -1 y 1‰. Fluidos de mayor temperatura, en la fase de maduración sedimentaria, explicarían valores más bajos en cementos carbonatados relacionados con fases más tardías de la diagénesis.

Los contenidos en elementos son coherentes con los de materiales carbonatados suficientemente bien preservados. Indicios de contaminación hidrotermal son revelados por la abundancia de Mg, Fe y especialmente Mn. La proximidad de previsibles fuentes de aporte hidrotermal (p.ej., la Cresta Volcánica del Subbético Medio) refuerzan las concentraciones mayores de Mn registradas en el perfil de Alamedilla. Se considera interesante que la temporización de la estabilización mineralógica de cada material carbonatado pueda indicar

las probabilidades de registro de un evento geoquímico post-sedimentario. Se propone una sucesión paragenética relativa para la estabilización mineralógica de los materiales carbonatados estudiados.

4. Distribución espacial de la geoquímica de carbonatos marinos del Jurásico tardío (Subplaca Ibérica)

Los perfiles estudiados del Jurásico Superior son analizados desde el punto de vista sedimentológico, estratigráfico y geoquímico. Su estudio proporciona un transecto de registros geoquímicos de varios cientos de kilómetros, desde enclaves neríticos de plataforma media a un variable espectro de ubicaciones en la franja epioceánica de los paleomárgenes meridional y oriental de la subplaca ibérica. Por medio de la comparación de la composición isotópica y elemental de diferentes materiales carbonatados, se concluye que los registros geoquímicos de la matriz micrítica en los depósitos epioceánicos (distales) estudiados representan adecuadamente las propiedades de las aguas marinas de fondo correspondientes. Por el contrario, la geoquímica que caracteriza los registros epicontinentales (proximales) estudiados revela un grado de complejidad mayor, que incluye la probable mezcla de señales geoquímicas marinas, continentales y diagenéticas.

El registro epioceánico de las señales isotópicas del carbono muestra tendencias estratigráficas comparables con las obtenidas en otros perfiles de referencia en paleomárgenes septentrionales del Tethys. Por el contrario, las señales isotópicas del oxígeno resultan enriquecidas en ^{18}O respecto a las publicadas, obtenidas en depósitos equivalentes. Este rasgo concuerda con la estabilización de las aguas intersticiales en el sedimento durante la diagénesis temprana. La interpretación termométrica basada en el registro isotópico del oxígeno se aplica a los valores del $\delta^{18}O$ de las matrices micríticas. Los resultados obtenidos son coherentes con efectos de distancia a la costa, diferencias en profundidad y/o patrones hidrodinámicos, y pueden reflejar factores de forzamiento local.

La abundancia de restos de conchas y otros restos esqueléticos carbonatados, y las concentraciones de manganeso, se comparan con la composición isotópica obtenida con la finalidad de identificar posibles desviaciones locales respecto a señales geoquímicas de ámbito regional amplio a global. Máximos de abundancia de bioclastos coinciden con picos positivos en los valores isotópicos del oxígeno. Dicha relación se discute en términos de

fluctuaciones del nivel relativo del mar, sus efectos en el registro sedimentario, y su potencial de registro geoquímico. Otros factores locales, tales como enriquecimientos en sílice, se atribuyen al aumento de nutrientes probablemente forzado por pulsos de emanación hidrotermal. Su interpretación se basa en la comparación de las tendencias registradas en valores isotópicos del oxígeno y en el registro del contenido en manganeso, y es soportada por el comportamiento en anti-fase entre ambos registros.

La base de datos obtenida pretende ser una aportación de valor para futuras investigaciones orientadas a esclarecer el significado de la distribución espacial de registros quimioestratigráficos en océanos mesozoicos

5. Sobre la procedencia de sedimentos basada en evidencias geoquímicas (Jurásico Superior, Isla de Mallorca)

Depósitos de facies ammonitico rosso en los perfiles de Cuber y Cala Fornells se comparan con los de la Formación Aumedrá, que representan una interrupción significativa en las condiciones estándar que caracterizan la sedimentación de mar abierto y su señal geoquímica en umbrales epioceánicos del Tethys.

Tasas de acumulación comparativamente muy altas, coloración marrón obscura en corte fresco y escaso contenido en bioclastos en las calizas de la Formación Aumedrá no han sido suficientemente explicadas hasta que se han contrastado con los datos geoquímicos presentados en la investigación realizada. El registro geoquímico obtenido proporciona las primeras argumentaciones que apuntan a la clarificación del origen de esta litofacies particular en sus contextos estratigráfico y paleogeográfico.

Valores más altos de lo esperado en $\delta^{13}C$ y $\delta^{18}O$, altas concentraciones en Sr y bajas en Mn y Fe en depósitos de la Formación Aumedrá son congruentes con un área de aporte o alimentación atípicamente somera en una situación de mar abierto. Una factoría aragonítica emplazada en aguas más someras y cálidas determinó la mineralogía de los sedimentos de la Formación Aumedrá. Procesos de transporte implicando removilización de sedimentos y selección granulométrica son congruentes con las diferencias observadas en aspectos macroscópicos, microscópicos y geoquímicos. Se considera que las áreas madre pudieron estar ubicadas al NE de la isla de Mallorca.

El axioma de que la impronta diagenética compromete la interpretación de la información paleoambiental registrada en carbonatos antiguos se considera una hipótesis simplificada. Se recaba atención sobre el interés de implementar la investigación realizada en casos análogos de intercalación de litofacies atípicas en umbrales epioceánicos.

6. Análisis estadístico del registro estratigráfico de elementos mayores y traza en el Jurásico Superior: facies Ammonitico Rosso, S-E Iberia

Los siete perfiles que comprenden el transecto proximal-distal presentado en el capítulo 4 son analizados y comparados en términos de su registro en los elementos seleccionados (Mg, Sr, Fe, y Mn). Con el soporte de un sofisticado análisis estadístico ha sido posible distinguir señales primarias (paleoambientales), muy tempranas o sinsedimentarias (sindeposicionales) y secundarias (relacionadas con fases tardías de diagénesis).

Las asociaciones de elementos proporcionadas mediante analítica de componentes principales (PCA) y de agrupamientos (conglomerados) jerarquizados (HC) revelan relaciones consistentes entre Mg, Fe y Sr. Esta asociación se considera en relación con el contexto del proceso que determina la formación de nódulos carbonatados en las facies ammonitico rosso, y se analiza la vía en la que cada elemento contribuye a dicho proceso. El manganeso resulta claramente independiente o separado del resto de parámetros analizados. Se consideran posibles factores locales responsables y se concluye en la mayor probabilidad de la incidencia de emanaciones hidrotermales dado el contexto de alto grado de actividad geodinámica en el fondo marino (seafloor spreading) durante el Jurásico tardío, y la concomitante acentuación de fracturación sinsedimentaria típicamente asociada a la reestructuración fisiográfica en el área estudiada de la franja epioceánica.

El tratamiento estadístico por medio de variogramas aplicado a datos geoquímicos de carbonatos antiguos es realizado por vez primera. Los resultados obtenidos revelan patrones de fluctuación del comportamiento geoquímico a lo largo del tiempo, que no han sido revelados por otros métodos. Los patrones obtenidos se analizan en términos de ciclidad y recurrencia temporal, así como de los mecanismos que pudieran ser responsables de los comportamientos recurrentes y de las tendencias.

7. Conclusiones

El capítulo de conclusiones muestra que el plan de investigación desarrollado representa un paso adelante respecto al estudio de los casos y materiales seleccionados, en términos de muestreo de campo, procesado de laboratorio y tratamiento de datos.

La fiabilidad del registro geoquímico proporcionado por matrices micríticas en ammonitico rosso y facies relacionadas deriva de detallados análisis comparativos entre diferentes enclaves de depósito, así como de su aplicación a diferentes materiales carbonatados con diferentes potenciales de preservación. Se han identificado tendencias regionales y globales para el registro epioceánico, con patrones estratigráficos compatibles con fluctuaciones del nivel relativo del mar, especialmente de periodo corto, para el Jurásico tardío, así como distribuciones espaciales coherentes con las diferencias paleogeográficas asumidas en el transecto proximal-distal estudiado.

Se propone implementar la investigación en el futuro asumiendo que toda información complementaria podrá ser valiosa para una mejor comprensión de la complejidad de factores que forzaron las dinámicas oceanográfica y ambiental durante tiempos mesozoicos, y de la manera en que tanto los factores como las dinámicas resultantes, fueron registrados en los cuerpos sedimentarios.

8. Apéndice: Conteo de pixeles para la estimación de porcentajes: aplicaciones en petrología sedimentaria.

La cuantificación de abundancias relativas mediante conteo de pixeles y estimación de porcentajes, para diferentes tipos de materiales identificables en lámina delgada, se presenta como una alternativa al uso de esquemas o gráficos de comparación visual u otros métodos de cuantificación que suelen consumir cierta cantidad de tiempo.

El método propuesto, automatizado y objetivo proporciona un nuevo parámetro comparable y compatible con otros conjuntos de datos cuantitativos. Se demuestra que el protocolo para el uso del conteo de pixeles con la finalidad de estimar porcentajes garantiza una vía rápida y fácil para resolver dificultades de cuantificación, y que su aplicación rinde resultados positivos en diferentes litofacies, morfologías, tamaños y color de las partículas.

1

Introduction

1.1- Carbonate production: depositional settings, precipitation modes, preservation potential

Carbonate materials precipitate in a wide range of environments, from marine to terrestrial realms (Fig. 1.1). Special attention has been given to marine carbonate precipitates because of their much greater extension and tight connection to oceanographic conditions, rendering to modern and ancient materials a high potential of preservation of paleoenvironmental changes.

Regarding marine carbonates, their distribution is widespread, from shallow, proximal areas to deep open ocean environments. Throughout this transect, the interplay between continental input, morphology of the platform (shelf type), oceanographic parameters (e.g., energy of currents, depth, turbidity, salinity, temperature) and related water masses, latitudinal changes and ocean/atmosphere interactions (coupling), result on a wide range of carbonate precipitates and relative abundance that may inform on the original conditions under which they form even through their geologic record.

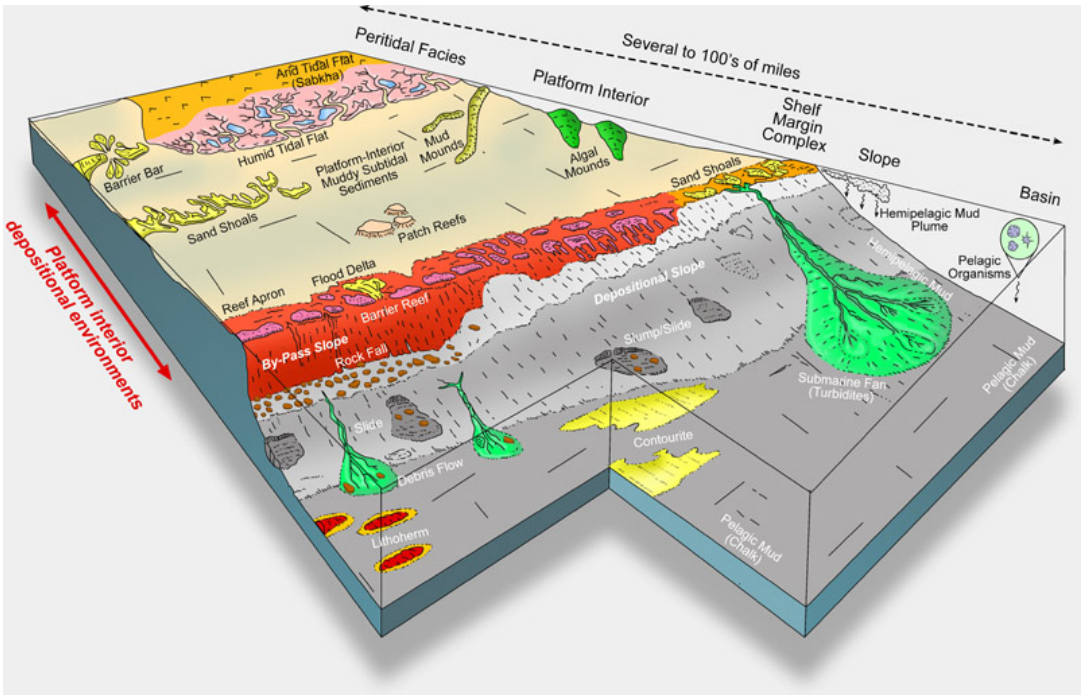

Fig. 1.1- Depositional environments associated to carbonate deposition along an hypothetical proximal to distal transect (in Loucks et al., 2003).

In addition, the dominant mineralogy of carbonate-rich sediments has been observed to change through geologic time (see below) according to Mg/Ca ratio from 1 to slightly higher than 5 (e.g., Lowestein et al., 2001). Aragonite and high-Mg calcite dominate the mineralogy of Holocene tropical shallow-water carbonate cements and skeletal debris, with Mg/Ca ratio values <2, while values close to 2 determine a threshold for the polymorphic mineralogy of precipitated carbonate (Sandberg, 1983), biotic and abiotic. From single to continuous trends from "Calcite to Aragonite Seas" (e.g., Sandberg, 1975; Milliken and Pigott, 1977; Wilkinson, 1979; Zhuravlev and Wood, 2009), numerous studies document ancient tropical shallow water carbonates composed originally of low-Mg calcite. (e.g., Mackenzie and Pigott, 1981; Sandberg, 1983; Stanley and Hardie, 1998; Wilkinson et al., 1984). Hence, changing carbonate mineralogy through geologic time has been recognized, and proposals for fluctuating "Calcite and Aragonite Seas" during Phanerozoic times have been common and accepted with successive adaptations (Sandberg, 1983, Hardie, 1996; Stanley and Hardi, 1998, 1999; Porter, 2007, 2010). In accordance, main carbonate mineralogy fluctuations throughout the geological record (Fig. 1.2), and a trend showing calcite and aragonite dominated intervals throughout ocean history is assumed following changes in seawater chemistry. However, debate exists with growing information about past coexistence of organisms with aragonite and calcite mineralogy irrespectively of dominant carbonate-mineralogy of the sea (e.g., Westphal and Munnecke, 2003), and even changes in Mg content during calcite precipitation are demonstrated for a given organism according to "Aragonite and Calcite seas" forcing conditions (e.g., Ries, 2004). Also debated are those main factors which control fluctuations in "Aragonite and Calcite Seas" conditions –i.e., the Mg content in the calcite lattice. The dominant hypothesis relates to the Mg/Ca ratio- being attributed to periods of intense seafloor activity and related effects (Sandberg, 1983, 1985; Spencer and Hardei, 1990; Hardie, 1996; Stanley and Hardi, 1998; Lowenstein et al., 2001; Steuber and Veizer, 2002), but refinement is on according to considerations about the role of factors such as pCO_2 (Hallock, 1997), salinity and/or temperature, the two latter even for a given situation (e.g., Adabi, 2004), and the role of particular settings (e.g., Arenas and Pomar, 2010).

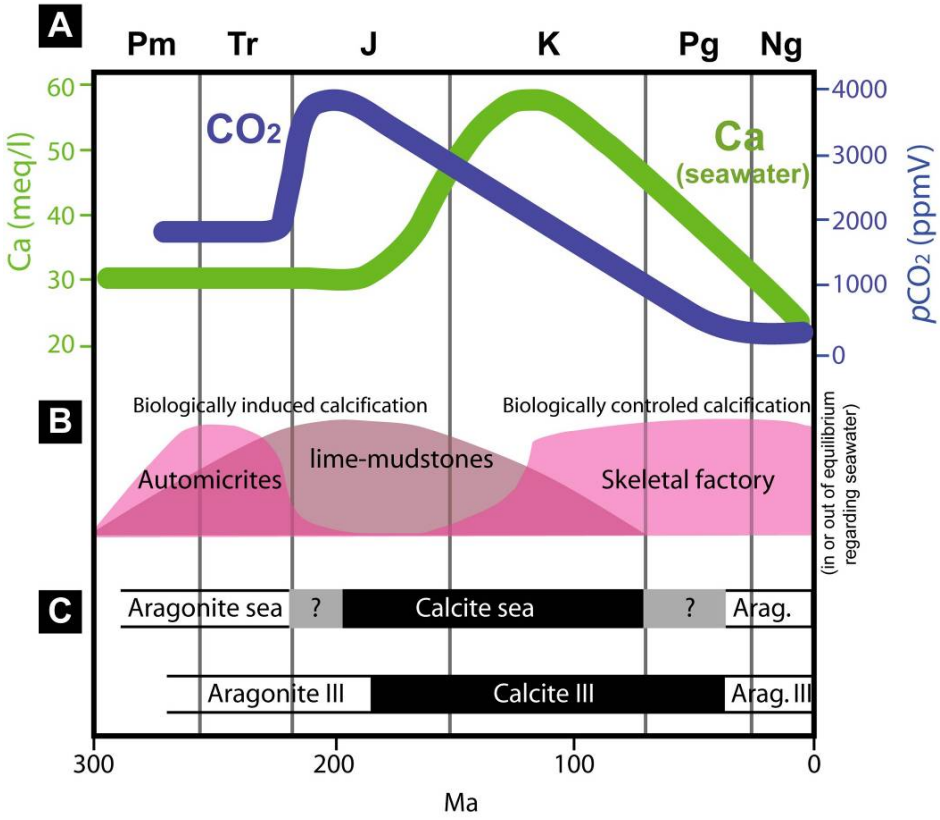

Fig. 1.2- Fluctuation in seawater chemistry and deposition modes along the geologic record (adapted from Pomar and Hallock, 2008). A: Seawater chemistry according to the model proposed by Hardie, 1996, from Stanley and Hardie, 1998. Note very high CO_2 concentrations during Early Jurassic times, with later decrease during the Late Jurassic and high increasing ratio of Ca concentration in seawater during the Mid-Late Jurassic; B: Fluctuations in recognized on carbonate factories, with dominance of biologically induced lime-mudstones throughout the Jurassic; C: Time distribution of non-skeletal carbonates according to Sandberg (1983) (above) and dominance of seawater precipitates (calcite vs. aragonite), according to Stanley and Hardie, 1998 (below).

The relevance of knowing carbonate polimorph dominance (mainly calcite versus aragonite) relates to their respective mineralogic stability degree under marine conditions, which ultimately will determine the amount of alteration through time (Fig. 1.3) solving a significant limitation for the right interpretation of ancient carbonate rocks. Whilst calcite (with variable amounts of Mg) is rather stable, aragonite is known to be highly unstable, experiencing mineralogic inversion into low-Mg calcite during a very early diagenetic stage. Despite these general considerations, the ancient carbonate record is far from being a straightforward matter. This because carbonate oozes are comprised of a variable mixture of components, from biotic counterparts as biomineralized skeletals with variable mineralogy, precipitated in or out of equilibrium with seawater, to mixed bioclasts incoming from

reworking and “pelagic rain or snow”, and abiotic precipitates of primary or secondary origin. All of this occurs under the influence of net sedimentary rates determining averaged carbonate assemblies per a given sediment/rock thickness.

The often called “micrite problem” (Bathurt, 1994; Munnecke and Samtleben, 1996; Immenhauser et al., 2002; Coimbra et al., 2009; Berkyová and Munnecke, 2010) demonstrates how intricate is the interpretation of its origin, if mainly biogenically mediated, resulting from variable tranport (allomicrites; e.g., Keim and Schlager, 1999; Neuweiler et al., 2003), or diagenetically induced at least in part by biodiagenesis- (Neuweiler et al., 2003), polymud fabrics included (Lees and Miller, 1985). In accordance, thorough and careful paleoenvironmental studies need to be in order to take into account this complex record to ensure the reliability of their interpretations. Notwithstanding, the potential of ancient carbonate oozes has been put in evidence by numerous publication either by a demonstrated extreme preservation of the studied materials (e.g., belemnite rostra) or by the fact that even when a pristine state is no longer the case, diagenesis is often conservative, at least in terms of trends along a studied time frame (e.g., Frank and Lohman, 1996).

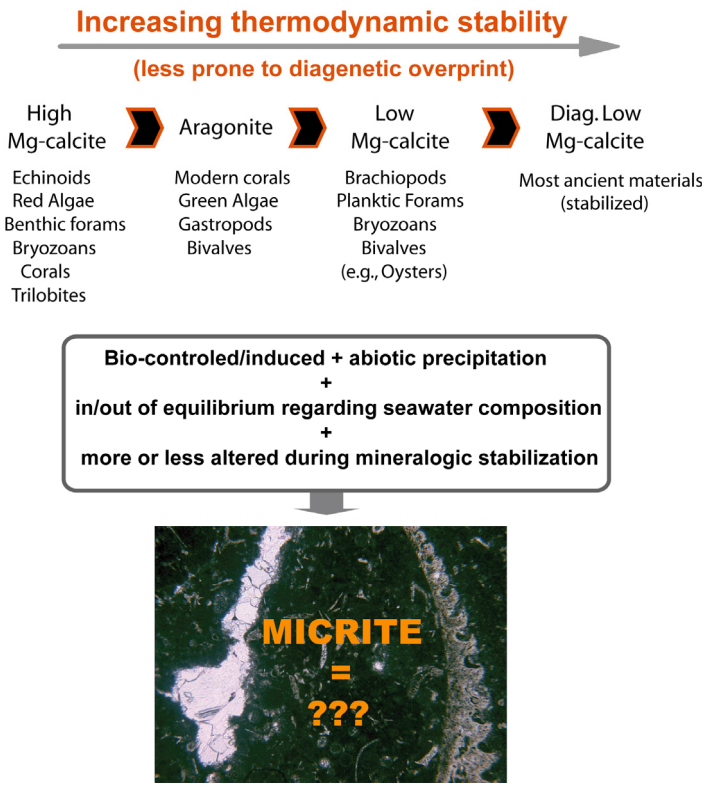

Fig. 1.3- Diversity of carbonate polymorphs: thermodynamic stability, selected organisms with carbonate skeletals (adapted from Kendall and Alnaji, SEPM Carbonate Diagenesis Image Gallery, 2009), and component variability accounting for micite composition. Representative image includes matrix micrite, encasing a high

diversity of skeletals (aptichus on the right) and latte carbonate cement infill.

1.2- Previous research, aims and relevance of this research

The investigation of hemipelagic and pelagic sediments as archives of recent climate and environment is nowadays a common procedure, increasingly developed since the implementation of the International Ocean Drilling Project (IODP). However, applying such a direct approach to ancient carbonate materials is not straightforward. For Jurassic times, examples of well exposed, extended carbonate record have been object of extensive studies (e.g., French and Swiss Jura Mountains), providing an archive of significant changes in oceanography and climate reorganization, potentially forced by local factors.

The study of condensed carbonate successions could seem at a first glance less attractive, since low averaged sedimentation rates and omission surfaces compromise the continuity or even the preservation of this record. But such materials, as the dominant Ammonitico Rosso facies from the Betic Cordillera, offer great/large exposures of Jurassic deposits, undoubtedly contributing with combined evidence of major tectonic/oceanographic changes and autocyclic factors controlling environmental conditions and carbonate geochemistry.

The major revision on the state of the art for the Jurassic of the Betic Cordillera was presented by Vera (1998) clearly pointing to the fact that geochemical approaches to Jurassic rocks of the Betic Cordillera was still sprouting during the nineties. Jiménez de Cisneros (1990, 1991 and 1993) provided the first milestones on the application of stable isotopes to unravel genesis and diagenesis of carbonate rocks at this sector of the north-west Tethyan margin. Interestingly, a direct mention to the need of developing specific work on paleotemperature acquisition for Jurassic times at the Betic Cordillera was made. This need becomes evident with the reference to “the first results on stable oxygen isotopes” by Jiménez et al., 1996, a record reported as significantly affected by diagenesis, hence compromising the paleoenvironmental interpretation.

Since the nineties, geochemical techniques have developed significantly due to the wide recognition of its potential, and increasing accuracy as a consequence of equipment and

analytical improvements, along with less time consuming techniques. Later researchers have taken advantage of this methodology on Jurassic materials from the Betic Cordillera.

The application of stable carbon isotope record as a correlation tool between pelagic successions is presented by Rey and Delgado (2002). These workers pay special attention to oxygen isotope record, often underestimated due to its higher susceptibility to diagenetic overprint (e.g., Marshall, 1992). In this work, and later ones (Rey and Delgado, 2005), the attempt was to differentiate between the behaviour of both carbon and oxygen isotope composition, by comparing swell areas to nearby troughs. This approach is clearly based on the recognition of the potential of isotope composition to record paleoenvironmental differences at a regional scale as well as differential diagenetic pathways.

Other interesting approaches dealing with geochemistry were proposed by O'Dogherty et al. (2006). Carbon isotope composition of Middle Jurassic Southern Iberian deposits is related not only to the record of the global carbon marine reservoir, but also a reflection of distinct environmental conditions under which different lithologies record the global trends, but with observed offsets attributed to local factors.

The advantages of geochemical studies (stable isotopes and elemental abundances) on belemnite rostra from the Subbetic zone were explored by Nieto et al. (2008). Well preserved specimens were selected based on their isotopic composition and elemental content and used to constraint the age of Jurassic condensed levels from the Subbetic Zone. More recently, work in progress by Reolid and Benito (2011) on belemnite rostra from the Prebetic Zone of the Betic Cordillera also have shown a good preservation potential revealed by their geochemical signature (among other traits). Investigated features on a total of 188 specimens are discussed in relation to encasing lithofacies and respective depositional settings (shelf and outer shelf environment).

The interest on the record of Jurassic anoxic events is revealed by the numerous articles dedicated to this topic worldwide (e.g., Jenkyns, 1998; Hesselbo et al., 2000; among many others).The investigation of these events was also undertaken on the Betic Cordillera. Using geochemical data to support environmental interpretations, Jiménez et al. (1996) proposed a linkage between regional carbon isotope variations and paleooceanographic conditions during the Early Toarcian Anoxic event. More recently, Rodriguez-Tovar et al. (2011) revisited the same Toarcian Oceanic Anoxic Event, complementing previous interpretations (Jiménez et al., 1996) with new geochemical data tied to trace fossil

assemblage analysis that allowed reinterpretations regarding the effect of the T-OAE on the endobenthic macrobenthos.

Examples of statistical evalutation of geochemical data are, in general, less common in the literature. A valuable contribution for this approach was presented by Jiménez-Espinosa et al. (1997), providing data reduction techniques (principal component analysis and correspondence analysis) on a set of geochemical proxies that elucidated on the factors that influence the genesis of Fe-Mn crusts.

Apart from the obvious interest of local working groups (Granada and Jaén, often in collaboration with researchers from other Universities), reference to features of Ammonitico Rosso facies from the Betic Cordillera are often mentioned in order to establish a comparison with other sites where this facies is also investigated (mainly Italy). Recent examples of this are presented by Préat et al. (2011), while investigating the regional validity of the term Rosso Ammonitico in Italy; Osete et al., 2011, that investigated Ammonitico Rosso facies (among others) due to their excellent palaeomagnetic signal in the context of the research on the consistency between the palaeomagnetic information and the tectonic models proposed for the western Mediterranean. The potential of these materials for paleomagentic studies had already been reported by previous workers that also took advantage of this feature (Osete et al., 1988; Ogg et al., 1984; Allerton et al., 1993).

From the previous, it becomes obvious that encouraging work has been developed by research groups on Jurassic deposits from the Betic Cordillera. Nevertheless, the approach here proposed arises from the recognition of a gap concerning the treatment of distinct carbonate materials regarding their geochemical composition within a spatial framework, i.e., changes along a proximal to distal transect covering hundreds of kilometres along the studied paleomargin. In this way, several aspects included in this contribution have never been approached in the context of the Betic Cordillera, namely:

- The comparison between the geochemical signal of matrix micrite, carbonate cements, belemnite rostra and neomorphic ammonite shells in order to access the differential diagenetic paths and establish the degree of preservations of the studied materials;

- The treatment of eight proxies: carbon and oxygen isotope composition, major and trace elements (Ca, Mg, Sr, Fe and Mn) and skeletal content, all of them integrated on a

statistic framework including linear correlation, principal component analysis and hierarchical clustering. Other available information as field observations and microfacies are also presented in order to contextualize, supporting and validating the interpretations;

- The comparative study of seven sections that in a whole comprise a transect from proximal (neritic mid-shelf) to more distal epioceanic settings with a spatial approach regarding the geochemical parameters investigated. This seems to be the first contribution of this kind on the Betic Cordillera, and also one of the few examples found on the literature dedicated to spatial analysis of paleomargins (e.g., van de Kooij et al., 2009).

The main goal that motivated the thorough methodology developed during this work was to obtain significant representation of a spatial proximal to distal transect across the epicontinental and epioceanic realms from the Late Jurassic platforms under scope. The geochemical characterization of this transect would allow the recognition of ancient water mass organization. The approach developed during this work aimed to distinguish between global from regional/local signals.

1.3- Geological setting and study areas

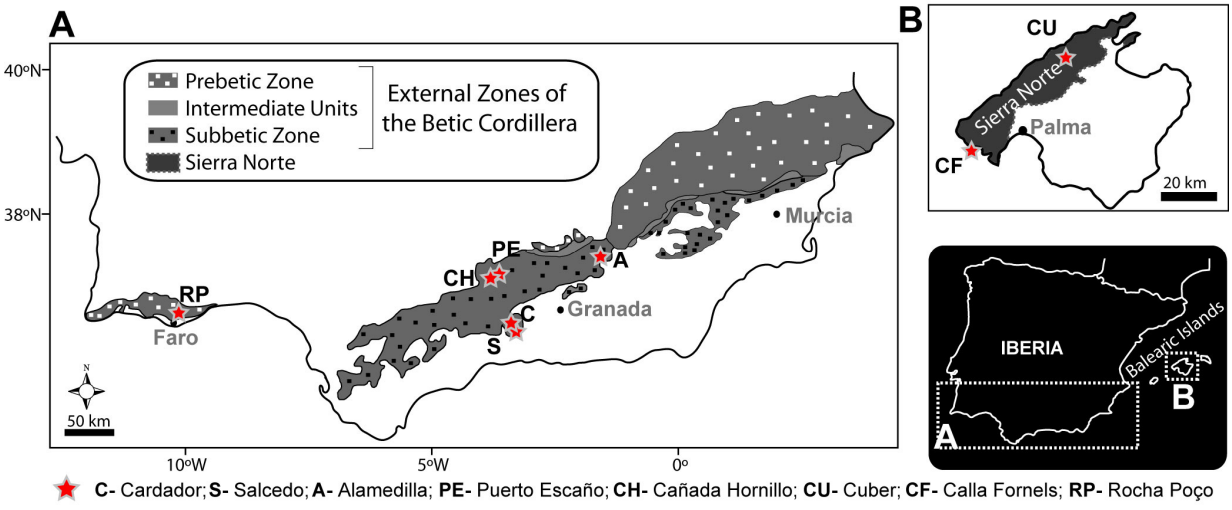

Fig. 1.4- Regional distribution of paleogeographic and geological units along the studied areas: A) Southern Iberia. B) Majorca Island (adapted from García- Hernández et al., 1980 and Caracuel and Olóriz, 1999). Stars indicate locations of studied sections (note key for abbreviations of sections studied)

Studied areas located in Southern Iberia (Spain and Portugal) and the Majorca Island provided carbonate samples from the External Zones of the Betic Cordillera and lateral equivalents (Fig. 1.4; see Olóriz et al., 2002a, Vera et al., 2004 and references therein for regional geology and detailed stratigraphy), as well as the southwestern part of the epicontinental shelf system in southern Iberia –i.e., the Algarvian Basin. During the Late Jurassic the south-eastern Iberian margin was an unstable area, as it was affected by relative movements between the Iberian and African plates (Fig. 1.5A and B) along the Maghrebian-Gibraltar Transform Zone – an extensional-transtensional margin closely linked to the geodynamic history of the central-north Atlantic Basin and the westernmost Tethys. As part of the NW Tethyan Margin (Fig. 1.5B), the physiography of south-eastern Iberia resulted in differentiation of two major paleogeographic areas: a more proximal, within a wide epicontinental shelf-system – the Prebetic zone and NE equivalents – and a more distal fringe, along the epioceanic realm – the Subbetic zone and lateral equivalents (Fig.1.4B and C). The Balearic Archipelago (Fig. 1.4B) has been interpreted as north-eastern extension of the Betic Cordillera (the Betic-Balear Domain in Fontboté et al., 1990). Pre-Cenozoic paleogeography and features in the Jurassic series have been noted; promoting differential interpretations including its understanding as a particular segment in the north–eastern extreme of the Betic Cordillera in correspondence with the eastern Iberian paleomargin during Jurassic times (Fig. 1.5C, see Olóriz et al., 2002a for references). Studied sections at the Majorca Island belong to the Sierra Norte domain (Figs. 1.4B and 1.5C, see Álvaro et al., 1984; 1989 and Caracuel and Olóriz, 1998 for regional geology and detailed Upper Jurassic stratigraphy).

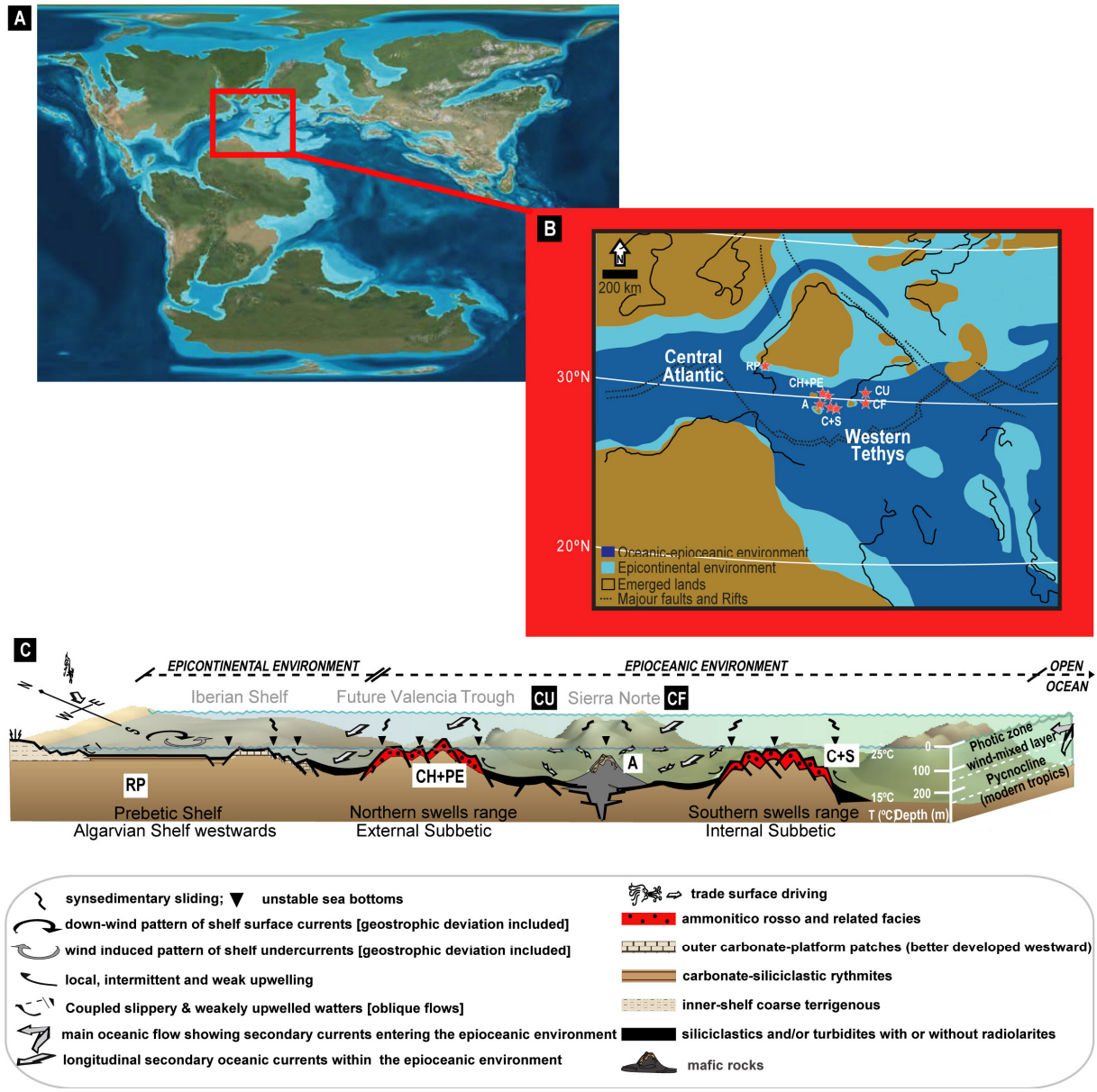

Fig. 1.5- Late Jurassic paleogeographic reconstruction at increasing detail. A: World map for Late Jurassic times (after Blackey, 2010); B: Late Jurassic paleogeographic reconstruction of western and central Tethys. Plate tectonic setting is from Stampfli and Borel (2002). Depositional environments are from Thierry et al. (2000 a, b). Schematic location of sections is indicated by stars; C: Composite schematic representation of the south and eastern Iberian paleo-margins showing assumed location of the studied sections (same abbreviations as in Fig. 1.4) and major paleo-environmental factors parameters affecting deposition (adapted from Olóriz, 2000).

In Southern Spain and the Island of Majorca, studied sections (Figs. 1.4 and 1.5) belong to the Subbetic Zone and lateral equivalents in the distal, epioceanic setting. The

Cañada del Hornillo, Puerto Escaño and Cuber sections represent an intermediate position from proximal to distal and correspond to the External Subbetic and NE lateral analogues (Figs. 1.4 and 1.5). The Cala Fornells section holds a similar, albeit somewhat more distal position compared to the Cuber section in tectonic-sheet IV of Álvaro et al. (1984) according to differential compression and shortening (Gelabert et al., 1992) in the piggy-back thrust-system of the Sierra Norte or Serra de Tramuntana in the Majorca Island. The most distal sections are considered those of Cardador and Salcedo belonging to the Internal Subbetic Zone (Figs. 1.4 and 1.5). Low, net accumulation rates on structural highs favoured the deposition of condensed, nodular, variably burrowed carbonates resulting in limestones widely known as Ammonitico Rosso and related facies (Fig. 1.5C). Typically, prevailing nodular pelagic-hemipelagic limestones are interbedded with more or less marly levels. More calcareous banks are a recurrent feature, sometimes useful for correlation (Fig. 1.6, A to D and F and Fig. 1.7 for stratigraphic distribution of studied lithofacies). Lateral and vertical colour changes are also a common feature, mainly from reddish to greyish (Fig. 1.6A to D and F).

The Upper Jurassic at Sierra Norte (Majorca Island) is dominated by Ammonitico Rosso facies (AR) (Caracuel and Olóriz, 1998, 1999 for details). The Alfabia Fm. (8-10 meters thick) is comprised of thin alternating horizons of AR and grey, more or less nodular marly limestones (Fig. 1.7 and 1.8A for detailed representation of the lithofacies at the Cuber section). Siliceous horizons occur occasionally. The Aumedrá Formation is characterized by expanded, well bedded brownish and macrofossil poor limestones (Fig. 1.7) (ca. 40 meters, i.e., 57% of total thickness and 6% of the time contained in Upper Jurassic deposits; Caracuel and Olóriz, 1999). The Son Torrelles Fm. (ca. 10 meters) shows returning AR depositional conditions, commonly with reworked sediments and siliceous horizons.

The studied outcrop in the surroundings of the village of Alamedilla (Fig. 1.4A) is located in the Middle Subbetic, corresponding to a trough separating two discontinuous ranges of seamounts (Fig. 1.5C) in the S-SE palaeomargin of Iberia (Olóriz et al., 2002a for a comprehensive review with extended references). The Alamedilla outcrop (Fig. 1.6E) displays reddish, brownish and pale-grey limestones, secondary marls, and dominant mafic rocks (Figs. 1.6E and 1.7). Limestones are locally rich in ammonites (condensed, pelagic, cephalopod-rich limestones), which preserve neomorphic shells infilled by fine sediment similar to the encassing deposits. Belemnites are relatively common.

Fig. 1.6- Field views of the studied outcrops. A: Cardador; B: Salcedo; C: Puerto Escaño; D: Cañada del Hornillo; E: Alamedilla; F: Cala Fornells; G: Cuber; H: Rocha Poço.

The most proximal end-member of the studied proximal to distal transect is represented by the Rocha Poço section (southern Portugal; Figs 1.4A, 1.5B and C, and 1.6H), covering mainly Lower Kimmeridgian deposits (see Fig. 1.7 for stratigraphic distribution of lithofacies). This section belongs to the epicontinental area of the south-western Iberian platform (Fig. 1.5 B and C, see Marques, 1983; Marques and Olóriz, 1989a, b; Olóriz et al., 1994), an expression of the epicontinental shelf system represented eastwards by the wider Prebetic Shelf. A 60 meters thick section is characterized by very distinct facies (Figs. 1.7 and 1.8B for detailed representation of the lithofacies registered at the Rocha Poço section). From a time of greater terrigenous influence, represented by the alternation of more or less detrital marly-limestones and marls at the base of this section (Fig. 1.6H), lithofacies gradually change with development of spongiolithic bioherms. These facies are topped by limestone banks upwards to the Upper Kimmeridgian (Figs. 1.7 and 1.8B).

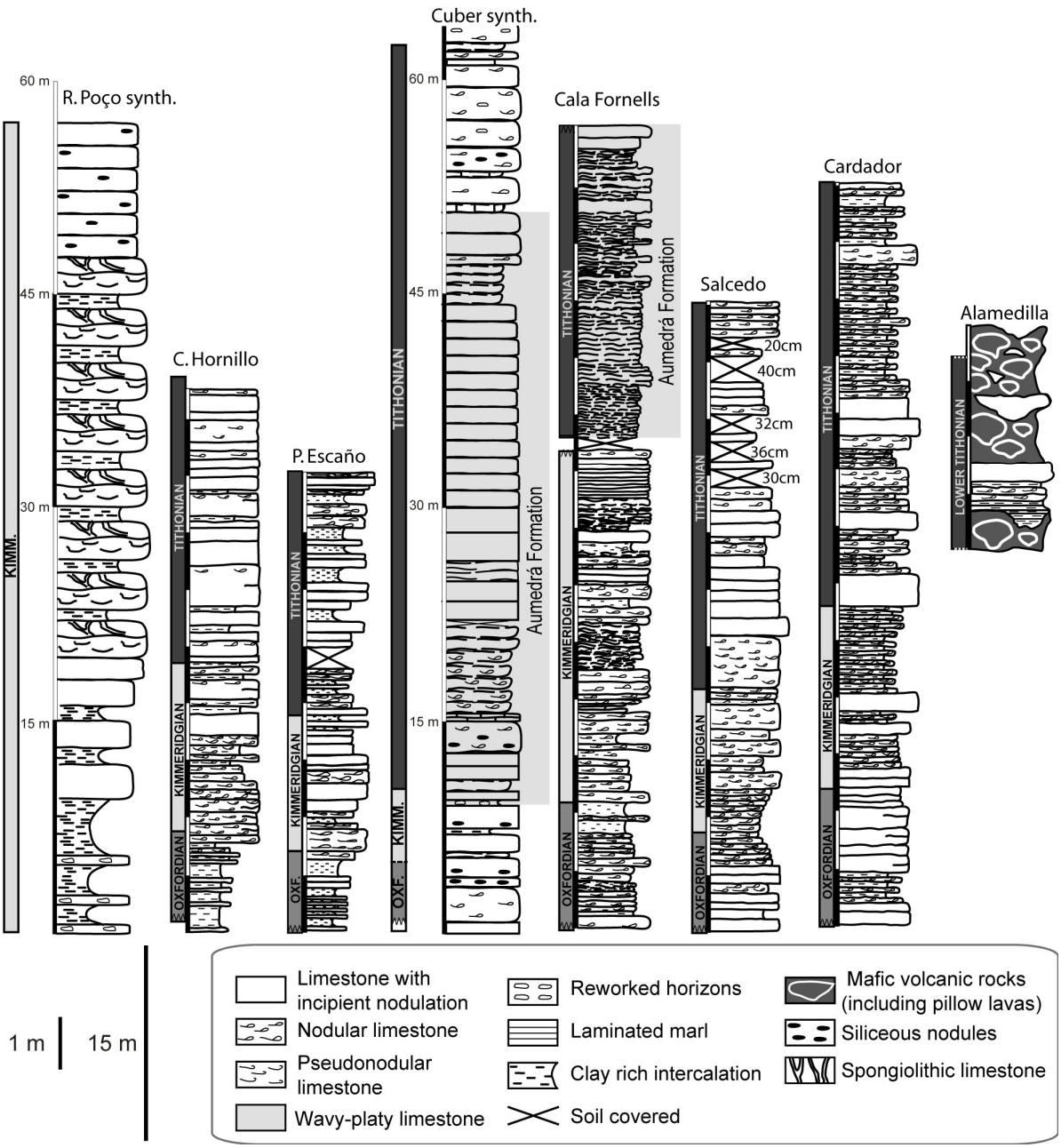

Fig. 1.7- Stratigraphic distribution of the studied lithofacies for each studied section. The sections at Cuber and Rocha Poço are presented in detail in Figure 1.8.

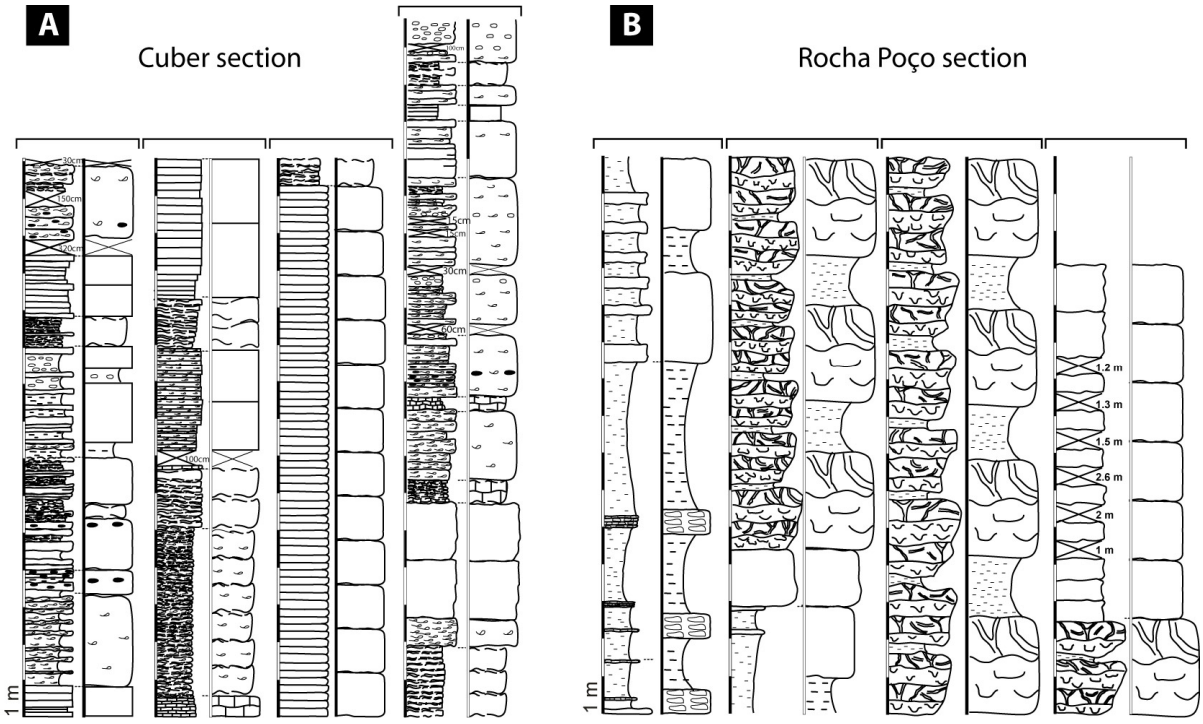

Fig. 1.8- Sections at Cuber (A) and at Rocha Poço (B) represented in detail and corresponding synthetic section.

1.3.1- General considerations on the paleogeographic and paleoenvironmental context of the studied sections

Two broad environmental realms are considered to contextualize the studied sections. Epicontinental areas refer to neritic environments represented by the Rocha Poço section in southern Portugal. Thus, in the case under study no epeiric seas are included. Epioceanic areas refer to depositional settings and water masses outside from neritic shelves and corresponding to the ecologically oceanic environment. These latter extend across the structured continental slope (continental crust) that precedes ocean floor regions more or less distant to oceanic spreading centers producing new ocean floor (oceanic crust emerging through oceanic ridges) –see D'Argenio (1974-76) for a geodynamic context of application to paleomargin structuring in the Mediterranean Tethys; Olóriz (1997) for reintroduction in terms of the eco-sedimentary context, and Olóriz (2000) for extended treatment. All the remaining sections studied in the Betic Cordillera and the Majorca Island are representative of the epioceanic fringe.

The most proximal section, Rocha Poço (Figs. 1.4 and 1.5B and C), presents the development of sponge bioherms allowing some inferences regarding the shallowest depth

reached by the studied epicontinental record. Depth estimations for sponge-microbialite buildups range from 25 m to slightly over 200 m water depth (e.g., Keup et al., 1990). Recent work on Jurassic coral- and sponge-microbialite bioconstructions assume depth ranges between 60-100 meters as probable, ensuring 10% of surface light availability vital for microbialite growth (Olivier et al., 2007). Eastwards along the south Iberian paleo-margin, Oxfordian buildups made by sponge-microbial consortia have been placed at mid-shelf depths (50-70m) in the Prebetic Zone (Olóriz et al., 2003a). Ramalho (1988) estimated depth euphotic zone in the range of 50-150m for the sponge reefs across the Rocha area. Following the above-cited works, the shallowest depths estimated for the most proximal section along the transect corresponds to a mid-shelf paleo-environment probably in the order of 50-60 meters deep (Fig. 1.5C).

The epioceanic record is dominated by the occurrence of nodular limestones deposited on structural highs (Fig. 1.5C). Low accumulation average rates favoured the deposition of carbonate muds resulting in condensed, nodular Ammonitico Rosso and related facies on structural highs, at maximum depths of around 250 meters, represented in Fig. 1.5C (Jenkyns, 1974; Olóriz et al., 1996, 1997; Olóriz, 2000). Nodule formation resulted from the complex interplay between sediment input and current sweep and winnowing, burrowing and pore-water circulation (Flügel, 2004; Coimbra et al., 2009).

Both sections investigated from the Island of Majorca (Figs. 1.4B and 1.5) are characterized by very distinctive lithofacies types (Figs. 1.7 and 1.8A). At the Cuber and Cala Fornells sections, thin intercalations of wavy to platy limestones, occasionally bearing silica nodules and/or discontinuous horizons suggest a locally higher silica input. Probable biotic silica sources included dissolution of marine siliceous skeletons (sponge spicules, diatoms, radiolaria) (Fanning and Schink, 1969; James et al., 2000). The conditions for silica nodule formation will be further discussed in the light of obtained geochemical data, as well as the effect of silica diagenesis on the encasing carbonate matrix micrite (chapter 4).

Another striking feature at the Majorca sections is the presence of the Aumedrá Formation. This comparatively extended, homogeneous deposit with distinctive dark brown colour in fresh samples and very fine grain size, markedly contrasts with standard deposition known from Jurassic epioceanic swells. Prior to this research, its origin was still enigmatic (Caracuel and Olóriz, 1998). Obtained geochemical data provided arguments to attempt new explanations for the development of such an atypical facies (chapter 5).

The studied outcrop in the surroundings of Alamedilla (Fig. 1.5A) is located in the Middle Subbetic, corresponding to a trough separating two discontinuous ranges of seamounts (Fig. 1.5C) in the S-SE palaeomargin of Iberia (Olóriz et al., 2002a for a comprehensive review with extended references). A longitudinal, volcanic structure 5-10km wide, exceeding the central sector of the Betic Cordillera in longitude (see Fig 1.5C for synthetic bottom physiography), and interpreted to be some hundred meters high locally, subdivided the Middle Subbetic Through (Comas, 1978). Shallow water carbonate deposition occurred on top of volcanic highs during the Middle Jurassic (e.g., Vera et al., 1997), evidencing patches of photic zone productive factories (Bahamian-type carbonates on guyots in Molina and Vera, 2000). Neritic depths have been interpreted for Upper Jurassic marl-limestone rhythmites with intercalated calcareous tempestites (Milanos Fm, cf. Vera and Molina, 1998) in relative low bottoms. Storm deposits also affected pelagic seamounts during early Tithonian times in the northern seamount range or External Subbetic (e.g., Checa et al., 1983; Molina et al., 1986, 1987). Lenticular lithosomes of condensed pelagic wackestones (described in chapter 3) with ammonites are here under scope due to the particular conditions that they represent, clearly deviated from any other studied section.

1.4- Working approach, studied materials and methods

Sample preparation (rock slabs, thin sections, polished surfaces of hand samples, vial cleansing, powder sampling), optical (petrography, SEM and CL), geochemical analysis and data treatment were performed at the facilities of the University of Granada (Depatment of Stratigraphy and Paleontology), and Centre of Scientific Instrumentation (CIC), Department of Geodynamics (Spatial Teledetection, GIS and Geoestatístics), as well as at the Institute for Geology, Mineralogy and Geophysics, Ruhr University Bochum, Germany. For details see below.

1.4.1- Different materials under scope

A total of 316 hand specimens were retrieved providing in average 5 samples per section meter for more condensed sections (Cardador, Salcedo, Puerto Escaño, Cañada del

Hornillo and Cala Fornells), and 1 sample per section meter for the two remaining ones (Cuber and Rocha Poço). From each hand sample, two slabs where cut: one for macroscopic inspection, microfacies analysis and cathodoluminescence, and the respective twin slab for geochemical investigations (Fig. 1.9).

Fig. 1.9- Upper view of some rock slabs. Each slab is approximately 1 to 2 cm thick.

Matrix micrite- Matrix micrite samples analyzed from the Upper Jurassic sections mainly correspond to Ammonitico Rosso nodular facies, intercalated with horizons with indistinct nodular structure (Fig. 1.6 A to D, F and 1.7). This is the main trend in five of the studied sections (Cardador, Salcedo, Cañada del Hornillo, Puerto Escaño and Cala Fornells). Several diagenetic models have been proposed for nodule formation (Hollmann, 1962, 1964; Jenkyns, 1974; Müller and Fabricius, 1974; Mullins et al., 1980; Farinacci and Elmi, 1981; Clari et al., 1984; Clari and Martire, 1996; Martire, 1996; Coimbra et al., 2009). Nodule formation is widely documented as an early diagenetic feature (references above), resulting from the interplay between current energy, sedimentary input and winnowing, burrowing and water pumping (Coimbra et al., 2009).

The presence of other facies adds complexity to this study. At the Cuber section, nodularity is commonly indistinct or harder to recognize, and silica bearing horizons are recurrent (Figs. 1.6G, 1.7 and 1.8A). Locally, probable silica sources include marine siliceous skeletons (e.g. diatoms, radiolarian) that by dissolution could provide enough silica supply (Fanning and Schink, 1969; James et al., 2000). The horizons that comprise the Aumedrá Formation (intercalated in the Cuber and Cala Fornells section, Figs. 1.7 and 1.8A) added diversity to the analyzed matrix micrite.

The Rocha Poço section adds further heterogeneity (Figs. 1.5H, 1.7 and 1.8B). More carbonate-siliciclastic facies, with more proximal influence are overlain by bioconstructed

horizons (example in Fig. 1.10D). The appearance of spongiolithic lithofacies, i.e., sponge-rich deposits represents a marine environment with favourable conditions for the extensive development of sponges in the form of large sponge meadows (Olóriz et al., 2003a).

In contrast to depositional and taphonomic histories typical for a Tethyan top-swell site (i.e., rather calcareous Ammonitico Rosso), matrix micrite from a pelagic cephalopod-rich limestone outcropping at Alamedilla (Figs. 1.5A and 1.6E) is compared with typical AR deposits (the Cardador section was used as reference). This peculiar lithofacies corresponds to events of carbonate-mud deposition, followed by rapid burial and early lithification, synsedimentary sliding and over imposition of mainly firmground horizons. Condensed, pelagic and ammonite-rich limestones are included as local, more or less stratified lithosomes encased by submarine mafic vulcanites in the Mid-Subbetic Volcanic Ridge (Fig. 1.5C and 1.6E). The peculiarity of this chosen example deserved special attention.

Geochemical characterization of such a variety of matrix micrites (Fig. 1.10) comes as a challenge towards the distinction between preservation of depositional environment information and potential diagenetic overprint.

Carbonate cements- Although not a frequent feature (from a total of 102 analysed features, 42% belong to the Cuber section, example in Fig. 1.10C) secondary blocky calcite was identified on several samples. Cathodoluminescence inspection was performed on several representative examples, and all carbonate cement samples were analysed for their stable isotope (C and O) ratios and elemental composition.

Belemnite rostra- Belemnite rostra are widely used on paleoenvironmental reconstructions (e.g. Price and Sellwood, 1994; Saelen et al., 1996; Podlaha et al., 1998; Jenkyns et al., 2002; Wierzbowski, 2002; Voigt et al., 2003; Rosales et al., 2004; McArthur et al., 2007; Price, 2010). Due to a more stable low-Mg calcite original mineralogy (Veizer, 1983; Sælen, 1989), belemnite rostra are generally less prone to diagenetic overprint. Therefore, marine paleotemperature reconstructions are often carried out on belemnite calcite data by means of isotope thermometry (e.g., Spaeth et al., 1971; Stevens and Clayton, 1971; Veizer, 1974; Naydin and Teys, 1976; Sælen et al., 1996; Price and Sellwood, 1997; Podlaha et al., 1998; McArthur et al., 2000; Jenkyns et al., 2002; Price and Groecke, 2002, McArthur et al., 2007). Recent works have contributed to a better knowledge on ecological and biogeographic effects

(Price et al., 2009; Rexfort and Mutterlose, 2009; Wierzbowski and Joachimski, 2009; Warnke et al., 2010) evidencing the relevance of vital effects on interpretations based on oxygen isotope signatures. Belemnite rostra were not very abundant on the studied materials (some examples are shown in Fig. 10A and E). All the available specimens were sampled and tested for their degree of preservation. The only case where belemnite abundance was higher corresponds to the selected cephalopod-rich limestone (Fig. 1.10E).

Neomorphic ammonite shells- Preservation of metastable aragonitic hardparts is not frequent due to metastability of aragonite under marine conditions (e.g. Veizer, 1983). Aragonitic ammonite shells may be stabilized through mineralogic inversion into neomorphic calcite. In the case of total dissolution of shell material, moldic porosity may be generated and latter occluded during recrystallization (Bathurst, 1971). Aragonite dissolution is thought to contribute to elemental supply for early nodule formation in Ammonitico Rosso facies (e.g., Jenkyns, 1974), significantly but not exclusively, substantiating the magnitude of this process. Notwithstanding, examples of neomorphic ammonite shells were found and analysed. Their scarcity on all studied AR sections (only 2 examples could be sampled, one example is shown in Fig. 1.10A) was contrasted by the very good preservation state for all the neomorphic ammonite shells (11 specimens) encased on the Alamedilla cephalopod-rich limestone (Fig. 1.10E).

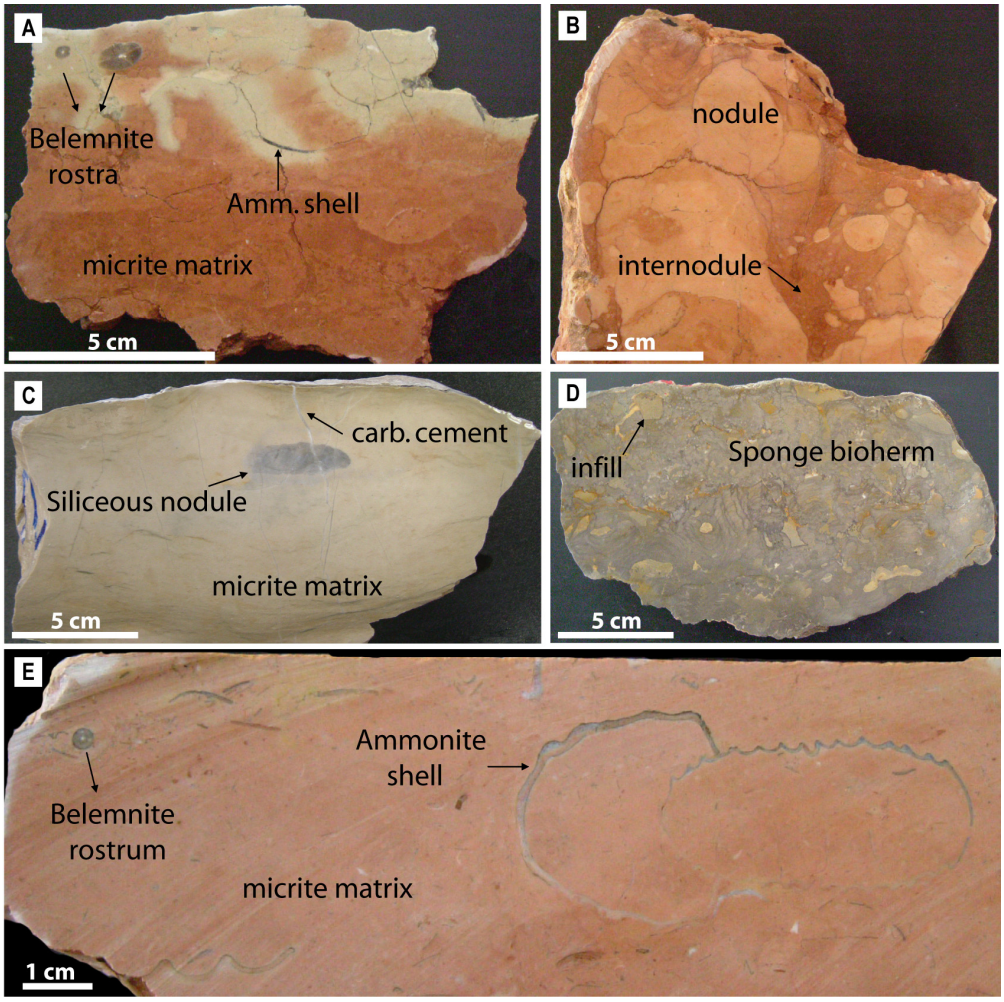

Fig. 1.10- Several examples of rock slabs that illustrate the applied sampling strategy. Note the diversity of sampled matrix micrites and also the variety of studied carbonate materials.

1.4.2- Working approach and applied methods

1.4.2.1- Field procedure

The selection of sections to be investigated was made according to their potential significance as paleogeographic and paleoenvironmental reference sections, all of this according to the principle of empirical parsimony. A detailed analysis bed-by-bed was conducted on the sections selected for this research, paying attention to lateral correlation of horizons within a given outcrop. Then, a precise numbering of beds and a selective sampling for lithofacies interpretation and geochemical analysis was programmed (Fig. 1.11) together with acquisition of precise thickness for bed and analyzed stratigraphic interval. In addition,

the appropriate refinement of the biostratigraphic information was accomplished. A comprehensive reference list on lito- and biostratigraphy concerning the studied areas can be found in Olóriz et al., 2002a and complementary references from the analyzed sections can be found in chapters 2 to 6. Rock samples with precise indication for bottom and top surfaces were differentiated between those for lito-biostratigraphy and those for geochemical analysis and related ones.

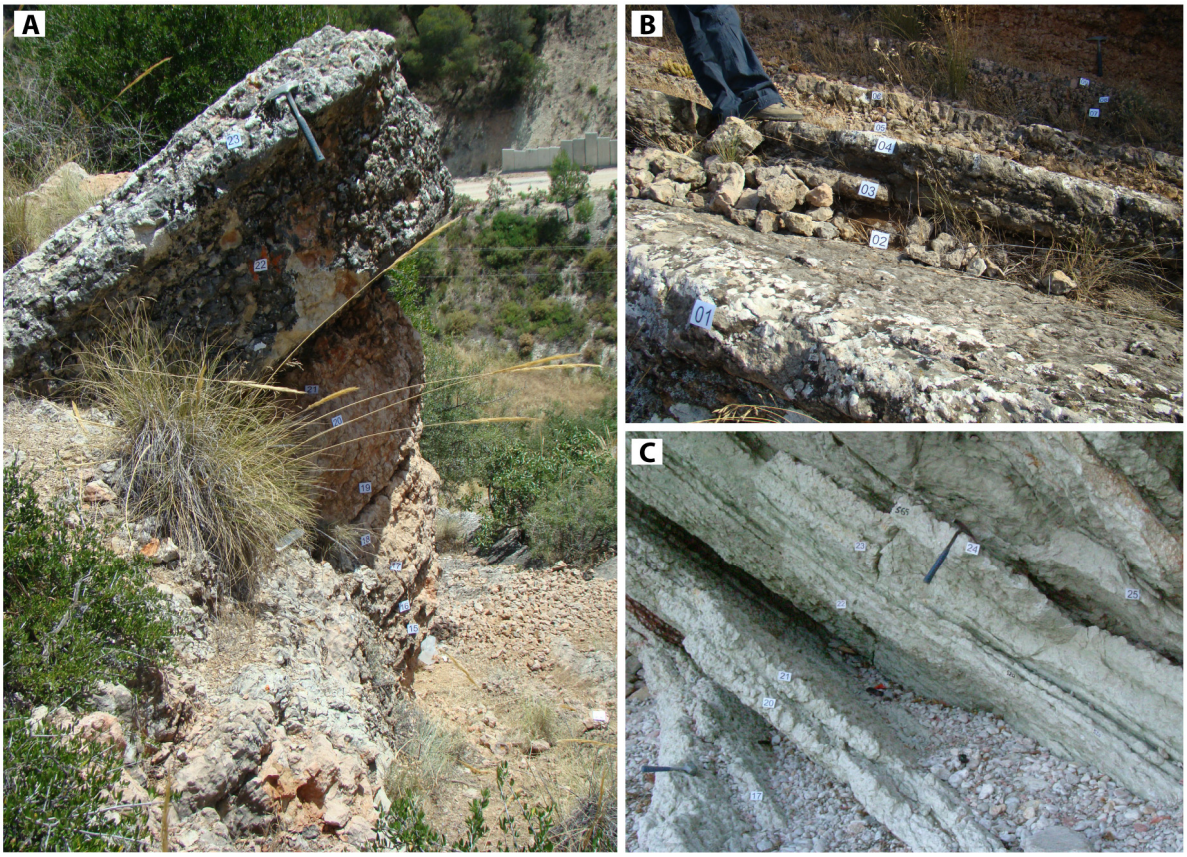

Fig. 1.11- Field aspects of distinct sections evidencing the sampling strategy applied during field work. A and B- Salcedo section; C- Cala Fornells section. Hammer for scale on all photos (for B at the upper right corner).

1.4.2.2- Petrographic parameters

Microfacies analysis was carried out on thin sections from each sampled horizon. Apart from detailed descriptions (see bellow), the skeletal abundance of the analysed thin sections was performed by means of pixel counting. The usefulness and innovation inherent to this method was worthy of a contribution to the journal *Computers and Geosciences*

(submitted the 31st of May of 2011). Since this contribution is mostly methodological, it will be included as Appendix (chapter 8).

Cathodoluminescence inspection was carried out for all different carbonate materials using a hot stage cathode luminescence (HC4- LM). The aim was on separating intrinsic (early) from orange luminescent (later diagenetic, secondary) carbonate materials in order to access the degree of diagenetic imprint (Fairchild, 1983; ten Have and Heijnen, 1985; Marshall, 1988; Machel and Burton, 1991; Machel et al., 1991; Bruckschen and Richter, 1994; Bruhn et al., 1995; Barbin et al., 1997).

Ultrastructure inspection of micrites was performed under Scanning Electron Microscope (SEM) LEO-Gemini 1530 on fresh fractured rock chips of 15 samples. These were mounted at the Center of Scientific Instrumentation of the University of Granada and at the Ruhr University (Bochum-Germany).

1.4.2.3- Geochemical parameters

A total of 1080 powder samples were analyzed for their elemental content and stable isotope (C and O) ratios. Sample preparation was carried out at the University of Granada. It consisted on preparing the vials used for storing the powder materials by means of thorough cleansing protocol; on producing the rock slabs used for analytic procedures; and on drilling the powder samples using a hand drill with a 1 mm diamond drill tip. Once the powder samples were collected, further analytical work was performed at the Institute for Geology, Mineralogy and Geophysics (Ruhr University Bochum, Germany). Stable carbon and oxygen isotopes were obtained on a ThermoFinnigan MAT delta-S mass spectrometer. Stable isotope data were collected from the CO_2 gas liberated by approximately 0.3 mg of bulk carbonate powder samples, after reaction with 100% phosphoric acid (following McCrea's (1950) method). Reproducibility ($\pm 1\sigma$) was controlled by NBS19 and internal standards, being better than ±0.03 and ±0.07‰ for, respectively, $\delta^{13}C$ and $\delta^{18}O$. Duplicate samples presented a maximum scatter of ±0.02‰ for $\delta^{13}C$ and ±0.08‰ for $\delta^{18}O$. Isotopic values are reported in the standard δ-notation in per mil (‰) relative to V-PDB.

All samples measured for isotopic analysis were also investigated for their Ca, Mg, Sr, Fe and Mn elemental composition using inductively coupled plasma- atomic emission spectrometry (ICP-AES). Dissolution of 1.5 mg of powdered sample in 1 ml of 3M HNO_3

(over 12 hours) was followed by further dilution with 2 ml of distilled water. A small amount insoluble residue was observed for most of the samples. This corresponds to a non-carbonate materials belonging to the detrital (clay) fraction, as silicate minerals (e.g., illite and montmorillonite, commonly present in AR facies (Jenkyns et al., 1974). This fraction is not dissolved during acid treatment of bulk micrite samples. Filtering the samples is crucial for an efficient functioning of the used equipment (correct flows and absence of clogging particles at the ICP nebulizer) and for ensuring that only carbonate bound elements are measured. Most of the samples were then filtered (ca. 90%). Maximum elemental scatter for duplicate runs was in the order of 3% for all elements.

1.4.2.4- Statistical approach

Descriptive statistics- When dealing with large data set it is often convenient to apply data reduction methods, in order to achieve a better overview of data distribution. Regarding the obtained dataset, the first step consisted on calculating the mean value for the three sub-samples analyzed for each rock slab. Respective mean values were used for further data evaluation, connected by full lines on all the presented stratigraphic trend plots.

Mean values were used to compute the boxplots (see Tukey, 1977; McGill et al., 1978 for detailed descriptions), representing the interquartile range (the difference between first and third quartiles); median and mean; maximum and minimum values. The ends of the whiskers represent the limits beyond which values are considered as non-representative. Since both average values of mean and median where available, the choice of connecting median values to interpret proximal to distal trends was based on the fact that the median is least affected by an extreme values (e.g., major peaks). Hence, the median represents better background situations, rather than deviating due to sudden changes in absolute values (here not considered as outliers since maximum peaks are associated to known environmental changes, further discussed bellow). Still, mean values were also tested, producing the same relative behavior as median values.

Filtering the samples before ICP measurements may affect total elemental abundance values since part of the initial weight of the samples is eliminated (retained on the filters). In order to correct the data set for this effect, all values were divided by measured Ca concentration (and multiplied by 100). This means that corrected elements loose their absolute abundance value. Despite this disadvantage, stratigraphic trends are preserved for all sections,

as further demonstrated (see chapter 6 dealing with elemental chemostratigraphy). In this way, statistical evaluations were preformed using the corrected data set (Sr/Ca, Mg/Ca, Fe/Ca, Mn/Ca), insuring minimum effects of sampling strategy inherent to elemental analysis.

Principal component analysis (PCA)- This statistic tool allows the establishment of patterns within large data sets through data reduction (Wold et al., 1987; see also Jolliffe, 2002 for detailed description). The eigenvectors of the correlation matrix are principal components (PC) and each original observation is converted into principal component scores by projecting it on the principal axes. The vales of the eigenvectors that are used to compute the scores of the observations are called principal component loadings. Typically, the raw data matrix can be reduced to two or three principal component loadings that account for the majority of the observed variance. The PC loadings can be examined to provide further insight into the processes that are responsible for the similarities between the proxies under evaluation.

Cluster analysis- Cluster analysis is used to group variables within a given data set. In clustering, similar objects fall into the same class (Danielsson et al., 1999, see also Everitt et al., 2001 for detailed description of this method). Hierarchical clustering joins observations that are progressively more similar to each other. The levels of similarity at which observations are merged are used to construct a clustering tree, designated as dendrogram. It is then possible to truncate the tree at a given level.

The proximity between two objects is obtained by measuring at what point they are similar (similarity) or dissimilar (dissimilarity). The agglomerative hierarchical clustering algorithm uses the dissimilar proximity type, but can be converted into similarity, if this is an advantage regarding the final goal of the performed analysis. In the case of geochemical composition here under scope, similarity is thought to be more adequate, since major differences can be established by PCA analysis.

To calculate the dissimilarity/similarity between two groups of objects, different agglomeration methods are possible. In the case of the available dataset, agglomeration was performed by using the "unweighted pair-group average linkage". It represents an intermediate approach regarding to compaction and dilation of the data space produced by simple and complete linkage (respectively), allowing a fair representation of the data space properties.

Geostatistical analysis of temporal variability- In recent years, geostatistical methods have become an essential tool to analyse spatio-temporal data. These methods are based on the "Theory of Regionalised Variables" (Matheron, 1970). This approach interprets experimental variables as regionalised variables, i.e., as variables which present a spatio-temporal distribution characterized by a spatial and/or temporal variability (or correlation) structure.

The concept of regionalised variable can be applied to this study concerning the analyzed geochemical parameters (and also petrographic) measured along the analysed series throughout the proximal to distal transect. Simple variogram function was applied for all proxies, applying the following equation:

$$\gamma_k(t) = \frac{1}{2n(t)} \sum_{i=1}^{n(t)} \{ z_k(x_i) - z_k(x_i + t) \}^2$$

where $z_k(x_i)$ and z_k (x_{i+t}) are the values of the z_k variable, observed in samples x_i and x_{i+t} of a series; n(t) is the number of pairs of distance data whose distance is the time vector t. It must be clarified in this study of the analysis of data temporal variability that vector t represents a relative time value, i.e., it corresponds to an ordinal value of separation of the experimental sample x_i and x_{i+t} in the series. It follows from the previous expression that a variogram is a vectorial function, which quantifies the variance of the first-order quadratic increments of the z_k variable. Both, its analysis and interpretation, are important to quantify the variable's temporal variability.

In the multivariate case, the cross-variogram function has been used to analyse the variability or joint correlation (coregionalisation) between two variables z_j and z_k:

$$\gamma_{jk}(t) = \frac{1}{2n(t)} \sum_{i=1}^{n(t)} \{ z_j(x_i) - z_j(x_i + t) \} . \{ z_k(x_i) - z_k(x_i + t) \}$$

The cross-variograms were performed only for those variables that showed certain similarity on their simple variograms. For the purpose of analysis and comparison of results the simple variograms have been normalised by the data variance; and in the case of the cross variograms, normalised by the variables covariance.

2

Matrix micrite $\delta^{13}C$ and $\delta^{18}O$ reveals synsedimentary marine lithification of Upper Jurassic Ammonitico Rosso limestones (Betic Cordillera, SE Spain)

Rute Coimbra [(a)], Adrian Immenhauser [(b)], Federico Olóriz [(a)]

[(a)] Departamento de Estratigrafia y Paleontologia, Universidad de Granada, Spain

[(b)] Institute for Geology, Mineralogy and Geophysics, Ruhr Universität Bochum, Germany

Sedimentary Geology 219 (2009) 332–348

Submitted 18th March 2009

Accepted 1st June 2009

Abstract

Matrix micrites are a commonly used carbonate archive for the reconstruction of past environmental parameters, but one that is submitted to known limitations. Main reasons for the often ambiguous value of many micrite-based isotope data sets are the unknown origin of the micrite components and their poorly resolved diagenetic history. Here we present carbon and oxygen-isotope data retrieved from Oxfordian to Tithonian Ammonitico Rosso nodular micrites sampled from three sections in the Betic Cordillera (Southern Spain). All three sections were correlated and sampled using a rigorous biostratigraphic framework. A noteworthy feature is that analyzed matrix micrites are more conservative in terms of their isotopic composition than other carbonate materials commonly considered to resist diagenetic alteration under favourable circumstances. Remarkably, this refers not only to $\delta^{13}C$ ratios, which reflect the typical Late Jurassic global trend, but also to $\delta^{18}O$ ratios that range around 0.3 ‰. The ^{18}O-enriched oxygen-isotope ratios are considered to represent diagenetic stabilization of carbonate ooze under the influence of marine porewaters within the sediment-water interphase (i.e., the immature sedimentary section, usually submitted to biogenic activity). This interpretation agrees with the very early lithification of micrite nodules with cements precipitated from marine porewaters, enriched by the dissolution of aragonite skeletals (i.e., ammonite shells). According to the model proposed, low sedimentation rates as well as rapid early marine differential cementation, under the influence of currents and seawater pumping, affected the sediment-water interphase of epioceanic swells where deposition resulted in early lithified Ammonitico Rosso facies. The data obtained show that special care must be taken to prevent oversimplified interpretations of carbonate archives, particularly in the context of epioceanic settings.

♦ ♦ ♦

2.1- Introduction

Biogenic, abiogenic and organomineralic carbonate materials are amongst the most important marine archives of global change. Spanning the Precambrian to the Recent, proxy data obtained from carbonates provide key information on seawater geo-chemistry, temperature and seasonality, pH, salinity or alkalinity (Shackleton and Opdyke, 1973; Walls et al., 1979; Carpenter et al., 1991; Savin, 1997; Spero et al., 1997; Rohling et al., 1998; Bruckshen et al., 1999; Veizer et al., 1999) and modelizations of the coupled surficial hydrosphere-atmosphere-biosphere-soil system have been proposed (e.g., Berner, 2005). Most studies either use biogenic shell material (Martin, 1995; Immenhauser et al., 2002; Brand et al., 2003), abiogenic marine cements (e.g., radiaxial fibrous cements; Lees and Miller, 1995; Tobin and Walker, 1996a, b) or lithified carbonate oozes (matrix micrites; Mennegati, et al., 1998, Jenkyns and Wilson, 1999; Stoll and Schrag, 2000; Jarvis et al., 2002; Rais et al., 2007) in order to extract information. Broadly, for neritic settings, well-preserved calcitic or aragonitic hardparts from sessile organisms (e.g., corals, brachiopods, rudist bivalves; Ross and Skelton, 1993; Carpenter and Lohman, 1995; Steuber, 1996; Mii et al., 1999; Gagan et al., 2000; Rosenfeld et al., 2003; Immenhauser et al., 2005; Pufahl et al., 2006) are perhaps the most reliable and time-resolved proxy archives for reconstruction of past environmental parameters.

From epicontinental and epioceanic domains, many authors refer to proxy data from belemnite rostra (Price and Sellwood, 1994; Saelen et al., 1996; Wierzbowsky, 2002; Rosales et al., 2004) or matrix micrites (Joachimski, 1994; Bartolini et al., 1999; Préat et al., 2006; Rais et al., 2008) but this approach is not exempt from problems. The nectonic behaviour of these cephalopods, which inhabited different water masses throughout ontogeny, adds complexity to the poorly understood composition and diagenetic alteration of the matrix micrite that encases them (Dickson and Coleman, 1980; Allan and Mathews, 1982). Despite considerable research (Friedman, 1964; Macintyre and Milliman, 1970; Blackwelder et al., 1982; Milliman et al., 1985; Reid et al., 1990; Keim and Schlager, 1999; Immenhauser et al., 2002), the origin of micrite remains an unresolved matter in carbonate sedimentology and paleoceanography. Micrite is polygenic in origin, and when diagenetically altered, its source is difficult to ascertain (the ‘micrite problem’). In addition, when lithifying, carbonate oozes undergo dissolution and reprecipitation processes (Steinen, 1982). The consequence is the

addition of variable amounts of secondary carbonate (micro-) cements and/or the diagenetic recrystallization of micritic carbonates. Despite the often poor knowledge about their origin and diagenetic history, time-series data of light stable isotope (C and O) ratios obtained from matrix micrites have been successfully applied in numerous geochemical studies (Jenkyns, 1980; Menegatti et al., 1998; Joachimski et al., 2002; Immenhauser et al., 2003; Jiang et al., 2007). Particularly, bulk data from IODP cores have shown surprisingly well preserved or even near-'pristine' geochemical records of global shifts in carbon-isotope data (e.g., Shackleton and Opdyke, 1973; Veizer, 1983; Renard, 1985). Nevertheless, to date the 'matrix micrite' approach is largely empiric, or at best, supported by data from diagenetically more stable carbonate materials. Hence, well-preserved marine isotope values obtained from micritic material are commonly interpreted through analogy with reported case studies (e.g., Weissert and Mohr, 1996), although the way in which micrite materials escaped alteration is poorly known.

Using the detailed biostratigraphic framework at the ammonite biozone-subzone level (Olóriz, 1978, 1996; Caracuel 1996; Olóriz et al., 1999), the matrix micrite, carbonate cements and belemnite carbon- and oxygen-isotope data from a series of carefully measured and dated outcrops in Upper Jurassic Ammonitico Rosso facies from southern Spain are presented and discussed in a process-oriented context. Remarkably, the micrite carbon- and oxygen-isotope data obtained are indicative of near-pristine marine-porewater values, whereas low-Mg belemnite rostra show evidence of diagenetic overprint. This pattern is uncommon and deserves attention. Consequently, the aim of this paper is threefold: (i) to document well-constrained, nodule versus inter-nodule isotope data from micrite, skeletal components and carbonate cements in three Oxfordian to Tithonian sections; (ii) to interpret isotope values in the context of their paleoceanographic and diagenetic evolution; and (iii) to assess potential mechanisms that resulted in the preservation of marine porewater isotope values in these micrites. The data and results obtained are therefore of broad significance for those concerned with the interpretation of geochemical data from matrix micrites in general.

2.2- Geological Setting and Sedimentological/Stratigraphical Context

The Betic Cordillera runs along SE Spain (Fig. 2.1) and is subdivided into two large geotectonic domains: the External and Internal Betics (Olóriz et al., 2002a and references therein; Vera et al., 2004 and references therein). During the Mesozoic, the External Zones of the Betic Cordillera were part of the NW Tethyan Margin (Fig. 2.2), differentiated into two different palaeogeographic areas: the Prebetic and the Subbetic zones. Due to their more distal, epioceanic setting, the Internal Subbetic Zone experienced very low average sedimentation rates and common omission/erosion on raised blocks (extended references in Olóriz et al., 2002a and Vera et al., 2004). This resulted in a deposition of condensed, nodular, intensely burrowed limestones widely known as Ammonitico Rosso and related facies. Despite the high level of stratigraphic condensation, Oxfordian, Kimmeridgian and Tithonian deposits are well recorded at the chosen localities and dated mainly based on well established ammonite biochronostratigraphy in agreement with the proposed standard zonation for the Western Tethys (Olóriz, 1978; Cariou et al., 1997; Geyssant, 1997; Hantzpergue et al., 1997) and later improvements (e.g., Caracuel et al., 1998; Moliner and Olóriz, 2008).

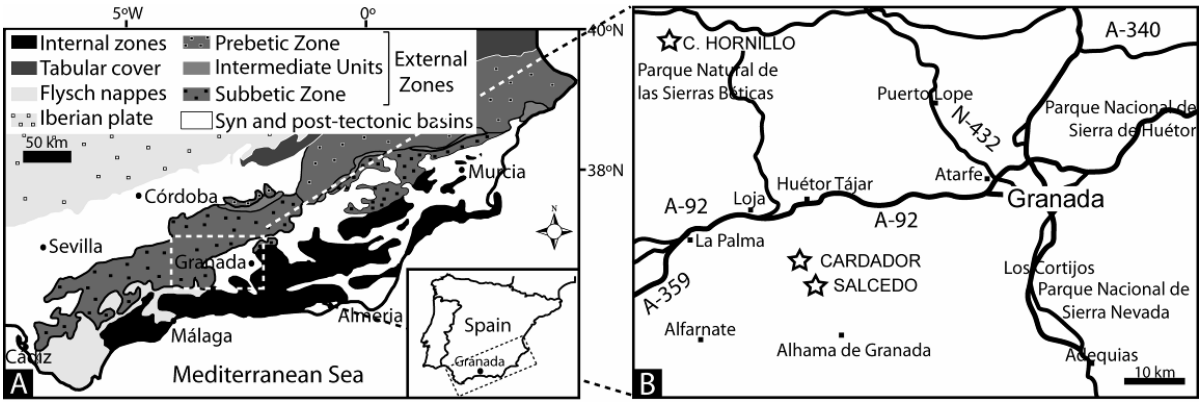

Fig. 2.1- A) Regional distribution of geological units along the Betic Cordillera (modified from García-Hernández et al., 1980). B) Stars for locations of the studied sections.

Three epioceanic sections were investigated. These include the Cardador and Salcedo sections, representative of more distal settings, and the Cañada del Hornillo section, a comparatively landward setting within the epioceanic fringe (Figs. 2.1, 2. 2).

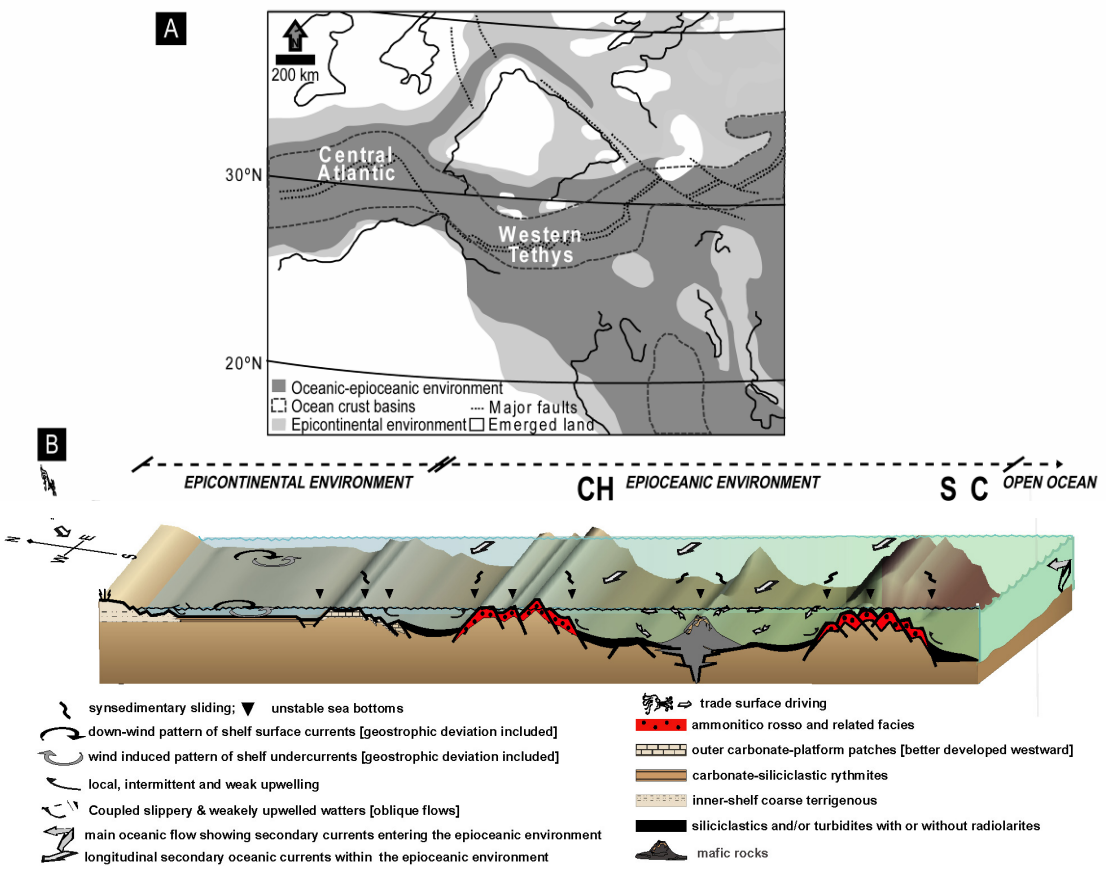

Fig. 2.2- A) Late Jurassic paleogeographic reconstruction of western and central Tethyan realm. Plate tectonic setting from Stampfli and Borel, 2002, and depositional environments after Thierry et al., 2000 a, b.; B) Palinspastic reconstruction of the South Iberian Margin and respective environments during the Late Jurassic (modified from García-Hernández et al., 1980, above, and adapted from Olóriz, 2000, below). Schematic location of sections is indicated (C = Cardador, S = Salcedo and CH = Cañada del Hornillo).

Nodular hemipelagic limestones are dominant (Fig. 2.3 for features identified on the field), interbedded with more or less marly levels. The recurrence of more calcareous banks is a marked feature in the study area, proving useful for correlation. Lateral and vertical colour changes are also a typical feature, ranging from greyish to reddish hues (brown is sometimes also present). Wackestones dominate the microfacies, showing variable content in radiolaria, calcisphaeres, dinoflagellates, plantik crinoids (*Saccoccoma*, mainly Kimmeridgian and Lower Tithonian), unidentifiable forams (plantiks and benthics) other than *Protoglobigerina* (Oxfordian), hyaline tintinnids (Tithonian), ostracods, cephalopods (ammonitella, i.e., embrionic shell of ammonoids), and fragments of juvenile and adult ammonite carcasses), along with broken mollusks, echinoderms (plates and spines), sponge spicules and pelagic

bivalves, among others; but locally, packstone horizons mainly composed by filaments and/or *Sacoccoma* sp. were identified (Caracuel et al., 1996, Olóriz et al., 1995). The Mn-coating of carbonate material occurring at the Salcedo section characterizes the base of the section (Middle Oxfordian).

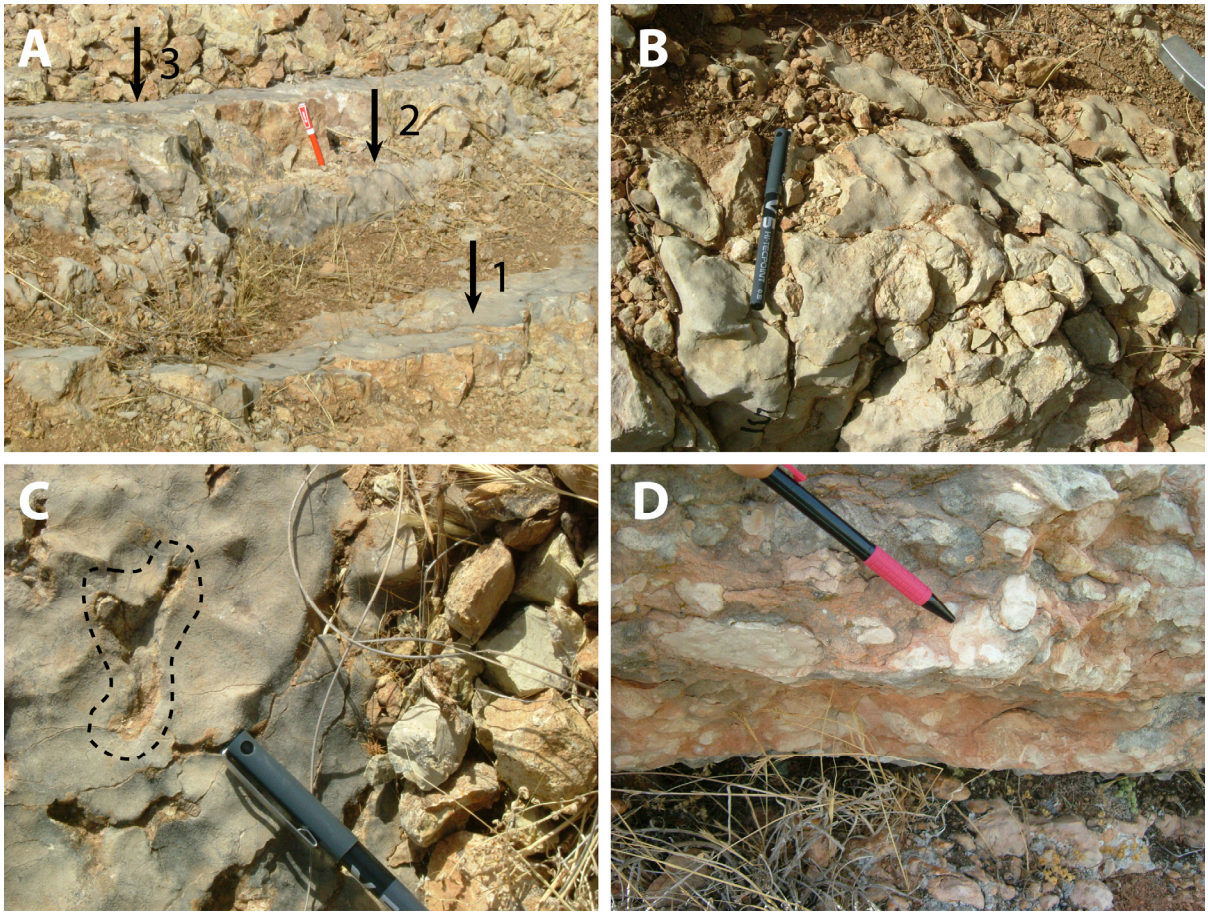

Fig. 2.3- Field close-up views of Upper Jurassic Ammonitico Rosso facies (pens used for scale are about 13 cm long). A) Combined omission-hardground surface labelled 1 marks the Middle/Upper Jurassic boundary; firmground surfaces indicated by 2 and 3 represent transient pauses in sediment deposition most probably related to enhanced current winnowing and relative short-lasting omission; B) Knobby omission surface indicating patchy subaquatic lithification; C) *Thalassinoides* (typical "Y" shape evidenced by a dashed line, indicating the depth of erosion reaching firmground levels); D) Ammonitico Rosso facies displaying variable nodule size and shape.

2.3- Methods (Field Sampling, Laboratory Processing) and Carbonate Materials

2.3.1-Field sampling

The sampling strategy was based on a bed-by-bed investigation of each of the selected sections, resulting in average sampling increases of one sample per 0.3 section meters. Ignoring the occurrence of common hiatuses in these sections, this translates as a time/sample relation of about 360 kyr per sample. Obviously, this overestimation is due to the considerable amount of time contained within omission surfaces (Fig. 2.3A) and diastems. To exemplify, for a time content per sample relation of the order of 180 kyr, 50% of the time duration for the complete section should be captured within omission surfaces. Nevertheless, since hiatuses are below biostratigraphic resolution, and hence cannot be quantified more precisely, these considerations must remain on the level of tentative assumptions. Furthermore, previously published average sedimentation rates between 0.5mm/kyr and 3.7 mm/kyr for other sections in the Subbebtic Zone (Comas et al., 1981; Molina, 1987) are not in agreement with the values suggested here (one sample would represent from 81 to 600 kyr). In addition, mean sedimentation rates depend on the selected geochronological scale and estimated duration of the Late Jurassic (15.7 Myr, according to Gradstein, 2004; Ogg and Przybylski, 2006).

One hundred and twenty-five hand specimens were collected under precise stratigraphic control. From each specimen, two slabs were cut using a diamond saw. One was chosen for macroscopic and optical microscope inspection and the respective mirror slab for geochemical analysis. Where possible, at each level sampled, three different carbonate subsamples were collected. These included (i) fine-grained nodular, micritic limestones; (ii) carbonate cement phases; and (iii) skeletals (mainly belemnite rostra). Drilling sites for subsamples were chosen based on visual inspection of slabs: two to four sites per slab for nodular matrix micrite and, finally, up to three more sites representing other features (inter-nodule micrite, carbonate cements and skeletal material) were chosen.

2.3.2- Laboratory processing

Thin sections were produced from all hand specimens for microfacies analysis. Representative portions of each thin section were photographed digitally under normal light. Using standard software (Adobe® Photoshop® CS2- version 9) the total amount of skeletal

components was estimated based on the pixel count for areas with distinct colour: matrix micrite (brown) and skeletal components (white).

Carbon- and oxygen-isotope analysis of five hundred bulk carbonate powder samples was performed using a ThermoFinnigan MAT delta-S mass spectrometer, (following McCrea's (1950) method) at the facilities of the Institute for Geology, Mineralogy and Geophysics (Ruhr University Bochum, Germany). Reproducibility (±1σ), controlled by NBS19 and internal standards, was better than ±0.08 ‰ and ±0.18 ‰ for, respectively, $\delta^{13}C$ and $\delta^{18}O$. Duplicate samples presented a maximum scatter of ±0.18‰ for $\delta^{13}C$ and ±0.25‰ for $\delta^{18}O$. Isotopic values are reported in the standard δ- notation in per mil (‰) relative to V-PDB.

Aliquots from the sampling material used for isotopic analysis were investigated for their Ca, Mg, Mn, Fe and Sr elemental composition using inductively coupled plasma-atomic emission spectrometry (ICP-AES) at the facilities of the Institute for Geology, Mineralogy and Geophysics at Bochum. Replicate samples presented an analytical precision of ± 2% or less for all these elements.

Cathodoluminescence microscopy was conducted focusing on the overall range of diagenetic features observed in all sections using a HC4-LM (Hot Cathode Luminescence Microscope). Ultrastructure inspection of micrites was performed under Scanning Electron Microscope (SEM) LEO-Gemini 1530 on fresh fractured rock chips of 15 samples. These were mounted at the Center of Scientific Instrumentation of the University of Granada.

2.3.3- Carbonate Materials Analysed

2.3.3.1- Matrix micrite

Ammonitico Rosso micritic limestones are present in their characteristic nodular facies in the investigated sections. Mechanisms of nodule formation have been debated for many years (e.g., Jenkyns, 1974; see below), with the premises for their appearance based on the study of ancient and modern equivalents (e.g., Hollmann, 1962, 1964; Müller and Fabricius, 1974; Mullins et al., 1980; Farinacci and Elmi, 1981 for an overview of diagenetic models; Clari et al., 1984; Clari and Martire, 1996; Martire, 1996). Hypotheses include (i) early, selective seafloor cementation, with precipitation of high-Mg calcite cements directly from seawater; (ii) low sedimentation rate to complete omission; (iii) bottom winnowing; and (iv)

active burrowing, forcing subsurface dissolution of aragonite skeletals (e.g., ammonite shells) as an important carbonate source. All the proposed models agree that nodule formation is a very early diagenetic feature, resulting from the formation of high-Mg calcite cements binding bioclastic micrites. Matrix micrite from the analysed nodular Ammonitico Rosso facies revealed good preservation of carbonate ultrastructure under SEM inspection (Fig. 2.4 C, D and E) and dull luminiscence under cathodoluminiscence microscopy (Fig. 2.4 A and B; Fig. 2.6A and B), both features considered as evidence for minor diagenetic overprint and recrystallization.

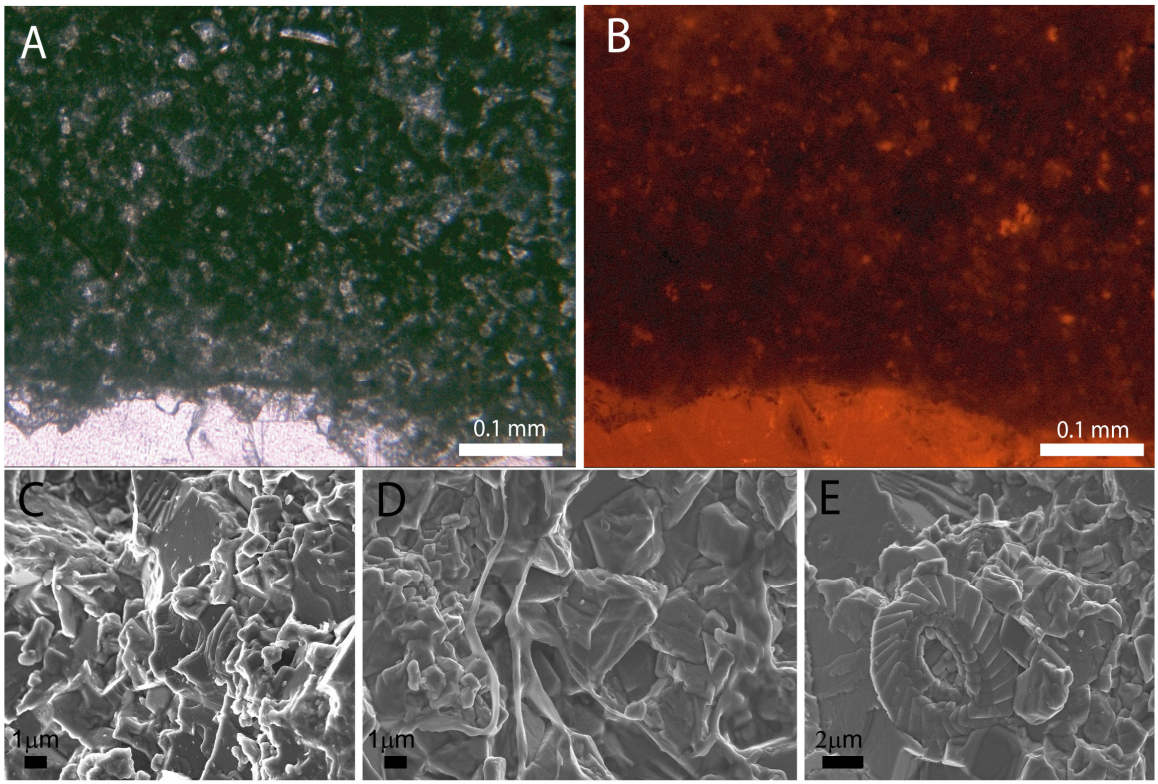

Fig. 2.4- Microscopic images of Ammonitico Rosso matrix micrite. A). Plane polarized light microscopic view of a wackstone; and B) Under cathodoluminescence; C) SEM image of micrite showing angular grains indicating high degree of preservation; D) SEM image of micrite with preserved bacterial and/or algal filaments; E) SEM image of well coccolith indicating well preserved carbonate ultrasctructure.

Based on optical inspection, ca. 80% from a total of about 500 hand-drilled powder samples correspond to homogenous micrite in nodular limestones (Fig. 2.5 A and C). Micrite representing inter-nodule material (Fig. 2.5 B) and burrow infills (Fig. 2.5 F) was likewise

collected in order to assess intra- and inter-nodule and host sediment (lower nodule differentiation) variability.

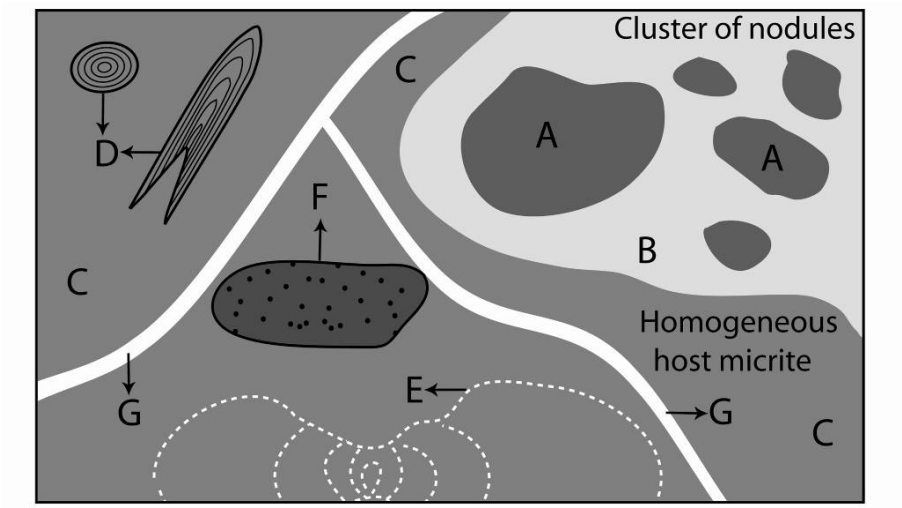

Fig. 2.5- Synthetic overview of carbonate materials sampled for geochemical analysis in Ammonitico Rosso facies. Cut and polished slabs are characterized by locally different staining, from reddish to greyish hues, indicated by variable grey shading in this figure. A) Intra-nodule micrite sample from nodule clusters; B) Inter-nodule micrite sample from nodule clusters; C) Homogeneous sample from host micrite; D) Belemnite rostra (transversal and longitudinal view); E) Ammonite mould with preserved neomorphic shell; F) Burrow infilled by coarser sediment; G) Calcite cement filled vein or fracture.

2.3.3.2- Carbonate cements

Inspection of carbonate cements under cathodoluminescence is a standard procedure for the assessment of diagenetic history. Distinctive cement phases can be differentiated by their degree of luminescence, which is ultimately related to the presence of the main activator – Mn^{2+}– and quenchers – Fe^{2+} or lattice defects (Fairchild, 1983; Marshall, 1988; Machel and Burton, 1991; Machel et al., 1991; Bruckschen and Richter, 1994). Although in-depth discussion of diagenetic evolution in the studied material is not the objective of this paper, general features are presented (Fig. 2.6) in view of their significance for the interpretation of the geochemical data obtained.

Veins and cement-filled fractures (Fig. 2.5 G) are relatively uncommon among the examined hand specimens. Where present, samples were drilled for isotope and elemental analysis and some samples chosen for further analysis under cathodoluminescence. All features display a directly comparable luminescence pattern (Fig. 2.6) indicative of a similar

diagenetic history. On the whole, cement-filled voids and veins are characterized by the presence of three cement generations. These include (i) a non-luminescent scalenohedral calcite phase (Fig. 2.6 B1), rimmed by (ii) a very bright orange phase (Fig. 2.6 B2), and (iii) dull luminiscent blocky calcites in the central parts of veins and cavities (Fig. 2.6 B3).

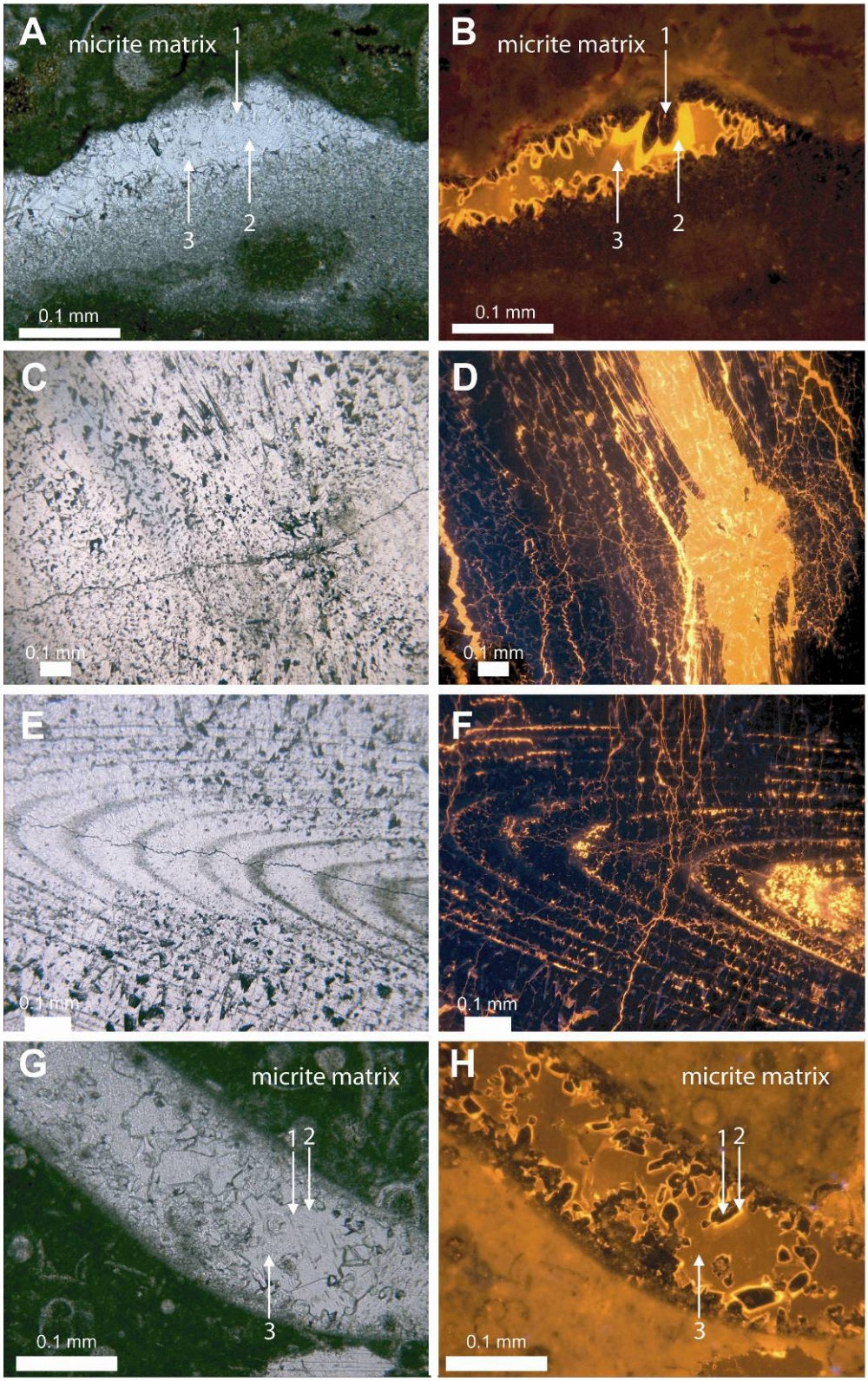

Fig. 2.6- Cathodoluminiscence images of matrix micrite, carbonate cements and skeletals. A) Carbonate cement filled void in matrix micrite (see text for description of cement phases 1 to 3); B) Same area under cathodoluminescence; C) Belemnite rostra in transversal cut, plane light; and D) Under

cathodoluminescence (note bright orange fractures); E) Belemenite rostra in tangent longitudinal cut, note growth increments; and F) Under cathodoluminescence (note bright orange between growth increments); G) Neomorphic ammonite shell with secondary calcite cement; and H) Under cathodoluminescence. Secondary calcite showing identical paragenetic phases as indicated in B).

2.3.3.3- Skeletal material

Most attempts to reconstruct Jurassic seawater properties use low-Mg belemnite rostra as archives in hemipelagites (Veizer, 1974). It has been proposed that oxygen-isotope data from well preserved rostra render reliable palaeotemperature estimations (Price and Sellwood, 1994; Saelen et al., 1996; Podlaha et al., 1998; Jenkyns, 2002; Wierzbowski, 2002; Rosales et al., 2004). The few belemnites (n = 6) found in the hand specimens (Fig. 2.5 D) collected at all three study sites were investigated under-cathodoluminiscence, and samples were drilled for geochemical analysis. Judging from the luminescence patterns observed, most rostra experienced a singificant diagenetic overprint including veining and alternating bright orange and dull luminescent laminae (Fig. 2.6 C to F).

Ammonite shells are characterized by a primary aragonite mineralogy stabilized to low-Mg calcite during diagenesis (e.g., Veizer, 1983; Ditchfield et al., 1994; Lécuyer and Bucher, 2006). In the studied sections, the complete dissolution of aragonite is a common feature resulting in the occurrence of frequent inner moulds. Preservation of neomorphic calcite of formerly aragonitic ammonite shells is uncommon in these sections. One example was found and investigated under cathodoluminescence (Fig. 2.6 G and H). The diagenetic phases observed are directly comparable to those of cement-filled voids or veins (Fig. 2.6 A and B).

2.4- Results of Stable Isotope and Trace and Minor Element Analysis

2.4.1- Carbon-isotope data

At all the sections studied, matrix values show values ranging from 1.1 to 3.3‰ (mean = 2.0‰; standard deviation (*s*) = 0.4‰) and likewise similar stratigraphic trends (Fig. 2.7). Carbon-isotope data increase from 2.4‰ at the base of the Oxfordian stratigraphic record to 3.3‰ during the Middle Oxfordian. Following a rather sharp 1‰_shift to lower values,

isotope maxima of 2.7‰ are present during the Late Oxfordian (a feature not recognized in the Salcedo section chemostratigraphy). The Kimmeridgian record has an overall decreasing trend that persists throughout most of the Tithonian, only to be interrupted during the Late Tithonian by a positive shift of the order of about 0.2‰. Thereafter, the isotope curve maintains the overall decreasing trend towards the Jurassic/Cretaceous boundary, reaching values of 1.5 ‰.

Inter-nodule areas showing differential packing degree of skeketals display very distinct aspects, depending on the stratigraphic level considered. Nevertheless, carbon-isotope data do not respond to these differences, nor to micrite colour or grain size, and range from 1.1 to 3.3 ‰ in all the studied features. Carbonate cements have $\delta^{13}C$ values similar to those obtained from matrix micrites (Fig. 2.9). Skeletal material presents a wider range in $\delta^{13}C$. In general, belemnite data are lower compared to micrite and cement data (values between 0.7 and 1.8‰). Some belemnite data points fall within the overall range of matrix data of their respective section (Fig. 2.9). When compared to matrix $\delta^{13}C$ obtained from the belemnite host micrite, however, carbon-isotope values are lower by about 1‰. Blocky cement samples in the inner mould of a replaced ammonite shell ($\delta^{13}C$ = 1.8‰) are, like belemnites, about 0.5‰ lower than the host matrix.

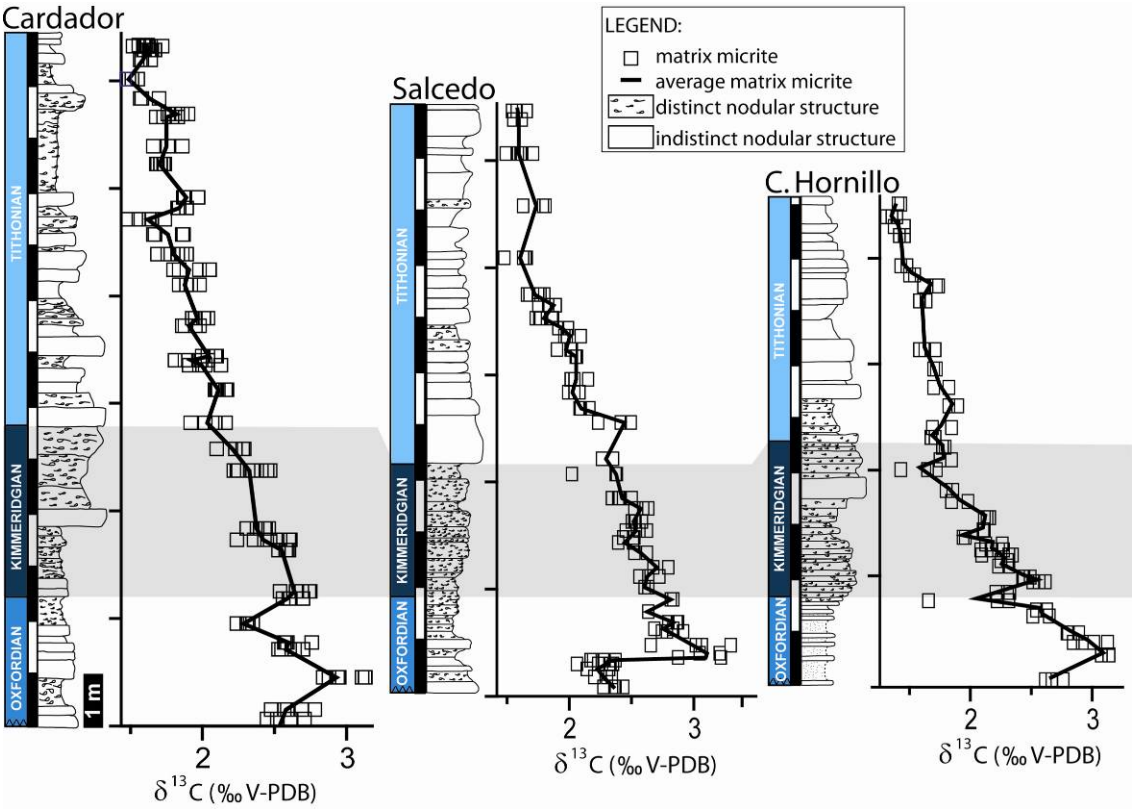

Fig. 2.7- Matrix micrite $\delta^{13}C$ stratigraphy from the Upper Jurassic sections studied. See overall post-Oxfordian decreasing isotope trend in all sections. Intra-sample isotopic variability is indicated for each investigated horizon. Line indicates the mean value of all subsamples for each hand specimen. Key to symbols for different lithologies is indicated.

2.4.2- Oxygen-isotope data

Oxygen-isotope data from micrite samples fluctuate between -2.0 and +0.9‰ (Fig. 2.8). The more seawards and nearby Cardador and Salcedo sections present a similar range (-0.3 to 0.9‰; mean values = 0.3‰; *s* = 0.2‰ and 0.1‰; *s* = 0.6‰, respectively). In contrast, the comparative landward and separate Cañada del Hornillo section is characterized by overall lower values ranging from -1.8 to 0.4‰ (mean value = -0.8‰; *s* = 0.6‰). Despite these differences in absolute values, a similar stratigraphic trend in $\delta^{18}O$ is observed in the three studied sections. Rather stable background isotope ratios of around 0‰ in the Cardador and Salcedo sections and of about -1‰ in the Cañada del Hornillo section dominate the Upper Jurassic record. These are followed by more positive values across the Middle Oxfordian, at the Kimmeridgian/Tithonian boundary and during the Late Tithonian.

As a non-quantitative assessment of potential diagenetic micrite alteration, palaeo-temperature estimates were calculated from oxygen-isotope values. Applying the equation of Anderson and Arthur (1983) to mean $\delta^{18}O$ values from each section and assuming $\delta_{seawater}$ of between -1 and +0.5 ‰ SMOW (Shackleton and Kennett, 1975), the following results were obtained: 11-17ºC for the Cardador section, 12-18ºC for the Salcedo section and 15-22ºC for the Cañada del Hornillo section. Acknowledging the fact that paleo-temperature estimates based on micrite $\delta^{18}O$ are commonly ambiguous, the results obtained for Cardador and the Salcedo sections are in agreement with values reported by other authors (e.g., Price and Sellwood, 1994).

Inter-nodule micrite and cavity infill $\delta^{18}O$ values do not differ significantly from nodular matrix micrite values, with intra-sample scattering below intersample isotopic differences. Carbonate cements are generally lower in $\delta^{18}O$ as compared to micrite values (Fig. 2.9). The cement phases sampled show minimum values of about -2.7‰ in the Cardador section (mean = -1.4, *s* = 1.1), about -1.8‰ in the Salcedo section (mean = -1.0, *s* = 0.6) and lower values of -5.9‰ in the Cañada del Hornillo section (mean = -2.6, *s*= 1.6).

Oxygen-isotope data from belemnites range from -3.9 to 0.0‰ (mean = -1.0, *s* = 1.3‰) and are thus more depleted than the matrix micrite $\delta^{18}O$ obtained from host micrites. One exception to this pattern is found in a belemnite rostrum retrieved from the Cañada del Hornillo section. Here, values of -0.1 and -0.6‰ overlap with those of the host micrite. The blocky cement filling the ammonite shell mould has $\delta^{18}O$ ratios of -1.1‰, again more depleted than the host matrix micrite.

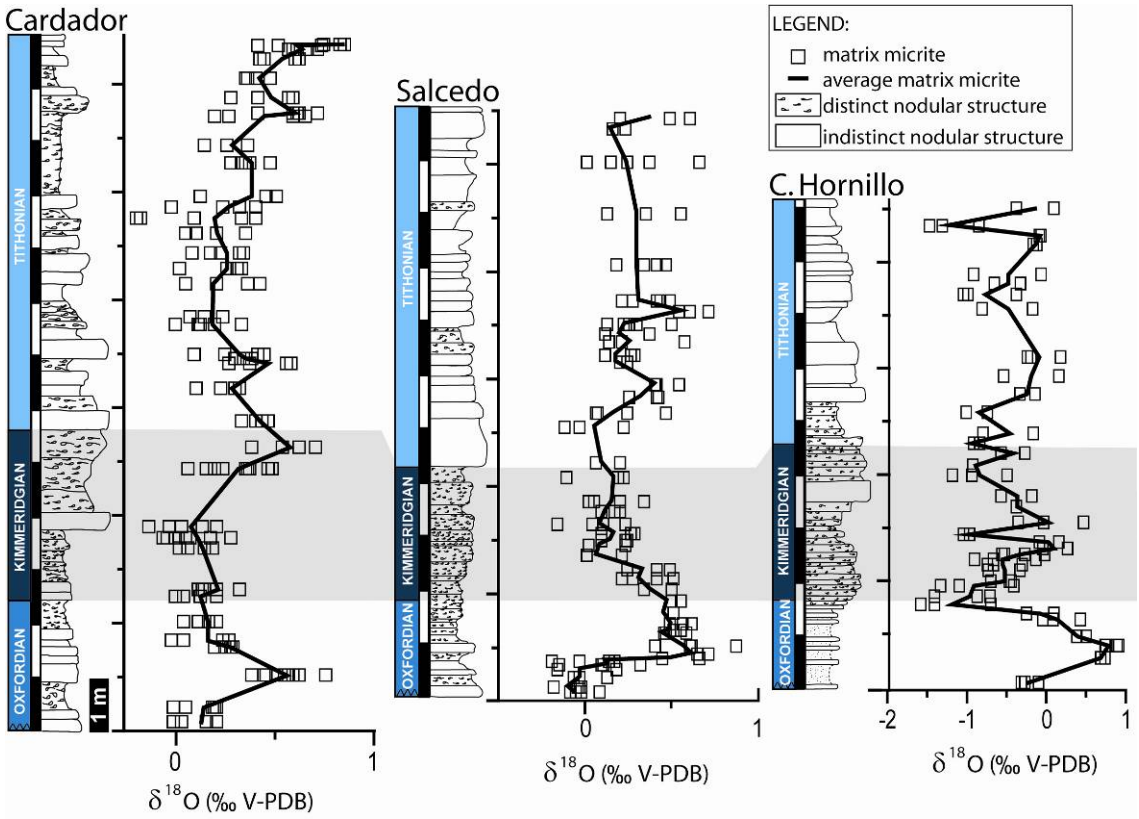

Fig. 2.8- Matrix micrite $\delta^{18}O$ stratigraphy from the studied Upper Jurassic sections. Intra-sample isotopic variability is indicated for each investigated horizon. Line indicates subsample meanvalue for each hand specimen. Key to symbols for different lithologies is indicated.

2.4.3- Patterns in $\delta^{13}C$ versus $\delta^{18}O$

A scatter diagram including isotope data from all carbonate materials analyzed is shown in Fig. 2.9. Three different clusters of data can be established. These include what we here term cluster 1, representing matrix micrite values for the Cardador and Salcedo sections with the sections overlapping in isotope scatter and range. Cluster 2 comprises data from the Cañada del Hornillo section. Overall, carbon-isotope values of cluster 2 are very similar to those of cluster 1, while the oxygen-isotope data are more depleted in this case. Cluster 3, in turn, lumps the carbonate cements and skeletal materials analyzed. The overall pattern in $\delta^{13}C$ from skeletals departs from that of micrite material, whereas cement data plot within micrite range. Cluster 3 shows more variable $\delta^{18}O$ values, ranging from slightly more negative than micrites to considerably more depleted values, the latter corresponding to carbonate cements.

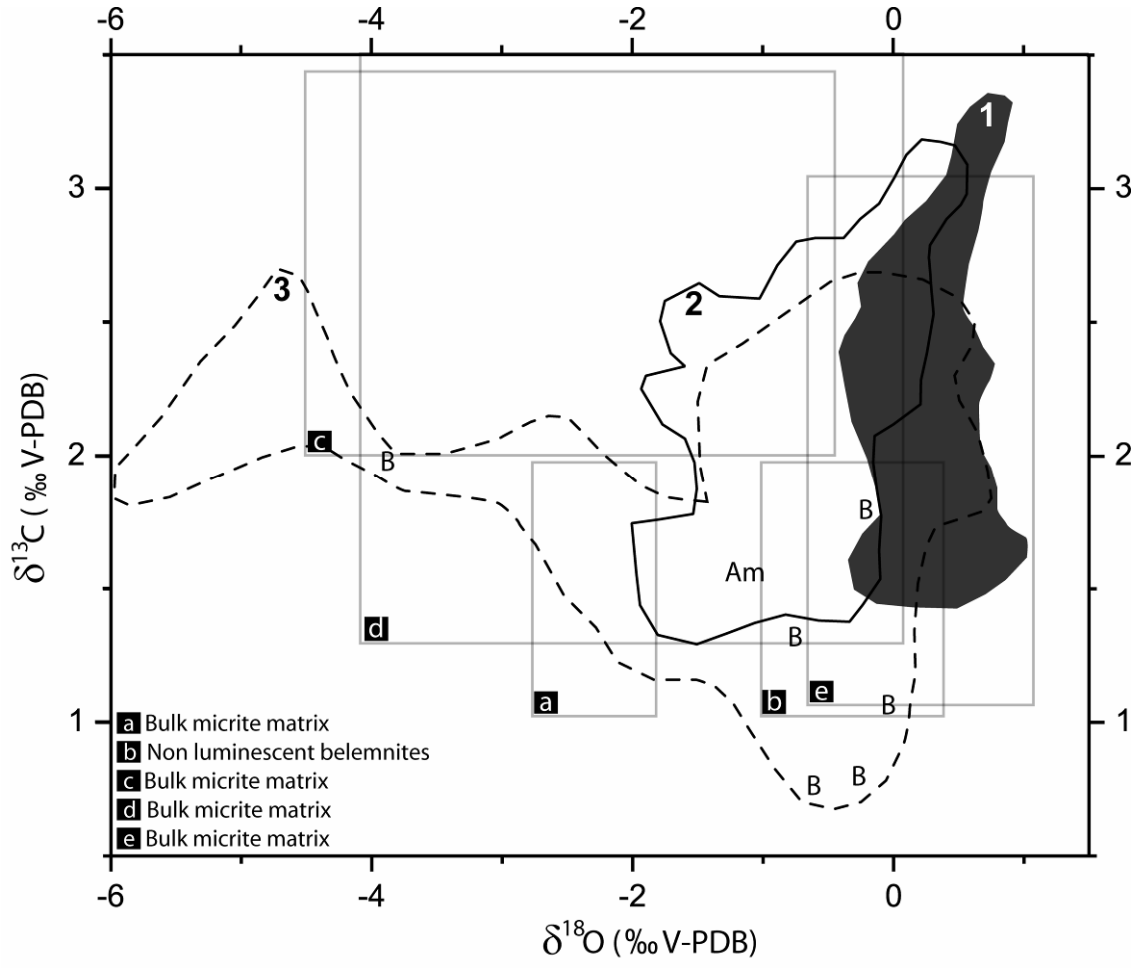

Fig. 2.9- Crossplot including all isotope data from the investigated sections. Cluster 1 combines all micrite data from Cardador and Salcedo sections and cluster 2 comprises micrite data from the Cañada del Hornillo section. Cluster 3 delineates data from the carbonate cement phases sampled. Neomorphic ammonite shell (Am) and belemnite rostra (B). Squares labelled a) to e) indicate ranges of Ammonitico Rosso isotope data according to: (a, b) Price and Sellwood (1994); Mallorca, Spain; (c) Préat et al. (2005); Trento Plateau, Italy; (d) Rey and Delgado (2002); Betic Cordillera, Spain; (e) Cecca et al. (2001); Monte Inici, Italy.

2.4.4- Intra-nodule isotopic variability

Individual nodules from the Lower Kimmeridgian Cardador and Salcedo sections (Fig. 2.10) were tested for their intra-sample isotopic variability. Results of two transects crossing from nodule margins through nodule centres to the opposite margins are characterized by very low intra-sample geochemical variability (< 0.3‰; average sample spacing of 5 mm; Fig.

2.10). Results are well correlated with positive and statistically significant parameters (r = 0.6 for $\delta^{13}C‰$ and 0.9 for $\delta^{18}O‰$ for a nodule from the Cardador section and r = 0.4 for $\delta^{13}C‰$ and 0.5 for $\delta^{18}O‰$ for a nodule from the Salcedo section).

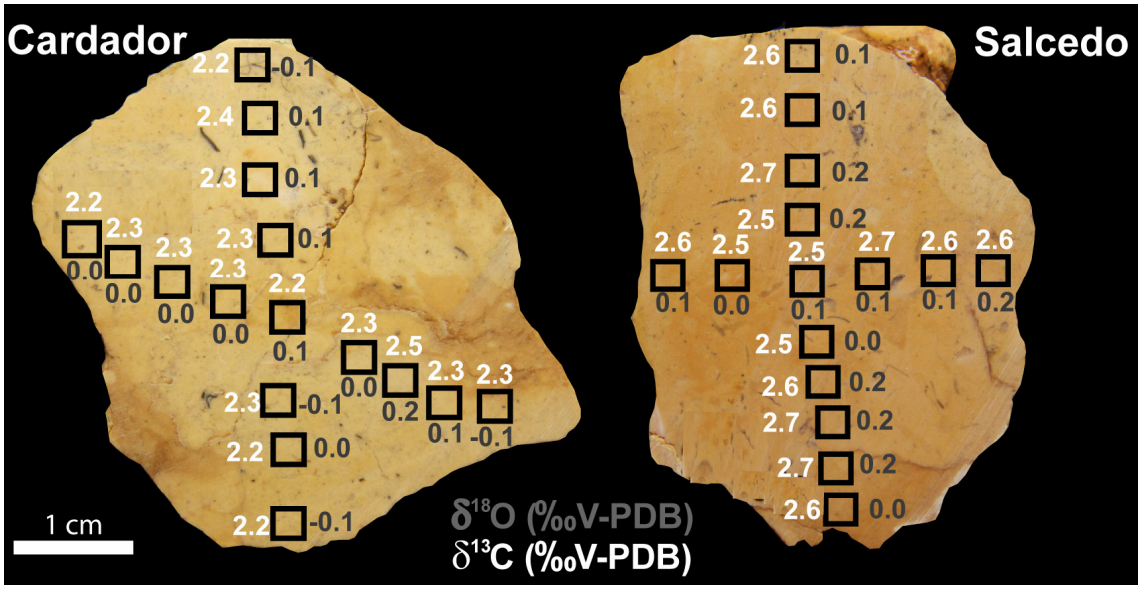

Fig. 2.10- Intra-nodule isotopic variability for representative cases from the Salcedo and Cardador sections. White numerals refer to carbon- and black numerals to oxygen-isotope data.

2.4.5- Trace elements

Elemental data obtained from micrite samples collected from Cardador, Salcedo and Cañada del Hornillo sections were investigated in order to evaluate potential spatial trends in relative values. Given the fact that micrites do not represent pure carbonates, and that samples were filtered prior to ICP-OES analysis, only relative values and shifts should be considered, as opposed to absolute values obtained for example from low-Mg calcite bivalves (Veizer, 1983; Klein et al., 1996a; Van der Putten et al., 2000). One of the remarkable features of the elemental stratigraphy is the identification of several pronounced Mn peaks recorded on the three sections, yet only identifiable as Mn-enriched horizonts in the Salcedo section. In line with previous work, a likely interpretation would invoke Mn derived from submarine hydrothermal activity (e.g. Kickmaier and Peters, 1990; Corbin et al., 2000) most probably related to the carbonate deposition crisis across the Middle/Late Jurassic transition (e.g., Wierzbowski, 2002). Assuming reactivated bottom physiography, hydrodynamic effects should be not ruled out.

2.5- Interpretation

2.5.1- Carbon-isotopes

Evidence for subaerial exposure and the influx of isotopically light soil-zone CO_2 (Allan and Matthews, 1982) is neither expected in these epiocenanic settings, nor supported by the data. Furthermore, field evidence for subaerial exposure of the carbonate seafloor (references in Immenhauser et al., 2008) is lacking. Matrix micrite $\delta^{13}C$ isotope ratios obtained reveal a consistency of data overall. This may or may not indicate that the carbon isotopic record has preserved its original signal, the second option suggesting a pervasive late diagenetic resetting resulting in geochemically homogenized samples. This interpretation is rejected, however, given the rather high values of these samples and, especially, the overall stratigraphic trend, in good agreement with previous data reported from other localities. The main $\delta^{13}C$ pattern observed, and the absolute values measured in all three sections (Cardador, Salcedo and Cañada del Hornillo), have also been reported from different Upper Jurassic localities along the north Tethyan European margin (e.g., Bartolini et al., 1999, central Italy; Jenkyns, 1996, central and southern Europe; Weissert and Mohr, 1996, overall Tethys review and Atlantic comparison; Joachimski, 1994, Jura Mountains). This is taken here as evidence that the studied sections recorded a Tethys-wide (and beyond) pattern in seawater $\delta^{13}C_{DIC}$ that is largely preserved to the present.

Such a notion obviously would not exclude some degree of diagenetic alteration; but commonly, the source of diagenetic carbonate precipitated as secondary phases is the host carbonate itself (Hudson, 1975). Although there may be no such thing as a closed system in nature, the overall geochemical pattern suggests a diagenetic system that mainly recycled $\delta^{13}C$ (sensu Veizer, 1983), a rather common feature conferring robustness to interpretations based on $\delta^{13}C$ values (e.g., Hudson, 1977; Dickson and Coleman, 1980; Marshal, 1992). Further supportive evidence is the fact that the late carbonate cement phases measured follow the same stratigraphical trend and overlap in terms of absolute values as those obtained for matrix micrite. This finding is significant in that bright luminescent phases are commonly considered to form under anoxic burial conditions.

Interestingly, skeletal components such as belemnites and a replaced, neomorphic ammonite shell are characterized by overall lower $\delta^{13}C$ values as compared to other analysed

carbonate materials. It may be that matrix micrites stabilized during a relatively early diagenetic stage, while skeletal components still underwent diagenetic alteration under deeper burial conditions. Late diagenetic fluids are commonly ^{13}C depleted relative to matrix carbonates, with low isotopic compositions often derived from the breakdown of organic material at depth. This would counter the often-cited notion of primary low-Mg shell hardparts being more reliable archives of past environmental conditions than instable matrix micrites, at least for the case examples investigated here.

2.5.2- Oxygen isotopes

Matrix micrite oxygen-isotope values are conspicuously higher than those reported by other authors for comparable depositional environments and time intervals (Pisera et al., 1992; Leinfelder et al., 1993; Price and Sellwood, 1994; Veizer et al., 1999; Bartolini et al., 2003; Préat et al., 2006). Oxygen-isotope values between -0.3 to 0.9‰, as measured from the Cardador and Salcedo matrix micrites, are uncommon in the literature. It is noteworthy that the few exceptions found include some Ammonitico Rosso-type examples (Cecca et al., 2001). Similarly elevated values are usually reported from well preserved low-Mg calcite materials, such as belemnite rostra (e.g. Price and Sellwood, 1994), i.e. the materials that undergo more pervasive alteration in the Subbetic sections investigated.

Mechanisms that result in ^{18}O enriched carbonate samples include seawater evaporation, as commonly seen in very shallow inner platform settings (Kievman, 1998; Immenhauser et al., 2002), which in general terms could be considered more similar to the ramp setting reported by (Wu and Chafetz, 2002) than the epioceanic settings here investigated. In fact, burial fluids, due to the commonly elevated temperatures of brines, tend to shift diagenetic calcites towards ^{18}O-depleted values as opposed to the ^{18}O-enriched ones found here. Similarly, sub-seafloor freshwater lenses, extending into marine basins have been reported from shallower settings to result in diagenetic alteration of $\delta^{18}O$ (Wu and Chafetz, 2002). Whereas the later interpretation has been proposed for a hemi-pelagic carbonate ramp setting, the stratigraphically condensed Ammonitico Rosso-type limestones investigated here were deposited on epioceanic topographic highs. This setting and the absence of porous facies, whatever their relative stratigraphic position, are able to evidence an absolutely distinct environmental scenario excluding the application of the interpretative model proposed by Wu

and Chafetz, (2002). Considering these arguments, it is suggested that the oxygen-isotope data presented in this study largely reflect the isotopic composition of the marine porewater in which early marine patchy lithification forced nodule formation.

Skeletal material $\delta^{18}O$ ratios vary more with respect to micrites, suggesting the influence of several stages of diagenetic alteration, with the most ^{18}O-depleted hardparts being the most affected. The lowest $\delta^{18}O_{skeletal\ material}$ are within the same range as the carbonate cement phases which, due to their bright luminescence and petrography, are considered to represent later burial stages.

Optical features point to a fair preservation of the studied material, consistent with the interpretation of near-pristine carbon and oxygen-isotope values. Overall, the carbonate ultrastructure of micritic material is well preserved (Fig. 2.4), as attested by the occurrence of filaments of boring algae (Jenkyns, 1971) or bacterial remains (Préat et al., 2006) and coccoliths. Early stabilization of carbonate matrix micrite is envisaged to be able to preserve these structures. The degree of preservation of coccoliths reinforces this interpretation, because micron-sized particles are especially prone to selective dissolution (Jenkyns, 1974). Furthermore, matrix micrite shows dull luminescence (as opposed to the bright luminescence often observed in micritic carbonate), indicative of limited diagenetic overprint. All the above attests to a good preservation state of the studied material.

2.6- Discussion

2.6.1- Paleoenvironmental parameters and matrix micrite geochemistry

The overall low degree of diagenetic overprint demonstrated for marine isotope data retrieved from Jurassic Ammonitico Rosso requires the discussion of two main issues: (i) The mechanisms responsible for the uncommonly low degree of diagenetic alteration of carbon, and more remarkably, of oxygen-isotope data; and (ii) the paleo-environmental significance of the major isotope shifts observed. The second issue is dealt with first, as its assessment is more straightforward.

2.6.2- Shifts in Upper Jurassic seawater $\delta^{13}C_{DIC}$: eustasy, nutrient levels and carbonate production

Unbiased carbon isotopes reflect changes in the balance of the different reservoirs of the carbon cycle (Berger and Vincent, 1986; de Boer, 1986; Weissert and Mohr, 1996), and more specifically, relative variations in the organic/inorganic carbon burial rates and differences between platform and basinal archives (Jenkyns, 1995; Ferreri et al., 1997; Swart and Eberli, 2005; Parente et al., 2007). The Upper Jurassic sections investigated are considered to reflect these parameters.

It has been suggested that a major mid-Oxfordian transgression is reflected in an overall positive trend in seawater $\delta^{13}C_{DIC}$ (e.g., Hoffman et al., 1991; Jenkyns, 1996; Weissert and Mohr, 1996; Bartolini et al., 1996, 1999; Colacichi et al., 2000), yet their direct cause-effect relationship has only recently been discussed (e.g., Pearce et al., 2005). As in previous studies of other epioceanic and epicontinental Tethyan areas (Bartolini et al., 1999; Cecca et al., 2001; Rey and Delgado 2002; Savary et al., 2003; Rais et al., 2007), $\delta^{13}C_{micrite}$ values in the Cardador, Salcedo and Cañada del Hornillo sections are seen to reflect this feature, reaching maximum values of around 3‰ (Fig. 2.7). The mid-Oxfordian transgressive event enhanced continental weathering during a phase of global warming (Bartolini et al., 1996; Colacichi et al., 2000; Wierzbowski, 2002), which resulted in increased nutrient levels forcing marine productivity, i.e. organic carbon production. Through biotic fixation of the lighter carbon isotope (^{12}C), and its increased burial on the sea bottom, the oceanic carbon pool was enriched in ^{13}C. This is reflected as the carbon isotope positive shift.

During the Kimmeridgian the sea levels rose globally. Superimposed on this long-term trend, short-term oscillations in relative sea level took place. Transgressive pulses are assumed to have enhanced marine productivity, as occurred during the comparatively major Mid-Oxfordian trangression, but no record of these events is preserved on the carbon isotope curve. The global enhancing of organic mater burial rates was probably buffered by a renewed growth of carbonate platforms that accompanied sea-level rise during Kimmeridgian times (e.g., Weissert and Mohr, 1996). A higher production rate of inorganic carbon provided a sink for ^{13}C, resulting in the stabilization of the C_{org}/C_{inorg} burial rate, which is reflected in the Tethyan carbon isotope record as a relatively stable phase. In light of previous research and published interpretations of the mid-late Upper Jurassic carbon-isotope record in other Tethyan sections, the decreasing $\delta^{13}C$ in the three Subbetic sections studied is in good agreement with what is generally considered the 'global' signature of seawater $\delta^{13}C_{DIC}$.

Throughout the Kimmeridgian and Tithonian series, an overall decreasing trend is recorded in the Subbetic sections studied. The shift in $\delta^{13}C$ to values beneath +1.5‰ reflected in the Cardador, Salcedo and Cañada del Hornillo sections during the late Tithonian is recognized in other Tethyan sections and the Atlantic realm as well (Weissert and Mohr, 1996), and is thus considered to constitute a provincial (at least) trend in nature, affecting both the intertropical western Tethys and the so-called Hispanic Corridor in the central North-Atlantic Basin. According to Weissert and Mohr (1996), the proposed reorganization of the global climatic system during Jurassic-Cretaceous boundary times was responsible for this feature. In particular, it has been hypothesized that the Jurassic monsoonal rainfall pattern gave way to increasingly zonal climate conditions during the earliest Cretaceous, thereby affecting carbonate-shelf dynamics (Weissert and Mohr, 1996).

In conclusion, the $\delta^{13}C_{micrite}$ record obtained from the Subbetic sections investigated would match that established for other Tethyan and Atlantic sections. The obtained $\delta^{13}C_{micrite}$ record may be best understood in the context of changes in the sea-level and climate coupled system, and resulting changes in seawater nutrient levels and carbonate production rates, as usually interpreted.

2.6.3- Sedimentation rate, porewater pumping and early marine lithification cause preservation of Jurassic seawater $\delta^{18}O$ ratios

Oxygen-isotope data from carbonate micrite archives are commonly affected by factors that include seawater temperature and salinity, changes in the ice-meltwater ratio and the primary mineralogy of the carbonate ooze. Once embedded in the sediment-water interphase and thus exposed to processes such as dissolution of metastable carbonate materials (aragonite) and/or loss of Mg (high-Mg calcite), the transformation to thermodynamically stable low-Mg calcites takes place (Veizer, 1983; Marshal, 1992). In the sediment-water interphase, mainly porewater geochemical properties – in turn controlled by factors such as porewater temperature and salinity, and the source of the diagenetic oxygen – control the isotopic composition of the secondary cement phases precipitated (Walls et al., 1979; Carpenter et al., 1991). It has been argued that the overall ^{18}O-enriched Ammonitico Rosso micrite isotope ratios from Southern Spain, and their comparison with well constrained data sets from other localities (Cecca, 2001) rule out a significant diagenetic alteration.

Likewise, porewater with elevated salinity, perhaps derived from surface seawater evaporation on shelves and subsequent basinward transport of density currents, can be ruled out as a factor controlling the oxygen-isotope record, for two reasons: (i) the paleo-geographic location of the studied sections on structural highs within the epioceanic environment, submitted to water depths of many tens of meters, renders the potential influence of platform-derived brines unlikely; and (ii) major changes in seawater salinity are expected to affect benthic communities in a significant manner. Relevant in this sense is the lack of evidence for faunal changes related to changing salinity levels, as demonstrated by previous research in the area (Olóriz 2000). Therefore, the process/factor interpretation can be focused on porewater temperature, which, close to the seafloor, is mainly controlled by the ambient seawater temperature.

Previous authors have attempted to assess Oxfordian, Kimmeridgian and Tithonian seawater paleo-temperature data based on well-preserved belemnite $\delta^{18}O$. From northern areas (England, Poland), seawater temperatures between 11ºC and 13ºC have been proposed for Oxfordian times with a Mid-Oxfordian peak of 26.7ºC (e.g., Longinelli et al., 2003), and an Early-Mid Oxfordian average temperature of 12ºC has been proposed for Central Poland, together with a slight incrase to 14.3ºC during Mid-Late Oxfordian times (Wierzbowski, 2002). Moreover, seawater temperature in Germany has been interpreted to fluctuate between 15.6-17^{o}C and 12-20^{o}C during Early to Late Kimmeridgian times, respectively (e.g., Bowen, 1961; and references in Price and Sellwood, 1994). Further northwards, in the Russian platform domain, lower seawater temperatures of 10-12ºC have been estimated for Late Kimmeridgian-Volgian times (Bowen, 1961; in Price and Sellwood, 1994). Price and Sellwood (1994) present well-preserved belemnites from Upper Jurassic Ammonitico Rosso facies exposed on the island of Mallorca that might reflect seawater paleo-temperatures between 13ºC and 16ºC for Kimmeridgian and Tithonian times. Applying the temperature equation of Anderson and Arthur (1983) to the $\delta^{18}O$ micrite data obtained here reveals a temperature range similar to that given by Price and Sellwood (1994). While acknowledging the limitations of such an approach, this observation is held as evidence for early lithification (i.e., early fossil diagenetic rather than biostratinomic phase) under the influence of marine porewater conditions.

In view of previous research on nodule formation of in Ammonitico Rosso facies, early marine dissolution of mainly aragonitic carbonates and subsequent reprecipitation,

causing lithification and hence nodule formation, must be considered. Factors that control early marine nodular lithification of micritic carbonates include physical (submarine winnowing of the carbonate seafloor), biological (alteration of sediment properties by burrowing) and chemical processes (selective, local dissolution and cementation; e.g., Jenkyns, 1974; Müller and Fabricius, 1974; Mullins et al., 1980; Clari et al., 1984; Clari and Martire, 1996). The reconstruction of accurate paleoceanographic conditions for the three study sites is hampered by only limited knowledge of Jurassic ocean dynamics, particularly when small regional sites are under consideration. Despite such limitations, physico-chemical factors affecting present-day guyot tops and open ocean seamounts might serve as a useful starting point for approaching processes potentially forcing the data observed (Fig. 2.11 for conceptual overview of mechanisms relevant for the interpretation of the obtained data set).

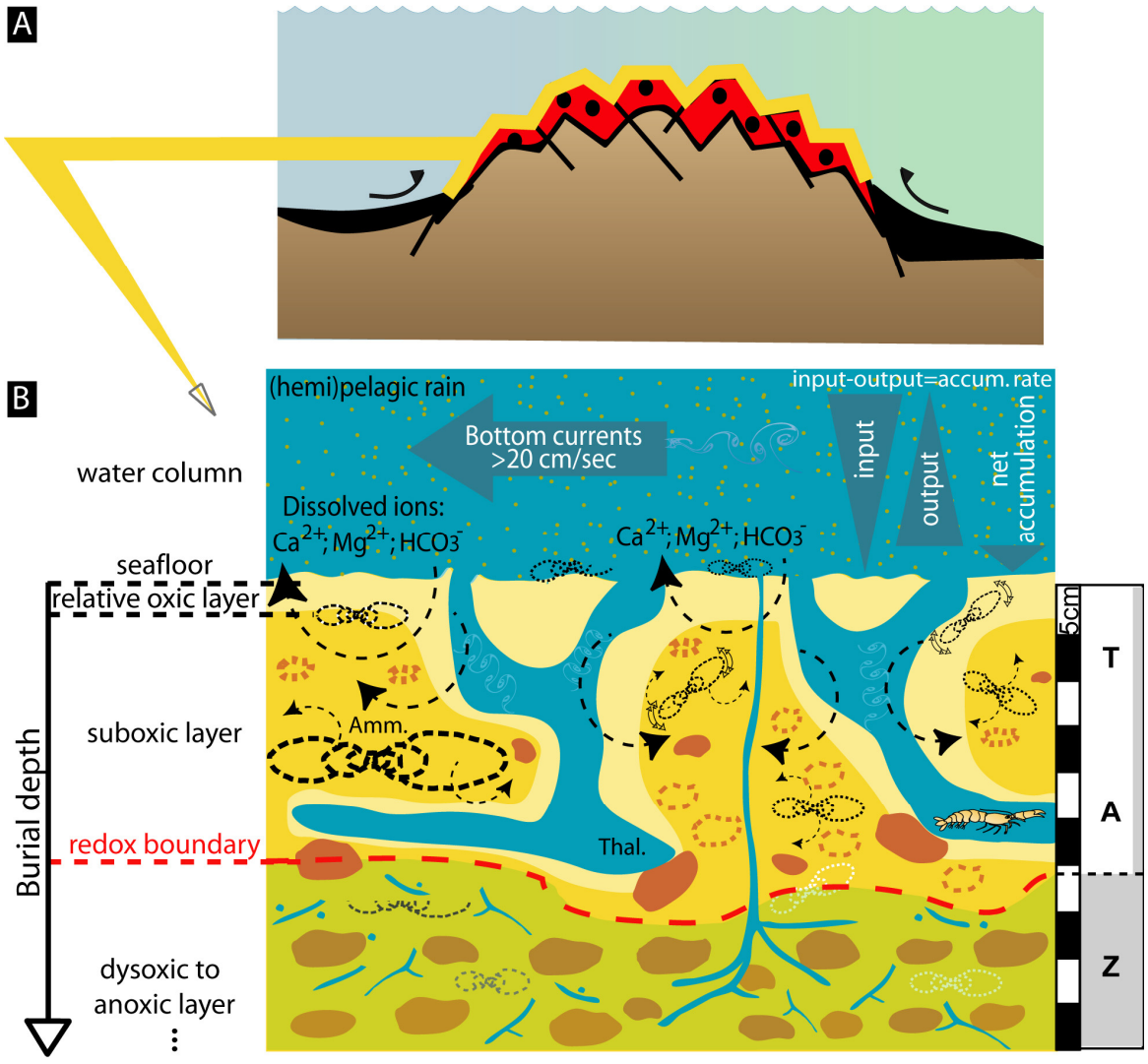

Fig. 2.11- Conceptual template for mechanisms significant for combined nodule formation and high degree of preservation of near-primary isotope signals in the Ammonitico Rosso sections investigated. A.) Hypothetical location of section on epioceanic swell area. B.) Cartoon showing processes relevant at the seawater – sediment interphase including out-side effect (pelagic-hemipelagic rain and currents) and in-side effects (dissolved ions in seawater, and burrowing where *Thalassinoides* is relevant, but not exclusive). Within substract oxygen stratification indicated to the left and relative sediment cohesion within the Taphonomically Active Zone (TAZ) to the right. Diagenetic stabilization and incipient microenvironmental differentiation (incipient nodulation) of matrix micrite takes place in the marine porewater zone close to the sediment – seawater interface. In contrast, cement precipitation and skeletal alteration occurs in deeper within the TAZ and the upper historical layer (not represented). In the right column note both grey bar for sediment cohesion and geochemically more active marine porewater above the dashed line.

2.6.4- Sedimentation rates and porewater stabilization of micritic carbonates on present-day guyots and seamounts

Topographically elevated localities in the oceanic-epiocenic domain are often sites of increased current intensity due to the interaction of the bottom currents with local topography. Lateral and circular vertical flows are commonly observed in the vicinity of subaquatic topographic highs (Hernández-Molina et al., 2006 and references therein), and enhanced currents are a common feature of isolated, open oceanic seamounts (e.g., Beckman and Mohn, 2002). Specifically, enhancement of current velocities over and near seamount-like structures and guyots is due to deflection mechanisms. From a longer-term perspective and ignoring local effects, currents also reflect the height of the water column above the seamount. As a rule of thumb, seamount-induced current systems would become more vigorous during sea-level lowstands.

Within the context of this case study, the subtle balance between sediment deposition and sediment winnowing apparently determined the sediment accumulation rate. Under common omission, the subaquatic lithification and/or mineralization resulted in the development of extensive hardgrounds (Marshall and Ashton, 1980; Fürsich et al., 1981, 1992; Pope and Read, 1997). Increased current velocities, however, also provide a mechanism for seawater circulation in the uppermost sediment column, i.e., the sediment-water interphase, hence providing Ca and carbonate ions for early cementation (McLaughlin and

Brett, 2004). This process triggers early marine lithification (Jenkyns, 1974; Mullins et al., 1980).

The Hancock seamount, at latitudes of approximately 30ºN on the Hawaiian Ridge, was selected as a tentative analogue for the assessment of Jurassic Ammonitico Rosso current dynamics at the Subbetic sites investigated. Similarities between the Hancock seamount and the Jurassic case examples include a number of features. The Hancock seamount presents a flat, two-kilometre-wide summit presently at depths of 265 meters below sea level. Sea surface temperatures of 26ºC during summer months (Boehlert, 1988) are similar to those proposed for Late Jurassic surface waters (estimated range of 12-30ºC and probably progressively but irregularly cooler at higher latitudes according to Ditchfield, 1994 and Longinelli et al., 2003, among others). For the Hawaiian Ridge, sea-surface temperatures decrease with water depth and reach 14ºC at 270 meters. Although present ocean dynamics and temperature zonation depend on a series of parameters, it is perhaps of significance that the reported value of 14ºC at 270 meters for the Hawaian Ridge is within the range of paleotemperature calculations from Ammonitico Rosso micritic carbonate data obtained here and Upper Jurassic belemnite rostrum data from study areas that lie geographically close to southern Spain (e.g, Price and Sellwood, 1994).

Depth estimations for the study area propose a maximum bathymetry of approximately 200 m, i.e., the maximum value expected for Upper Jurassic seamounts at structured margins (Jenkyns, 1971), but this value cannot be tested here. The assumed Jurassic bathymetry of the structural high summits on which the Ammonitico Rosso facies was deposited is poorly constrained. Based on sedimentological, palaeoecological and regional evidence (Olóriz, 2000; Olóriz et al., 2002b) however, it is assumed to be at depths lower than 250 m, the preferred depth range for Late Jurassic epioceanic ammonites (Olóriz et al., 1996, 1997, 2002).

Current velocities of 22 cm/s at 10 meters below sea-level are reported for the Hancock seamount (Boehlert, 1988). This rate is sufficient for mobilizing fine-grained sediment and to winnow the carbonate seafloor as shown by McCave and Hall (2006). The authors predict a combination of selective deposition and removal of finer particles for current velocities in the range of 10-20 cm/s, above which erosional winnowing results in a relative increase in grain size (mud-size particles are only intersticial in sandy sediments). Another modern case example, the Fieberling Guyot (32ºN, summit at 438 depth) experiences current

velocities ranging between 10 and 20 cm/s (Eriksen, 1991). Atop the Fieberling Guyot, currents result in mobilization of clay to sand-sized particles, consistent with the ranges proposed by McCave and Hall (2006). Assuming an average current velocity of approximately 20 cm/s for standard hydraulic regime conditions at paleo-seamount ridges in the Subbetic range, the relation between flow speed and sediment accumulation (e.g., McCave and Hall, 2006) predicts an accumulation rate of perhaps 2 cm/kyr, i.e., a value that is one order of magnitude greater than the average accumulation rate calculated (0.1 and 0.2 cm/kyr) for the study area. This might either imply that the assumed current velocity (20 cm/s) is too low or that factors other than winnowing reduced the overall sedimentation rate in these settings (or a combination of these two scenarios). Factors might include temporarily reduced production, or storm events forcing erosive currents across seamount ridges. Obviously, an increased current velocity (and hence a decreased sediment accumulation) would be expected during periods of sea-level lowstand, such as perhaps after the Late Kimmeridgian sea level maximum (Haq et al., 1988; Hardenbol et al., 1998; Ogg and Przybylski, 2006).

Although speculative at this stage, a preliminary working hypothesis proposes low (~20 cm/s) background current velocities punctuated by episodically higher velocities resulting in the formation of omission surfaces. The former would represent background environmental conditions prone to nodule formation, most probably within the lower to lowermost transitional layer and the upper historical layers. The latter episodes are related to lowered sea level and/or ephemeral changes in the pattern of currents and might be reflected in the commonly observed firmgrounds and/or omission surfaces present in all three sections analyzed. In contrast, hardgrounds, i.e. lithified surfaces characterized by borings and secondary iron and manganese encrustations, are not observed in the sections studied, except for the hardground at the base of the Cañada del Hornillo section. Nevertheless, exhumed *Thalassinoides*-like burrows with no relevant difference in burrow filling with respect to encasing sedimentary rocks point to erosion, most probably proceeded by rather common relative short-time omission, but without significant increase of shelly material transportation. This is supported by the assumption of *Thalassinoides*-makers commonly burrowing firmgrounds (i.e., cohesive substrates; e.g., Martin and Pollard, 1996) under variable oxygenation levels, usually higher than severe dysoxia (e.g., Griffis and Suchanek, 1991; Kristensen, 2000; Monaco and Giannetti, 2002; Ekdale and Bromley, 2003) within a wide spectrum of environmental conditions and with no precise indication about water depth (see

below). Assuming usual bioturbation depth for *Thalassinoides*-makers in Ammonitico Rosso-like facies (ca. 20-30cm taking decompaction into account; e.g., Caracuel et al., 2000), a rough estimante of the eroded sedimentary column could be gained from *Thalassinoides* horizons with a mean thickness of 30 cm for the substract affected by *Thalassinoides*-makers. As usually interpreted for Ammonitico Rosso sections, observations made in the studied sections agree with alternating sediment deposition, albeit at rates relatively low but clearly higher than deduced from usual average estimations, and omission-erosion events.

2.6.5- Burrowing and nodule formation

The extent to which porewater geochemistry reflects water column marine conditions clearly relates to both the organic matter content within the substrate (immature and uppermost mature section; e.g., Sadler, 1993) as well as the occurrence of endobenthic and burrower organisms within the so-called taphonomically active zone (TAZ e.g., Davies et al., 1989) down to the final burial depth (e.g., Olszewski, 2004). Thus, biotic contribution (microenvironments, see Stolp, 1988) is relevant inasmuch as it forces geochemical dynamics and carbonate dissolution/precipitation equilibria in the interstitial environment (from high-Mg calcite, followed by aragonite, and finally low-Mg calcite), which can result in nodule formation during early diagenetic stages. The surface area available for diffusive solute exchange is considerably enhanced through irrigation of the sediment by burrowers. The most surficial layer of sediment usually remains oxic only at the first centimeters below the surface for relatively shallow marine settings (Revsbech, 1980, Kristensen, 2000), though oxidizing (suboxic) conditions can be mantained just above the redox boundary that separates the suboxic layer from the anoxic zone (Froelich et al., 1979); its depth depends on the combination of biotic (e.g., organic-matter content and degradation, dissolution prone skeletals) and abiotic (e.g., grain size and bottom currents) factors, which cause within-sediment heterogeneity in bio-beochemical conditions – i.e., microenvironmental dynamics (e.g., Munn, 2004). Trace fossils of the *Thalassinoides* type were found in the study area (Fig. 2.3C), a biosedimentary structure known from Paleozoic to present-day sediments (Myrow, 1995) and clearly related to different, poorly known trace makers (mainly but not exclusively crustaceans decapods; e.g., Bromley, 1996) in different environments (e.g., Pemberton et al., 1976; MacEachern et al., 1992; Martire, 1996; Schlirf, 2000; Monaco and Giannetti, 2002). In

contrast to the common occurrence of horizontal frames, vertical shafts were not unequivocally identified and related to *Thalassinoides*-like structures, although *Thalassinoides* without vertical shafts has been described from shallow depths within the substrate (Myrow, 1995). While the absence of vertical shafts has been related to their low preservation potential in relatively less-cohesive deposits (e.g., MacEachern et al.,1992), some examples of shaft preservation have been reported from Ammonitico Rosso facies in the Trento Plateau (Late Bajocian to Early Callovian RAI; Martire, 1996) as well as from Late Jurassic mudstones deposited post-carbonate shelf drowning in the Cracow-Wielun Upland Poland (latest Oxfordian-to-earliest Kimmeridgian; Matyszkiewicz, 1996). Thalassinideans decapods, one of the burrowers making Y-shaped *Thalassinoides*-like traces, bioturbate up to 3-meters-deep within the substrate (e.g., Pemberton et al., 1976) forcing within-sediment relative oxygenation (e.g., Libes, 1992), as well as changes in bacterial occurrence and microbiologically induced chemo-dynamics (e.g., Kinoshita et al., 2003). Information about Y-shaped *Thalassinoides*-like burrows within the first 30-40 cm of the sedimentary column (envisaged critical depth for nodule formation) indicates increasing of the water-sediment reaction interphase area from 1 to 9 m^2 per each m^2 of sediment (e.g., Griffis and Suchanek, 1991). Taking into account that oxygen diffusion is possible through several millimeters of sediment adjacent to *Thalassinoides*-like tunnel walls, the oxygenation effect may be enhanced up to 70% in comparison to one-dimensional diagenetic stratification (Kristensen, 2000 and references therein). Water pumping efficiency can reach values similar to tidal flux in modern coastal settings (Mukai and Koike, 1984), guaranteeing elemental supply from overlying marine water down to the first 30-40 cm of the sediment column. This within-sediment depth coincides with the estimated depth for nodule formation of modern analogues (Mullins et al., 1980), whereas deeper intra-tunnel irrigation showing a decreasing gradient is known from deeper Thalassinideans burrows under relative hypoxic conditions (e.g., Astall et al., 1997). Accordingly, the early diagenetic red pigmentation of micrites in Ammonitico Rosso facies could be a within-sediment process occurring deeper than envisaged by Mamet and Préat (2005; 2006).

The effectiveness of the chemical processes of cementation depends on the permeability of the sediment, controlled by physico-chemical and biological factors. Surface and near-surface cementation is possible when currents are competent enough to remove fine sediment, enlarging interstitial volume and consequently increasing permeability (pumping of

seawater through the uppermost, mostly immature sediment column) and ionic availability (Ca^{2+}, Mg^{2+}, CO_3^{2-}) necessary for chemical processes to take place. Omission surfaces, taphonomic features and bioclastic infilling of irregular cavities (including the so-called "tubular tempestites" identified in the context of this study or deducible from the literature; e.g., Martire, 1996) agree with this scenario of episodical, tractive bottom currents in a depositional context, which will result in Ammonitico Rosso facies. In this context, the abundance of ammonoid carcasses and accompanying calcite skeletals in the epiocenic environment plays an important role, as the very early onset of the dissolution of ammonite aragonitic shells (e.g., Clari and Martire, 1996) contributes to increase porewater elemental content, favouring an even more rapid nodule formation as envisaged by Palmer and Wilson (2004). This process is independent of the present seawater mode (i.e., "aragonitic" or "calcitic" e.g., Gruszczyński, 1998).

Although nodule formation in Mesozoic deposits is still under debate, the authors favour the hypothesis predicting nodule formation in a relatively shallow sedimentary horizon (most probably the lower immature to uppermost mature section) early during diagenesis (Fig. 2.11). This horizon is affected by differential movement of pore fluids i.e., geochemical gradients linked to sedimentary overburden, microbial activity and soft-to-firmground burrowing, although bioturbation in more cohesive firmground substrate is also envisaged (Fig. 2.11). Given the fact that examples of *Thalassinoides*-like tunnels affecting nodule periphery occur, the space for within-sediment nodule origin would correspond to the sedimentary column between the lower boundary of TAZ (Olszewski, 2004) and a imprecise, variable depth within the upper mature section (Sadler, 1993). The process determining early diagenetic nodules, as considered here, differs from that commonly defined (e.g., Martire, 1996) as due to incipient compaction (i.e., forcing selective dissolution identifiable with no deformation) as a trigger factor for the onset of nodulation inside the sedimentary column.

After diagenetic nodules originated, the observed geochemical preservation can be explained by the reduced intranodular fluid circulation (Jenkyns, 1974 and references therein; Clari and Martire, 1996; Martire, 1996). This results as compaction expels pore fluids upwards and further geochemical exchange between fluid and nodules is therefore more limited. The very low intra-nodule geochemical range observed for two representative Kimmeridgian nodules is in agreement with a rapid, relative pressure-solution and cementation effect within the marine porewater domain. Similarly, within the sedimentary

column, nodule growth seems to cease when burial depth exceeds a critical threshold value perhaps defined by the depth limit at which diffusion, and hence elemental supply, is possible (e.g., Jenkyns, 1974; see Farinacci and Elmi, 1981 for extended references in Ammonitico Rosso facies).

2.6.6- Matrix micrite geochemistry for interpreting Ammonitico Rosso facies

Having established a causative relation between sediment accumulation rate, early marine cementation (i.e., formation of nodules) endobenthic biogenic activity and isotope values, it is of interest to apply these findings to other case studies of Jurassic Ammonitico Rosso facies. The following ones are used here for comparison (isotopic values shown in Fig. 2.9): Price and Sellwood, 1994, from Mallorca, Spain; Préat et al., 2006, from the Trento Plateau, Italy; Rey and Delgado, 2002, from the Betic Cordillera, Spain; and Cecca et al., 2001, from Monte Inici, Italy. On the basis of available data, however, it appears that the only study providing similarly elevated oxygen-isotope values is that reported by Cecca et al. (2001). Other studies document significantly lower $\delta^{18}O$ values ranging from -4 to 0‰ (Fig. 2.9). Comparing assessments of sediment deposition rates from these studies with mean oxygen-isotope values provides no clear relation between low sedimentation rates and elevated $\delta^{18}O$ values and higher sedimentation rates combined with more depleted $\delta^{18}O$. The reasons for this lack of association are obviously complex, yet might include differential diagenetic histories, burial depth, degree of geological overprint, differences in the original sediment composition, differences in current velocities, or topographical differences, all of which are difficult to evaluate.

2.7- Conclusions

Three carefully correlated Upper Jurassic Ammonitico Rosso stratigraphic sections from the Betic Cordillera were analysed in terms of their geochemical signature and paleoenvironmental regime. The strict biochronostratigraphic control and the comparison with direct measurements reported from modern analogues proved to be of value for the characterization of the ancient distal-epioceanic swells environments under scope.

The material retrieved from the Subbetic range revealed good preservation of the matrix micrite on SEM and cathodoluminiscence analysis. The geochemical data obtained (i.e., marine $\delta^{18}O$ ratios) agrees with the favourable preservation verified by optical inspection techniques.

The carbon isotope stratigraphy matches the well known pattern commonly described along the Tethyan margins, reflecting the Middle Oxfordian marine trangression and the later, rather progressive change in paleoenvironmental conditions during the Late Jurassic.

Oxygen-isotopes values are higher than commonly expected for Upper Jurassic micritic carbonates. These values are interpreted as corresponding to a close-to-original isotopic signal. Assuming that this interpretation is correct, the data obtained allow for the reconstruction of past environmental parameters, in terms of relative seawater depth and paleotemperature, as well as fluctuations in porewater conditions.

Early diagenetic nodule formation is thought to be a key factor for interpreting the obtained geochemical data set. The interplay between current velocity, sedimentary input and winnowing, burrowing and water pumping would be crucial in providing favourable conditions for the early occurence of nodules, which remained remarkably resistant to subsequent diagenetic alteration.

In this context, paleoenvironmental conditions during and just after deposition can be assessed, contributing to a better understanding of the Ammonitico Rosso facies studied. On the assumption of available data from modern analogous settings, the proposed scenario is coherent with upper water depths, current swept and discontinuous net deposition, endobenthos acitivity, and resulting within-substrate differential microenvironments that forced nodularity and hence the "freezing" of isotopic signals.

Acknowledgements

We wish to thank Dieter Buhl, Ulrike Schulte, Beate Gehnen and Barbara Raczek (Ruhr Universität Bochum-RUB) for their support during laboratory measurements; Rolf Neuser (RUB) for the cathodoluminescence analysis; Matthias Born (RUB) and Alberto Montes (University of Granada-UGR) for the preparation of thin sections; and Alicia González, Concepción Hernandez and Hoda Khaldy (CIC-UGR) for collaboration during SEM analysis and preparation of laboratory material. This research was supported by Projects CGL2005-01319 and CGL2008-05251-E (MICINN) and the Research Group RNM-178 Junta de Andalucía, Spain. We appreciate comments and suggestions made by Luca Martire (Univ. Torino, Italy), Henry Chafetz (Univ. of Houston, USA) and the editors on an early draft of this paper.

3

Contrast comparison of differential diagenetic pathways of Lower Tithonian carbonate materials from the Betic Cordillera (S Spain): Evidence for physico-chemical paleo-seawater properties

Rute Coimbra [(a)], Federico Olóriz [(a)]

[(a)] Departamento de Estratigrafia y Paleontologia, Universidad de Granada, Spain

Submitted to Palaeogeography, Palaeoclimatology, Palaeoecology (April 2011)

Abstract

The reconstruction of palaeoenvironmental conditions is based on the study of ancient rock materials. For this purpose, skeletal materials are often assumed as having higher preservation potential, sometimes favoured against the use of matrix micrite. However, factors such as ecology, depositional setting, mineralogy and diagenetic processes may obscure original geochemical signals, and care must be taken when reading such an intricate record. This work provides a thorough comparison between geochemical signatures of different carbonate materials, interpreted in the light of their palaeoenvironmental significance. Burial and diagenetic processes are taken into account, contextualized by ammonite and belemnite ecology.

Two sections deposited in epioceanic Tethyan areas and corresponding to the same Lower Tithonian ammonite biozone are under scope: a condensed, pelagic and cephalopod-rich limestone (the Alamedilla sector) intercalated in marls and mafic rocks, and a typical Ammonitico Rosso facies (the Cardador section). In contrast to depositional and taphonomic histories typical for a Tethyan top-swell site (i.e., rather calcareous Ammonitico Rosso), events of carbonate-mud deposition, rapid burial and early lithification, synsedimentary sliding and over imposition of firmground horizons characterize pelagic cephalopod-rich limestones. Differential taphonomy of carbonate skeletals agrees with differential preservation, favouring inner-cast preservation in Ammonitico Rosso and shell preservation (neomorphic calcite) in pelagic cephalopod-rich limestones.

Stable carbon and oxygen isotopes, together with trace element data (Sr, Mg, Fe, Mn) are presented for a wide range of carbonate materials: matrix micrite, neomorphic ammonite shells, belemnite rostra and carbonate cements. Optical inspection (including cathodoluminescence imaging) suggests a fair preservation of analysed materials, except for diagenetic marine burial carbonate cements, also supported by geochemical data. Carbon isotope values fall within the typical Tethyan Late Jurassic range (ca. 2‰), except data from belemnite rostra which are depleted around -1‰, which is interpreted as resulting from metabolic fractionation. Oxygen isotope values are more variable, but a rather conservative diagenesis agrees with the clustering of different carbonate materials within a narrow range of values from -1 to 1‰. Warmer burial fluids explain lower values in later diagenetic carbonate cements. No evidence of pervasive diagenetic imprint is revealed by elemental composition,

and recognition of hydrothermal contamination is detected by increased abundance of Mg, Fe, and specially Mn, up to 1500 ppm. Proximity to hydrothermal sources (the Mid-Subbetic Volcanic Ridge) accords with higher Mn concentration at the Alamedilla site. Interestingly, the timing of mineralogical stabilization of each carbonate material seems to reveal the potential record of a post-sedimentary geochemical event.

The obtained information demonstrates the complexity of ancient carbonate records, and encourages future research focused on the preservation potential of geochemical proxies throughout time.

3.1- Introduction

The complex, polygenic nature of matrix micrite is a feature that has recently been addressed (Immenhauser, 2002; Turpin et al., 2008). Furthermore, unresolved palaeoecology of often used skeletal materials (as belemnite rostra) and variable degrees of diagenetic imprint on distinct carbonate materials (e.g., secondary calcite, skeletal remains, matrix micrite), illustrates that palaeoenvironmental interpretations may sometimes be hard to ascertain.

Geochemistry has proved to be useful when applied to matrix micrite, especially true for carbon isotopes, even reflecting local signals superimposed on more global signatures (e.g., Swart and Eberli, 2005). In the case of stable oxygen isotopes, usually considered to be prone to diagenetic overprint (e.g., Marshal, 1992), a reliable record of porewater palaeotemperature may be preserved in the case of early lithification of matrix micrite (e.g., Coimbra et al., 2009).

Metastable carbonate materials tend to alter their original signal during stabilization into low-Mg calcite (e.g., Veizer, 1983). This argues in favour of using originally low-Mg calcite skeletal materials such as belemnite rostra, which are widely reported as suitable for reconstructing palaeoceanographic conditions (Podlaha et al., 1998; Wierzbowski, 2002; Voigt et al., 2003; Rosales et al., 2004; McArthur et al., 2007; Price, 2010). Since some debate still exists on aspects regarding belemnite lifestyle/habitat (e.g., Mutterlose et al., 2010), care must be taken with direct interpretations of geochemical proxies retrieved from belemnite rostra. Other skeletal components, such as ammonite shells, may also be suitable for palaeoenvironmental conditions despite their less stable original mineralogy. Original aragonitic shells, when preserved, may inform on ontogenic C and O isotope variations (e.g., Lécuyer and Bucher, 2006; Lukeneder et al., 2008). Combined with the ecologic context of the organisms under study, isotope shifts serve to the interpretation of changing palaeoceanographic conditions. In cases of aragonite stabilization into low-Mg calcite, porewater conditions may potentially be preserved at a very early diagenetic stage (e.g., Hendry et al., 1995; Maliva, 1995; Brachert and Dullo, 2000). For latter diagenetic stages, some features (e.g., secondary calcite veins) can complete an overview of the diagenetic history of studied materials, informing on post-depositional phenomena. Thus, an integrated geochemical approach is fundamental to unravel syn- and post-depositional conditions.

Condensed, pelagic and cephalopod-rich limestones are one of the typical facies in the Late Jurassic of Tethyan regions. In fact, this particular lithofacies is commonly related to sedimentary contexts in which Ammonitico Rosso facies are recorded (e.g., Farinacci and Elmi, 1981 for extended overview with references). However, the so-called condensed, pelagic, cephalopod-rich limestones clearly differ from typical Ammonitico Rosso facies in two relevant traits: (i) they are not nodular limestones; and (ii) they typically contain ammonites with a comparatively well-preserved shell, in contrast to the inner-cast preservation very common to typical for Ammonitico Rosso deposits. Moreover, the so-called condensed, pelagic, cephalopod-rich limestones are typically recorded from extremely condensed sections, at least in upper Jurassic deposits. The latter are known in the Betic Cordillera, and the selected case study exemplifies deposition on a volcanic ridge which was more active during the Middle and the Late Jurassic in the Median Subbetic Trough of the Betic Cordillera in southern Spain. Thus, studied materials are considered suitable for an integrated geochemical and ecologic approach, as they represent a variety of carbonate materials retrieved from different settings.

Precise sedimentological observation of rock slabs, together with consideration of cephalopod ecology and taphonomy (the latter especially for ammonites), provide a favourable context to interpret diagenetic pathways through geochemical data (stable isotopes of C and O and trace elements) gathered from matrix micrite, ammonite shells and its sedimentary infilling, and belemnites. Under strict biostratigraphic control, comparisons are made with geochemical data obtained from a typical nodular Ammonitico Rosso section in the Internal Subbetic of the Betic Cordillera. We investigate the possibility that matrix micrite geochemical signals could be less averaged than usually interpreted, thus providing favourable conditions for evaluating potential relationships of porewaters with local overlying marine bottom waters as well as with the marine water from which biogenic carbonates precipitated.

3.2- Geological context

Sections from the localities at Cardador and Alamedilla are here under scope (see Fig. 3.1A to D for major geological units, location of sections and field aspects).

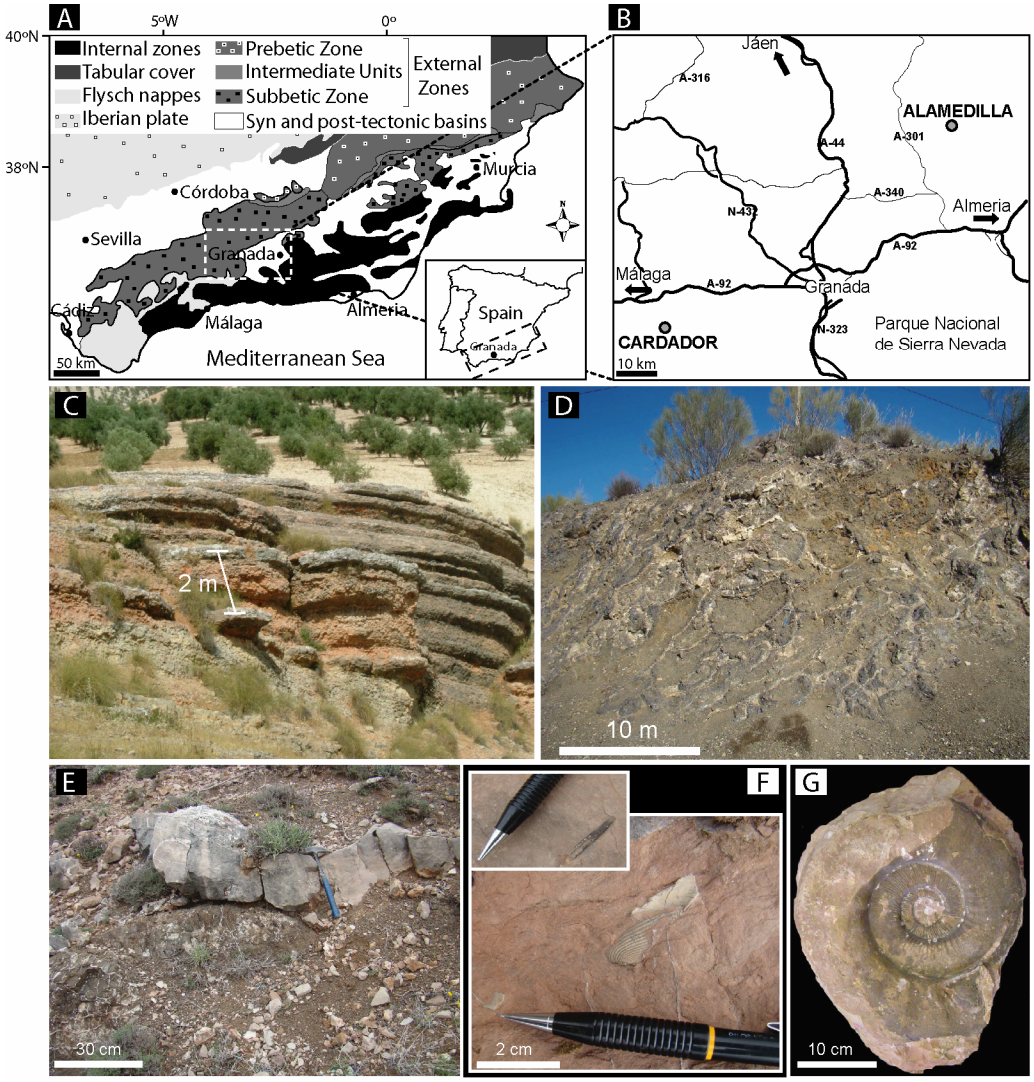

Fig. 3.1- Distribution of major geological units along the Betic Cordillera (modified from Garcia-Hernández et al., 1980). B: Location of studied sections, Cardador and Alamedilla (grey circles). C: Field view of the Cardador section, with evident nodularity. D: Field view at the Alamedilla sector, showing pillow lava structures (westward from Alamedilla). E to G: Close up views from the Alamedilla sector. E: Red limestone bed resting on pillow lava; F: Belemnite and aptychi in red marly limestone; G: Ammonite from the sampled block of pelagic cephalopod-rich limestone.

The Cardador section is located at the External Zones of the Betic Cordillera (Fig. 3.1A) corresponding to the Internal Subbetic Zone in a distal seamount range of the Subbetic zone (Fig. 3.2) (Olóriz et al., 2002a).

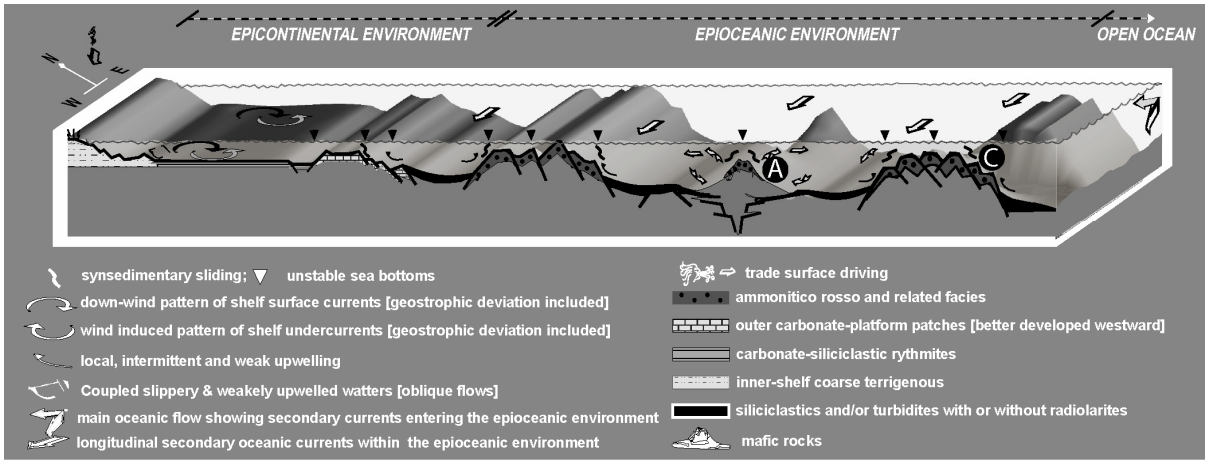

Fig. 3.2- Synthetic bottom physiography and major palaeoenvironments in the South Iberian Margin during the Late Jurassic (adapted from Olóriz, 2000). Location of the studied outcrops indicated by A-Alamedilla and C-Cardador.

The studied outcrop in the surroundings of the village of Alamedilla is located in the Median Subbetic, corresponding to a trough separating two discontinuous ridges of seamounts (Figs. 1A, B, D and 2) in the S-SE palaeomargin of Iberia (Olóriz et al., 2002a for a comprehensive review with extended references). A longitudinal, volcanic structure 5-10km wide, exceeding the central sector of the Betic Cordillera in longitude (see Fig 2 for synthetic bottom physiography), and interpreted to be some hundred meters high locally, subdivided the Median Subbetic Through (Comas, 1978). Shallow water carbonate deposition occurred on top of volcanic highs during the Middle Jurassic (e.g., Vera et al., 1997), evidencing patches of photic zone productive factories (Bahamian-type carbonates on guyots in Molina and Vera, 2000). Neritic depths have been interpreted for Upper Jurassic marl-limestone rhythmites with intercalated calcareous tempestites (Milanos Fm, cf. Vera and Molina, 1998) in relative low bottoms. Storm deposits also affected pelagic seamounts during early Tithonian times in the northern seamount ridge or External Subbetic (e.g., Checa et al., 1983; Molina et al., 1986, 1987). Lenticular lithosomes of condensed pelagic wackestones with ammonites (Fig. 3.1E), showing parallel and/or cross bedding and intercalated packstone horizons with abundant small bivalves (2-4 mm) and secondary brachiopods and crinoids were deposited on volcanic highs in the Median Subbetic Trough at the same age (Comas and Olóriz, 1986), the latter evidencing persistence of most probably small, scattered shallow carbonate factories. The relatively huge bottom topography locally persisted during early Cretaceous times (Molina and Vera, 2008). An analogous situation was described by Gill et al. (2004), who interpreted

photic to slightly subphotic depths for typical pelagic deposits (condensed ammonite-rich limestones) on submarine highs adjacent to troughs in Central Apennines. These authors recognized close lateral relations between condensed ammonite-rich limestones and radiolarian cherts, and interpreted a general depth context shallower that previously considered for typical upper Jurassic Tethyan lithofacies (e.g., Ammonitico Rosso, nodular *aptychus* limestone).

Condensed, pelagic and ammonite-rich limestones included as local and more or less stratified lithosomes encased by submarine mafic vulcanites in the Mid-Subbetic Volcanic Ridge have been identified (e.g., Comas, 1978; Comas et al., 1981; Rey, 1993). The averaged sedimentation rate interpreted for these cephalopod-rich limestone horizons (mudstone-to-mainly wackestone) was interpreted as 0.5mm/ky and exceptionally 1mm/ky (e.g., Comas et al., 1981).

The studied outcrop near Alamedilla shows some lithosomes of the so-called red-beige, condensed, pelagic and ammonite-rich limestones intercalated among mafic rocks (Fig. 3.1E). In the studied block (Fig. 3.1G), the content in macrofossils and the close analysis of cut-sections of hand samples show good preservation of ammonites (Fig. 3.3B-a to d), some of them with shell-width of several centimetres (Fig. 3.3B-b) as well as subtle, more or less irregular surfaces separating limestone horizons with different content in fossil remains and or matrix colours (Fig. 3.3B-b, c and g). Hence deposition in these horizons was likely far more rapid than the average values mentioned above and resulted from episodes of sudden carbonate precipitation of hemipelagic muds, thus favouring rapid burial, early diagenetic processes and good preservation of shells in ammonites and others skeletal remains.

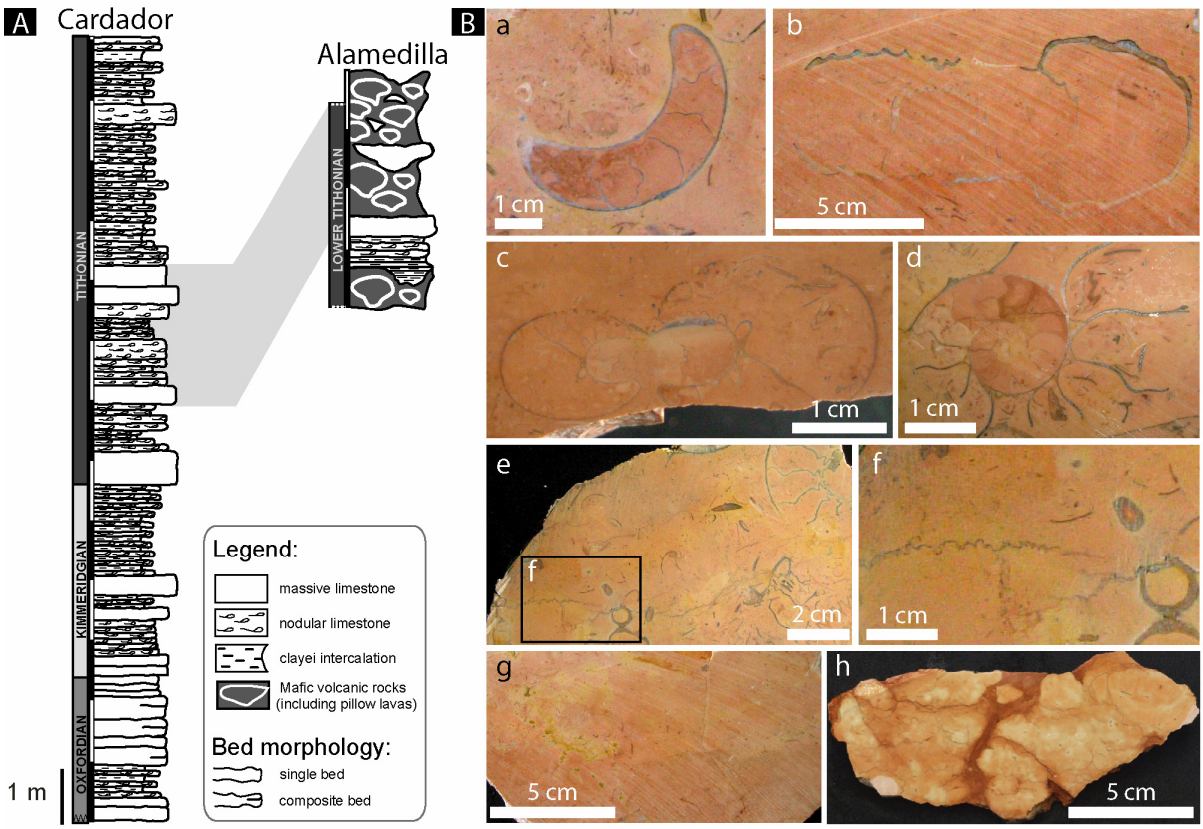

Fig. 3.3- A: Cardador section and Alamedilla outcrop, with grey bar indicating chronostratigraphic correspondence between both sections. B: polished surfaces showing features relevant for sedimentologic and taphonomic interpretation; a) to g) from the Alamedilla outcrop (note shell preservation) and h) from the Cardador section. a) Ammonite phragmocone infilled by bioclasts-free and partly burrowed sediment, differing from encasing matrix micrite; b) Ammonite body chamber preserved in volume with sediment infilling equivalent to surrounding matrix and containing shelly fragments of probable broken septa; c) Ammonite phragmocone (geopetal in inner whorls) preserved in volume, not reworked, showing shell breaking with small displacement of fragments, shell puncturing, no plastic deformation, and selective accumulation of shelly fragments. d) Equatorial section of ammonite phragmocone with differentiated infill (note colour changes), and missing the ventral zone of the carcase evidencing selective dissolution of shell and no difference with the surrounding matrix (intraclasts and skeletals) except for inner chambers protected through preservation of the ventral part of their shell; e) Bioclast-rich sediment matrix showing stylolite and no compaction of subtle and selectively preserved shell remains; f) detail of stylolitic truncation of recrystalized bioclast; g) Within-bed sedimentary horizon evidenced by scoured changing colour along scoured and/or biogenically elaborated surface; h) nodular structure typical for the Ammonitico Rosso facies in the Cardador section showing clayey dissolution seams among irregular nodulation of burrowed sediments.

3.3- Materials and Methods

In the context of this study, four different carbonate materials from two localities were investigated. These include: (i) matrix micrite from the Cardador section (*n*=21) and from the Alamedilla outcrop (*n*=31); (ii) carbonate cements from the Cardador section (none were observed for the Alamedilla outcrop) (*n*=6); and skeletal materials encased on Alamedilla matrix micrite: (iii) neomorphic ammonite shells (seven specimens, *n*=11); and (iv) belemnite rostra (five specimens, *n*=6).

Thin sections were prepared from each hand specimen for Tithonian horizons from the Cardador section and for representative samples from the Alamedilla outcrop. Cathodoluminescence inspection was carried out for all different carbonate materials using a hot stage cathode luminescence (HC4- LM). The aim was on separating intrinsic (early) from luminescent (later diagenetic, secondary) carbonate materials in order to access the degree of diagenetic imprint (Fairchild, 1983; ten Have and Heijnen, 1985; Marshall, 1988; Machel and Burton, 1991; Machel et al., 1991; Bruckschen and Richter, 1994; Bruhn et al., 1995; Barbin et al., 1997). Ultrastructure inspection of micrite samples from both localities was performed under Scanning Electron Microscope (SEM) LEOGemini 1530 on 8 fresh fractured rock chips at the Center of Scientific Instrumentation at the University of Granada and at the facilities the Institute for Geology, Mineralogy and Geophysics at Bochum, Germany.

Isotope analysis (carbon and oxygen) was preformed on a total of seventy six hand drilled bulk carbonate powder samples using a ThermoFinnigan MAT delta-S mass spectrometer (procedure according to McCrea, 1950). Analytical precision (±1σ) was controlled by NBS19 and internal standards, and was better than ±0.03 and ±0.08‰ for $\delta^{13}C$ and $\delta^{18}O$, respectively. Duplicate samples presented a deviation of ±0.08‰ for $\delta^{13}C$ and ±0.11‰ for $\delta^{18}O$. Obtained values are expressed in the conventional delta notion as ‰ relative to the V-PDB standard.

Aliquots from powder sub-samples analyzed for isotope ratios were investigated for Ca, Mg, Mn, Fe and Sr elemental concentrations using inductively coupled plasma-atomic emission spectrometry (ICP-AES). Duplicate samples allow for an assessment of the maximum scatter for measured elements in the order of 0.4%. All analytical procedures were carried out at the laboratory facilities of the Institute for Geology, Mineralogy and Geophysics at Bochum, Germany.

Sedimentologic observations carried out on the field were complemented by precise analysis of rock slabs, parallel and perpendicular to bedding, to control sedimentary and

biogenic structures (fine lamination, burrowing and/or boring, shell fragmentation and orientation, and the sedimentary fabric). Special attention was given to taphonomic traits and to precise biostratigraphy at the ammonite biozone level. In order to support the interpretation of geochemical data in a palaeoenvironmental context, considerations about cephalopod palaeoecology were taken into account.

3.4- Results

3.4.1- Field evidence and microscopic inspection of sample material

The Cardador section (Fig. 3.1C) is characterized by variable calcareous, reddish and grayish Ammonitico Rosso facies (Fig. 3.3B-h). Amongst the carbonate facies, wackestones dominate. These contain radiolaria, calcisphaeres, calcareous dinoflagellates, planktic crinoids (*Saccocoma*), unspecified benthic foraminifera, ostracods and cephalopods (rare ammonitella or embrionic shell of ammonoids and aptychi included; belemnites). Fragments of juvenile and adult ammonite carcasses along with broken molluscs, echinoderms (plates and spines), sponge spicules and pelagic bivalves occur locally. Occasionally, packstone horizons mainly composed by filaments (young, planktic bivalves) are recorded. Fossil preservation is moderate and dominated by inner moulds. Preservation of neomorphic shell is extremely rare and restricted to spots on inner moulds. Among macrofossils, ammonites dominate including more or less complete specimens showing phragmocones and body chambers, but peristomal structures are rare. Sedimentary condensation varies, reworking without biostratigraphic relevance is common, and no stratigraphic condensation has been demonstrated (e.g., Olóriz, 2000).

The Alamedilla outcrop (Fig. 3.1D) displays reddish, brownish and pale grey limestones, secondary marls, and dominant mafic rocks. Limestones are locally rich in ammonites (condensed, pelagic, cephalopod-rich limestones), which preserve neomorphic shells infilled by fine sediment similar to the encassing deposits. Belemnites are relatively common (Fig. 3.1F). Within-bed orientation relates to shell size showing common horizontal settling for ammonites greater than 60-70mm. In the Alamedilla outcrop, cephalopod-rich wackestones contain a variable amount of radiolaria. Among skeletal components (Fig. 3.4A to L) are common to abundant calcareous dinoflagellates, occasional planktic crinoids

(*Saccocoma*), benthic foraminifera (*Lenticulina*), ostracods, cephalopods (common ammonitella or embrionic shell of ammonoids included), and fragments of juvenile and adult ammonite carcasses, rare aptychi and belemnites (Fig. 3.1F and G). Along with broken mollusks, subordinate small gastropods, juvenile bivalves, rare brachiopods and echinoderms (plates) as well as a variable amount of filaments (pelagic-planktic bivalves) are found (Fig. 3.4B to L).

In a detailed analysis of sampled blocks and slabs (Fig. 3.3B-a to g), macrofossils show: (i) typical shell preservation; (ii) specimens with and without preserved bodychamber occur together; (iii) sediment infilling indistinguishable from that of the enclosing matrix dominates, although rare examples of partially hollow shells occur (druse calcite infilling); (iv) local shell breaking and/or shell loss, and thus isolate shell fragments of variable size; (v) absence of macroscopic encrusters; (vi) no size selection; and (vii) larger shells showing sub-horizontal settling but smaller ones showing a more variable within-sediment orientation (Fig. 3.3B-a to f and Fig. 3.4D).

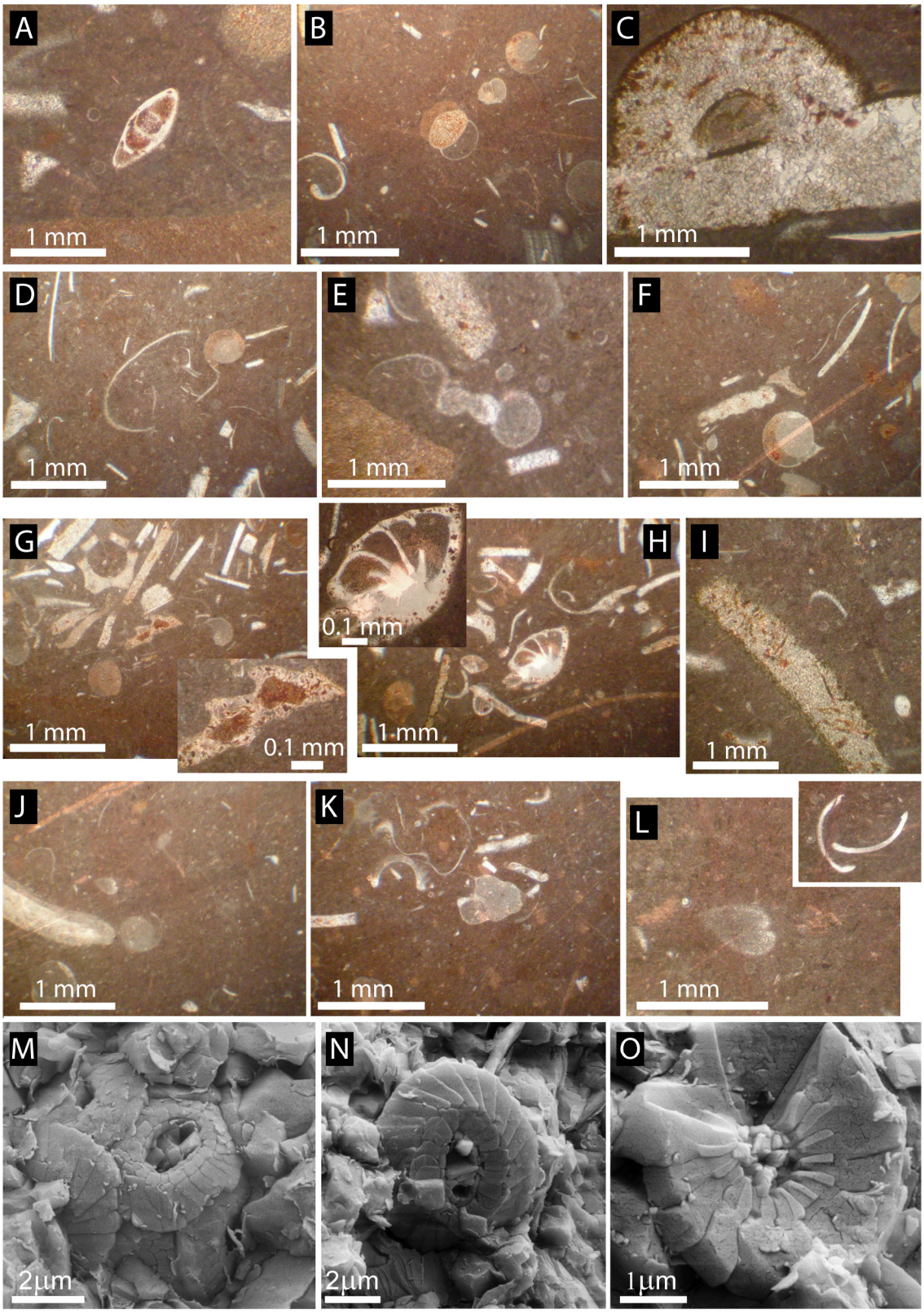

Fig. 3.4- Microscopic images of Alamedilla matrix micrite. A: Net surface boundary between within-bed subhorizontal sedimentary horizons (bioclast-rich with coarser size fragments above and bioclast poorer with smaller, finer fragments below). B; Well preserved ammonitellas with differential infill (recrystalized whitish

aspect in the protoconch and matrix micrite infill of different colours very early in the phragmocone); note remains of molluscs (gastropods, bivalves), radiolaria and dinoflagellates, with no evident deformation but slight variation in geopetals' orientation. C: Recrystallized mollusc structure showing microboring and remarkable coating/pigmentation by iron oxides. D: Broken but uncrushed ammonite shell; note ammonitella and fragments of septal structure, equinoderms, bivalves and indeterminate molluscs (a single valve of lamellaptychus out of view on the left); E) Ammonite shell with broken yet undeformed body chamber and recrystallized inner whorls; note sedimentary infill with no difference with respect to the surrounding matrix showing dynoflagellate cysts, probable single valve of ostracod and indeterminate shelly remains. F: Common preservation of ammonitellas, a structure very prone to early dissolution, evidencing an overall good degree of preservation of commonly incomplete skeletals (gastropods, bivalves, ostracods?, dynoflagetllate cysts, echinoderms). Gastropods and dinoflagelates are also present. G: Bioclast-rich horizon overlying a subtle depositional boundary separating differential packing, relative density and size of skeletals; note fragmentation without crushing and microboring (close-up of broken aptychus showing intense microboring and iron oxide pigmentation but no coating). H: Abundance of undeformed broken skeletals (mainly molluscs) with variable microboring (close-up of benthonic foraminifera with iron oxide inclusions) and example of iron oxide coating on recrystallized, indeterminate fragment. I: Detail of coarse skeletal fragment (probably from bivalve) showing intense microboring on potentially coated surface. J: Differential preservation of ammonitellas in volume (no compression), including the primary varyx; K) Bioclast-rich matrix micrite with abundant radiolaria ghosts and dynoflagellate cysts, indeterminate shell remains and gastropod with differentiated infill; note preservation of subtle, arched structures (no compaction). L: Undeformed bivalve shell. Close up of well preserved, disarticulated but uncrushed ostracod close to indeterminate and dynoflagellate cysts (out of view on the right). M to O: Coccoliths (probable coccosphere on M).

In accordance with the context described above, the large specimen of Lithacoceratinae (most probably macroconch showing more than 5cm of adoral shell width) analyzed for carbon and oxygen stable isotopes and trace elements (Fig. 3.1G) shows: preserved phragmocone with trace of the line of whorl overlapping that corresponds to the missing anterior part of the body chamber (field sampling?); no evidence for edge fracturing, edge rounding, and crushing by sediment loading; and no macroscopic encrusting.

Concerning belemnites, incomplete rostra of Belemnopseidae (*Hibolithes*-like forms) are scattered, without preferential accumulation. Azimuthal orientation (oblique or near-vertical specimens) is common. No particular orientation in horizontal planes has been identified. Fragmented specimens dominate but neither bioerosion nor encrusting is identifiable.

Cathodoluminescence (CL) images were produced for each carbonate material investigated (Fig. 3.5). Cathodoluminescence images of micritic carbonates from the

Cardador section (Fig. 3.5B) are characterized by duller luminescence when compared to the Alamedilla block micritic matrix analyzed (Fig. 3.5D). Secondary blocky calcite cement from the Cardador section (Fig. 3.5B) reveals zoning and is rimmed by bright orange luminescent micrite. Skeletal material from the Alamedilla outcrop reveals overall intrinsic dark luminescence. The neomorphic ammonite shell (Fig. 3.5F) discussed here presents large blocky calcite crystals with intrinsic luminescence. Belemnite rostra (Fig. 3.5H) reveal overall intrinsic luminescence, cross-cut by very fine veins and occasional bright luminescent laminae.

Ultrastructure inspection under SEM revealed an overall abundance of well preserved coccoliths (Fig. 3.4 M to O; see also Coimbra et al., 2009 for SEM images from the Cardador section). The preservation of filaments (algal and/or bacterial, see Coimbra et al., 2009 for the Cardador section) was not observed in samples from the Alamedilla outcrop.

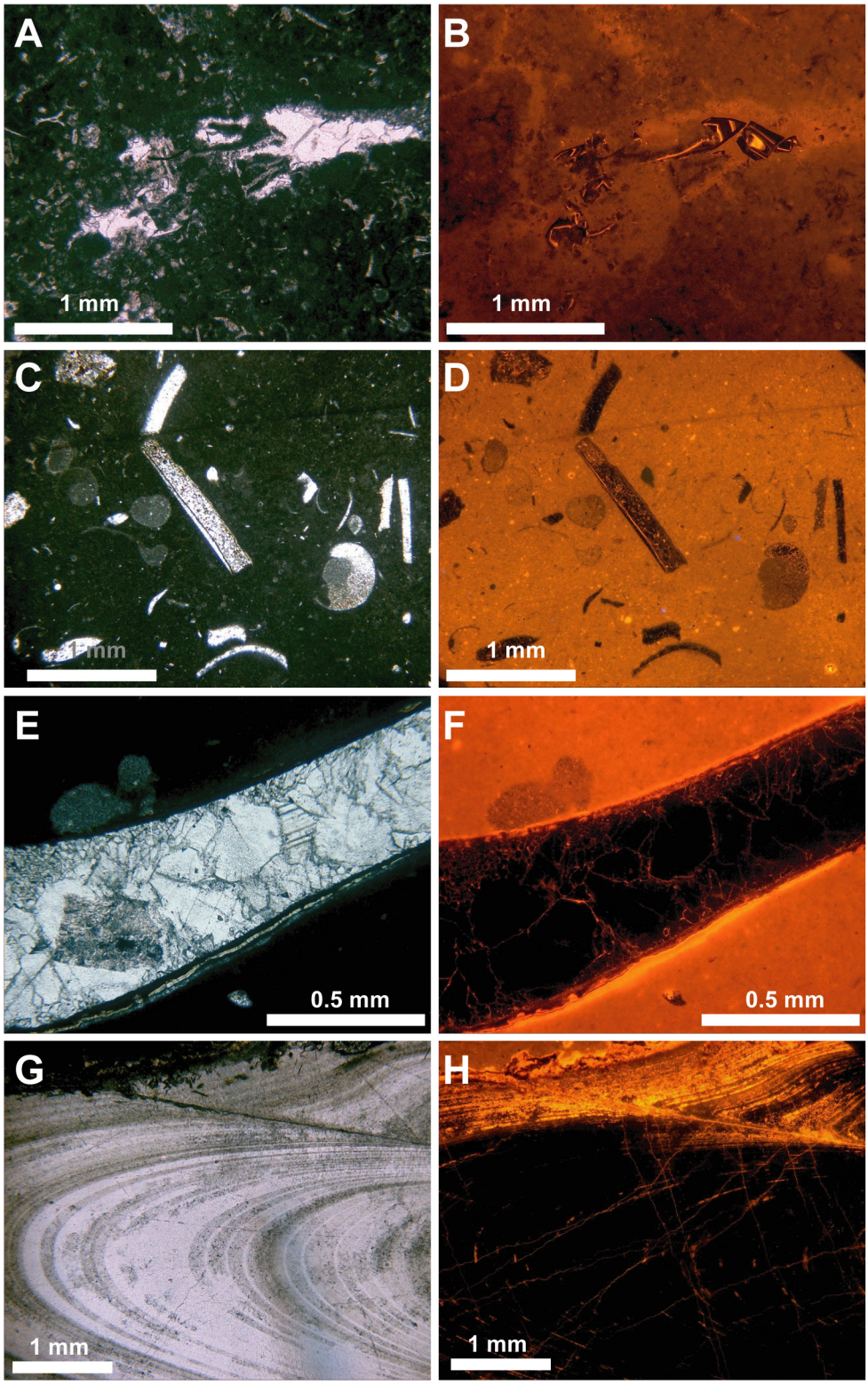

Fig. 3.5- Cathodoluminescence images representative of all sampled materials (micrite matrix, carbonate cements and skeletal materials). A: Matrix micrite from the Cardador section showing a cemented void (no equivalent features are recorded in the Alamedilla section. B: Under cathodoluminescence. C: Matrix micrite from the Alamedilla block showing relative abundance of microfauna. D: Under cathodoluminescence. E:

Neomorphic ammonite shell. F: Under cathodoluminescence, note intrinsic luminescence. G: Belemnite rostra (transversal cut). H: Under cathodoluminescence. Note luminescence contrast between belemnite rostrum laminae and the encasing micrite.

3.4.2- Carbon and oxygen isotope data

Carbon and oxygen isotope values are presented in Fig. 3.6 (mean values and standard deviations are summarized on Table 3.1).

		$\delta^{13}C$ (‰)	$\delta^{18}O$ (‰)	Sr (ppm)	Mg (ppm)	Fe (ppm)	Mn (ppm)	n
Cardador section	Micrite	1.80 ±0.2	0.37 ±0.2	138 ±86	3118 ±184	1068 ±398	202 ±152	21
	Carb. cements	1.83 ±0.1	-2.2 ±0.7	258 ±65	3973 ±777	382 ±207	1230 ±502	6
Alamedilla outcrop	Ammonite Shells	1.52 ±0.9	0.40 ±0.4	106 ±16	4117 ±470	1195 ±681	284 ±83	10
	Micrite	1.55 ±0.6	-0.66 ±0.5	177 ±27	4028 ±621	1956 ±1035	744 ±257	31
	Belemnite rostra	-0.78 ±0.6	-0.95 ±0.2	1108 ±63	2848 ±774	57 ±29	74 ±71	6

Table 3. 1- Mean values and standard deviations calculated for isotope composition and elemental data for all the types of carbonate materials analysed from both localities.

Micrite matrix (clusters "a" and "b" in Fig. 3.6, including data from both sections, Cardador and Alamedilla), secondary blocky calcite cements (cluster "c") and neomorphic ammonite shells (included on cluster "a") display $\delta^{13}C$ ratios between 1.5 and 2.1‰. Belemnite rostra (cluster "d") present lower $\delta^{13}C$ ratios, from -1.6 to 0.1‰. Regarding oxygen isotope composition, a higher overall variability is observed. Cluster "a" presents the least depleted values, with values ranging from 0.1 to 0.9‰, followed by cluster "b" plotting from -0.9 to -0.1‰. Cluster "d"data fluctuate between -1.2 to -0.7‰, overlapping with the lower end of cluster "b". Cluster "c" comprises ^{18}O depleted values ranging from -2.7 to -1.8‰.

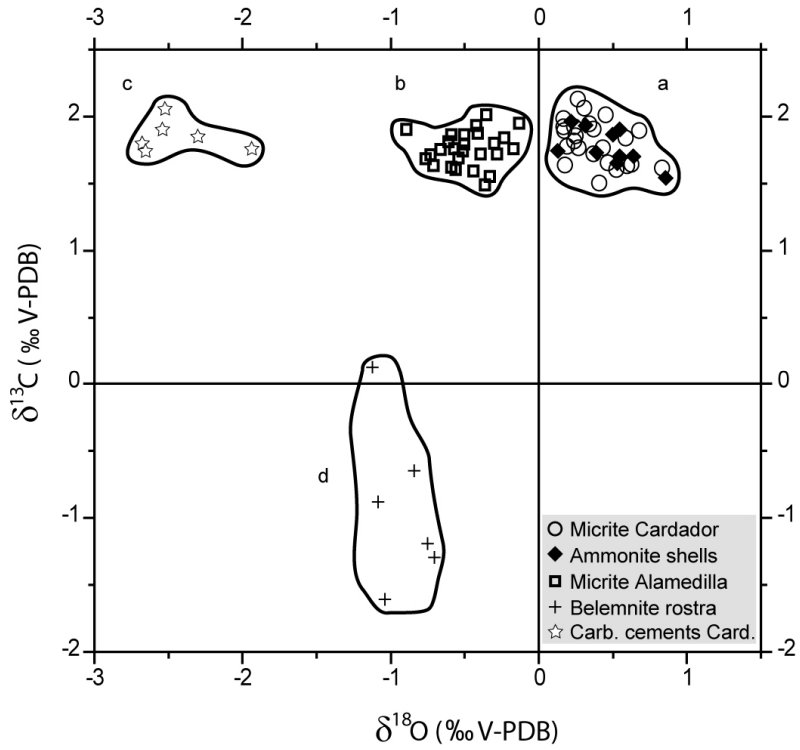

Fig. 3.6- Crossplot of the stable isotope values observed for all the carbonate materials analysed. Group "a" includes matrix micrite from the Cardador section and neomorphic ammonite shells; group "b" represents matrix micrite from the Alamedilla block; group "c" includes carbonate cements from the Cardador section; group "d" gathers data from belemnite rostra. Mean values and standard deviations summarized on Table 3.1.

3.4.3- Elemental composition data

Trace element concentrations are presented in Fig. 3.7A (Table 3.1 for mean values and respective standard deviations). Matrix micrite elemental composition for the Cardador section presents overall lower values when compared to matrix micrite data from the Alamedilla sample containing the ammonites and belemnites analyzed (Table 3.1). At Alamedilla, whilst strontium and magnesium values are only slightly increased, iron and manganese concentrations stand out due to higher values (Fig. 3.7A, up to 4000 and 1500 ppm, respectively). In contrast, background Mn concentration for micrite samples from the Cardador section is around 200 ppm (dashed line "a" in Fig. 3.7A). At this location, local Mn peak values (750 ppm, dashed line b) occur during the lowermost Tithonian and are similar in

range to Alamedilla matrix micrite values. Higher Mn values in Cardador correspond to carbonate cement samples (dashed line "c" in Fig. 3.7A).

Each skeletal material analysed shows characteristic values that conspicuously differ from elemental values obtained for host Alamedilla outcrop matrix micrite. Neomorphic ammonite shells have overall similar Sr and Mg elemental values, but Fe and Mn concentrations increase relative to matrix micrite range in Alamedilla (see Table 3.1 and Fig. 3.7A). Belemnite rostra average values (see Table 3.1 and Fig. 3.7A) show higher Sr (1108 vs. 177 ppm), lower Mg (2848 vs. 4028 ppm) and very low Fe and Mn values (57 vs. 1956 ppm and 74 vs. 744 ppm, respectively) relative to encasing Alamedilla matrix micrite samples.

Strontium abundances plotted against Mn (Fig. 3.7B on the left) show no relation between these two elements, with different carbonate materials plotting within different ranges and clear separation of ammonite shells from belemnites according higher Sr-contents in the latter. When comparing the Sr/Mn ratio with $\delta^{18}O$ variations (Fig. 3.7B on the right) no clear trend is identified, but a comparatively high ratio corresponds to belemnite rostra.

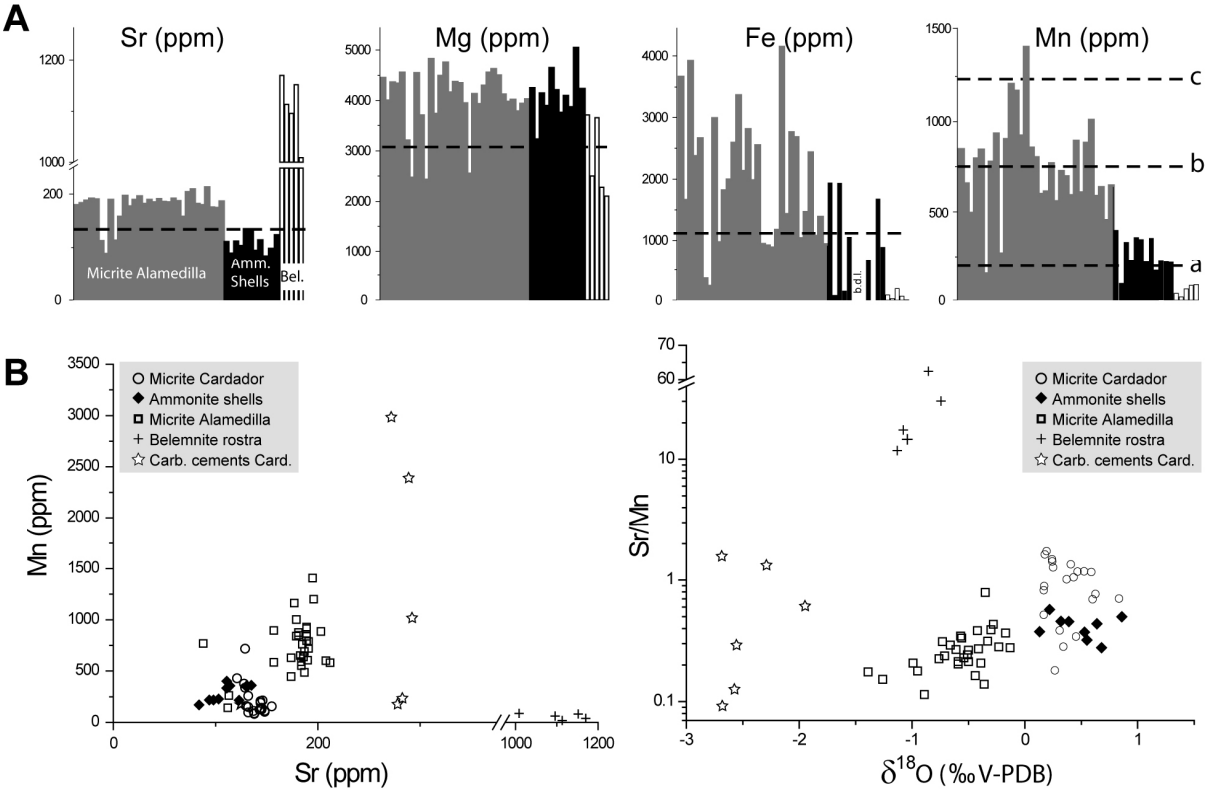

Fig. 3.7- Elemental composition for the carbonate materials studied. A: Absolute concentrations of Sr, Mg, Fe and Mn for micrite from the Alamedilla block, neomorphic ammonite shells and belemnite rostra (b.d.l.- bellow detection limit). Dashed horizontal lines represent mean values for micrite matrix from the Cardador section.

Letters on horizontal dashed lines on the Mn plot designate reference values in the Cardador section for (a) matrix micrite average; (b) maximum matrix micrite Mn peak; (c) carbonate cement average value; see Table 3.1. B: Mn vs. Sr biplot and Sr/Mn ratio vs. $\delta^{18}O$. Note the clustering of each carbonate material on different regions of both plots and the lack of (at least) visual correlation, especially evident for belemnite elemental data.

3.5- Data Interpretation

3.5.1- Ecological remarks

Given controversy and/or variability in the palaeoenvironmental interpretation of isotope and trace element values obtained from biogenic carbonate sources such as cephalopods (mainly but not exclusively belemnites in Jurassic deposits; see below), the following comments serve to show the ecological scenario assumed, in which the data are interpreted.

Ammonite ecology is a long-time discussed topic. Nowadays there is a wide consensus about variable behavior in the water column according with basic shell types (e.g., Westermann, 1996), and colonization of waters showing salinity other than normal marine water has been accepted (e.g., Westermann, 1996; Olóriz and Villaseñor, 2010). According to recent revisions, epioceanic ammonites mainly inhabited upper waters in the range of neritic depths as slow swimmers, specially the longidome and heavy sculptured specimens (e.g., ataxioceratids), and included cases of demersal behavior has been proposed (see Olóriz and Villaseñor, 2010 for extended treatment with references), even for colonizers of fluctuating environments below the wave base (e.g., Paul et al., 2008). Post-mortem transport without biogeographic significance (rare expatriation) has been widely interpreted and experimentally demonstrated as the most common case for Jurassic ammonites (e.g., from Chamberlain et al., 1981 to Olóriz and Villaseñor, 2010 and references therein). Examples of post-mortem drift have been related to the record of epibionts on the ammonite shells, both as intra- and extrathalamous epizoa (e.g., from Seilacher, 1971 to Tintant, 1980, 1983 and more complex treatment in Maeda and Seilacher, 1996), but precise evaluations could be difficult even for present cephalopods (e.g., Dauphin, 1979a, b).

Belemnite ecology is also a controversial issue (e.g., Mutterlose et al., 2010), especially in that concerning the precise interpretation of isotope derived palaeotemperatures since no conclusive data exists about both general and ontogeny related behaviours.

Moreover, the way in which carbon is fixed and the role of metabolism in calcite precipitation is still under discussion (e.g., Podlaha et al., 1998; Williamson, 2006; Rexfort and Mutterlose, 2006, 2009), especially when different taxa are compared (e.g., McArthur et al., 2004). Variable temperatures have been reported from genera of the same age and basin (e.g., from Ditchfield, 1997 to Mc Arthur et al., 2004), and a rather variable ecology and behaviour is being considered for belemnites (e.g., Dutton et al., 2007), which are mainly interpreted as neritic organisms with assumed potential for wide horizontal movements and change of inhabited water masses during ontogeny (e.g., Wefer and Berger, 1991; Doyle, 1992; Huber et al., 1995; Williamson, 2006; Dutton et al., 2007). Palaeoenvironmental factors affecting neritic specimens, including recognition of unfavourable conditions in inner-to-innermost shelves, are far better known than those forcing epioceanic ones, but deposition in and/or colonization of photic depths seaward from epicontinental shelves have been proved (e.g., Combé-Morel and Mariotti, 1986 for lower Tithonian examples). The potential role of deep oceanic waters as ecological barriers has been proposed (e.g., Stevens, 1965) as well as deeper habitats relative to ammonites (Dutton et al., 2007), but these two interpretations could have local rather than general applications. In fact, colonizers of the upper ocean layers could minimize this effect being more dependant of prey distribution, among other ecological factors than effective depth. However, consensus exists about belemnites being good swimmers predators, those showing comparatively slender and longer rostra considered as the closets analogs (i.e., nektonic life style) to present-day coleoids' behaviour, especially pelagic teuthids (e.g., Rexfort and Mutterlose, 2006, 2009; Lewy, 2009; Malkoč and Mutterlose, 2010; Mutterlose et al., 2010). Their predatory behavior in the water column could extend not only to "soft" but also ectocochleate preys (e.g., Klompmaker et al., 2009). Their favoured interpretation as demersal organisms on the basis of comparatively lower temperatures in agreement with those obtained from benthics (e.g., Wierzbowski, 2002; Dutton et al., 2007; Wierbowski and Joachimski, 2009; Price and Teece, 2010) could be forced. In fact, no conclusive data about the potential depth of the thermocline are given, and the water column between the thermocline and the seafloor could show no significant difference in temperature. In addition, examples of belemnites recorded from black shells reinforce their interpretation as pelagic animals (e.g., Rexfort and Mutterlose, 2009; Mutterlose et al., 2010; but see Mitchell, 2005).

3.5.2- Taphonomic and sedimentologic remarks

Data above agree with the scenario of more or less complete ammonite carcasses accumulated on a muddy seafloor, resting exposed for a short time in which shell breaking most probably resulted from impacts and/or biogenic activity (scavengers) as well as from potential corrasion (s. Brett and Baird, 1986) in a low-energy environment (Figs. 3Bc and 4D). Lacking shell imbrications, preferential convex-up orientation of fragments, and relict of sediment lamination and gradation exclude significant environmental energy affecting exposed skeletals. However, burial was a rapid process according to the high potential dissolution of aragonitic shells during long-lasting bottom exposure, and/or hydrothermal activity. This contrasts with averaged sedimentation rates previously calculated (see above), and lacking relevant, pervasive bioerosion. Preservation history can be summarized according to disintegration of potential periostracum, shell puncturing, and fine sediment percolation as well as infilling of the same fine sediment together with small skeletal remains throughout the aperture and sites of local shell collapse (Fig. 3.3B-a, c and d). Selective dissolution occurred (Fig. 3.3B-d). High-energy infilling of shells is not documented (no dense accumulation of skeletals inside shells, in body chambers or phragmocone chambers below sites of collapsed carcasses; e.g., Fig. 3.4D and E). Sedimentation episodes (note burial of centimeter-width shells) preceded very early cementation-lithification (syndepositional cementation most probably occurred) and much later pressure solution phenomena (e.g., stylolites, Fig. 3.3B-e and f), but fossil remains were not affected by sedimentary load (no crushing identified, Figs. 3.3B and 3.4). Therefore, geopetals and no plastic deformation are observed (Fig. 3.3B-c). Occurrence of early cementation agrees with dissolved aragonite and precipitation of Mg-calcite in sediments evolving to rather firm- to stiffground better than strictly soft conditions, after progressing dehydration and microbial degradation of sedimentary organic matter. This early diagenetic pathway is even known from recent Bahamian-type carbonates (e.g., James et al., 2005 and references therein) with potential incidence on carbon isotope signatures in "marine-lake" situations (e.g., De Leeuw et al., 1995), which clearly differs from the case study. No preserved lamination in the sampled block (Fig. 3.1G) could agree with both extensive burrowing of mixed and shallow transitional rather than historical layers (i.e., more cohesive sediment implicating boring but not burrowing). No reworking with biostratigraphic relevance has been identified and, therefore, low-grade time-averaging is assumed clearly

below biostratigraphic resolution. Muddy bottom instability (e.g., seismicity related or unrelated to volcanism) forcing small-scale sliding (potential mud-flows included) capping previous but analogous semi-consolidated horizons is assumed. Alternatively, or complementarily, storms affecting shallower bottoms would export biogenic carbonates (i.e., nepheloid, aragonite-rich "clouds") accumulating as a blanket. On the basis of the above considered, we interpret the combination of rapid burial and cementation preceded by a short-time exposure on the muddy-carbonate sea bottom with possibility for a within-habitat but short necroplanktic transport.

Within-bed orientation of belemnites observed on the sampled block show common azimuthally oriented specimens indicates settling on soft to firm bottoms, and potential mixing (s. Sadler, 1993) by burrowing and/or limited sediment sliding. In addition, preservation of azimuthal orientations accords with small-to-absent effects forced by sedimentary load, which agrees with preservation in volume of ammonite shells, as well as with rapid lithification. In such a case, instable orientation of whatever fossil remains should be better explained by settling on muddy bottoms most probably affected by biogenic, bulldozer activity. Rapid cementation before sedimentary load resulted in avoiding potential compaction with reorientation of ammonite carcasses of greater sizes (above 60-80mm). Given the fine hemipelagic sedimentation, rapid cementation allowing 3D preservation of shells could be triggered by episodes of rapid carbonate sedimentation (hemipelagic ooze or muddy events of deposition) providing importation of "aragonitic waters" from productive areas in seamount tops (see above) better than sourced from the occurrence of highly packed, shelly horizons (e.g., Tomašových and Schlög, 2008).

At present, Late Jurassic carbonate factories related to volcanic highs in the Median Subbetic Trough can only be macroscopically deduced from local records of consumers as those of dense packed shelly horizons showing high mortality of small bivalves (coquina beds) together with less abundant brachiopods and crinoids (Comas and Olóriz, 1986). However, the precise type of carbonate producers is not clear. In contrast to the Florida-Bahamian type factory which was active during the Middle Jurassic in the area (e.g., Vera et al., 1997) a mud-mound type factory (e.g., Schlager, 2003) for the case study could better adapt to the absence of evidence for significant oolitic sediments in a low-energy but potentially more mesotrophic environment due to the combination of huge bottom topography, related currents and volcanic activity.

3.5.3- Cathodoluminescence imaging

Cathodoluminescence imaging of matrix micrites from the two studied localities (Cardador and Alamedilla; Fig. 3.1) reveal orange bright luminescence with somewhat more intense luminescence for samples from the Alamedilla outcrop. Secondary blocky calcite (Fig. 3.5B) presents an alternating pattern between intrinsic and yellow luminescence (zonation). This implies cement precipitation or alteration under shallow marine burial conditions (Bruckschen and Richter, 1994). Skeletal material is characterized by intrinsic luminescence (Figs. 5F and H), suggesting low diagenetic overprint. Within the limitations of this method, the intrinsic luminescence of skeletal calcites might point to a relatively well-preserved carbonate material that is potentially suitable for palaeoenvironmental reconstructions. Analysis under SEM evidenced good preservation of common coccoliths attesting for limited alteration of matrix micrite at both locations (Fig. 3.4M to O; see Coimbra et al., 2009 for the Cardador section).

3.5.4- Carbon isotope data

Carbon isotope values for matrix micrite, neomorphic ammonite shells and secondary blocky calcite from the Cardador and Alamedilla localities plot within the same range of values. The data obtained are comparable to published results from other Tethyan margin settings (Joachimski, 1994; Jenkyns, 1996; Weissert and Mohr, 1996; Bartolini et al., 1996) that were considered to reflect late Jurassic seawater carbon isotope composition by most authors. Pervasive meteoric influence and diagenetic resetting of these isotope values is therefore tentatively excluded (Lohman, 1987; Allan and Mathews, 1992) in absence of co-variation of $\delta^{18}O$ and $\delta^{13}C$ (e.g., McArthur et al., 2004; Mutterlose et al., 2010). Potential influence of low salinity water forcing low values in these ratios (e.g., Podalha et al., 1998) seems to be less probable within the epioceanic environment. Belemnite rostra $\delta^{13}C$ values are depleted by as much as 3.8‰ relative to host matrix micrite. This observation merits attention as low-Mg belemnite data are commonly considered to be relatively conservative carbonate archives (Mutterlose and Wiedenroth, 2008), notwithstanding being metabolically mediated during cephalopods ontogeny, especially in those experiencing rapid growth (Rexfort and

Mutterlose, 2006, 2009). Potential explanations for deviations from the isotopic signal of the surrounding seawater during calcite precipitation include the presence of isotopically light organic carbon from decaying organic tissue in the intraskeleton of the belemnite, or fractionation of seawater $\delta^{13}C_{DIC}$ due to metabolic processes, out of equilibrium precipitation (Price and Page, 2008; Price et al., 2009). This may imply that, in the specific cases analyzed, belemnite rostra should be considered as a less reliable archive relative to encasing matrix micrite data. Lines of evidence include metabolic processes as recently reported in Rexfort and Mutterlose (2009) and Malkoč and Mutterlose (2010), water masses influenced by continental runoff and uncoupled from open sea hydrodynamics (e.g., Price and Teece, 2010), warmed water masses (e.g., Williamson, 2006) and diagenetic alteration (Immenhauser et al., 2003; Dutton et al., 2007), all of which resulting in $\delta^{13}C_{belemnite}$ depletion when compared with matrix micrite. The most reliable evaluations arise from combined interpretations along with oxygen isotope and trace elements values.

3.5.5- Oxygen isotope data

Oxygen isotope ratios analyzed display a wide range but cluster into specific domains for each carbonate material analyzed (Fig. 3.6). According to previous work (Coimbra et al., 2009) matrix micrite from the Cardador section preserved a near-seawater isotopic composition due to early stabilization and lithification resulting in nodular structure under the influence of marine porewater. When compared to matrix micrite data from the Alamedilla block sample, the observed 1‰ offset in $\delta^{18}O$ is probably related to slightly warmer bottom waters (4ºC or slightly less per 1‰ shift in $\delta^{18}O$; Marshal, 1992 and McArthur et al., 2004, respectively).

Late blocky calcite presents the most depleted values in the data set, which is interpreted as resulting from comparatively elevated temperatures of burial fluids (e.g., Mitchell et al., 1997). Ammonite neomorphic shells and belemnite rostra are characterized by primary aragonite and low-Mg calcite mineralogies, respectively. It seems most likely, that different skeletal compositions may undergo differential diagenetic pathways, which can be inherited from differential palaeoenvironments and/or palaeoecology (e.g., Wierzbowski, 2002, McArthur et al., 2004, Joachimski, 2006 and Mutterlose, 2010 for information including belemnites). If this holds true, then different $\delta^{18}O$ patterns are expected to result.

3.5.6- Elemental composition

Matrix micrite samples from the Cardador and Alamedilla localities (Fig. 3.1) do not present the same elemental distribution. At the Alamedilla outcrop, matrix micrite shows only slightly higher Sr, but higher Mg and Fe and a striking Mn enrichment. In the case of significant diagenetic overprint of carbonate materials, elemental enrichment in Fe and Mn would be expected (e.g., Podlaha et al., 1998; McArthur et al., 2004; Williamson, 2006; Dutton et al., 2007; Schneider et al., 2009; Wierzbowski and Joachimski, 2009). But in such case, the inverse trend should be recorded for both Mg and Sr (e.g., Veizer, 1983), which is not verified at the Alamedilla outcrop. Localized elemental enrichment, especially evident on manganese concentration has been commonly attributed to regional hydrothermal/volcanic activity (Milliman, 1971; Shanmugam and Benedict III, 1983; Kickmaier and Peters, 1990; Corbin et al., 2000). In our case, elemental enrichment in Alamedilla due to hydrothermal/volcanic activity is supported by the geological context and will therefore be interpreted as an environmental signature, rather than a latter diagenetic imprint.

Neomorphic ammonite shells elemental abundances are in agreement with those analyzed in host matrix micrite (Alamedilla block sampled) with the exception of lower Fe and significantly lower Mn concentration. The notable Mn-deviation is perhaps best explained by differential mineralogic stabilization. Similar Sr concentrations for neomorphic ammonite shells and encasing Alamedilla matrix micrite is a feature that may relate to mineralogical stabilization from original aragonite into neomorphic calcite during early diagenesis (e.g., Munnecke and Samtleben, 1996). In fact, all extant mollusc shells provide high Sr content (e.g., Price and Teece, 2010), and selective lower Sr values in calcitic fossils are expected from diagenetic overprint (e.g., Veizer et al., 1999; Schneider et al., 2009), except for places with high-Mg content related to distorted calcitic frames (e.g., Wierzbowski and Joachimski, 2009). According to earlier and preferential dissolution of aragonitic- vs. HMC-shells (e.g., Munnecke and Westfall, 2005), ammonite shells would contribute with trace elements to porewaters and then to limestone cementation very early during diagenesis (i.e., a rather open system in correspondence with low clayey content of limestones). Note that less than 20% in aragonite content triggers carbonate redistribution and differential diagenetic pathways (e.g.,

Munnecke et al., 2001), and that contrasting abundances of Sr and Mg deduced from Fig. 3.7A indicate limited diagenetic overprint in ammonite shells from the Alamedilla outcrop.

Theoretic demonstrations of such elemental mobilizations can be gained from Veizer (1983) and Tucker and Wright (1990). For original skeletal aragonite with Sr concentration of 9000 ppm and high-Mg calcite with 1200 ppm (precipitated in equilibrium with seawater) the resulting stabilized low-Mg calcite is 350 ppm for the aragonitic precursor and 150 ppm for high-Mg calcite precursor (2:1 ratio). Hence, average values of 106 ppm for ammonite shells and 177 ppm for surrounding micrite do not seem to record the previous ratio. This evidence is consistent with dissolution/reprecipitation occurred in a somewhat open pore system, flushing Sr into the surrounding sediments. This elemental supply from aragonite dissolution would contribute to a faster lithification and result in a homogenization of Sr values in both materials: neomorphic ammonite shells and encasing matrix micrite. This mechanism would also imply contribution of all other aragonitic sources embedded in the matrix, apart from the studied ammonite shell.

Belemnite rostra present elemental concentrations that can be directly compared with those published from well preserved coeval rostra for a relative close area in the eastern palaeomargin of Iberia (e.g., Price and Sellwood, 1994), and are within the ranges of assumed good preservation for belemnites in different settings and Mesozoic ages (e.g., Anderson et al., 1994; Ditchfield, 1997; McArthur et al., 2004; Williamson, 2006; Price and Rogov, 2009; Schneider et al., 2009; Price and Teece, 2010), except for cases of very low Mn-contents (e.g., Mn<25 ppm in McArthur et al., 2004). Hence, cut-offs values applied for interpreting good preservation are Mg<5.000 ppm, Sr>800-1.000 ppm; Fe<100 ppm; Mn<100 ppm. Concentrations of Mn and Fe plot with the range of pristine to near-pristine elemental concentrations (Voigt et al., 2003; Nunn et al., 2009; Price, 2010) except for Fe in one small sample (191 ppm) that could be close to the belemnite apex and potentially overprinted by diagenesis or, alternatively, considered compatible with good preservation (e.g., McArthur et al., 2004; Price and Teece, 2010). Strontium concentrations are very close to the cut-off values proposed by Wierzbowski and Joachimski (2007) rather than Wierzbowski and Joachimski (2009). Manganese and Fe concentrations plot outside the range of well-preserved material as proposed by these authors that provide examples of extremely low values compared with those accepted by other authors (citations above). Care must be taken to not overrate these geochemical screening approaches. The combination of limited knowledge

about metabolic processes and/or palaeoecology (short-term and ontogenetic behaviour included) in extinct life forms (here belemnites) make this approach debatable (e.g., Brand and Veizer, 1980; Ditchfield, 1997; Wierzbowski, 2002; Brand et al., 2003; McArthur et al., 2004; Rexfort and Mutterlose, 2006, 2010; Dutton et al., 2007; Wierzbowski and Joachimski, 2009). Nevertheless, within the limitations of this approach, it is suggested that elemental values of belemnite rostra point to rather well preserved material.

3.6- Discussion

The data set suggests a particular diagenetic setting that deserves attention focused on interplaying factors of which the two dominant ones are addressed. These are: (i) Differences in environmental parameters and diagenetic pathways in two spatially separated settings (study localities near Cardador and Alamedilla); and (ii) differential carbonate mineralogy of matrix micrite, neomorphic ammonite shells and belemnite rostra.

3.6.1- Palaeogeography and diagenetic setting

Micrite matrix from Cardador and Alamedilla localities present geochemical differences that may, at least to some degree, relate to differential palaeogeographic settings. The Cardador section corresponds to a more distal swell, characterized mainly by open oceanic conditions. The palaeogeographic setting of the Alamedilla outcrop corresponds to active areas in a relative high, the Mid-Subbetic Volcanic Ridge, rising from a trough lined by pelagic swells (Fig. 3.2). Thus, two local and clearly different contexts are envisaged for respective water columns and water-sediment inter-phases, the latter determining typical processes associated to sedimentary maturation (s. Sadler, 1993).

Accepting the shortcomings of this approach, oxygen isotope values point to a relative difference in bottom water temperatures in the order of about 4ºC between the two localities, with higher temperatures found in the Alamedilla outcrop. This difference is in agreement with the notion of a standard open marine environment for the Cardador section, resulting in cooler bottom water masses. In contrast, the vicinity of hydrothermal/volcanic sources would contribute to warmer bottom waters at the Alamedilla locality.

Reconstructing the precise palaeoceanographic setting of both study sites is difficult due to limited knowledge of Jurassic ocean dynamics and particularly so when relatively minor regional variations are considered. Nevertheless, lessons learnt from present day settings suggest that even moderate hydrothermal influence may account for the observed differences. At the Mid-Atlantic Ridge, for example, low temperature hydrothermal activity results in a locally elevated seawater temperatures (up to 7ºC), comparing to adjacent bottom seawater (Dias and Barriga, 2006). Combined with locally elevated seawater temperatures, elemental enrichment of sediments is also registered and attributed to hydrothermal activity, namely Mg, Fe and Mn (Dias and Barriga, 2006). Similar cases of local hydrothermal activity with Mn enrichment are not uncommon and are also recognized from ancient records (Milliman, 1971; Shanmugam and Benedict III, 1983; Kickmaier and Peters, 1990; Corbin et al., 2000). Interestingly, most of these examples show very similar geochemical patterns as those found at the Alamedilla outcrop, located at the vicinity of a hydrothermal source, and conspicuously different in elemental composition and isotopic values from those obtained at the Cardador section.

Cathodoluminescence imaging of matrix micrite also shows distinct degrees of orange luminescence, attributed to relative abundance of manganese (see above), in this case due to hydrothermal contamination. Considering the differences in Mn concentration obtained for both studied sites (200 and 744 ppm for the Cardador section and Alamedilla outcrop, respectively) the brighter orange luminescence of Alamedilla matrix micrite, relative to Cardador, is in good agreement with the measured geochemical properties (Figs. 5 and 7).

In summary, both oxygen isotopic and elemental patterns are in good agreement with localized hydrothermal activity at the Alamedilla sector, and luminescence imaging support this notion. Assuming that differences in micrite oxygen-isotope values are at least in part related to differences in seawater temperature, localized hydrothermal activity is a reasonable explanation for the observed pattern. Differences in water mass temperatures between the two study sites are envisaged but difficult to quantify with precision.

3.6.2- Metastable carbonate materials and paragenetic succession of diagenetic events

Carbonate materials analysed reflect a range of primary carbonate mineralogies including low-Mg calcite belemnite rostra (e.g., Veizer, 1983), assumed high-Mg calcite

composition for micrite matrix nodules (e.g., Milliman and Müller, 1973; Jenkyns, 1974; Mullins et al., 1980; Cecca et al., 1992) and aragonitic mineralogy of ammonite shells (see above). It is well known that diagenesis will lead to Mg-loss of magnesian calcites and replacement of aragonite by low-Mg calcite mineralogy (Brand and Veizer, 1980; Veizer, 1983). Stabilization timing and associated open system fluid dynamics will crucial. Whereas metastable aragonite and magnesian calcite stabilize under the presence of near-marine porewater, later diagenetic stages (deep marine burial and/or late meteoric diagenesis) may affect all carbonate materials, including primary low-Mg calcite.

As laid out above, cathodoluminescence imaging and geochemical data reject pervasive late burial or late meteoric diagenesis (Coimbra et al., 2009). In contrast, all lines of evidence point to an early diagenetic, open system stabilization of nodular limestones under marine porewater conditions (Coimbra et al., 2009). Hydrothermal influence, evident at the Alamedilla area, is supported by $\delta^{18}O$-depleted values and notable elevated manganese concentrations leading to brighter orange luminescence.

Remarkably, neomorphic ammonite shells encased on Alamedilla matrix micrite do not share geochemical signal of their encasing sediments. In contrast, $\delta^{18}O_{ammonite}$ is similar to that of the Cardador matrix micrite, displaying no manganese enrichment accompanied by dark intrinsic luminescence. Clearly, this pattern must be interpreted in the context of the timing and environment of aragonite stabilization relative to lithification of the host matrix micrite. Metastable ammonite aragonite was dissolved and re-precipitated/re-crystallized as low-Mg calcite early during diagenesis. Given the highly unstable aragonite mineralogy, this mineral inversion took place prior to surrounding micrite stabilization (Fig. 3.8A1 and A2). Similar diagenetic patterns have been described before. Price and Sellwood (1994) interpreted very early diagenetic stabilization of aragonite to low-Mg calcite in neomorphic ammonite shells where calcite re-precipitation occurred in close equilibrium with seawater as proved by $\delta^{18}O$ values close to those obtained from well preserved belemnites. Maliva (1995) reported a $\delta^{18}O$ composition of modern neomorphic calcite from the Great Bahama Bank similar to marine porewater values. Hendry et al. (1995) suggested early diagenetic stabilization for Jurassic aragonitic bivalve shells. Brachert and Dullo (2000) presented evidence for modern aragonitic skeletal components that were diagenetically stabilized prior to the lithification of the host sediment.

A possible paragenetic model summarizing the observed geochemical and mineralogical patterns is illustrated in Figure 3.8. During early marine diagenesis (Fig. 3.8, A1 to C1 and A2 to C2) inversion of skeletal aragonite (ammonite shells) into low-Mg calcite is the first mineralogic stabilization taking place on the inmature sedimentary column (Fig. 3.8B1 and B2).

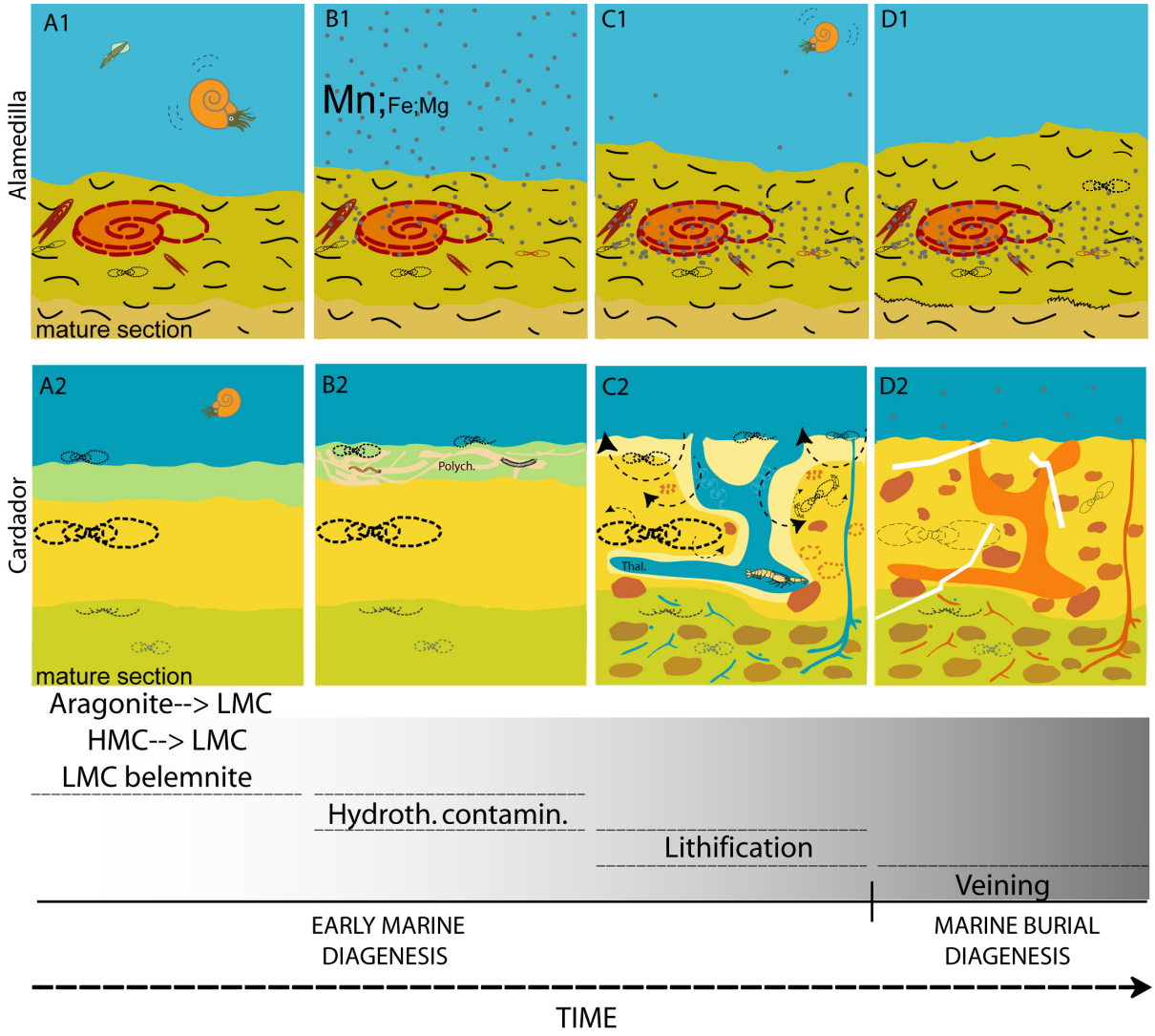

Fig. 3.8- Diagram showing a possible paragenetic pathway at the Alamedilla locality (A1 to D1) and the corresponding one for the Cardador section (A2 to D2). A1 and A2: Respective background marine conditions, in which skeletal aragonite is stabilized into neomorphic calcite; belemnite rostra original mineralogy is maintained (low-Mg calcite- LMC) and High-Mg calcite is stabilized into Low-Mg calcite. B1: Hydrothermal contamination increases Mn concentrations in seawater, flushed into the sediment. B2: No evidences of hydrothermal contamination are observed during this stage, and the uppermost sediment layer is disturbed by polychaetes cohorts (assumed with no influence as figurative trace fossils). C1: Manganese enriched layer is covered by more recent sediment, incorporating hydrothermal Mn on early lithified micrite. C2: Incipient

nodule formation takes place, with Thalassinoid boring enhancing water pumping and irrigation. D1 and D2: No late veining is observed on Alamedilla samples (D1) while veins and fractures occurring during an early burial stage in the Cardador section (D2) are filled with secondary blocky calcite, the only features showing Mn enrichment.

Belemnite rostra, with a more stable mineralogy (see below) preserve their pristine state (Fig. 3.8A1 to D1). Hydrothermal contamination of seawater spreads into the sediment via porewater circulation, strongly affecting the geochemistry of Alamedilla sediments due to proximity of hydrothermal sources, the Mid-Subbetic Volcanic Ridge (Fig. 3.8B1). Alternatively, bottom instability may have occurred between stage A1 and B1 (not represented in Fig. 3.8) during local physiographic reconfiguration related to volcanic/hydrothermal activity –stage B1. Only materials stabilized after stage B1 will incorporate high manganese concentrations and reflect higher temperature (Fig. 3.8 C1). Incipient lithification during warmer porewater conditions occurred at Alamedilla, and nodule formation at Cardador, occurred with no record of thermal influence during this stage in the Cardador section (Fig. 3.8C2). Later during marine diagenesis veining was registered at Cardador (Fig. 3.8D2), filled by secondary blocky calcite showing a very distinct geochemical signature when compared to materials only affected by early marine diagenesis (Figs. 3.6 and 3.7). In the equivalent stage in Alamedilla only pressure-solution phenomena have been recognized (stylolite formation; Fig. 3.8D1).

Belemnite rostra, may or may not undergo mineralogical stabilization into diagenetic low-Mg calcite (Veizer, 1983) and generally are less prone to compositional and structural changes, although no strict lineal relationships exist in belemnite preservation and diagenesis (e.g., Podlaha et al., 1998). For this reason, belemnite rostra are widely used for palaeoenvironmental reconstructions (e.g., Price and Sellwood, 1994; Saelen et al., 1996; Podlaha et al., 1998; Jenkyns et al., 2002; Wierzbowski, 2002; Voigt et al., 2003; Rosales et al., 2004; McArthur et al., 2007; Price, 2010). Belemnite rostra from the Alamedilla outcrop present intrinsic luminescence, representing optical evidence of minor diagenetic overprint. Belemnite $\delta^{18}O$ is depleted relative to that of the host micrite but this differential oxygen-isotopic signature is probably to a large degree a primary one (see above). Matrix micrite is lithified on the marine floor, and when well preserved, may reflect porewater temperature and chemistry. In contrast, belemnites are nektonic organisms known to migrate vertically (and laterally) on the water column, recording different isotopic compositions during ontogeny

(e.g., Rexfort and Mutterlose, 2006, 2009; Price and Page, 2008; Wierzbowski and Joachimski, 2009; see discussion in Immenhauser et al., 2008 and revision in Mutterlose et al., 2010). Applying the palaeotemperature equation of Anderson and Arthur (1983), with $\delta_{seawater}$ between -1 and +0.5‰ SMOW according to Shackleton and Kennet (1975), belemnite $\delta^{18}O$ point to seawater palaeotemperatures of 16 to 22ºC. Nevertheless, when compared to host matrix micrite, their warmer palaeotemperatures evidence shallower (nutrient rich) waters, clearly differentiating between upper and bottom water masses.

In summary, differences in geochemical signatures from the distinct studied carbonate materials relate to relative mineralogical stability. Hydrothermal contamination in Alamedilla provides a geochemical timeline, allowing the establishment of a paragenetic sequence. Well preserved belemnite rostra owe their signature to differences in water masses, reflecting shallower depths than those corresponding to their encasing matrix micrite.

3.7- Conclusions

Petrographic and geochemical data from five different Tithonian carbonate materials are presented and interpreted in a process-oriented context. Overall fair preservation was demonstrated for matrix micrite from both studied sites (Cardador and Alamedilla) and also for neomorphic ammonite shells and belemnite rostra encased on Alamedilla matrix micrite. Latter carbonate cements provide the only record of more pervasive diagenetic overprint.

The overall fair degree of preservation of primary geochemical signals allow for the distinction of two specific palaeogeographic settings. Geochemical signatures from the Cardador section are considered to reflect cooler, bottom seawater masses. By comparison, the Alamedilla outcrop data are characterized by elevated seawater palaeotemperatures and pronounced higher manganese concentrations, indicative of a nearby hydrothermal source.

A relative paragenetic succession for the mineralogical stabilization of the studied materials is proposed. Aragonitic ammonite shells were probably neomorphized prior to lithification of the surrounding sediments, recording early marine porewater conditions.

Acknowledgements

We wish to thank Dieter Buhl, Ulrike Schulte, Beate Gehnen and Noushin Arshadi (Ruhr-University Bochum-RUB) for their collaboration during measurements; Rolf Neuser (RUB) for the cathodoluminescence

analysis and SEM inspection; Matthias Born (RUB) and Alberto Montes (University of Granada) for the preparation of thin sections. Adrian Immenhauser (RUB) is thanked for to the help in improving earlier text versions. This research was supported by Projects CGL2005-01319 and CGL2008-05251-E (MICINN) and the Research Group RNM-178 Junta de Andalucía, Spain.

4

Spatial geochemistry of Upper Jurassic marine carbonates (Iberian Subplate)

R. Coimbra [(a)], A. Immenhauser [(b)], F. Olóriz [(a)]

[(a)] Departamento de Estratigrafia y Paleontologia, Universidad de Granada, Spain

[(b)] Institute for Geology, Mineralogy and Geophysics, Ruhr Universität Bochum, Germany

Submitted to Journal of Sedimentary Geology (August 2011)

Abstract

Chemostratigraphy applied to ancient marine carbonates is often based on one-dimensional (stratigraphic) sections or core-material. As demonstrated from modern oceans, this approach probably underestimates the spatial complexity of physico-chemical seawater properties. Here, the results of a several-hundred-kilometer long geochemical transect, ranging from the neritic middle shelf to settings in the epioceanic fringe across the south and eastern paleo-margins of the Iberian sub-plate are documented. Seven Upper Jurassic sections are analysed for their sedimentologic, stratigraphic and geochemical records. The comparison of the isotopic and elemental data from different carbonate materials (matrix micrite, carbonate cements, belemnite rostra and neomorphic ammonite shells) sheds light on differential diagenetic pathways. Epioceanic (distal) matrix micrite geochemical data represent reasonable proxies for paleo-seawater properties. In contrast, the coeval epicontinental (proximal) record shows a higher level of complexity including the potential admixture of marine, continental and diagenetic geochemical signals. Epioceanic sections are characterized by a carbon-isotope stratigraphy that is in agreement with Upper Jurassic reference sections from northern Tethyan margins. Oxygen isotope ratios are ^{18}O-enriched relative to those previously reported for equivalent deposits, a pattern consistent with early diagenetic porewater stabilization. Tentatively using $\delta^{18}O$ as proxy for paleo-seawater temperatures across the transect investigated, the results obtained are in agreement with increasing distance from shore, inferred depth variations and/or hydrodynamics and probably reflect local forcing factors. Of particular significance is the relationship between punctuated isotope ($\delta^{18}O$), elemental (Mn) and skeletal content shifts placed against relative sea-level changes. Overall, the record agrees with global and regional patterns. Local deviations in chemostratigraphy are traced back to site-specific changes in paleoceanographic parameters, as based on case examples from ancient and modern oceans. The data set shown here is of relevance for those concerned with the spatial chemostratigraphy in Mesozoic oceans.

♦ ♦ ♦

4.1-Introduction

The record of Earth's climate and changes in marine seawater properties through geological time is largely based on evidence provided by a wide range of proxies, usually lithofacies, fossil assemblages or geochemical information (e.g., Veizer et al., 1999; Cicero and Lohmann, 2001; Dromart et al., 2003; Immenhauser, 2005; Katz et al., 2005; Sellwood and Valdes, 2006; James and Austin, 2008). In Earth sciences, one-dimensional, stratigraphic geochemistry from a given section or core, or an averaged "composite curve" from several localities is commonly the favoured approach (e.g., Weissert and Erba, 2004; Dera et al., 2011). This stratigraphic perspective assumes that changes in seawater properties - and hence the geochemical proxy record of these changes - take place in site and time. Whilst the validity of time-series data sets is not questioned here, modern oceans clearly show that water masses are organized in a complex, three-dimensional manner and changes in physico-chemical seawater properties take place both in space and time (Astraldi et al., 2002; van der Kooij et al., 2009; Cardin et al., 2011). Moreover, in near-coastal settings or in shallow epeiric seas, local parameters intermingle with regional or global ones, usually through relative sea-level forcing and climate change driving changes in continental runoff (Holmden et al., 1998; Fanton et al., 2002; Panchuk et al., 2005, 2006; Dopieralska et al., 2006; Immenhauser et al., 2008).

Oceanographers deal with spatial records of marine dynamics at all scales, from global latitudinal distribution of chemical elements in marine sediments, to for example the distribution of calcium carbonate in Atlantic Ocean surface sediments (Chester, 2000). The connection between vertical and lateral structuring of water masses and other oceanic system components has significantly improved the knowledge of modern ocean dynamics (Cacho et al., 2000; Gutjahr et al., 2010; Voelker et al., 2010). On a smaller scale (e.g., Great Bahamas Bank), the complexity of proximal-to-distal transects has been demonstrated (Swart and Eberli, 2005; Turpin et al., 2008). Interpreting the spatially complex architecture of oceanic water masses from the proxy record of ancient carbonates and adding (stratigraphic) changes with geologic time remains a challenging – and at present underexplored – research area. The inherent incompleteness of the stratigraphic record (e.g., Wetzel and Allia, 2000; El Kadiri, 2002; Dogan et al., 2006; McLaughlin et al., 2008), diagenetic alteration (Dickson and

Coleman, 1980; Cicero and Lohman, 2001), and the lateral discontinuity of facies belts commonly limits attempts to separate signals from noise (Bhattacharya, 2011).

Regarding Jurassic times, detailed paleo-climatic interpretations have been proposed by several authors (Hallam, 1993, 2001; Abbink et al., 2001; Gröke et al., 2003; Cecca et al., 2005; Dera et al., 2009). Still, links between driving mechanisms and related climatic changes are less than clear (Hallam, 2001; Sellwood and Valdes, 2006). On a larger scale, modelling has provided useful latitudinal information. Some examples include Boreal/Tethyan water mass characterization and general climate inferences (Hallam, 2001); latitudinal characterization of ocean temperature in relation to upwelling influence (Gröcke et al., 2003; Muttoni et al., 2005); or the establishment of latitudinal climate belts based on sediment and fossil records (Hallam, 1993).

In an attempt to test Upper Jurassic micrites as archives of the potentially complex three-dimensional organization of paleo-water masses, seven sections from the Iberian sub-plate (Spain and Portugal) have been investigated for their sedimentological, stratigraphic and geochemical records. As a pre-requisite for spatial characterization of a mixed carbonate-siliciclastic platform and adjacent seaward deposits, a well-established biochronostratigraphic control based on ammonites was available (Olóriz, 1978; Marques, 1983; Marques and Olóriz, 1989a, b; Cariou et al., 1997; Geyssant, 1997; Hantzpergue et al., 1997; Caracuel and Olóriz, 1998; Olóriz et al., 2002a,b). This allowed for a biochronostratigraphic correlation of spatially separated sections across different depositional environments and lithofacies types

The aims of this paper are to (i) present a detailed Late Jurassic geochemical seawater record from seven spatially separated sections in Southern Iberia forming a several-hundert-kilometer long proximal-to-distal transect; to (ii) interpret and separate transect-wide spatial and temporal variations of paleo-seawater properties (signals) from local and diagenetic (noise) features; to (iii) compare and contrast these data against published coeval records.

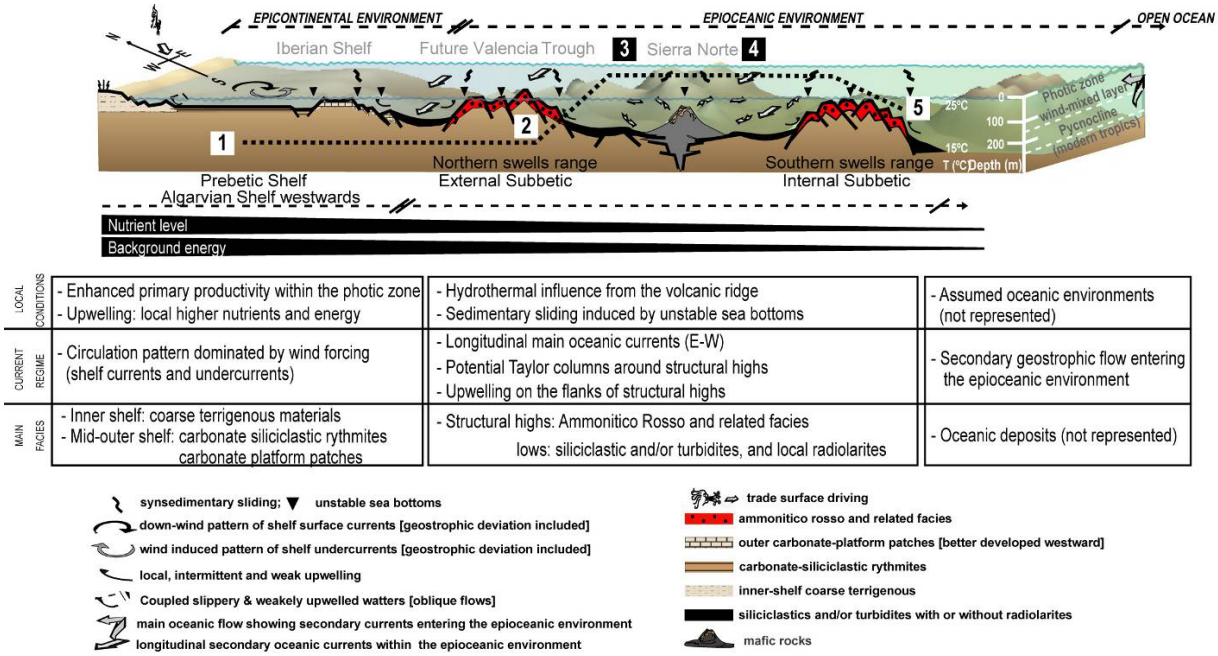

Fig. 4.1- Composite schematic representation of the south and eastern Iberian paleo-margins showing assumed location of the studied sections (1 to 5) and major paleo-environmental factors parameters during deposition (adapted from Olóriz, 2000).

4.2- Regional setting and study areas

4.2.1.-Regional setting

Studied areas located in Southern Iberia (Spain and Portugal) and Majorca Island provided carbonate samples from the External Zones of the Betic Cordillera (Fig. 4.2A; see Olóriz et al., 2002a, Vera et al., 2004 and references therein for regional geology and detailed stratigraphy).

During the Late Jurassic the south-eastern Iberian margin was an unstable area, affected by relative movements between the Iberian and African plates (Fig. 4.3A) along the Maghrebian-Gibraltar Transform Zone – an extensional-transtensional margin closely linked to the geodynamic history of the central-north Atlantic Basin and the westernmost Tethys. As part of the NW Tethyan Margin (Figs. 4.1 and 4.3A), the physiography of south-eastern Iberia resulted in differentiation of two major paleogeographic areas: a more proximal, within a wide epicontinental shelf-system – the Prebetic zone and NE equivalents – and a more distal

fringe, along the epioceanic realm – the Subbetic zone and lateral equivalents (Figs. 4.1, 4.2 and 4.3A).

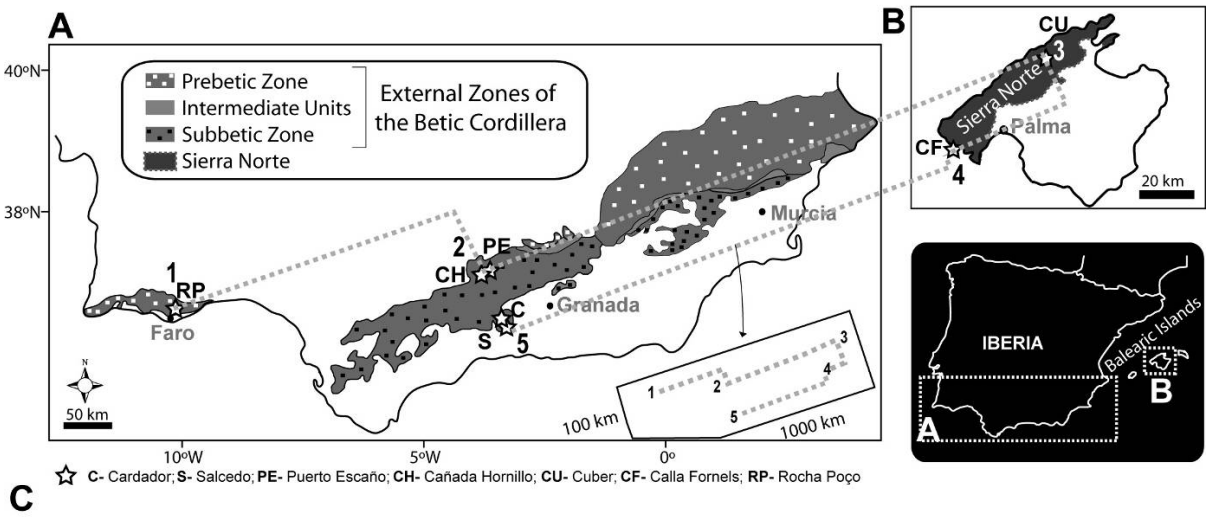

	Section	Stratigraphy	Thickness	Main lithofacies	References
Proximal	1	Kimmeridgian	60 m	- Silty marly-limestones and marls; - Sponge bioherms overlain by cherty limestones.	Marques 1983, 1985 Ramalho 1988
Relative distance from shore	2	Late Jurassic	10 m 9 m	- Nodular Ammonitico Rosso limestones interbedded with marly limestone levels and marls. - Recurrence of more calcareous Ammonitico Rosso.	Olóriz et al. 2002 Coimbra et al. 2009
	3	Oxf. - Tithonian	20m+ 40m Aum.	- Nodular marly limestones alternating with more wavy-platy limestones (ocasional cherty horizons); - Aumedrá Formation: brown, wavy-platy macrofossil poor limestones; - Bioclastics horizons and reworking.	Alvaro et al. 1989 Caracuel and Olóriz 1998
	4	Oxf. -Lower Tith.	9m + 5m Aum.		
Distal	5	Late Jurassic	11 m 13 m	- Nodular Ammonitico Rosso limestones interbedded with more or less marly levels; - Recurrence of more calcareous banks.	Olóriz et al. 2002 Coimbra et al. 2009

Fig. 4.2- Regional distribution of geological units along the studied areas: **A)** Southern Iberia. **B)** Majorca Island (adapted from García- Hernández et al., 1980 and Caracuel and Olóriz, 1999). Stars indicate locations of studied sections (note key to abbreviations for sections studied). **C)** Main oceanographic, bathymetric and sedimentological parameters of studied sections with indication of sources used.

The Balearic Archipelago (Figs. 4.1, 4.2B and 4.3A) has been interpreted as north-eastern extension of the Betic Cordillera (the Betic-Balear Domain in Fontboté et al., 1990). Pre-Cenozoic paleogeography and features in the Jurassic series have been noted; promoting differential interpretations including its understanding as a particular segment in the north–eastern extreme of the Betic Cordillera in correspondence with the eastern Iberian paleomargin during Jurassic times (see Olóriz et al., 2002a for references). Studied sections at the Majorca Island belong to the Sierra Norte domain (see Alvaro et al., 1984; 1989 and

Caracuel and Olóriz, 1998 for regional geology and detailed Upper Jurassic stratigraphy). The location of each section and the respective bio-chronostratigraphic range, thickness, main lithofacies and references for more detailed descriptions are presented in Figs. 4.2 and 4.3.

The erosion of coastal zone deposits in the area counterbalance potential limitations of ammonite biochronostratigraphy in inner-shelf settings. This study includes neritic depths (< 60 m) from the middle shelf seawards to the epioceanic fringe (ca. 250 m) according to assumed preferred habitat depths for ammonites and sponge buildups (Fig. 4.1; Olóriz et al., 1996; Olóriz et al., 2003a; Olóriz and Villaseñor, 2010).

4.2.2- The epioceanic setting

In Southern Spain and the Island of Majorca, six (out of seven) studied sections (Figs. 4.1 through 4.3) belong to the Subbetic Zone and lateral equivalents in the distal, epioceanic setting. The Cañada del Hornillo, Puerto Escaño and Cuber sections represent an intermediate position from proximal to distal and correspond to the External Subbetic (Figs. 4.1 through 4.3). The Cala Fornells section (Figs. 4.1, 4.2B and 4.3) holds a similar, albeit somewhat more distal position compared to the Cuber section in tectonic-sheet IV of Álvaro et al. (1984) according to differential compression and shortening (Gelabert et al., 1992) in the piggy-back thrust-system of the Sierra Norte or Serra de Tramuntana in the Majorca Island. The most distal sections are those of Cardador and Salcedo belonging to the Internal Subbetic Zone (Figs. 4.1, 4.2A and 4.3).

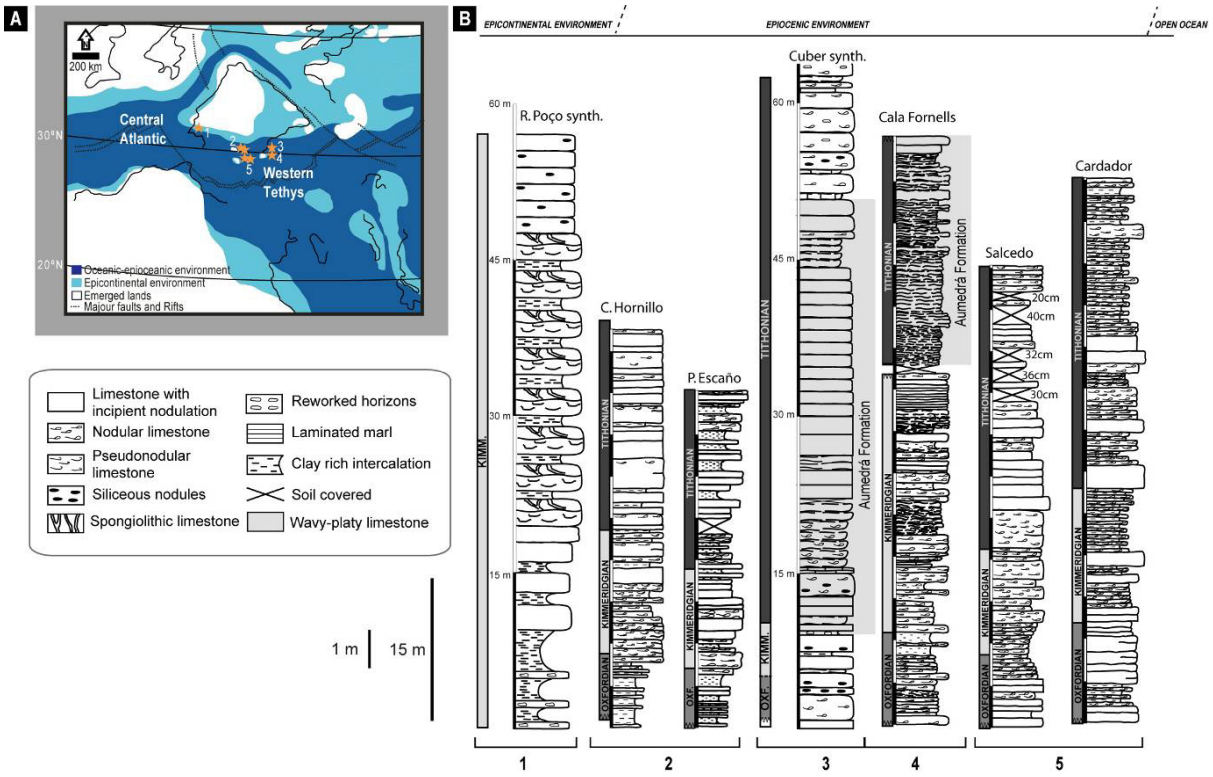

Fig. 4.3- **A)** Late Jurassic paleogeographic reconstruction of western and central Tethys. Plate tectonic setting is from Stampfli and Borel (2002). Depositional environments are from Thierry et al. (2000 a, b). Schematic location of sections is indicated by stars and labelled 1 through 5. **B)** Stratigraphic overview columns of studied sections.

4.2.3- The epicontinental setting

The most proximal end-member of the studied proximal to distal transect is represented by the Rocha Poço section (southern Portugal; Figs. 4.1, 4.2A and 4.3), covering mainly Kimmeridgian deposits (interpreted paleo-water depths above). This section belongs to the epicontinental area of the south-western Iberian platform (Figs. 4.1, 4.2A and 4.3A; Marques, 1983; Marques and Olóriz, 1989a, b; Olóriz et al., 1994), an expression of the epicontinental shelf system represented eastwards by the wider Prebetic Shelf.

4.2.4- Environmental significance of studied lithofacies

The most proximal section, Rocha Poço (Figs. 4.1 through 4.3), presents the development of sponge bioherms during the Early Kimmeridgian (Marques, 1985; Ramalho,

1988), a lithofacies type that points to neritic depths ranging from 25 to about 200 m paleo-water depth (Keup et al., 1990; revision with references in Olóriz et al., 2003a). Depth estimations for sponge-microbialite buildups range throughout neritic depths, from 25 m to slightly over 200 m water depth (e.g., Keup et al., 1990; revision with references in Olóriz et al., 2003a). Recent work on Jurassic coral and sponge-microbialite buildups assume depth ranges between 60-100 meters as probable, ensuring 10% of surface light availability vital for microbialite growth (Olivier et al., 2007). Eastwards along the south Iberian paleo-margin, Oxfordian buildups made by sponge-microbial consortia have been placed at mid-shelf depths (50-70m) in the Prebetic Zone (Olóriz et al., 2003a). Ramalho (1988) estimated depth euphotic zone in the range of 50-150m for the sponge reefs in the Rocha area. Following above-cited work, the shallowest depths estimated for the most proximal section along the transect corresponds to a mid-shelf paleo-environment probably in the order of 50-60 meters deep.

The epioceanic record is dominated by the occurrence of nodular limestones deposited on structural highs. Low accumulation average rates favoured the deposition of carbonate muds resulting in condensed, nodular Ammonitico Rosso and related facies on sub-aquatic highs (Fig. 4.1), at maximum depths of around 250 meters (Jenkyns, 1974; Olóriz et al., 1996, 1997; Olóriz, 2000). Nodule formation resulted from the complex interplay between sediment input and current sweep and winnowing, burrowing and pore-water circulation (Flügel, 2004; Coimbra et al., 2009). Nodular structure formed during an early (porewater) diagenetic stage (Jenkyns, 1974; Müller and Fabricius, 1974; Mullins et al., 1980; Clari et al., 1984; Clari and Martire, 1996) resulting in an early diagenetic stabilization of thermodynamically instable carbonate mineralogies (Jenkyns, 1971).

Both sections from the Island of Majorca (Figs. 4.1 through 4.3) are characterized by very distinctive lithofacies types. At Cuber and Cala Fornells, thin intercalations of wavy to platy limestones, occasionally bearing silica nodules, suggest a locally higher silica input. Probable biotic silica sources included dissolution of marine siliceous skeletons (sponge spicules, diatoms, radiolaria) (Fanning and Schink, 1969; James et al., 2000).

Another striking feature at the Majorca sections is the occurrence of relatively thick (ca. 40 meters) brown tabular, fossil poor limestones of the Aumedrá Formation (uppermost Kimmeridgian/lowermost Tithonian; Figs. 4.2C and 4.3B). An in-depth analysis of the poorly

understood origin (Álvaro et al., 1989; Caracuel and Olóriz, 1998) of these limestones is beyond the scope of this paper.

4.3- Methods and materials

4.3.1- Sampling strategy and analytic procedures

A total of 316 hand specimens were collected from the seven studied sections. This resulted in an average of 19 samples per section meter for more condensed sections (Cañada del Hornillo, Cardador, Puerto Escaño and Salcedo), and one sample per section meter for the Cuber and Rocha Poço sections (Fig. 4.3B). From each hand sample, two slabs where cut: one for macroscopic inspection (microfacies and cathodoluminescence) and the respective twin slab for geochemical investigation. Thin sections were produced from each hand specimen. Microphotographs of thin sections were used for a quantitative estimate of skeletal abundance. Cathodoluminescence inspection was performed on selected samples, using a hot stage cathodoluminescence microscope (HC4- LM at the facilities of the Institute for Geology, Mineralogy and Geophysics, Ruhr University Bochum, Germany). The purpose was to evaluate the degree of preservation of matrix micrites, different carbonate cements and skeletal material (belemnite rostra and neomorphic ammonite shells), based on their luminescence patterns (Fairchild, 1983; ten Have and Heijnen, 1985; Marshall, 1988; Machel and Burton, 1991; Machel et al., 1991; Bruckschen and Richter, 1994; Bruhn et al., 1995; Barbin and Schvoerer, 1997).

Matrix micrite powder sub-samples were drilled based on visual inspection of slabs: in average, four powder samples per slab were collected, resulting in a total of 1150 matrix micrite sub-samples. Where present, up to four more samples representing other features where also drilled. These included carbonate cements (n=102), neomorphic ammonite shells (n=2) and belemnite rostra (n=30). At the Cuber section (Figs 1 through 3) the silica nodules were tested for the potential influence of silica diagenesis on carbonate geochemistry. Three transects crossing nodule areas where sampled, resulting on a total of 51 matrix micrite samples.

Geochemical analysis were performed at the facilities of the Institute for Geology, Mineralogy and Geophysics; Ruhr University Bochum, Germany. Carbon- and oxygen-

isotope ratios were analyzed on a ThermoFinnigan MAT delta-S mass spectrometer following McCrea's (1950) procedure. Analytical precision (±1σ), controlled by NBS19 and internal standards, was better than ±0.03 and ±0.07‰ for $\delta^{13}C$ and $\delta^{18}O$, respectively. Duplicate samples presented a deviation of ±0.02‰ for $\delta^{13}C$ and ±0.08‰ for $\delta^{18}O$. Isotopic values are reported in the standard δ-notation in per mil (‰) relative to V-PDB. The paleotemperature equation of Anderson and Arthur (1983) was applied to distinct carbonate materials, considering a $\delta_{seawater}$ between -1 and +0.5‰ SMOW according to Shackleton and Kennet (1975).

Aliquots from each sample were investigated for their Ca, Mg, Mn, Fe and Sr elemental composition using inductively coupled plasma-atomic emission spectrometry at Bochum (ICP-AES). Maximum elemental scatter for duplicate samples was in the order of 3%.

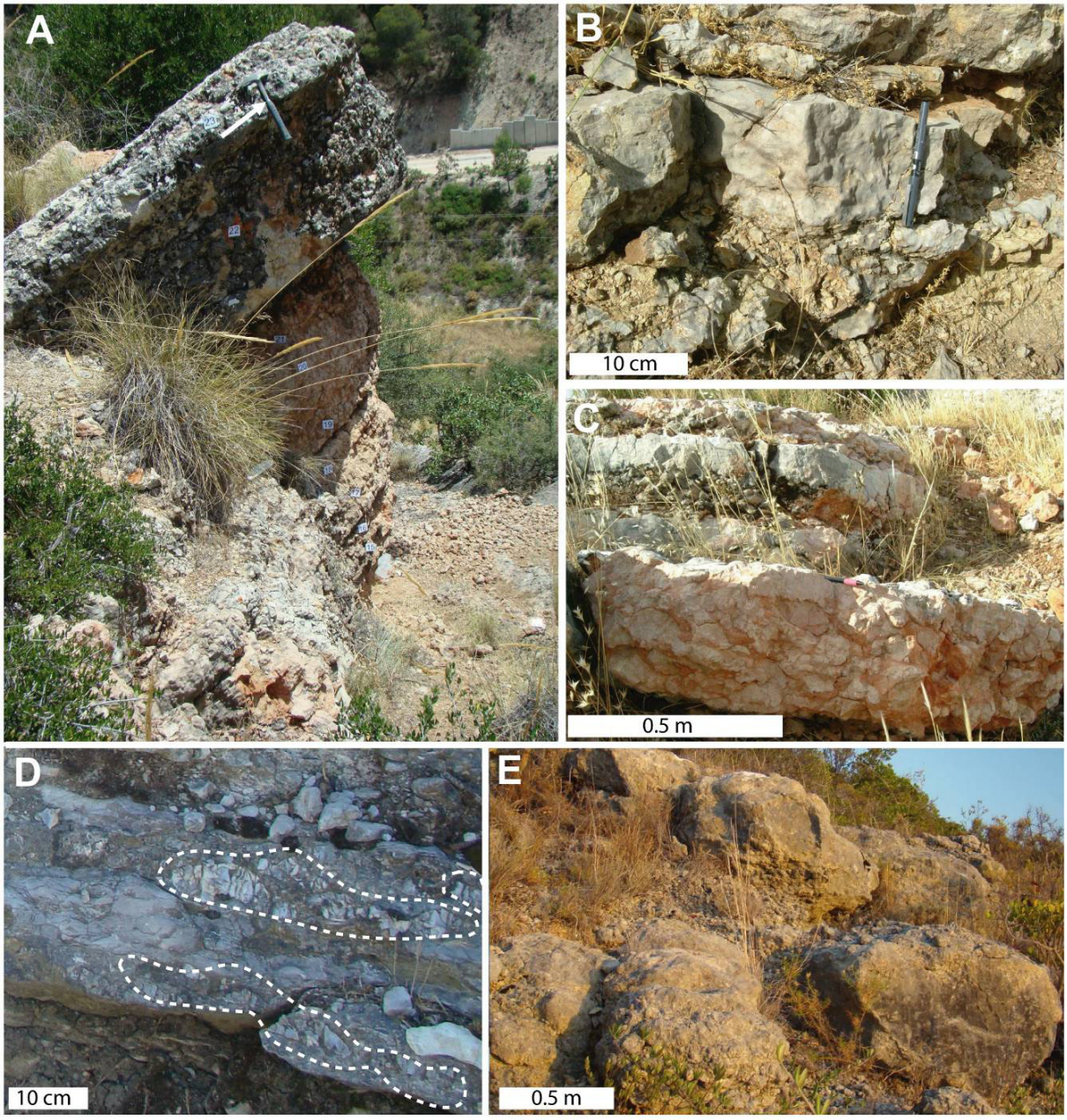

Fig. 4.4- Field images documenting sampling strategy and lithologic features. **A)** Typical Ammonitico Rosso succession of the Salcedo section with numbers in white indicating sampled horizons. Hammer for scale, white arrow. **B)** Calcareous Ammonitico Rosso horizon (Cardador section). **C)** Detail of nodular structure (Cardador section). **D)** Siliceous nodules intercalated in Ammonitico Rosso succession (Cuber section). **E)** Spongiolithic bioherms (Rocha Poço section). For macroscopic details see Figure 4.5.

4.3.2- Carbonate and silica materials

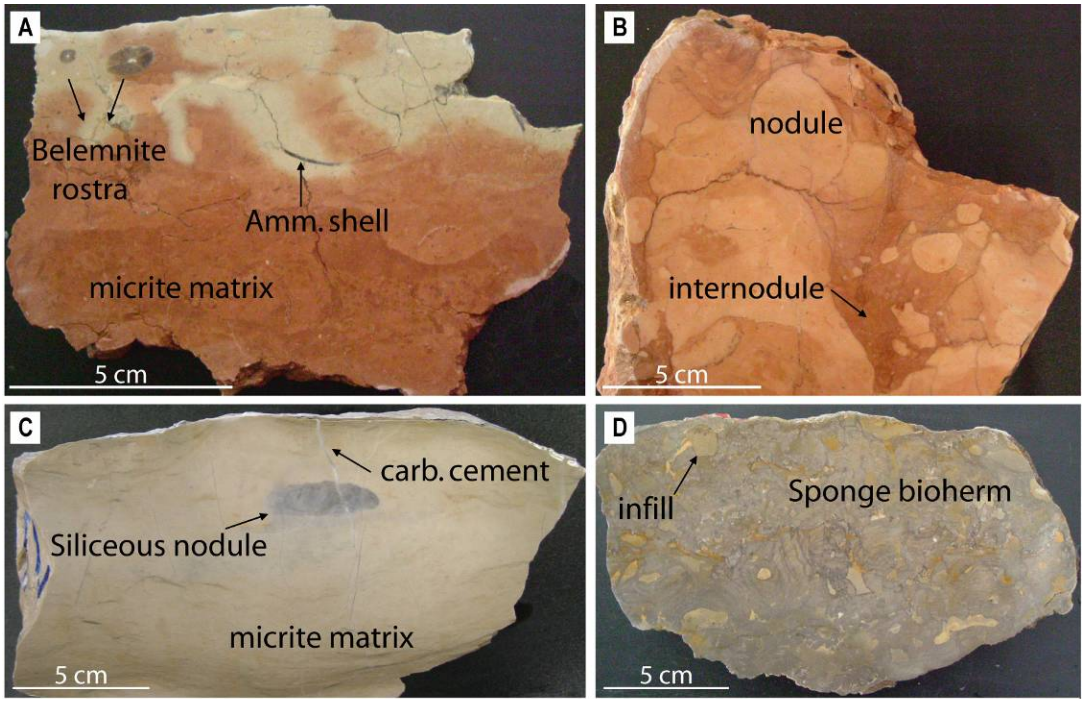

Fig. 4.5- Cut and polished slabs showing macroscopic features. **A)** Indistinct nodularity in Ammonitico Rosso facies with macrofossils (Salcedo section). **B)** Ammonitico Rosso nodule and internodule (marked with arrows) facies with characteristic red colour pattern (Cardador section). **C)** Siliceous nodule in wackestones matrix and cross cut by late burial carbonate vein (Cuber section). **D)** Spongiolithic bioherms (Rocha Poço section). Arrow indicates fine-grained sediment infilling primary cavity.

Matrix micrite

Matrix micrite samples are dominated by nodular Ammonitico Rosso facies (Figs. 4.4A, C and 4.5A, B) alternating with horizons characterized by indistinct nodular facies (see Figs. 4.2C and 4.3B for facies distribution, and Fig. 4.4B). The occurrence of facies other than Ammonitico Rosso adds complexity. At the Cuber section, silica nodules (Figs. 4.4D and 4.5C) are a common feature. Silty limestones and bioconstructed horizons (Figs. 4.4E and 4.5D) at the Rocha Poço section were investigated too.

Carbonate cements

Overall, cement-filled voids are uncommon in the carbonate slabs investigated, but blocky and other calcite cement were identified and sampled where possible. Cathodoluminescence (CL) inspection revealed three cement generations (1 to 3 in Fig. 4.6B). The first generation (1) is a non-luminescent, scalenohedral calcite phase, followed by a bright-luminescent

orange generation 2. The latest cement generation 3, is a dull orange luminescent blocky calcite, occluding the center of voids.

Belemnite rostra

Belemnite rostra are widely used for paleoenvironmental reconstructions by means of carbon and oxygen isotope analysis (e.g. Price and Sellwood 1994; Saelen et al., 1996; Podlaha et al., 1998; Wierzbowski 2002; Voigt et al., 2003; Rosales et al., 2004; McArthur et al., 2007; Price 2010). Due to their low-Mg calcite mineralogy (Veizer, 1983; Sælen, 1989), belemnite rostra are often considered to be less sensitive to post-mortem diagenetic alteration, a view that may or may not require a re-evaluation (Richter et al., 2011). All belemnite rostra data shown here (n=19) were screened for their degree of diagenetic alteration using elemental and visual (CL) approaches (Fig. 4.6D, F) in order to avoid material with more than a minor diagenetic overprint.

Neomorphic ammonite shells

Preservation of aragonitic skeletal parts is not frequent due to metastability of aragonite under marine conditions (Veizer 1983). Within the Ammonitico Rosso facies, aragonite shell dissolution is a common feature, attested by the abundance of ammonite inner casts. Notwithstanding, two examples of neomorphic ammonite shells were identified from the samples collected. Cathodoluminescence inspection revealed the presence of the same luminescence pattern (generations 1 through 3) recognized from cement-filled voids (Fig. 4.6H).

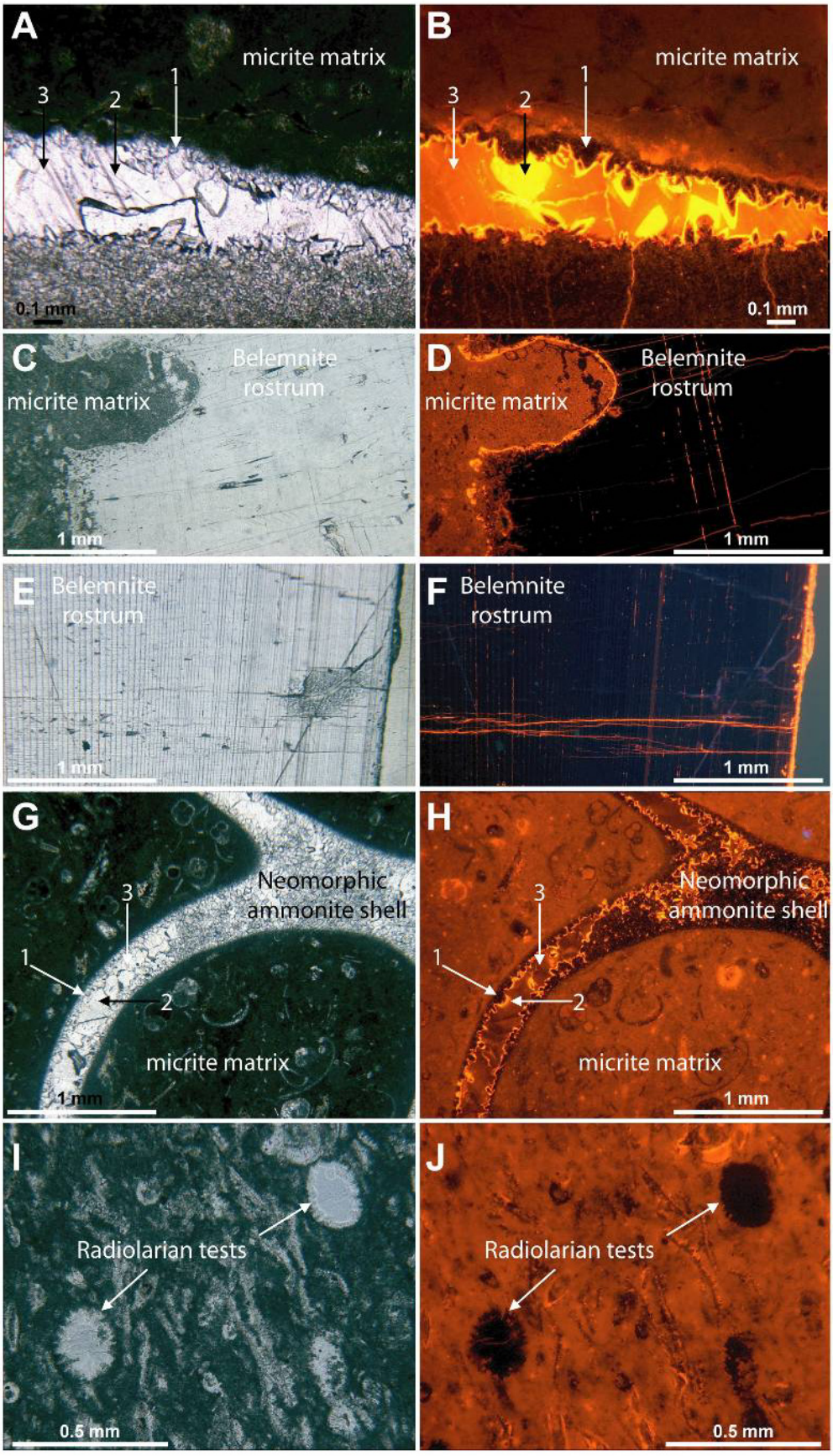
A
micrite matrix
1
2
3
0.1 mm
B
micrite matrix
1
2
3
0.1 mm
C
Belemnite rostrum
micrite matrix
1 mm
D
Belemnite rostrum
micrite matrix
1 mm
E
Belemnite rostrum
1 mm
F
Belemnite rostrum
1 mm
G
Neomorphic ammonite shell
3
1
2
micrite matrix
1 mm
H
Neomorphic ammonite shell
3
1
2
micrite matrix
1 mm
I
Radiolarian tests
0.5 mm
J
Radiolarian tests
0.5 mm

Fig. 4.6- Comparison of transmitted light (images to the left) and cathodoluminescence imaging (to the right) of characteristic features. A/B) Typical cement paragenesis. Cement phases are labelled 1 to 3. Matrix micrite presents dull luminescence. C/D) Belemnite rostrum. Note overall intrinsic blue luminescence, cross-cut by bright orange veinlet. Rare interlaminae orange luminescence is present. E/F) Belemnite rostrum. Belemnite rostrum shows similar luminescence pattern as D; G/H) Neomorphic ammonite shell showing characteristic paragenetic phase as shown in A/B. I/J) Matrix micrite radiolarian tests filled with non-luminescent secondary silica.

4.4- Data presentation

4.4.1- Microfacies analysis

Microfacies data (mainly carbonate grains and texture)- Sections characterized by typical Ammonitico Rosso facies (Cardador, Salcedo, Cañada del Hornillo, Puerto Escaño, Cuber and Cala Fornells; Figs 1 through 3) are predominantly formed by wackestones showing variable contents of radiolaria, calcisphaerulids (calcarerous dinoflagellate cysts), planktic crinoids (*Saccoccoma*, mainly Kimmeridgian and Lower Tithonian), unidentifiable foraminifera (planktic and benthic forms) others than *Globuligerina* (Oxfordian Conoglobigerinidae), hyaline tintinnoids (Upper Tithonian), ostracods, radiolarian tests, green algae zoospores (*Globochaetes*), foraminifera, calcisphaerulids (calcarerous dinoflagellate cysts) cephalopods (ammonitella and fragments of juvenile and adults ammonite carcasses and *aptychi*), mollusk fragments (gastropods included), brachiopods, echinoderms (plates and spines), sponge spicules and pelagic bivalves. Locally, packstone horizons mainly composed of filaments and/or *Sacoccoma* sp. were identified. Locally (lower portion of the Cuber section) subordinate packstones with calcareous planktic foraminifera (*Conoglobigerinidae*), radiolaria, *Saccocoma* sp., filaments, and undetermined foraminifera occur.

The Aumedrá Formation in the Majorca sections (Fig. 4.3B) presents relatively monotonous microfacies, mainly represented by mudstones, with scarce *Saccocoma* sp., filaments, radiolarian, and green algae zoospores (*Globochaetes*). Occasionally, undetermined foraminifera are present, along with sponge spicula, gastropods, *aptychi* and bivalves.

The more proximal Rocha Poço section will be described in detail, since its epicontinental setting favoured distinct biogenically induced sedimentary structures and peculiar microfacies of relevance for further geochemical interpretations. Below the first

occurrence of sponge build-ups, the lower part of the section is characterized by silty mudstones to wackestones with variable abundance of ammonites, bivalves, plant remains and less common gastropods. Microfacies analysis from silty to marly intervals shows ostracods and rather scarce small benthic foraminifera dominated by agglutinated and calcareous forms (lituolaceans, nodosariaceans). The overlying spongiolitic facies belongs to the "biohermes stromatolitiques à spongiaires silicieux" Ramalho (1988) within the Peral Formation (Marques, 1985). Microfacies analysis shows dominant peloidal wackestones, very locally packstones, with well preserved microbial/algal structures (planar-to-wavy laminated or stromatolitic microbialites, and thrombolites), sometimes encasing clotted peloidal fabrics. Microbial encrustation of skeletals is widespread. Microbial/algal oncoids and lumps are common, include skeletals (commonly sponge spicules in their nuclei) and appear more or less floated in brown micrite matrix or pale-grey microspar patches (voids infilling?). Some nuclei are a relatively large recrystallized void (algal air bladder, gas bubble or decayed fleshy material), and there are cases of no clear differentiation from the surrounding pale-grey matrix typical of interstitial spaces (potential micritized inner cast of bivalve or burrow?). These microbial/algal growths include benthic foraminifera (nubeculariids) or are encrusted by them. Angulose and mainly subrounded micritic (automicrite) intraclasts and micritized aggregate grains (lumps) are common. *Tubyphites* and tuberoids exist, and cortoids occurs at the top of the section (Jordana Formation; Marques, 1985). Small grains of monocristaline quartz variably occur, mainly at the bottom and top of the section. Bioclast abundance varies showing common sponge frames (dictyonals) and spicules, echinoderms (plates, spines, ossicles), fragments of mollusks (benthic and pelagic bivalves, gastropods), rare articulated small bivalves (articulate oyster with local micrite coating included) and ammonites (two-three incomplete phragmocones from the middle and the upper part of the section, one of them with preserved ammonitella), and broken brachiopods (valves and a single case with preserved part of the brachidium). Less abundant are neomorphized worm tubes (serpulids), rarely preserved as local patches, and remains of probable filamentous algae. Benthic foraminifera are sparsely scattered, represented by calcareous (nodosariaceans –*Lenticulina*; robertinaceans –epistominins?; rare involutinids -*Trocholina*), porcelanous (miliolaceans – nubeculariids, miliolids including ecuatorial sections of *Nautiloculina* or *Meandrospira*) and agglutinated forms (nonseptate ammodiscids?; uniserial and more scarce biserial, planispiral and trochopiral lituolaceans –*Reofax*, *Textularia,* lituolids, ataxophragmiids?). Transverse and

oblique sections of tubes due to biogenic activity (boring, burrowing) show very fine mudstone (automicrite?)-to-microspar infilling, and locally interrupt microbialite layering. Interspaces (open spaces) show microspar, and larger spaces (most probably traces made by biogenic activity) are filled by coarser particulate sediment including rare intraclasts derived from the enclosing wackestone. Uncommon geopetals show pale-brown filling containing rounded intraclasts, skeletal fragments and pellets. Silicification is common above levels with large sponges. Macrofossils are usually fragmented sponges, small corals and very rare juvenile ammonites.

Skeletal abundance estimated for all epioceanic sections revealed fluctuations in bioclast content from 1 to 45% (Fig. 4.7A, mean value of 15%). This information was combined with other analyzed proxies and interpreted in the light of its environmental significance according to their stratigraphic distribution (Fig. 4.7; for relationship with oxygen isotope composition see below). The epicontinental record was not quantified. This because the lower part of the Rocha Poço is quartz rich but practically barren in microbioclasts and also because the overlying spongiolithic facies are biogenically constructed and hence, the matrix is largely biogenically induced (automicrite).

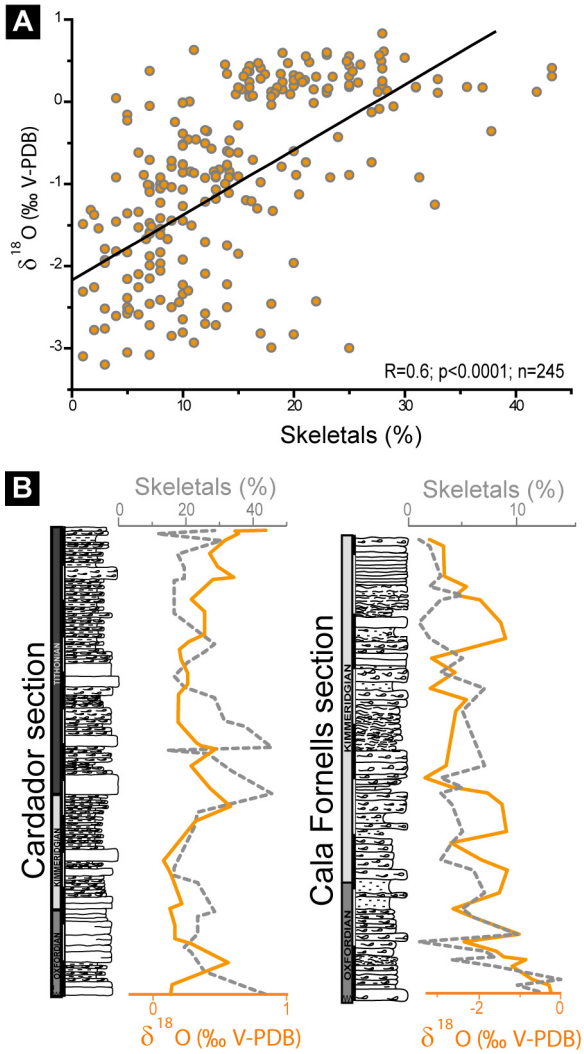

Fig. 4.7- Skeletal abundance plotted against oxygen isotope chemostratigraphy: A) Statistically relevant, linear correlation computed for data from all epioceanic sections. B) Exemplary stratigraphic distribution of skeletal abundance (dashed line) and oxygen isotope composition (full line) for the Cardador and Cala Fornells sections. Note co-variance.

Cathodoluminescence patterns- CL microscopy of matrix micrites revealed dull to slightly bright luminescence (Fig. 4.6B, D, H and J) patterns. Carbonate cements and neomorphic ammonite shells showed a typical luminescence pattern characterized by the occurrence of three cement generations (Fig. 4.6H). Belemnite rostra show an overall intrinsic luminescence with the exception of rare, orange luminescent growth increments and are cross-cut by bright-orange veinlets, (Fig. 4.6D, F). Pixel counting allowed an estimation of relative volumetric significance of each cement generation (Fig. 4.8A to D). Radiolarian test identified on siliceous horizons are non luminescent (Fig. 4.6J).

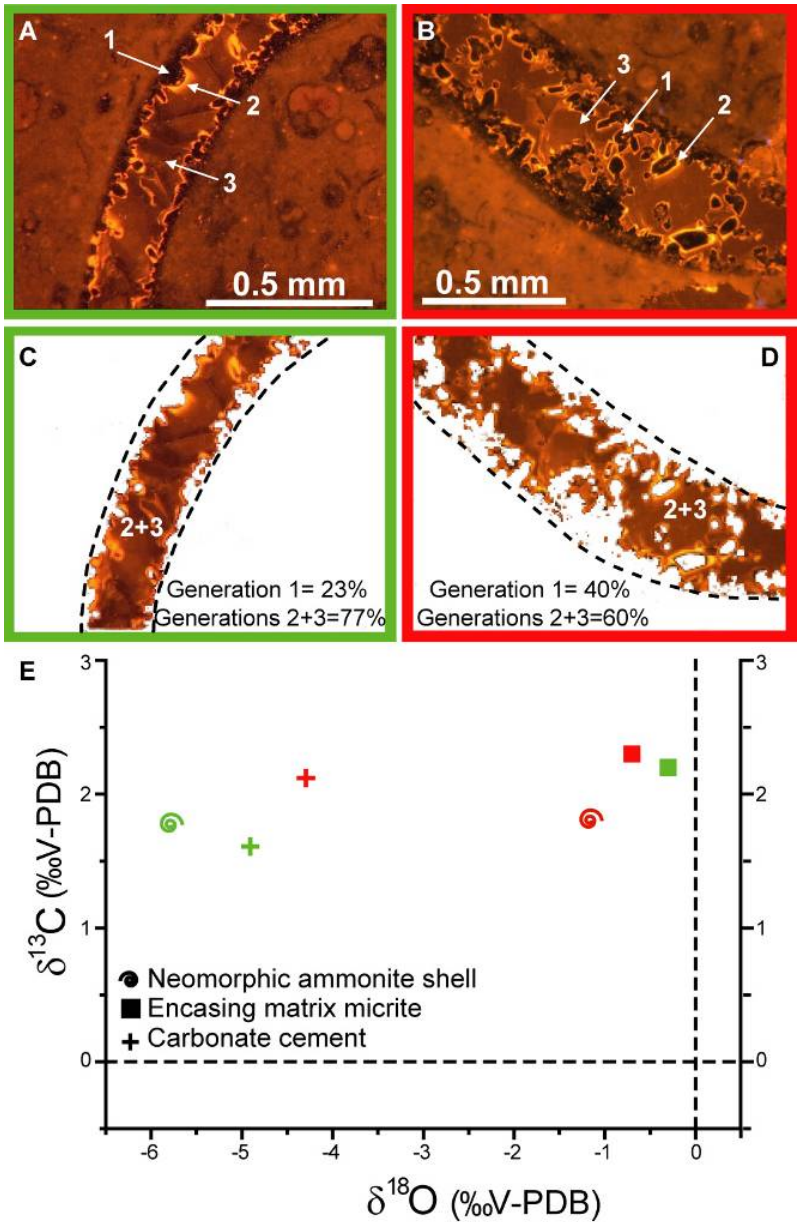

Fig. 4.8- Cathodoluminescence images from neomorphic ammonite shells in relation to their C and O isotope composition. A) and B) Cathodoluminescence images obtained from two neomorphic ammonite shells from Puerto Escaño and Cañada del Hornillo sections, respectively. Typical paragenetic phases labelled 1 to 3 (see Fig. 6B). C) and D) Same images applying pixel counting (cement generation 1 was eliminated, dashed line outlines the shape of the shell). E) Carbon and oxygen isotope composition for neomorphic ammonite shells, host matrix micrites and mean carbonate cement values. Note different significance of cement phase 1 in each example, and differences in oxygen isotope composition of neomorphic ammonite shells.

4.4.2- Carbonate geochemistry

Carbon isotope ratios

Mean carbon isotope ratios obtained for each carbonate material are shown in Table 4.1. Values range from 1.9 to 2.0‰, with the exception of belemnite rostra (mean of 0.4‰).

	$\delta^{13}C$ ‰ (V-PDB)	$\delta^{18}O$ ‰ (V-PDB)	n
Matrix micrite	1.9 ± 0.8	-1.3 ± 1.5	1150
Belemnite rostra	0.4 ± 0.7	-0.6 ± 0.3	19
Marine cement	2.0 ± 0.3	-3.7 ± 1.9	102

Table 4.1- Mean stable isotope (C and O) composition.

A more detailed overview for each studied locality is provided in Figures 4.9 and 4.10. All epioceanic sections present similar matrix micrite carbon isotope compositions, between 1.0 and - 3.5‰. Carbon-isotope values from the epicontinental Rocha Poço section are significantly lowered and range between -6.2 and 2.3‰. Carbonate cements (Fig. 4.9) and neomorphic ammonite shells (Fig. 4.8E) plot within the range of their encasing matrix micrite. Belemnite rostra generally present lower $\delta^{13}C$ values with respect to their host matrix micrite (-1.4 to 1.8‰; Fig. 4.9). Specimen collected from the most proximal setting (Rocha Poço; Figs. 4.1 through 4.3) represent an exception with $\delta^{13}C$ values plotting within the range of matrix micrite data.

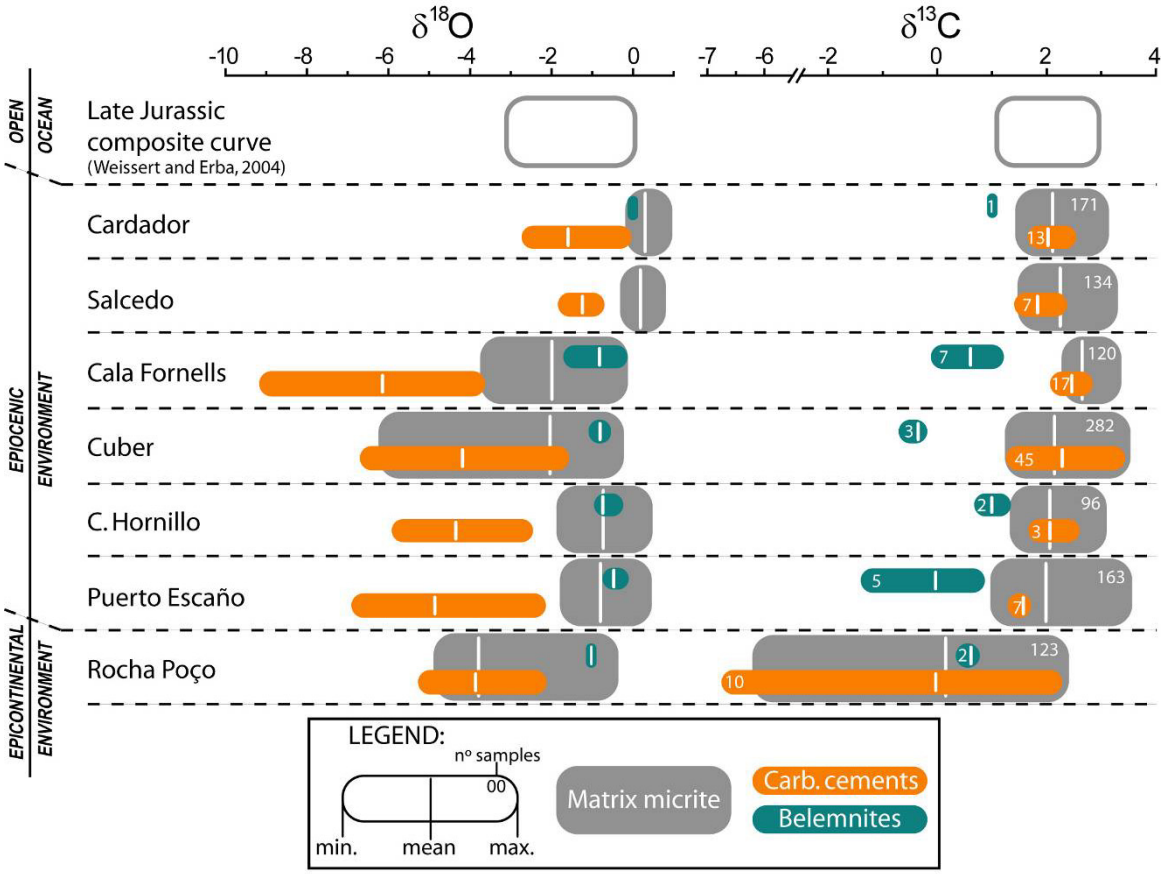

Fig. 4.9- Overview of carbon and oxygen isotopic composition of matrix micrites, carbonate cements and belemnite rostra from all sampled locations. Mean values and average values are presented for each analyzed studied material and section (vertical lines), as well as maximum and minimum values (width of bars). Note narrow $\delta^{13}C$ range (except belemnites) and fairly homogeneous $\delta^{18}O$ ratios (except carbonate cements).

All epioceanic sections (Cañada del Hornillo, Puerto Escaño, Cuber, Cala Fornells, Salcedo and Cardador) share similar stratigraphic trends (Fig. 4.10). Absolute values may fluctuate between sections, but range between 2 to 2.5‰ at the base of the recorded Oxfordian, whilst a pronounced positive shift of about 1‰ is observed during the Middle Oxfordian. Carbon isotope ratios progressively decrease during Kimmeridgian and Tithonian times. Late Jurassic minima of ca. 1‰ are reached for the topmost Tithonian of the epioceanic sections. In the Cuber section, $\delta^{13}C$ ratios for carbonate cements are plotted against matrix micrite (indicated red in Fig. 4.10A) revealing exactly the same trend. The only exceptions to the described trend are found at the two sections from the Majorca Island, for the Aumedrá Formation, discussed elsewhere.

The most proximal section, Rocha Poço (Figs. 4.1 through 4.3), is characterized by ^{13}C-depeleted values near the base of the Kimmeridgian. Further upsection, isotope values progressively increase from -6 to +2‰, with the most pronounced shift across the boundary to spongiolithic limestone (Fig. 4.10A) facies. In the latter, a distinction is made between samples retrieved from the sponge buildups itself and samples from sediment filling cavities (Fig. 4.10A). At the onset of this facies, infill material differs from the biogenically mediated sediments, showing depleted values. Once this facies is fully established, this distinction is no longer detected in the $\delta^{13}C$ signature of these materials (overlapping values). An abrupt decrease of about 6‰ is observed at only one spongiolitic sample. Generally, positive $\delta^{13}C$ ratios are maintained throughout the Kimmeridgian. Matrix micrite samples from silica nodule-bearing horizons in the Cuber section (Fig. 4.10A) display no particular carbon isotope pattern (filled grey squares on Figure 4.10A).

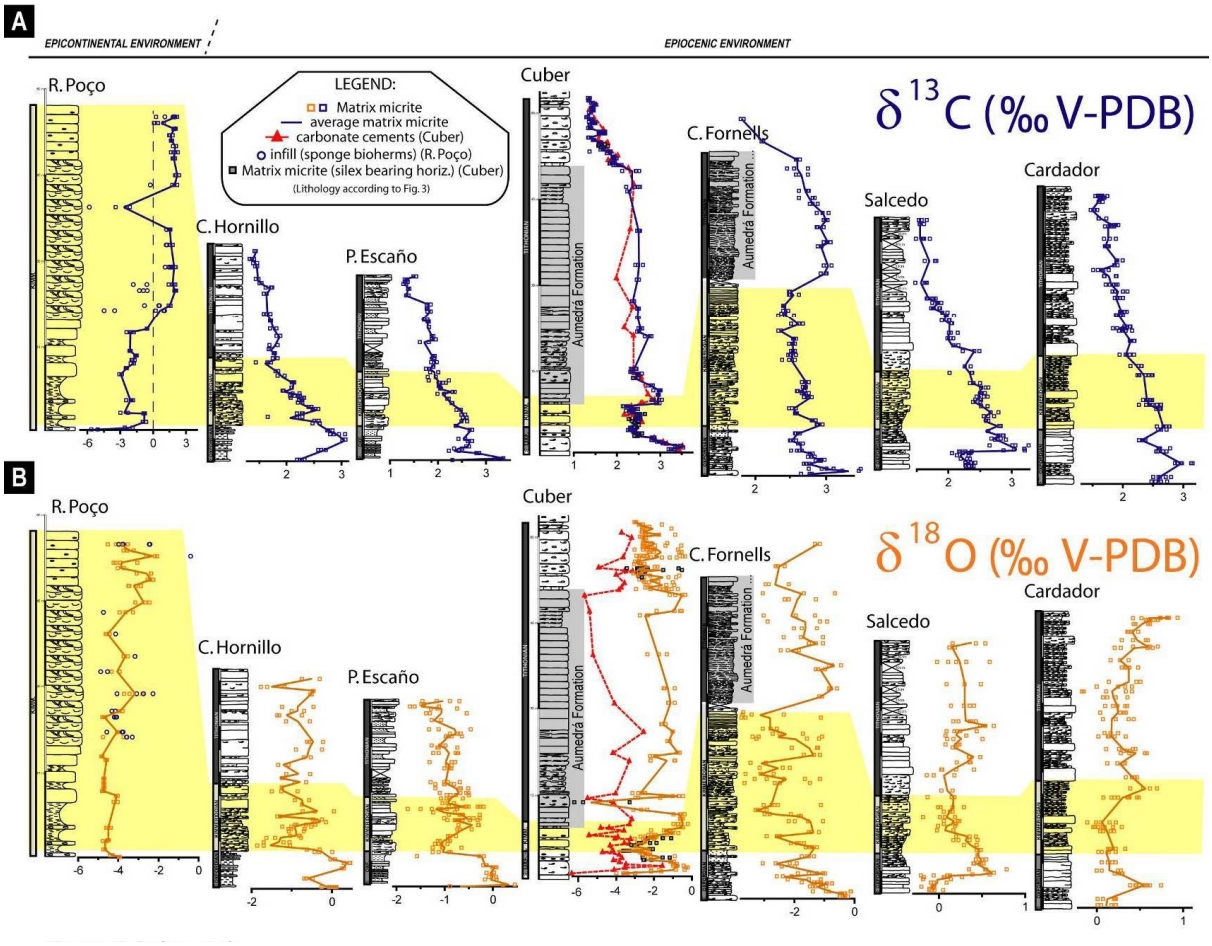

Fig. 4.10- Spatial chemostratigraphy: **A)** carbon isotope composition and **B)** oxygen isotope stratigraphy of all studied sections. Intra-sample isotopic variability is indicated for each investigated horizon. Line indicates the

mean value of all subsamples for each hand specimen. Key to symbols for different analyzed materials is given. The portion of the sections that represents the Kimmeridgian time interval is underlain in yellow for comparison.

Oxygen isotope ratios

An overview of the $\delta^{18}O$ characteristics of different carbonate materials is presented in Table 4.1. Matrix micrite samples present mean values around -1.3‰, whilst carbonate cements are the most depleted set of samples, with average of -3.7‰. Regarding skeletal components, $\delta^{18}O_{belemnite}$ values are higher than the average $\delta^{18}O_{micrite}$ values. Neomorphic ammonite shell data sets differ from each other with one plotting near the host matrix micrite value (-1.2‰) and the other approaching diagenetic cement values of -3.4‰ (Fig. 4.8E).

The geochemical signatures from different carbonate materials are presented in Figures 4.8E, 9 and 4.10B. Sections from the epioceanic realm can be grouped based on their matrix oxygen isotope values. More landward sections (Cañada del Hornillo and Puerto Escaño; Figs. 4.1 and 4.3) display similar values between -1.9 to 0.5‰. The Cala Fornells and Cuber sections from Majorca Island (Figs. 4.1 through 4.3) present the same average $\delta^{18}O_{micrite}$ (-2‰), similar maximum value (-0.2‰), the Cuber section reaching lower values (-6.2‰) than the Cala Fornells section (-3.7‰). Matrix micrite data from the more distal, epioceanic sections of Cardador and Salcedo share the same range of $\delta^{18}O_{micrite}$ (-0.3 to 0.9‰, mean of 0.2‰; Fig. 4.9). The epicontinental, most proximal section at Rocha Poço is characterized by the lowest mean $\delta^{18}O_{micrite}$ value of all investigated sites (-4.9 to -0.4‰).

Carbonate cements can be separated in two groups (Fig. 4.9). One with $\delta^{18}O$ values lower than those obtained from matrix micrites (Cardador, Salcedo, Cañada del Hornillo, Puerto Escaño and Cala Fornells sections; Figs. 4.1 though 4.3) and a second group with carbonate cement samples at least partly overlapping with matrix micrite data (Cuber and Rocha Poço sections; Figs. 4.1 through 4.3).

Belemnite $\delta^{18}O$ is relatively constant and ranges from -1.7 to -0.2‰ (Fig. 4.9). Most samples plot within the more positive end of the range of matrix micrite data.

Similar to carbon isotopes, neomorphic ammonite shells from the Cañada del Hornillo section are characterized by $\delta^{18}O$ ratios that are close to their host matrix (-1.1 and -0.7‰; Fig. 4.10B), whilst the specimen from the Puerto Escaño section plots with a value similar to that of $\delta^{18}O_{cements}$ from the same locality (-4.9 and -5.7‰).

The oxygen chemostratigraphy of all sections is shown in Figure 4.10B. A $\delta^{18}O$ fluctuation of ca. 1‰ is observed during the mid-Oxfordian in all epioceanic sections (Puerto Escaño, Cañada del Hornillo, Cala Fornells, Cuber, Salcedo and Cardador). The Kimmeridgian and Tithonian record is more variable, but the first-order isotope pattern as found in the Cardador section is recognized in all other epioceanic sections too (Fig. 4.10B). After the mid-Oxfordian positive shift, $\delta^{18}O$ ratio decrease towards the Oxfordian/Kimmeridgian boundary (-1‰ at Puerto Escaño and Cañada del Hornillo; -2 and -3‰ at Cala Fornells and Cuber, respectively and 0‰ at Salcedo and Cardador; Fig. 4.10B). During the Kimmeridgian, increasing of $\delta^{18}O$ values are observed and the Tithonian record reflects the return to $\delta^{18}O$-depleted values that again shift to more positive values towards the end of the Late Jurassic.

Overall, a significant negative shift in $\delta^{18}O$ values coincides with silica nodule bearing horizons (Figs. 4.10B and 4.11). Micrite and carbonate cement records reflect the same stratigraphic trend, although the latter are shifted towards more negative values, about 4‰ lower. In the epicontinental Rocha Poço section (Fig. 4.10B), the Early Kimmeridgian record is rather stable (ca. -4‰; Fig. 4.10B), with a gradual increase towards $\delta^{18}O$-enriched average values of -2.7‰ upwards in Lower Kimmeridgian strata.

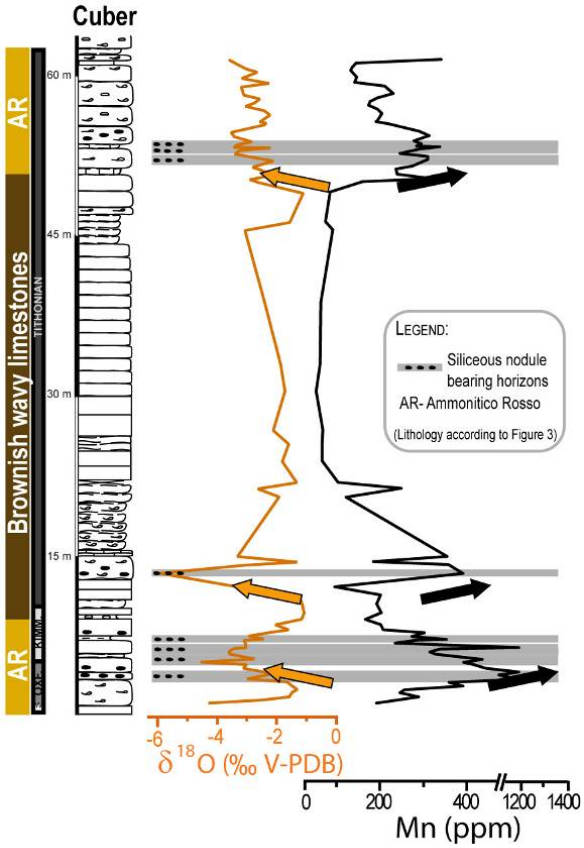

Fig. 4.11- Stratigraphic distribution of $\delta^{18}O$ and Mn abundances from epioceanic Cuber section. Note the anti-correlation of both proxies, with marked shifts across horizons bearing siliceous nodules.

Elemental geochemistry

An in-depth description of elemental data for different carbonate material analyzed from all sections is beyond the aims of this study. Nevertheless, elemental evidence is significant when dealing with differential preservation of belemnite rostra data or more generally, with the reconstruction of diagenetic patterns. Previous work established elemental threshold values separating well preserved belemnite rostra from altered ones (Voigt et al., 2003; Rosales et al., 2004; Nunn et al., 2009; Price 2010; Malkoč and Mutterlose, 2010), but no consensual values are reported. From 30 analysed samples, 19 fall within published ranges of the elemental composition of well-preserved belemnite low-Mg calcite (Veizer, 1974, 1983; Saelen, 1989; Podlaha et al., 1998; van de Schootbrugge et al., 2000; Niebuhr and Joachimski, 2002; Voigt et al., 2003; Rosales et al., 2004; Nunn et al., 2009; Price, 2010; Malkoč et al., 2010; Tables 4.2, 4.3). Regarding matrix micrite elemental abundances (research in progress), only manganese content at the Cuber section is compared with oxygen isotope composition (Fig. 4.11) in order to reinforce the interpretation of the latter proxy.

	Mg (ppm)	Fe (ppm)	Mn (ppm)	Sr (ppm)	n
Matrix micrite	2707	1657	331	213	1150
Belemnite rostra*	2575	150	45	1040	19
Carb. cements	3165	2379	757	278	102

* only best preserved specimens (see Table 3).

Table 4.2- Mean trace element concentrations for matrix micrite, carbonate cements and belemnite rostra (bellow "cut-off" values).

	$\delta^{13}C$ ‰ (V-PDB)	$\delta^{18}O$ ‰ (V-PDB)	Mg (ppm)	Fe (ppm)	Mn (ppm)	Sr (ppm)	$\Delta\delta^{18}O$* ‰ (V-PDB)	$\Delta\delta^{13}C$* ‰ (V-PDB)
C	0.9	-0.5	3381	126	100	971	- 1.0	- 1.5
S	xx	xx	xx	xx	xx	xx	xx	xx
CH	0.8	-0.3	2000	163	47	926	0.0	- 1.6
	1.3	-0.8	3038	79	30	987	0.0	- 1.2
CU	-0.2	-0.9	2398	107	22	1129	+ 2.7	- 2.7
	-0.6	-0.5	2340	62	6	1171	+ 1.8	- 2.1
	-0.2	-0.8	2488	185	27	935	+ 1.5	- 1.8
PE	0.8	-0.5	2896	465	61	821	0.0	- 1.8
	0.1	-0.5	2243	99	34	1213	0.0	- 2.0
	0.8	-0.3	2600	512	70	1180	+ 0.5	- 1.2
	-0.5	-0.6	2130	89	54	1085	+ 0.3	- 2.5
	-1.4	-0.1	2229	65	20	1266	+ 1.0	- 3.5
RP	0.7	-0.9	2684	45	1	1286	+ 3.0	- 1.0
	0.4	-0.9	3249	53	1	1187	+ 3.0	- 1.0
CF	0.3	-0.6	2147	273	100	847	+ 0.5	- 2.6
	-0.0	-0.1	1909	51	65	1019	+ 1.0	- 2.4
	1.2	-0.5	2611	187	25	774	+ 1.0	- 1.2
	0.5	-1.0	2622	248	42	906	+ 1.0	- 2.0
	0.8	-0.7	3781	440	75	914	+ 1.0	- 2.0
	1.0	-1.5	2170	239	58	842	+ 1.0	- 1.5

* offset between C and O isotope composition of belemnite rostra and neighbouring encasing micrite matrix.

Table 4.3- Stable isotope composition (C and O) for belemnites with elemental concentrations bellow cut-off values. Offset between each belemnite C and O composition and respective encasing matrix micrite is indicated by $\Delta\delta$ (positive for belemnite values higher and negative for lower).

4.5- Interpretation and discusison

4.5.1- Late Jurassic paleoceanography, sea-level fluctuations and variations in seawater geochemistry

In order to establish a link between major paleoceanographic events and how they may relate to observed geochemical trends along the studied proximal-to-distal transect, background parameters of the Jurassic world must be taken into consideration.

During Jurassic times, intensified seafloor spreading and volcanic activity increased atmospheric CO_2 and triggered changes in the global climate setting (Weissert and Mohr, 1996; Price, 1999; Weissert and Erba, 2004). Plate tectonics had a major influence on relative sea level changes during the break-up of Pangea (Hallam, 2001) and the evolution of the Central North Atlantic Basin was of importance for the westernmost Tethys. To some extent, glacio-eustasy may have also contributed, since the presence of high-latitude ephemeral and/or permanent inland ice caps and/or sea ice has been postulated (Moore et al., 1992; Rowley and Markwick, 1992; Valdes et al., 1995; Price, 1999; Dromart et al., 2003; Immenhauser, 2005), but causes are controversial (Dera et al., 2011).

During the Jurassic "greenhouse" mode, higher temperatures lead to increased evaporation at low latitude shallow seas (Ziegler et al., 2003), resulting on the formation of Tethyan relative warm saline bottom waters (Arthur et al., 1987). As a consequence, the Jurassic Tethys most likely acted as source of warm and saline waters for much of the world's oceans (Kutzbach and Gallimore, 1989).

Linking chemostratigraphic evidence of marine carbonate archives and paleoceanographic patterns has the potential to shed additional light on Late Jurassic climates. As a response to changes in seawater composition, chemostratigraphic changes in carbon and oxygen isotope ratios may reflect oceanographic events. During the early Late Jurassic, a major Tethyan transgression is recognized for the mid-Oxfordian throughout the Tethyan realm (Bartolini et al., 1999; Cecca et al., 2001; Rey and Delgado, 2002; Savari et al., 2003; Rais et al., 2007) as well as in the Central North Atlantic Basin and the Mexico-Caribbean areas (Olóriz et al., 2003b; Cobiella-Reguera and Olóriz, 2009 and references therein).

Increased continental weathering, coupled with increased nutrient runoff to the ocean is evidenced in seawater $\delta^{13}C_{DIC}$ (Bartolini et al., 1996; Colacichi et al., 2000; Wierzbowski,

2002) since higher nutrient levels triggered increased primary productivity. Due to elemental fractioning by biomass, fixation of ^{12}C is preferred by primary organic carbon producers (Schidlowsky, 1987). Enhanced burial of sedimentary organic carbonate (^{12}C rich) results in a ^{13}C enriched oceanic DIC pool (Hoffman et al., 1991; Jenkyns, 1996; Weissert and Mohr, 1996; Bartolini et al., 1996, 1999; Colacicchi et al., 2000). The effects of this major oceanographic event are less debated in terms of changes in $\delta^{18}O$ (see Dera et al. (2011) for global interpretations).

During Kimmeridgian and Tithonian times, the long-term global sea-level rise is superimposed by lower order fluctuations (Haq et al., 1988; Hardenbol et al., 1998; Hallam, 1998) most probably driven by complex geodynamic and coupled ocean atmosphere interactions. Expansion of carbonate platforms during sea-level highstands resulted in higher precipitation rates of inorganic carbon in shallow, enlarging subtropical seas (Weissert and Mohr, 1996). Organic/inorganic carbon burial rate is thereby modulated and an overall comparatively stabilized Kimmeridgian and Tithonian $\delta^{13}C_{DIC}$ pattern results (e.g., Weissert and Mohr, 1996). This trend is observed along Tethyan paleomargins (Weissert and Mohr, 1996; Bartolini et al., 1999; Cecca et al., 2001; Rey and Delgado, 2002; Savari et al., 2003; Rais et al., 2007; Coimbra et al., 2009).

It is not obvious if the temperature-depth structure of Late Jurassic oceans should be compared with that of modern tropical seas (Ziegler et al., 2003). In a context of irregular bottom physiography, as largely recognized for the epioceanic fringe in the northern Tethyan margin, to approach “detailed” structuring of paleo-water masses is a difficult task. In absence of direct data (e.g., sclerothermometry) the possibility to reconstruct water-mass boundaries (e.g., thermocline, chemocline, pycnocline) is limited. Carbonate deposition on epioceanic swells represents an admixture of suspended mud and “planktonic rain”, and the possibility for secondary episodes of fine sediment reworking. Among preserved skeletals, those of vagrant organisms (cephalopods) overwhelmingly dominate in our record, without option to retrieve the required information.

4.5.2- Preservation and reliability of C and O records obtained

Carbon and oxygen isotope ratios may present a wide range of values, depending on primary parameters (including carbonate mineralogy, seawater physico-chemical properties,

the presence or absence of metabolic effects and precipitation kinetics) and their subsequent diagenetic history (Dickson and Coleman, 1980; Allan and Matthews, 1982; Bickert, 2000; Melim and Scholle, 2002).

Carbon-isotope ratios reflect balance changes among components of the carbon cycle (Berger and Vincent, 1986; de Boer, 1986). Neomorphism, dissolution of metastable carbonate mineralogies or latter recrystallization processes may alter the original marine $\delta^{13}C$ composition (Given and Lohmann, 1985; Carpenter and Lohmann, 1989, 1997). The source of diagenetic carbonate precipitated is often the host carbonate itself (Hudson, 1975) and therefore, this proxy is rather conservative. Pervasive diagenetic processes can be reflected by depleted carbon isotope values, since late diagenetic fluids are commonly ^{13}C depleted relative to matrix carbonates (e.g., Carpenter and Lohmann, 1997; Schneider et al., 2008; van der Kooij et al., 2009).

Oxygen isotope composition of marine carbonate materials largely reflects changes in seawater temperature and/or salinity (Craig and Gordon, 1965; Marshall, 1992). Other factors may cause oxygen isotopic fractionation, such as mineralogy or the biotic versus abiotic origin of different carbonate materials (see Marshall, 1992 for details). Large reservoir of oxygen in pore waters buffers $\delta^{18}O$ composition of later carbonate precipitates (Allan and Mathews, 1977; Lohmann**,** 1987). Post depositional changes are usually accompanied by increased fluid temperature in the burial realm or the influence of ^{18}O depleted meteoric fluids (Given and Lohmann, 1989; Hoefs, 1997), causing original $\delta^{18}O$ values to be significantly lowered (Plunkett, 1997; Bartolini et al., 2003; van der Kooij et al., 2009).

A diagenetic model summarizing the imprint of shallow marine burial to meteoric fluids is shown in Figure 4.12. In accordance, $\delta^{13}C$ and $\delta^{18}O$ of matrix micrite from epioceanic sections reflect isotope signals from open marine bottom waters, while carbonate cements from these settings fall within the range of shallow marine burial to later diagenetic phases. In contrast, a clear separation between primary environmental influences and meteoric imprints is not straightforward in shallow epicontinental settings due to the potential mixing of continental and marine signals.

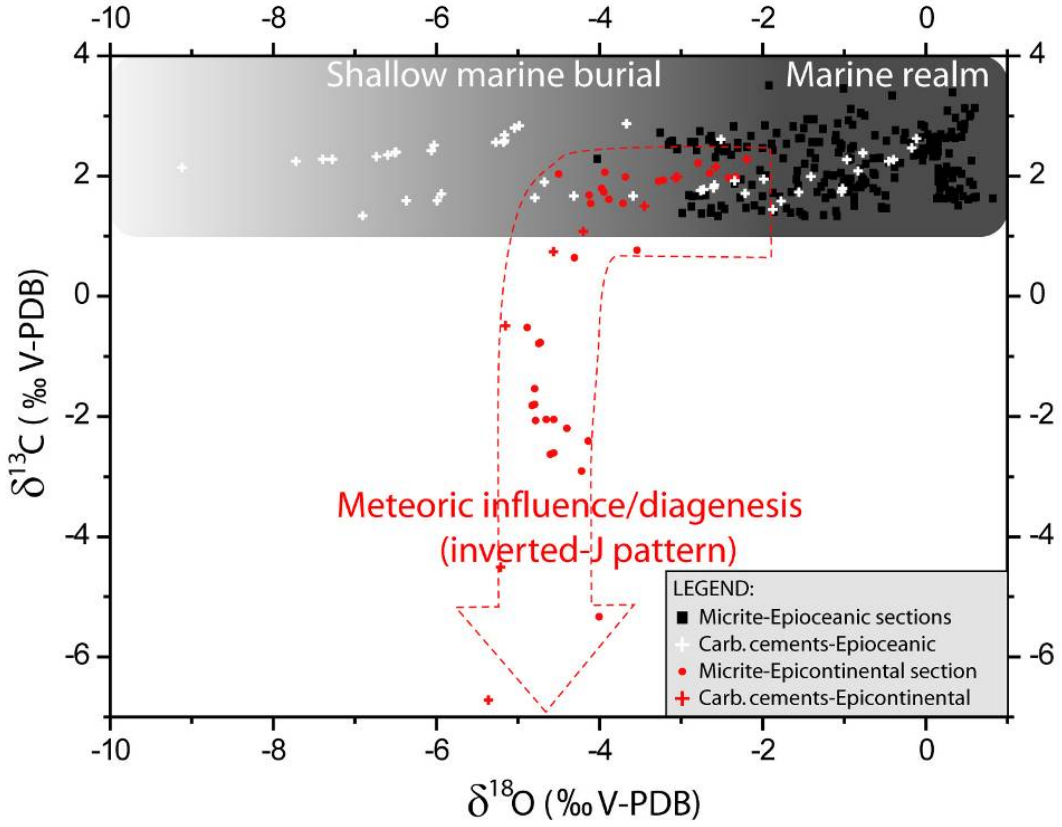

Fig. 4.12- Crossplot including major diagenetic domains identified for the studied carbonates. Epioceanic matrix micrite samples fall within the marine domain while carbonate cements agree with progressively more depleted $\delta^{18}O$ ratios typical for the shallow marine burial domain. Data from epicontinental samples reveal a more complex pattern due to the interference of Tethyan with local paleoceanographic patterns and a differential diagenetic pathway including a possible meteoric diagenetic overprint.

Carbon isotope composition

Most analysed carbonate materials oscillated around $\delta^{13}C$ values of 2‰, a value that is in good agreement with previous data from Upper Jurassic Tethyan margins (Joachimski, 1994; Jenkyns, 1996; Weissert and Mohr, 1996; Bartolini et al., 1999). A noteworthy exception is represented by belemnite rostra and matrix micrites from the lower part of the Rocha Poço section (Fig. 4.9).

Depleted $\delta^{13}C$ ratios (< 2‰) from the lower part of the Rocha Poço section (Fig. 4.10A) stratigraphically coincide with more silty facies. Isotope data obtained from these horizons are depleted as much as 8‰ relative to the overlying facies. The diagenetic origin of these values is probably best explained in the context of differential porosity and permeability and an increased fluid flow during burial (van der Kooij et al., 2009). Biogenically mediated

spongiolitic facies in the upper part of the Rocha Poço section show an equivalent, decreasing $\delta^{13}C$ trend of similar values when compared to Lower Kimmeridgian epioceanic records (not evident due to scale difference in Fig. 4.10A). This reflects the reliability of the marine $\delta^{13}C$ signal, buffering a local deviation to mesotrophy in a mid-shelf setting by comparison to dominant oligotrophy in the epioceanic fringe.

The observed 2‰ depletion of belemnite guards in respect to their host matrix micrite deserves attention (Fig. 4.9). This because low-Mg calcite belemnite guards are commonly considered a diagenetically stable carbonate archive (Longinelli et al., 2003; Brand, 2004). Possible interpretations for these low values include the incorporation of metabolic ^{13}C-depleted organic carbon. Given the non-luminescent nature of the rostra (Fig. 4.6D, F), significant diagenetic alteration is excluded. Following previous authors (Price and Page, 2008; Price et al., 2009), the $\delta^{13}C_{Belemnite}$ ratios are therefore interpreted as representing calcite precipitation in metabolic non-equilibrium with sea water through vital fractionation. Alternative interpretations for the low $\delta^{13}C$-values in belemnites include the decay of organic laminae (*laminae obscurae*, Müller-Stoll, 1936) that alternate with inorganic ones. Assuming a closed system, isotopically light organic carbon is potentially contained in early secondary cements occluding pore space in the belemnite guards. All of these interpretations are geologically reasonable but difficult to prove and evidence is circumstantial at best. It seems obvious, however, that a non-critical application of belemnite data in paleoceanographic studies must be discouraged because of controversial interpretation of ecology and/or metabolism (Podlaha et al., 1998; Mc Arthur et al., 2004; Price et al., 2009; Richter et al., 2011).

Oxygen isotope composition

Matrix micrite oxygen isotope values from the Spanish sections are ^{18}O-enriched relative to data from coeval similar depositional settings reported elsewhere (Price and Sellwood, 1994; Veizer et al., 1999; Bartolini et al., 2003; Preát et al., 2006). Following the arguments brought forward in Coimbra et al. (2009), changes in Ammonitico Rosso $\delta^{18}O_{micrite}$ values are perhaps best interpreted in terms of changes in water masses including factors such as up- or downwelling, bottom currents and related spatial paleotemperature and paleosalinity distribution. Particularly, $\delta^{18}O_{micrite}$ ratios from Cardador, Salcedo and Cañada del Hornillo sections (Fig. 4.10B) are considered to represent the uncommon case of micrite isotope values

representing near-seawater isotopic composition. This is probably due to early marine stabilization of thermodynamically instable carbonate phases and near-seafloor lithification of sediments to nodular carbonate rocks under the influence of marine pore waters.

Dense and saline bottom waters have the potential to affect marine porewater diagenesis (Immenhauser et al., 2002; van der Kooij et al., 2009). With reference to the epioceanic sections studied here (Figs. 4.1 through 4.3), relevant changes in bottom water salinity are discarded based on ecologic evidence (Olóriz, 2000). Moreover, the epioceanic setting, distant from shelf areas where surface seawater evaporation may result in the formation of dense, saline water masses or plumes, disagrees with salinity as the main driver of $\delta^{18}O_{micrite}$.

Sections investigated on the Island of Majorca (Figs. 4.1 through 4.3) are characterized by some lithological differences relative to sections from southern Spain (Figs. 4.2 and 4.3). In essence, the lithofacies in Majorcan sections is less nodular and siliceous horizons and reworked horizons are more common. Considering early, near-seafloor lithification and nodule formation (Coimbra et al., 2009), this features might point to a differential diagenetic path. Nevertheless, as (i) the chemostratigraphy of Majorca sections is very similar to that from southern Spain, and (ii) $\delta^{18}O_{micrite}$ values clearly differ from those of late diagenetic cements in these sections, significant diagenetic alteration is excluded. This observation is encouraging as the chemostratigraphic patterns observed are largely facies-independent in all sections investigated.

Oxygen-isotope values from different bright luminescent cements phases (Fig. 4.6B) are several per mil lower than those from the encasing matrix micrite (Fig. 4.9). This is evidence for burial fluids (Fig. 4.12) characterized by elevated temperatures and different geochemical composition. Apparently, $\delta^{18}O_{micrite}$ was diagenetically stabilized at a shallow burial marine porewater stage and was not affected significantly by later burial fluids.

The epicontinental oxygen isotope record obtained at the Rocha Poço section is the most depleted, from -4.9 to -0.4‰. The lower part below the occurrence of spongiolitic limestones fluctuates around -4.5‰, which is interpreted as effect of the continental water entering porous sediments prone to diagenetic imprint. In contrast, slightly higher values (-3.5‰ in average) in the overlying spongiolitic facies suggest decreasing influence from continental inflow, and deserves special attention. This averaged value agrees with values of -4‰ reported for Upper Jurassic analogues (Keupp et al., 1993; Ruff et al., 2005). In

comparison with modern examples that precipitate in equilibrium with seawater, and in which diagenetic imprint is negligible, a 4‰ offset is observed (values around 0‰ are reported by Keupp et al., 1993).

The most reliable record of water column oxygen isotope composition for the Rocha Poço section, i.e., with insignificant diagenetic overprint, was retrieved from an exceptionally well preserved belemnite rostrum with a value of -0.9‰ (Table 4.3). The latter represents water column conditions (16-23ºC), against benthic signals as retrieved from modern microbialites. This 1‰ offset is comparable with modern temperature gradient in tropical upper water layers (up to 100 meters), and paleodepths close to 60m adapt to this scenario (Steph et al., 2006). In this way, diagenesis would have reset $\delta^{18}O$ values from a pristine value of -1‰ to a significantly altered value of -3.5 to -4‰ (this work and Keupp et al., 1993; Ruff et al., 2005). A rather complex diagenetic course is envisaged to account for this depletion. The first imprint must have been forced by biodiagenesis (Neuweilwer et al., 2003; Olivier et al., 2006; Desrochers et al., 2007; Neuweiler et al., 2007), since microbially induced automicrite was recycled into detrital allomicrite (Neuweiler et al., 2003). A limited reworking combined with what might have been the contribution from inner-shelf carbonates and fine clastics is envisaged. The resulting bulk carbonate followed the standard early marine burial pathway, depleting oxygen isotope values towards values of -3.5‰. The relative contribution of biodiagenesis to this value is difficult to quantify based on the data set available.

Overall, $\delta^{18}O_{belemnite}$ values of screened specimens oscillate around a value of -0.6‰ (σ =0.3‰). Paleotemperature estimates obtained from $\delta^{18}O_{belemnite}$ may provide some evidence on the preferred habitat of these nektonic organisms. Based on the obtained data, the analyzed belemnites inhabited preferentially water masses with temperatures in a range between 15-21ºC. This paleotemperature range is in agreement with well preserved coeval belemnite data gathered from Majorca Island (Price and Sellwood, 1994) and also consistent with direct temperature measurements from what might be analogous modern settings with a similar bathymetry. Examples include the waters masses above the present-day Hancock seamount, situated at latitudes of approximately 30°N on the Hawaiian Ridge (Boehlert, 1988).

Ammonite shells present very comparable luminescence patterns (Fig. 4.8A, B), whilst $\delta^{18}O_{ammonite}$ ratios are variant (Fig. 4.8E). Cathodoluminescence images where used for pixel counting in order to quantify the relative proportion of specific different paragenetic phases

(Fig. 4.8C, D). Phase 1 cements are abundant in some cases (images B and D in Figure 4.8), occluding a total of 40% of the former shell. Oxygen-isotope values of phase 1 cements match those of $\delta^{18}O_{micrite}$. Here, given the predominance of phase 1 cements, bulk ammonite isotope ratios plot close to the assumed marine values. In the other neomorphic ammonite shell analyzed, phase 1 cement comprises only about 20% of the total bulk shell material (Fig. 4.8C). As a consequence, $\delta^{18}O_{ammonite}$ from this sample plots closer to early burial values (Fig. 4.8E), more specifically the data are consistent with shallow marine burial isotope ratios (Bruckschen and Richter, 1994).

Silica diagenesis

The occurrence of siliceous horizons characterizes the Cuber section and mainly occurs in Upper Oxfordian, Kimmeridgian and Middle to Upper Tithonian deposits. Marine siliceous skeletons, e.g., sponge spicules, diatoms, and radiolarian, provide biogenic opal A via dissolution of metastable opaline SiO_2 (Fanning and Schink, 1969; James et al., 2000). Given the open marine setting under discussion, spongae are discarded as source of opal A. Elevated contents in manganese (Fig. 4.11) may agree with a hydrothermal influence (Bender et al., 1970; Kickmaier and Peters, 1990; Corbin et al., 2000). Judging from the overall depleted $\delta^{18}O_{micrite}$ of silica-bearing horizons, lacking evidence for diagenesis, biogenic silica accumulation was perhaps related to locally warmer water masses and increased nutrient gradients (Jones and Jenkyns, 2001). This view is in agreement with the observed anti-correlation of $\delta^{18}O_{micrite}$ and Mn abundances (Fig. 4.11).

4.5.3- The epioceanic record

Having considered possible diagenetic alteration, isotope data are now placed in their paleogeographical context across the proximal-to-distal transect sampled. A comparable carbon-isotope stratigraphic pattern is recorded in all epioceanic sections (Fig. 4.10A). This pattern matches previously published data from Upper Jurassic Tethyan sections (Bartolini et al., 1996, 1999; Weissert and Mohr, 1996; Cecca et al., 2001; Rey and Delgado, 2002; Savary et al., 2003; Rais et al., 2007; Coimbra et al., 2009). Epioceanic sections shown here thus recorded an, at least Tethys-wide, chemostratigraphic evolution of seawater $\delta^{13}C_{DIC}$.

The mid-Oxfordian transgression is recorded as a positive peak in $\delta^{13}C_{micrite}$ in all epioceanic sections. Later, decreasing values towards Late Tithonian times are observed. Thus, local paleo-oceanographic features do not overprint the overall Tethyan epioceanic pattern. This observation is relevant given the very complex bottom physiography in the studied transect (Fig. 4.1). Spatially complex, local productivity changes similar to modern oceans are expected due to up- and downwelling patterns (Boehlert, 1988; Beckmann and Mohn, 2002, Auster et al., 2005), as well as associated local hydrodynamics. Accepting the overall significance of the data obtained, these local features were buffered by the isotope signature of the open, oceanic water masses.

Similar to carbon, the $\delta^{18}O_{micrite}$ record of all epioceanic sections is relatively homogenous. Overall, excursions in $\delta^{18}O_{micrite}$ tend to be more pronounced in the most distal section (Cardador section; Fig. 4.10B) but are still recognized in more proximal ones. Interestingly, $\delta^{18}O_{micrite}$ seems to follow relative changes in sea level, with values being significantly more positive (1‰ higher) during periods of higher sea level. Examples include the Mid-Oxfordian transgression and the eustatic maximum towards the end of the Kimmeridgian. Relative differences in absolute values, as observed in different epioceanic sections, could relate to local differences in paleo-geographic setting and paleo-hydrodynamics.

Acknowledging the fundamental problems of comparative seawater temperature estimates, the paleotemperature equation of Anderson and Arthur (1983) was also applied to matrix micrite $\delta^{18}O$ from epioceanic sections. Averaged $\delta^{18}O_{micirte}$ ratios from each epioceanic section proposed, from proximal to distal, a seawater paleotemperature range of 15-22ºC for the Cañada del Hornillo and Puerto Escaño sections, temperatures of 20-27ºC for Cuber and Cala Fornells sections and 11-17ºC for the Cardador and Salcedo sections (Figs. 4.1 through 4.3). The most distal sections (Cardador and Salcedo; Figs. 4.1 through 4.3) record relative cooler marine porewater paleotemperatures of 11 to 17ºC. In comparison, the Cañada del Hornillo and Puerto Escaño sections (Figs. 4.1 to 4.3), i.e., the less distal epioceanic sections, seem to reflect slightly warmer pore water paleotemperatures of 15-22ºC. If genuine, this trend is consistent with their paleogeographic location and the concept of increasingly cooler temperatures with increasingly more oceanic (deeper?) sections.

The sections from the Majorca Island (Figs. 4.1 to 4.3) recorded the overall warmest paleotemperatures of 20 to 27ºC. Considering the limitations of an essentially diagenesis-

sensitive proxy such as $\delta^{18}O$, this might either place these sections at an overall less distal, shallower setting characterized by warmer water masses within the epioceanic fringe, or reveal local differences in paleo-oceanographic parameters with respect to sections from southern Spain. A departure from the general trends described above is the 1‰ positive shift recorded in sections on Majorca (Cuber and Cala Fornells; Fig. 4.10B). The underlying reasons are at present unclear.

4.5.4- Oxygen isotope ratios and skeletal abundance in epiocenic sections

A statistically significant linear correlation is observed between oxygen-isotope composition of matrix micrite and the estimated abundance of bioclasts for all epioceanic sections (Fig. 4.7A). When stratigraphically plotted (Fig. 4.7B), $\delta^{18}O$ maxima and peak maxima in skeletal abundance are nearly coincident (Fig. 4.7B). A particular case is that of calcareous, less nodular, grayish marker beds characterized by both $\delta^{18}O$ and skeletal maxima that were used for lateral correlation of time-equivalent portions of sections (Coimbra et al., 2009) deposited close to the Kimmeridgian/Tithonian boundary. This pattern requires an explanation. Earlier, it has been suggested that the $\delta^{18}O$ record of the epioceanic sections shown here follows Late Jurassic sea level fluctuations (Coimbra et al., 2009). Specifically, cooler seawater temperatures during higher sea levels are recorded by more positive $\delta^{18}O$ values (Fig. 4.10B).

The relation between oceanographic parameters and depositional conditions has been considered before (McCave et al., 1995a, b). In a context of sea level change, initial transgressive phases are often recorded as ravinement surfaces (i.e., bioclastic-rich horizons) with rising sea level bottom-current energy is commonly decreased, resulting in reduced winnowing, sorting and changes in net accumulation rates on epioceanic swells. It must be emphasized, however, that these relations are less than trivial and the concepts presented here represent simplifications (Immenhauser, 2009). The case of less nodular, grayish marker beds that correlate with the eustatic maximum near the Kimmeridgian/Tithonian boundary might support to the above considerations. The higher accumulation rate recorded is supported by laminated fabrics (sacoccomites) associated to reworking and presumably higher bottom water oxygenation related to bottom instability. The later factors might be independent from the eustatic maximum.

According to previous studies dealing with Ammonitico Rosso pigmentation (Berner, 1969; Jenkyns, 1971; Mamet and Préat 2003, 2006; Préat et al., 2006, 2008; van der Kooij et al., 2007), gray carbonate facies represents reducing porewater conditions often attributed to higher sedimentation rates and suboxic pore waters (Boulvain et al., 2001 and references above). Case studies from modern settings indicate that in many cases, oxygen levels and seawater temperature are inversely covariant (Weiss, 1970; Chester 2000; Keeling et al., 2010). Assuming normal seawater salinity (3.5‰) the observed decrease in bottom temperature from 15ºC (Coimbra et al., 2009) to 11ºC, i.e., 4ºC cooler in agreement with the observed 1‰ increase in $\delta^{18}O$ as suggested by Marshall (1992) would result in an increase of about 10% in the concentration of dissolved oxygen in seawater (Kester, 1975, 1975). In this way, field observations and geochemical data account for higher oxygenation levels referring to specific paleoceanographic conditions on epioceanic swells.

4.5.5- The epicontinental record

The epicontinental domain of the studied transect is represented by the Rocha Poço section (Figs. 4.1 to 4.3). The development of sponge bioherms above more silty facies with ammonites agrees with changing ecological conditions including the deterioration of living conditions for ammonites. This pattern is perhaps related to carbonate margin progradation following proposed relative sea level trends (Olóriz, 2000), including a decrease in detrital input and bottom stabilization favouring growth of sponge buildups. An ammonite-bearing marker bed interrupting spongiolithic facies during the peak Early Kimmeridgian transgression (Divisum Chron) supports this interpretation. The characteristic marine carbon isotope signature of 2‰ deduced from the epioceanic sections is present in bulk samples from sponge bioherms and stratigraphically overlying limestones (Fig. 4.10A). In the lowermost part of the spongiolithic facies, detrital carbonate material with more depleted $\delta^{13}C$ values (about 5‰) fills primary pore and interstitial spaces in the carbonate fabric. These depleted values are not found where the spongiolithic facies is fully developed (Fig. 4.10A). This feature may reveal the transitional environmental phase between the previous silty limestone facies and the environmental conditions favouring the growth of sponge-algal consortia (see microfacies description).

Within this comparatively shallow, proximal setting the only potential subaerial exposure surface was recorded in the spongiolitic facies. Evidence for subaerial exposure is both geochemical, i.e., a negative carbon saw tooth shaped isotope shift (Fig. 4.10A; ^{18}O depleted rainwater and ^{13}C depleted soil zone CO_2; Allan and Matthews, 1982) and petrographic features such as epi-karstic dissolution cavities.

The epicontinental section analyzed at Rocha Poço shares some similarities with the studied epioceanic sections whilst relevant differences are observed mainly in the stratigraphically lower portions of the section. Matrix micrite $\delta^{13}C$ and $\delta^{18}O$ values from the more silty, lower portion of the Rocha Poço section (Figs. 4.2 and 4.3 for facies distribution) are depleted with respect to the overlying facies and other sections (Figs. 4.9, 4.10 and 4.12). Possible mechanisms include (i) differential diagenetic alteration, (ii) changes in local water mass properties, or (iii) an admixture of carbonate material from different source areas, (iv) a combination of these factors. Given that this section is the only epicontinental record among all the sampled localities, inner-to-mid platform derived material contribution is expected. Longer residence time of seawater on platforms results on aging of the affected water mass during which the input of ^{12}C from remineralized organic carbon may lower the $\delta^{13}C$ values up to 4‰ (Immenhauser et al., 2002, 2008). Depleted oxygen isotope values agree with silty to fine sandy limestone and marls comparatively rich in quartz and small plants remains. The above considerations confirm the higher level of complexity found in epicontinental sections and their sedimentological and geochemical record. The comparison with a data set that includes information on both spatial as well as temporal changes, however, allows for an improved understanding of these complex archives.

4. 6- Conclusions

The geochemical analysis of different Upper Jurassic carbonate materials collected across a several-hundred-kilometer long proximal-to-distal transect in southern Spain, the Balearic Islands and southern Portugal allows for the following conclusions:

1. The contrast comparison of geochemical data from Ammonitico Rosso matrix micrites, different carbonate cements, neomorphic ammonite shells and belemnite rostra allowed for a separation of noise – specifically the differential diagenetic overprint and local to regional features – from signals forced by Tethys-wide paleo-oceanographic patterns.

Cathodoluminescence suggests a fair preservation of matrix micrites and belemnite rostra, as well as shallow marine burial precipitation of secondary carbonate cements as neomorphic ammonite shells and different void-filling carbonate phases.

2. Stratigraphic trends in carbon and oxygen isotope composition across all epioceanic sections are in good agreement with major Late Jurassic paleoceanographic features. The Middle Oxfordian Tethyan transgression is recorded as carbon-isotope maxima related to higher productivity levels. Sea-level highs are reflected in ^{18}O-enriched values, probably reflecting relatively cooler water masses. Variations in $\delta^{18}O$ are perhaps best interpreted as local differences in current patterns driven by relative bottom physiography and related oceanographic features.

3. In contrast to the commonly held view regarding the reliability of belemnite data, carbon-isotope data compiled here most likely reflect vital effects that differ from oceanic $\delta^{13}C_{DIC}$. This is in agreement with belemnite oxygen-isotope ratios, apparently not affected by metabolic processes, which are in agreement with proposed seawater values. Interestingly, Ammonitico Rosso matrix micrite geochemical data –often considered as less reliable relative to those from belemnite rostra – are in good agreement with proposed seawater values.

4. Whilst most geochemical patterns are recognized as at least Tethys wide in significance, regional features are present too. An example for this is found in the silty carbonate-clastic facies registered at the base of the epicontinental Rocha Poço section. The source of this material is most likely the inner platform domain not investigated in the context of this study. Isotope data from this interval deviate from the first-order patterns recognized elsewhere.

5. Two lower-order features require attention: (i) Skeletal abundance maxima coincide with peak values in geochemical data. This pattern points to a complex relation between relative sea level, productivity, sediment entrainment and the geochemical record. (ii) Silica-bearing intervals reveal increased nutrient levels potentially triggered by hydrothermal pulses. Evidence for this comes from the anti-correlation of manganese elemental abundances and oxygen isotopic composition.

6. The data obtained represent a strong motivation for a spatial assessment of patterns in chemostratigraphy as opposed to the one-dimensional approach presented in many studies. The main significance lies in a much improved set of arguments for the separation of signal from noise.

Acknowledgements

We wish to thank Dieter Buhl, Ulrike Schulte, Beate Gehnen and Noushin Arshadi (Ruhr Universität Bochum-RUB) for their support during laboratory measurements; Rolf Neuser (RUB) for the cathodoluminescence and SEM analysis; Matthias Born (RUB) and Alberto Montes (University of Granada-UGR) for the preparation of thin sections; and Alicia González, Concepción Hernandez and Hoda Khaldy (CIC-UGR) for collaboration during SEM analysis and preparation of laboratory material. We also thank Beatriz Marques (University of Lisbon) for background information and field support in S Portugal. This research was supported by Projects CGL2005-01319 and CGL2008-05251-E (MICINN) and the Research Group RNM-178 Junta de Andalucía, Spain.

5

Sediment provenance supported by geochemical evidence (Upper Jurassic, Majorca Island)

Rute Coimbra[1], Federico Olóriz[1]

[1] Departamento de Estratigrafía y Paleontología, Universidad de Granada, Spain

Submitted to Terra Nova (August 2011)

Abstract

The notion that diagenetic imprint on ancient carbonates significantly compromises paleoenvironmental interpretations is revealed as an oversimplification. The enigmatic case within the scope of this research is the extended, homogeneous deposit with distinctive dark brown colour and very fine grain size, which markedly contrast with standard deposition known from Jurassic epioceanic swells. Geochemical data of distinct carbonate materials is used to unravel its interpretation. Obtained results are compared with under- and over-lying deposits, as well as to coeval sections. Conspicuously higher than expected carbon (and oxygen) isotope signatures, together with strontium enrichment and atypically low iron and manganese concentrations favour a distant, shallower, probably aragonitic sedimentary supply. Modern and ancient examples of carbonate deposition are integrated with possible hydrodynamic conditions justifying transport along the studied area. The potential source area is envisaged towards the NE.

♦ ♦ ♦

5.1- Introduction and geological setting

The Balearic Archipelago (Fig. 5.1A), is an extension of the Betic Cordillera (Fontboté et al., 1990; but see Olóriz et al., 2002a and Sabat et al., 2011), showing late Jurassic brown limestones at the Sierra Norte of the Majorca Island. These are exceptional deposits on west Tethyan epioceanic swells, otherwise dominated by Ammonitico Rosso facies. We clarify these bizarre depositional conditions through verifiable arguments, including information from potential recent analogous.

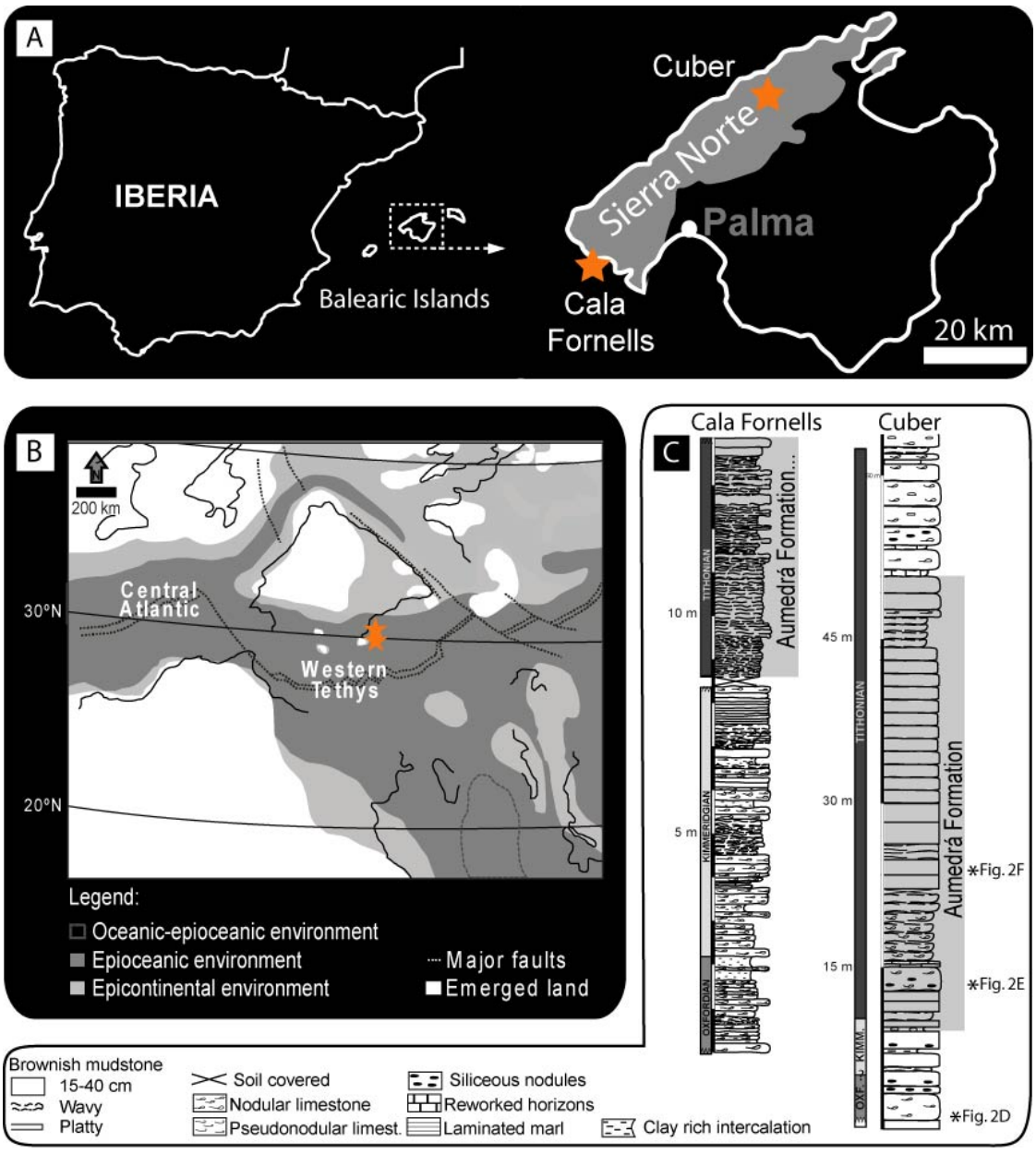

Fig. 5.1- A: Location of the studied sections (indicated by stars). B: Late Jurassic paleogeographic reconstruction of western and central Tethyan realm. Plate tectonic setting from Stampfli and Borel, 2002, and depositional environments after Thierry et al., 2000a, b. Locations of study sections is indicated by stars. C: Stratigraphic distribution of the studied lithofacies along both sections. Asterisks refer to microfacies photographs presented in Fig. 5.2.

The Cuber and Cala Fornells sections (Fig. 5.1A to C) crop out in Sierra Norte, Majorca (Alvaro et al., 1984 and Sabat et al., 2011 for structural interpretation). The Upper Jurassic at Sierra Norte is dominated by Ammonitico Rosso facies (AR) (Caracuel and Olóriz, 1998, 1999 for details). The Alfabia Fm. (8-10 meters thick) is comprised of thin alternating horizons of AR and grey, more or less nodular marly limestones. Siliceous horizons occur occasionally. The Aumedrá Fm. is characterized by expanded, well bedded brownish and macrofossil poor limestones (Figs. 5.1C and 5.2) (ca. 40 meters, i.e., 57% of total thickness and 6% of the time contained in Upper Jurassic deposits; Caracuel and Olóriz, 1999). The Son Torrelles Fm. (ca. 10 meters) shows returning AR depositional conditions, commonly with reworked sediments and siliceous horizons.

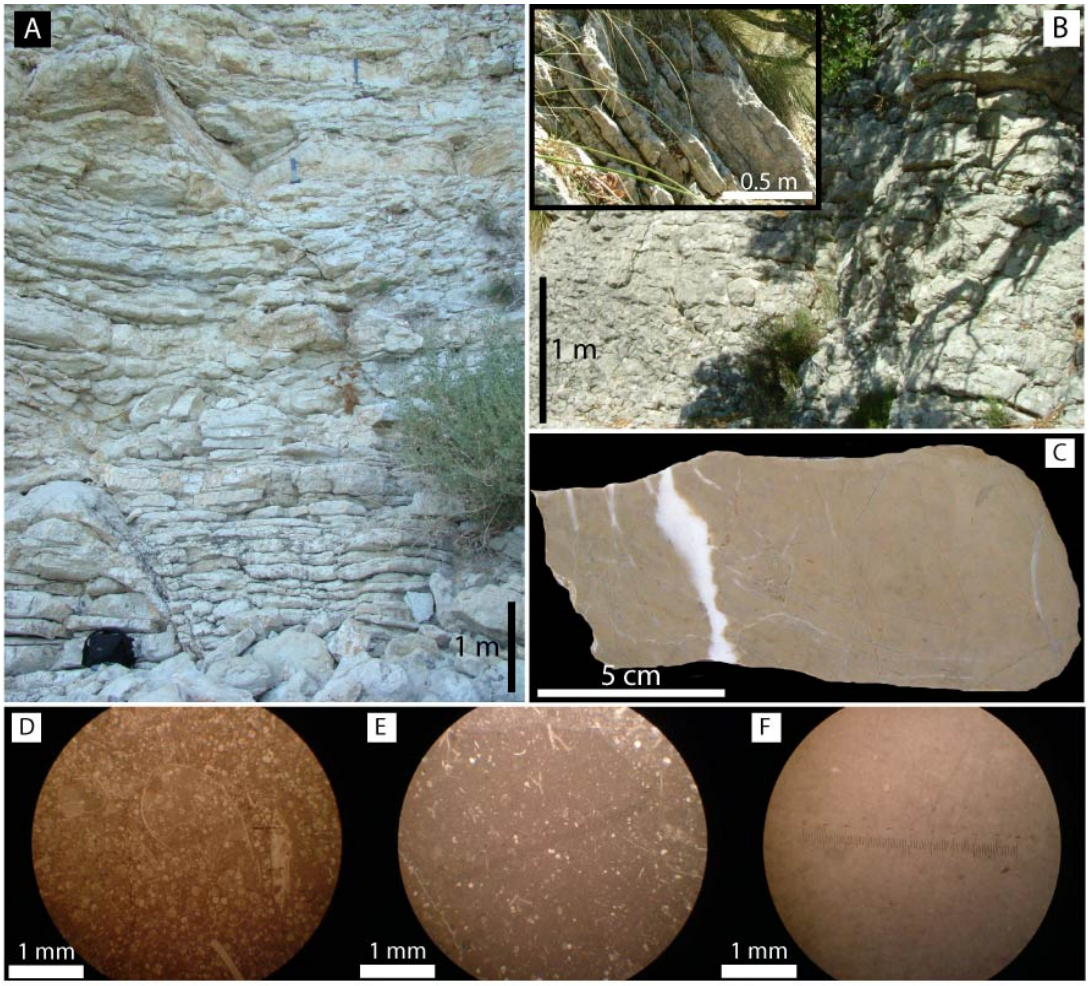

Fig. 5.2- Examples of distinctive aspects of Aumedrá Fm. horizons. A and B: Typical tabular aspect of the Aumedrá Fm. at the Cala Fornells and Cuber sections, respectively. C: Hand sample slab from the Aumedrá Fm. showing the typical dark brown colour. Note the presence of distinct carbonate materials (matrix micrite and carbonate cements). D to F: Microfacies views (see stratigraphic position in Fig. 5.1C) illustrating the variability of bioclast content. Note scarcity of bioclasts in samples from the Aumedrá Fm. (E and F) in comparison to Oxfordian Ammonitico Rosso (D).

5.2- Methods

Hand samples (n=122) were collected under precise ammonite biostratigrahy (Olóriz et al., 2002a,b) from the Cala Fornells and Cuber sections, covering Middle Oxfordian to uppermost Tithonian deposits (Fig. 5.1C).

Rock slabs were examined for microfacies, cathodoluminescence and geochemistry. Cathodoluminescence was preformed using a hot stage cathode luminescence microscope

(HC4-LM at Ruhr University Bochum, Germany) to evaluate the degree of preservation of matrix micrite, carbonate cements and belemnite rostra (e.g., Machel et al., 1991; Bruckschen and Richter, 1994; Barbin and Schvoerer, 1997).

Bulk powder sub-samples were drilled for geochemical analysis of matrix micrite (n=380), carbonate cements (n=61) and belemnite rostra (n=16).

Stable C and O isotopes and trace element analysis was performed at Ruhr University. A ThermoFinnigan MAT delta-S mass spectrometer was used for isotope analysis, following McCrea's (1950) method. Analytical precision (±1σ), controlled by NBS19 and internal standards, was better than ±0.03 and ±0.05‰ for $\delta^{13}C$ and $\delta^{18}O$, respectively. Duplicate runs presented deviations of ±0.01‰ for $\delta^{13}C$ and ±0.05‰ for $\delta^{18}O$. The standard δ-notation in per mil (‰) relative to V-PDB is used.

Aliquots of samples used for isotopic analysis were investigated for Ca, Mg, Mn, Fe and Sr elemental composition using inductively coupled plasma-atomic emission spectrometry (ICP-AES). Elemental scattering for duplicate runs was ca. 3%.

5.3- Results

5.3.1- Optical inspection

Microfacies analysis commonly revealed a low abundance of microfossils in brown carbonates (Fig. 5.2E and F, Fig. 5.2D shows AR for comparison).

The Alfabia Fm. (AR) is mainly composed of wackestones (occasionally packestones) showing Conoglobigerinidae, radiolaria, *Saccocoma* and filaments. Undetermined benthic foraminifera, gastropods, bivalves, brachiopods, ammonoids and some aptychi also occur. The Aumedrá Fm. presents relatively constant microfacies, mainly mudstones, with scarce *Saccocoma*, filaments and radiolarians. Occasionally, undetermined benthic foraminifera are present, as well as sponge spicules, gastropods, aptychi and bivalves. The Son Torrelles Fm. (AR) is mainly composed of wackestones with radiolarians and *Saccocoma*, and less commonly ammonoids, bivalves, gastropods, benthic foraminifera, sponge spicules, dinoflagellate cysts and ostracods.

Cathodoluminescence of matrix micrite revealed varying luminescence, from bright to duller orange (Fig. 5.3B and D for AR and Aumedrá Fm., respectively). Carbonate cements

(blocky calcite) show three generations with distinct luminescence (Fig. 5.3F). The earliest is dark, rimmed by a discrete brighter orange phase. The most luminescent blocky calcite is the latest, showing medium to bright orange zonation, cross-cut by duller veining (Fig. 5.3D). Belemnite rostra revealed intrinsic luminescence (Fig. 5.3F and H) with interlaminae of bright orange luminescent cement, also identified on small fractures in secondary blocky calcite (Fig. 5.3H).

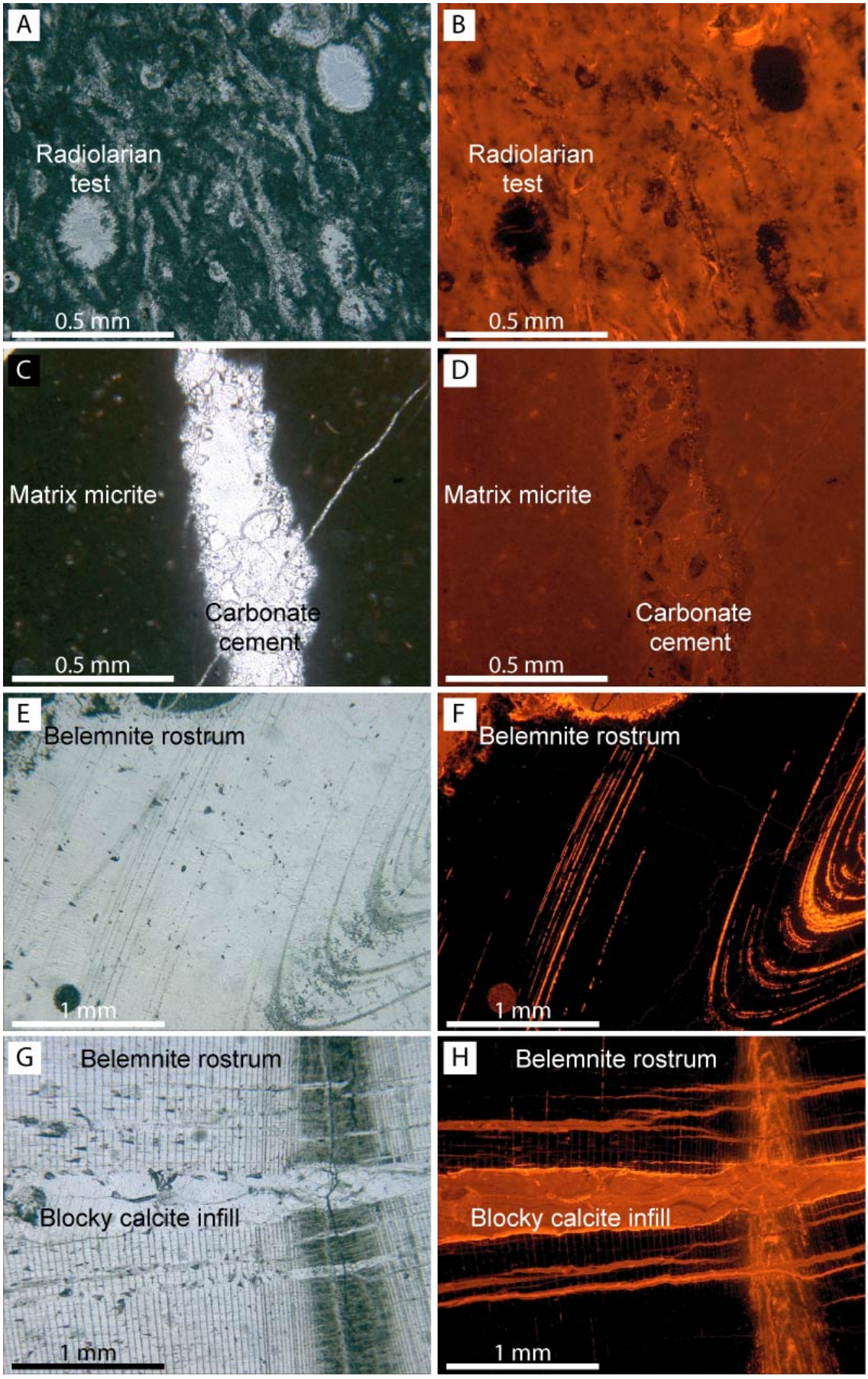
A
Radiolarian test
0.5 mm
B
Radiolarian test
0.5 mm
C
Matrix micrite
Carbonate cement
0.5 mm
D
Matrix micrite
Carbonate cement
0.5 mm
E
Belemnite rostrum
1 mm
F
Belemnite rostrum
1 mm
G
Belemnite rostrum
Blocky calcite infill
1 mm
H
Belemnite rostrum
Blocky calcite infill
1 mm

Fig. 5.3 Cathodoluminescence images of the distinct carbonate materials analysed. A: Matrix micrite from an Oxfordian sample showing the presence of radiolarian tests and filaments (bivalves). B: The same area as A, under cathodoluminescence (note orange luminescence); C: Carbonate cement encased in matrix micrite, sample from the Aumedrá Fm.. D: The same area as C, under cathodoluminescence. Note duller orange luminescence of matrix micrite and of carbonate cement generations filling the void. E: Tangent longitudinal cut of belemnite rostrum. F: Same specimen as E, under cathodoluminescence, showing overall intrinsic luminescence (by contrast note the very fine bright orange luminescence veins and interlaminae areas). G: Close up of belemnite rostrum in tangent longitudinal cut (note the blocky calcite infill that heals a fracture). H: Same area as G, under cathodoluminescence, showing areas of intrinsic luminescence and very bright orange carbonate cement infill.

5.3.2- Analytical results

Carbon and oxygen isotope values for all carbonate materials are summarized bellow.

	$\delta^{13}C$ ‰ (V-PDB)		$\delta^{18}O$ ‰ (V-PDB)		
	Average (± stand. dev.)	Range [min.;max.]	Average (± stand. dev.)	Range [min.;max.]	n
Matrix micrite	2.3±0.6	[1.3;3.4]	-2.1±0.7	[-3.9;-0.4]	89
Matrix micrite (A. Fm.)	2.6±0.2	[2.2;3.0]	-1.4±0.7	[-3.2; 0.5]	33
Carb. cements	2.3±0.4	[1.3;3.5]	-4.8±1.3	[-9.1;-3.1]	61
Belemnite rostra	0.8±0.7	[0.9;1.8]	-0.7±0.5	[-1.9; 0.2]	16

(A. Fm.- Aumedrá Formation; Carb. cements- carbonate cements; stand. dev.- standard deviation)

Table 5.1- Range and average values for carbon and oxygen stable isotope ratios.

The respective crossplot is presented in Fig. 5.4A. Cluster (a) includes matrix micrite values (average values of 2.3 and -2.1‰, for $\delta^{13}C$ and $\delta^{18}O$, respectively). Cluster (b) includes only Aumedrá matrix micrite samples (average of 2.6‰ and -1.4, for $\delta^{13}C$ and $\delta^{18}O$, respectively) within the range values of cluster (a). Cluster (c) gathers secondary carbonate cements showing the same $\delta^{13}C$ range as cluster (a), but with depleted $\delta^{18}O$ values (up to -9.1‰). Cluster (d) includes all analysed belemnite rostra samples, providing the lowest values of $\delta^{13}C$ (-0.6 to 1.8‰) and a narrow range of slightly higher $\delta^{18}O$ values (-1.9 to 0.2‰). The average $\delta^{18}O_{belemnite}$ value of the best preserved specimens (Fig. 5.4A and Table 5.3) was used for paleotemperature estimations, following Anderson and Arthur (1983), with $\delta_{seawater}$ from -1 to 0‰ SMOW.

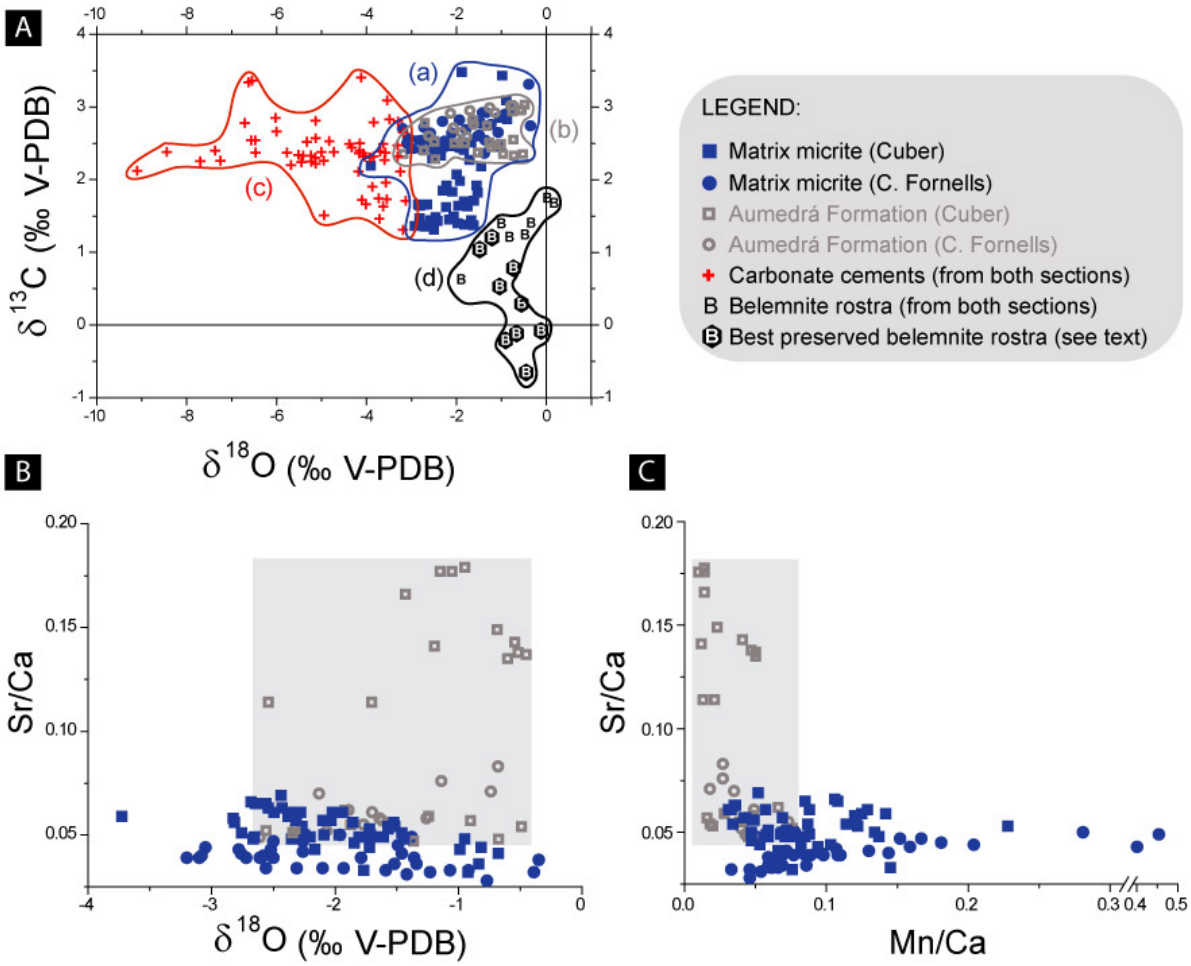

Fig. 5.4- Geochemical data obtained from the distinct materials analysed. A: Crossplot including all studied materials, grouped into clusters. Cluster (a)- matrix micrite samples from the Alfabia, Aumedrá and Son Torrellles Fms. for both sections; cluster (b)- matrix micrite samples from the Aumedrá Fm.; cluster (c)- carbonate cements from both sections; cluster (d)- belemnite rostra from both sections (best preserved specimens indicated, see legend). B and C: Strontium/Ca vs. oxygen stable isotope ratio and Mn/Ca, respectively, for matrix micrite samples from both sections (samples from the Aumedrá Fm. are differentiated, see legend).

No covariance is observed between strontium concentrations and $\delta^{18}O_{micrite}$ or Mn (Fig. 5.4B and C). Increasing Sr concentration relates to a wide range of $\delta^{18}O_{micrite}$ values and very low Mn content.

Stratigraphic variation in $\delta^{13}C_{micrite}$ and $\delta^{18}O_{micrite}$ is presented in Fig. 5.5, along with carbonate cement values. Overlapping $\delta^{13}C$ values were obtained for both materials, but $\delta^{18}O_{cements}$ is 2‰ lower than encasing $\delta^{18}O_{micrite}$. A significant positive shift was registered at

the base of both sections (Middle Oxfordian) and higher $\delta^{13}C$ values were recorded for Aumedrá Fm. horizons. The same applies for the obtained $\delta^{18}O$ record.

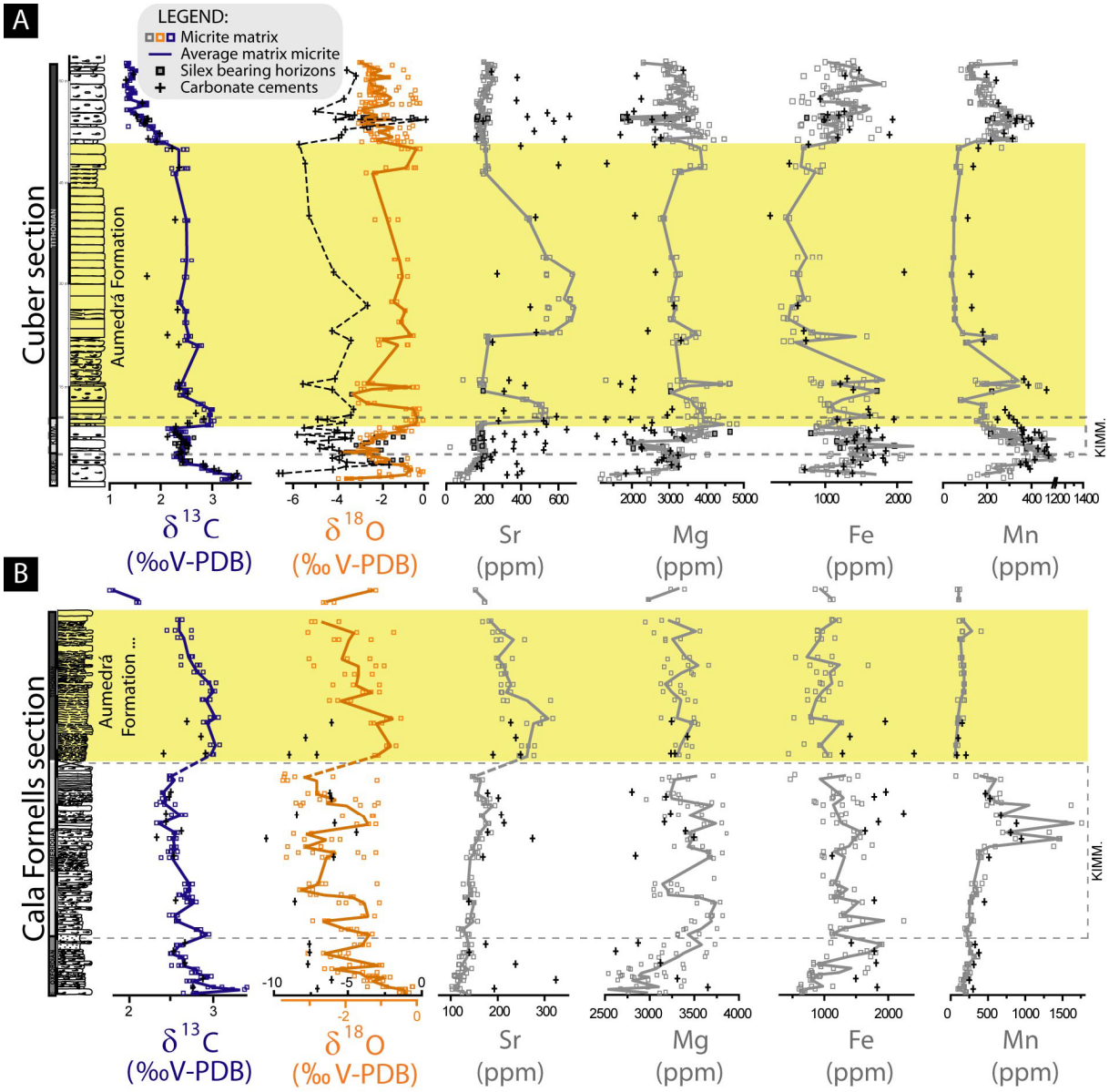

Fig. 5.5- Matrix micrite and carbonate cement C and O stable isotope ratios and elemental stratigraphy (Sr, Mg, Fe and Mn) from both Upper Jurassic sections studied (A: Cuber section and B: Cala Fornells section). Intra-sample isotopic variability is marked with squares, and lines connect mean values calculated at horizon level. Lithologies are according to Fig. 5.1.

Elemental composition of matrix micrite and carbonate cements is presented in Fig. 5.5A and B (see Table 5.2). The onset of Aumedrá deposition relates to striking variations. Strontium increases up to 700 ppm, on average 93% higher than under- and overlying horizons; Fe concentrations decrease (22% lower); and Mn concentrations are remarkably

lower, about 100 ppm (58% lower). Magnesium concentrations remain rather stable. Carbonate cements offer lower Mg concentrations and an overall increase in Sr, Fe and Mn abundances.

	Cala Fornells section				Cuber section			
	MM	MM (A. Fm.)	CC	CC (A. Fm.)	MM	MM (A.Fm.)	CC	CC (A. Fm.)
Mg (ppm)	3336	3356	3090	3164	3144	3502	2570	2426
Sr (ppm)	142	234	204	223	188	418	408	423
Fe (ppm)	1233	1001	1944	1613	1188	910	1509	1147
Mn (ppm)	434	152	533	179	279	129	427	195
n	34	12	13	14	53	21	36	14

(MM-matrix micrite; CC- Carbonate cements; A. Fm.- Aumedrá Formation)

Table 5.2- Average elemental concentrations for matrix micrite and carbonate cements.

	$\delta^{13}C$ ‰ (V-PDB)	$\delta^{18}O$ ‰ (V-PDB)	Mg (ppm)	Fe (ppm)	Mn (ppm)	Sr (ppm)	$\Delta\delta^{13}C$* ‰(V-PDB)	$\Delta\delta^{18}O$* ‰ (V-PDB)
Cuber section	-0.2	-0.9	2398	107	22	1129	-2.7	+2.7
	-0.6	-0.5	2340	62	6	1171	-1.8	+2.1
	-0.2	-0.8	2488	185	27	935	-1.5	+1.8
Cala Fornells section	0.3	-0.6	2147	273	100	847	-0.5	+2.6
	-0.0	-0.1	1909	51	65	1019	-1.0	+2.4
	1.2	-0.5	2611	187	25	774	-1.0	+1.2
	0.5	-1.0	2622	248	42	906	-1.0	+2.0
	0.8	-0.7	3781	440	75	914	-1.0	+2.0
	1.0	-1.5	2170	239	58	842	-1.0	+1.5

(*) offset between belemnite rostra and encasing matrix micrite (see text for details).

Table 5.-3 Isotope (C and O) and elemental composition for the best preserved belemnite rostra (see text for selected "cut-off" values).

5.4- Interpretation and Discussion

5.4.1- Regional/global record vs. diagenetic overprint

Cathodoluminescence inspection reveals duller luminescence for Aumedrá deposits. Cathodoluminescence interpretations (e.g., Boggs and Krinsly, 2006 and references therein) are controversial concerning interactions and absolute concentrations of luminescence

activators ($Mn^{2+, 4+}$, Fe^{4+}, trivalent rare earth elements, lattice defects) and quenchers (mainly Fe^{2+}; but also Mn^{2+} at high concentrations by self quenching). It is widely accepted that very low Mn^{2+} concentration activates luminescence (10 to 30 ppm; e.g., ten Have and Heijnen, 1985; Barbin and Schvoerer, 1997), with linear relationship between intensity and Mn^{2+} concentration (up to 200 ppm, ten Have and Heijnen, 1985 or 400 ppm, Barbin and Schvoerer, 1997) assuming that Fe^{2+} was not actively quenching. Yet, reported quenching thresholds for Fe^{2+} vary from 30-60ppm to 3000-4000 ppm (e.g., Machel, 2000; Götte and Richter, 2009). Regarding the samples under scope, obtained Mn concentrations show pronounced peaks up to 1500 ppm, recognized on coeval sections (Coimbra et al., 2009). Manganese enrichment is attributed to hydrothermal activity (rather than diagenetic overprint) occurring during geodynamic readjustments (e.g., reported from Shanmugam and Benedict III, 1983 to Corbin et al., 2000). In Aumedrá samples, lower Mn and Fe contents (58 and 22%, respectively, Table 5.2) result in duller orange luminescence (Fig. 5.3D). Absolute values (Table 5.2) agree with reported activation and quenching thresholds (see above).

Changes in redox potential during early shallow marine burial (Bruckschen and Richter, 1994) explain differential luminescence in carbonate cements (Fig. 5.3D). Belemnite rostra present intrinsic luminescence (Fig. 5.3F and H), reflecting pristine preservation. Elemental screening agrees with this interpretation for 60% of the analysed specimens (Table 5.3 and Fig. 5.4A), with elemental concentrations within the assumed range for pristine belemnites (from Anderson et al., 1994 to Price and Teece, 2010 for "cut-off" values).

Overall, matrix micrite $\delta^{13}C$ values are comparable with those reported for epioceanic settings of similar age (e.g., Weissert and Mohr, 1996; Bartolini et al., 1999). This holds true also for $\delta^{13}C_{cements}$, but not for $\delta^{13}C_{belemnite}$. For the latter, lower values should derive from metabolic fractionation during growth (ontogenic variations and precipitation out of equilibrium with seawater; e.g., Price et al., 2009) or, alternatively, distinct water masses. Interestingly, $\delta^{18}O_{belemnite}$ presents the lightest and narrowest range of values, rendering seawater paleotemperatures of 15-19ºC. This agrees with published data from coeval settings nearby (Coimbra et al., 2009 and references therein). The minor depletion of $\delta^{18}O_{micrite}$ compared to $\delta^{18}O_{belemnite}$ values, indicates slightly warmer, shallow marine burial fluids. Latter carbonate cements are expected to record higher burial temperature ($\delta^{18}O_{cements}$ as low as 9‰). Obtained $\delta^{13}C$ and $\delta^{18}O$ show stratigraphic trends comparable to known Upper Jurassic records from northern Tethyan margins (e.g., Bartolini et al., 1999; Coimbra et al., 2009).

Similar carbonate cement stratigraphic trends attest to the preservation of relative fluctuations throughout the studied stratigraphic interval (e.g., Frank and Lohman, 1996 for similar observations). The only exception is Aumedrá deposition, discussed below.

Matrix micrite was tested for diagenetic imprint by plotting the most sensitive geochemical indicators (here Sr, Mn and $\delta^{18}O$), which revealed no covariance (Fig. 5.4B and C; see from Veizer, 1983 to Immenhauser et al., 2003 and van der Kooij et al., 2009). This suggests that the elemental record is less affected by the mild diagenetic imprint verified in the $\delta^{18}O$ record. This holds true also for Aumedrá horizons.

5.4.2- Aumedrá deposits: sediment provenance and transportation

Aumedrá deposits clearly deviate from AR by exceptional, rapid deposition of platy to slightly irregular, dark brown limestone beds (ca. 20 cm tick, Fig. 5.2A to C) and bioclast scarcity (Fig. 5.2D to F).

In contrast to AR geochemical background consistent with regional and global signals (see above), striking geochemical traits of Aumedrá limestones require clarification. Higher C and O isotope ratios and high Sr concentrations, coupled with low Mn and Fe abundances point to an alternative sedimentary source. Particular paleoceanographic conditions may account for differences in accumulation rate, color, skeletal content and geochemistry.

Aumedrá deposits show very high average accumulation rate (40 meters during 1 Myr, without decompaction, vs. metre thick AR biozones). This indicates rapid, persistent hemi-pelagic contribution, hence episodes of enhanced carrying hydrodynamic capacity are envisaged (gravity driven processes included). Modern examples help to illustrate certain hydrodynamics that may account for the special case under study. Present knowledge of sediment distribution and recognition of sedimentary structures in modern basins improves understanding of redistribution mechanisms for particulate material suspended throughout the water column (from Moore, 1969 to McCave and Hall, 2006). Nepheloid layers carry suspended material comprising the dynamically sensitive fraction from 10 to 63µm (sortable silt; McCave et al., 1995a, b). Hence sorting by lateral transport could account for the fine grain size (< 100 µm) and for the absence of coarser skeletals in Aumedrá deposits, and thus, deposition resulted from decreased current energy (ca. 10 cm/s to avoid winnowing and removal of finer grains).

In this context, relatively elevated $\delta^{13}C$ values (Fig. 5.5) may have two possible sources, with and without isotope signatures typical for open marine settings or even their combination. In the first proposed scenario, $\delta^{13}C$ enrichment in Aumedrá deposits could indicate a shallower, more productive open-sea provenance area. In the second proposed scenario, higher than expected $\delta^{13}C$ values in Aumedrá sediments derived from sorting during sediment redistribution. Allocthonous sediments could reflect a $\delta^{13}C_{DIC}$ reservoir, at least as bulk signal. Sediment sorting during transportation would remove coarser components that then no longer contribute to $\delta^{13}C$ bulk signals. If so, Aumedrá deposits represent the finest size of originally heterogeneous sediments. This could potentially shift bulk signal towards higher $\delta^{13}C$ values, as reported for modern sediments (e.g., Swart, 2008; Swart et al., 2009).

Mineralogy can also be responsible for $\delta^{13}C$ variations, as seen in modern carbonate platforms. Aragonite-dominated sediments in shallow areas of the Great Bahama Bank, reveal enriched $\delta^{13}C$ values relative to pelagic deposits (Swart and Eberli, 2005). The dominance of aragonite enriches $\delta^{13}C$ compared to low-Mg calcite precipitated under similar equilibrium conditions (Rubinson and Clayton, 1969; Romaneck et al., 1992). Petrographic and geochemical data suggests aragonite precursors in the shallow water Upper Jurassic Mozduran limestone (as interpreted by Adabi and Rao, 1991), while local mineralogy is calcite-dominated in deeper areas (Adabi and Rao, 1996; Lasemi, 1996). The unusual combination of high Sr and low Fe and Mn abundances in Aumedrá samples (Table 5.2) agrees with aragonitic parent mineralogy. Moreover, crystallographic differences between calcite and aragonite influence elemental abundances, since incorporation of cations of ionic radii equal to or greater than that of Ca^{2+} (e.g., Sr) are favoured by aragonite, excluding smaller ions (Mn, Fe or Mg). Hence, lower Mn and Fe content in aragonitic lattices dictate concentrations as low as 20 ppm for warm water examples (e.g., Rao and Adabi, 1992). During aragonite precipitation, Mg is strongly discriminated against, with Mg/Ca values in aragonite 5 to 10 times lower than in calcite (e.g., James et al., 2005). Thereby, strontium concentrations may reach 8000 ppm (Veizer, 1983). Under normal marine conditions aragonite metastability forces a relatively fast neomorphism into a more stable low-Mg calcite. However, differences in elemental contents can be preserved after mineralogic stabilization, accounting for observed differences in Aumedrá deposits. Aragonite stabilization at the source area is favoured because dissolution and/or neomorphism would at least partially reset the geochemical record into the local marine signal (not verified). A rather

uniform Mg concentration attests for the openness of the system, which allows for Mg-redistribution during stabilization into low-Mg calcite (2000-4000 ppm; e.g., Veizer, 1983).

Shelf carbonates in Majorca (Fornós et al., 1988) are consistent with a north-east sediment source (Artá area), where bottom instability during the highest Jurassic relative sea level forced sediment remobilization and Aumedrá deposition.

5.5- Conclusions

Carbonate deposits in the Cuber and Cala Fornells sections demonstrate a mild, rather conservative diagenesis. Atypical Aumedrá carbonates disrupt background conditions for Tethyan open marine sedimentation and geochemical record on swells, observed in under- and overlying AR facies.

Macroscopic features such as very high accumulation rates, dark brown colour and scarce skeletals in Aumedrá limestones remained enigmatic until contrasted with the geochemical data presented here. Higher than expected $\delta^{13}C$ and $\delta^{18}O$ values, high Sr and low Mn, Fe concentrations, support the plausibility of an open-sea sedimentary supply for Aumedrá sediments. There, an aragonite factory in a shallower, warmer setting dictated the mineralogy of the sediments, which were remobilized and sorted during transport from source areas to the NE of the Majorca Island.

The notion that diagenetic overprint compromises the paleoenvironmental information retrieved from ancient carbonates is demonstrated to be oversimplified. The application of this approach to analogous cases of intercalation of atypical lithofacies is encouraged.

Acknowledgements

We wish to thank Adrian Immenhauser for productive discussions; Dieter Buhl, Ulrike Schulte, Beate Gehnen and Noushin Arshadi (Ruhr-University Bochum-RUB) for their collaboration during measurements; Rolf Neuser (RUB) for the cathodoluminescence analysis and SEM inspection; Matthias Born (RUB) and Alberto Montes (University of Granada) for the preparation of thin sections. Mara Schiro is thanked for the final linguistic revision. This research was supported by Projects CGL2005-01319 and CGL2008-05251-E (MICINN) and the Research Group RNM-178 Junta de Andalucía, Spain.

6

Statistical analysis of elemental chemostratigraphy in Upper Jurassic Ammonitico Rosso

Rute Coimbra [(a)], Adrian Immenhauser [(b)], Federico Olóriz [(a)], Víctor Rodríguez [(c)], Mario Chica-Olmo[(c)]

[(a)] Departamento de Estratigrafia y Paleontologia, Universidad de Granada, Spain

[(b)] Institute for Geology, Mineralogy and Geophysics, Ruhr Universität Bochum, Germany

[(c)] Departamento de Geodinámica, Universidad de Granada, Spain

Submitted to Chemical Geology (September 2011)

Abstract

Elemental concentration in seawater is known to fluctuate both in time and space, to be incorporated in carbonate lattices, and recorded as an intricate mixing of original differences in abundance and those resulting from variable degrees of diagenetic alteration. Data from seven sections corresponding a proximal to distal transect along the S-E Iberian paleomargin are presented. Major and trace elements (Ca, Sr, Mg, Fe and Mn) are discussed in terms of their stratigraphic and spatial variations. From more common to novel methods, a thorough statistic approach is proposed. Elemental abundances from the epicontinental record revealed a clear continental influence, coupled with a high degree of diagenetic overprint. However, the epioceanic record proved to be closer to original elemental signatures, reflecting sin-depositional to very early diagenetic processes. Thus distance from epicontinental shelves acts as a major buffering to differentiate major paleoenvironments on the studied paleomargin.

Elemental associations provided by principal component analysis (PCA) and hierarchical cluster analysis revealed a consistent relation between Mg, Fe and Sr. Early diagenetic nodule formation in Ammonitico Rosso facies is the interpreted process responsible for their incorporation in the carbonate lattice, shedding light on the significance of this elemental association. The clear decoupling of manganese behavior is reported and related to bottom instability. The latter was forced by high seafloor spreading rates during the Late Jurassic, resulting physiographic structuring of the paleomargin and related hydrothermal seepage throughout the epioceanic fringe under scope.

Variogram computation is, to our knowledge, applied for the first time to geochemical data of ancient carbonates revealing time-fluctuations patterns for geochemical behavior. Late Jurassic paleoceanographic conditions could be coupled with the observed trends in time, most likely forced by relative sea level dynamics superimposing fluctuations of variable order.

♦ ♦ ♦

6.1- Introduction

Chemical elements enter the oceans in their ionic form, as aquo-complexes or as compounds via riverine input (e.g., Martin and Withfield, 1983; Marcus, 2009), airborne dust (e.g., Mahowald et al., 1999; Muhs et al., 2007; Rodrigo-Gamiz et al., 2011), seepage (Birgel et al., 2011 and references therein) and from hydrothermal sources, vents associated to hotspots or mid-ocean ridges (e.g., Dias and Barriga, 2006, Middag et al., 2011). Carbonate deposition and seafloor redox dynamics act as depositional sink as major and trace elements are incorporated in the carbonate lattice, even known from mid-Ocean ridges environments (e.g., Coggon et al., 2010; Elderfield, 2010).

Coastal and epeiric water masses are – due to their shallow depth and direct vicinity to land masses – strongly affected by continental runoff relative to "blue" oceanic water masses (Immenhauser et al., 2008). Continental runoff is characterized by markedly lower contents of magnesium and strontium when compared with seawater (e.g. Banner and Hanson, 1990; Cicero and Lohman, 2001; Tipper et al., 2006) and by significant elemental supply of Mn and Fe resulting from continental weathering (e.g., Vincent et al., 2006). Depending on the mixing ratio of riverine runoff and coastal marine waters, considerable geochemical and physical (density, salinity, temperature, pH) gradients are observed in near-coastal aquafacies. In contrast, oceanic water masses – albeit highly complex in their ocean wide spatial organization – carry a distinct geochemical signature (e.g., Hongo et al., 2006).

Proxy data from fossil carbonate materials provide clues for parent water chemistry in ancient oceans (e.g., Wadleigh and Veizer, 1992; Malchus and Steuber, 2003; Eggins et al., 2003; Rosales et al., 2004; Pufahl et al., 2006; Nunn and Price, 2010; van der Kooij et al., 2009; Coimbra et al., 2009). Nevertheless, precipitation conditions (temperature, salinity, pH, mineralogy, vital and/or kinetic effects and post depositional/post mortem diagenesis may compromise the reliability of their carbonate archive and its geochemical proxies (Veizer, 1974; Brachert and Dullo, 2000; Rexfort and Mutterlose, 2006, 2009). During diagenesis, thermodynamically instable carbonate phases (aragonite, high-Mg calcite) are stabilized to a more stable calcite polymorph, commonly low-Mg calcite (Al-Aasm and Veizer, 1982; Veizer, 1983; Immenhauser et al., 2002; Tynan and Opdyke, 2011). The degree of water-rock interaction will determine the amount of elemental supply during dissolution/reprecipitation, while partition coefficients (k) for each element rule their relative abundance on secondary

diagenetic carbonate phases (Veizer, 1983; Tucker and Wright, 1990, Möller et al., 1991, Yasutaka and Mami, 2006; Morse et al., 2007). Notwithstanding, even where a moderate degree of diagenesis modifies the primary elemental composition, the first order trends contained in a time-series (stratigraphic) dataset are, pending favourable conditions, preserved (Frank and Lohmann, 1996). Thus, whilst carbon and oxygen isotope chemostratigraphy is now widely used as a correlation tool for paleoenvironmental conditions between spatially distant stratigraphic sections (Jenkyns, 1980; Immenhauser et al., 2002; Rais et al., 2007; da Silva and Boulvain, 2008; Coimbra et al., 2009; van der Koij et al., 2009; Huck et al., 2010). Comparatively, the use of carbonate major and trace elemental chemostratigraphy is clearly underexplored and the number of studies dealing with this paleoenvironmental approach is limited (e.g., Vincent el al., 2006, Renard et al., 2007; Boulila et al., 2010).

Here, the chemostratigraphic trace and major elemental archive of seven stratigraphic sections, representing a proximal-to-distal transect across an Upper Jurassic paleomargin in southern Iberian plate, is presented and discussed in a process oriented manner. Calcium, Mg, Sr, Fe and Mn elemental abundances from different carbonate materials are combined with carbon and oxygen isotopic and sediment petrographic information. In the framework of the multi-proxy approach used here, the extraction of significant stratigraphic patterns from thousands of data points is performed through statistical methods (e.g., Chen et al., 2007; Basaham, 2009; Monien et al., 2010, Dias et al., 2011). The use of a rigorous statistical framework, including linear correlations, principal component analysis, hierarchical cluster analysis and variogram computation allows for an integrated and quantitative assessment of the complete geochemical dataset. Furthermore, variogram computation is, to our knowledge, applied for the first time to geochemical data from spatially distant sections along an ancient proximal-to-distal transect. In recent years, these geostatistical methods based on the "Theory of Regionalised Variables" (Matheron, 1970) have become an essential tool to analyse spatio-temporal datasets. This approach interprets experimental parameters as regionalised variables, i.e., those which present a spatio-temporal distribution characterized by a spatial and/or temporal variability (or correlation) structure resulting from interdependence.

The purpose of this paper is (i) to test the informative potential of elemental chemostratigraphy from ancient marine carbonate materials in a proximal-to-distal transect; and (ii) to establish a statistical protocol for the comparison of elemental and isotopic time-series data from matrix micrites. The obtained outcome might encourage those interested in

chemostratigraphy, palaeoceanography and carbonate proxy research to further explore this novel tool and documents its potential and limitations.

6.2- Case setting

Stratigraphic sections investigated in the context of this project are located in Southern Iberia and on the Island of Majorca (Fig. 6.1A and B). The Upper Jurassic limestones studied belong to the External zones of the Betic Cordillera (Fig. 6.1A; Olóriz et al., 2002a, Vera et al., 2004). During the Late Jurassic, the South Iberian margin was a tectonically unstable area affected by relative movements between the Iberian and African plates (Fig. 6.1C). The studied sectors and segments of the South Iberian plate sedimentary cover represent a transect ranging from the more proximal epicontinental areas into the more distal epioceanic realm (Fig. 6.1D). Carbonates sampled were deposited in a paleo-bathymetric range corresponding to upper layer waters equivalent to mid-to-deep neritic water depths (Fig. 6.1D). In its present-day setting, the transect spans over a distance of about 100 km. In paleogeographic terms, distances of several hundred kilometers result (see Fig. 6.1). Age control of the sections studied is based on a well established ammonite biochronostratigraphy in agreement with the proposed standard zonation for the Western Tethys (Olóriz, 1978; Cariou et al., 1997; Geyssant, 1997; Hantzpergue et al., 1997; Caracuel et al., 1998, 2000) and appropriate local application to the Majorca Island (Caracuel et al., 1995; Olóriz et al., 1995a, b, 1998; Caracuel and Olóriz, 1998, 1999a, b).

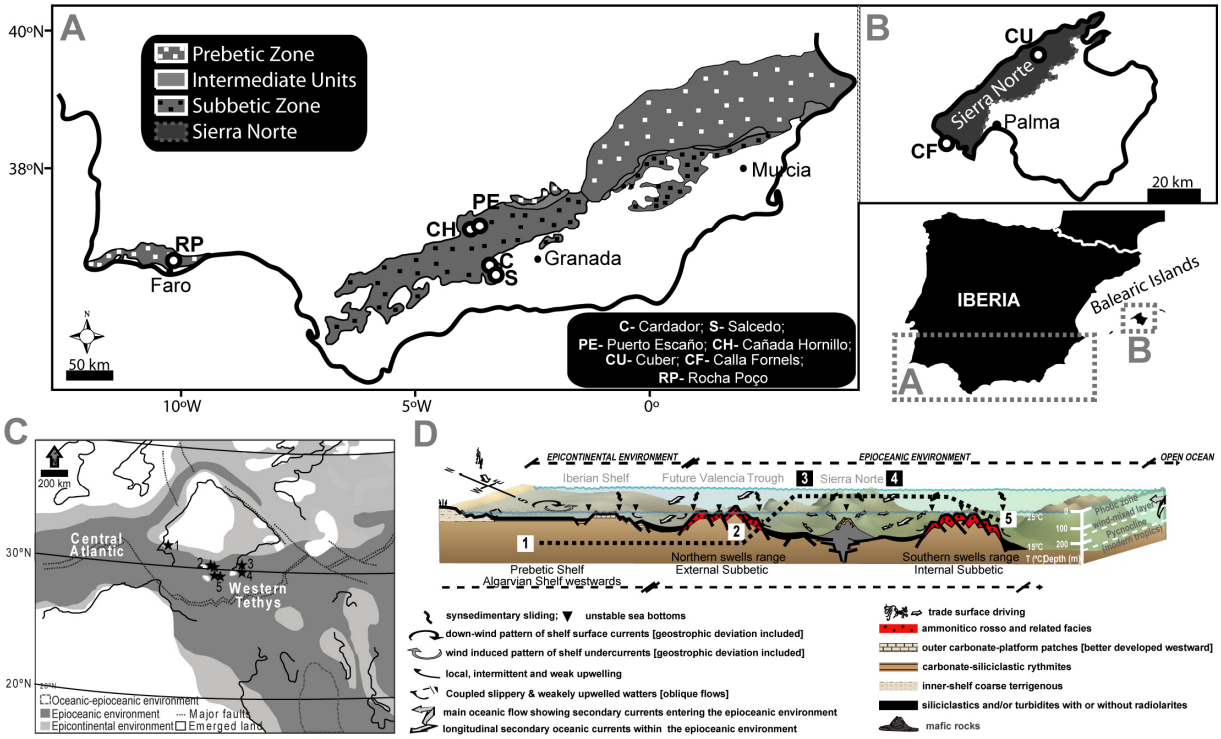

Fig. 6.1- Regional distribution of paleogeographical and geological units along the studied areas, and Late Jurassic paleogeographic reconstruction of western and central Tethyan realm: A- Southern Iberia; B- Majorca Island (modified from García- Hernández et al., 1980 and Caracuel and Olóriz, 1999). Circles indicate the location of the studied sections, used abbreviations for studied sections are indicated; C- Plate tectonic setting from Stampfli and Borel, 2002, and depositional environments after Thierry et al., 2000 a, b. Stars indicate the paleogeographic location of the sampled sections; D- Physiographic sketch of the South and East Iberian margins and respective environments during the Late Jurassic (adapted from Olóriz, 2000).

6.3- Methods

6.3.1- Field sampling and analytical methods

The sampled stratigraphic levels from seven spatially distributed Upper Jurassic sections (Fig. 6.1A and B) provided 316 hand samples. Average sampling density was between 1 to 5 samples per section meter. Two rock slabs were cut from each hand sample: one for geochemical investigations and one for thin section optical inspection. Thus, thin

sections were produced for each sampled horizon for microfacies characterization and skeletal abundance estimation (see Coimbra et al., 2009; and chapter 4 for details) and selected samples were chosen for cathodoluminescence and scanning electron microscopy (SEM) analysis.

Cathodoluminescence inspection was performed on selected samples, using a hot stage cathode luminescence (HC4-LM) at the facilities of the Institute for Geology, Mineralogy and Geophysics, Ruhr University Bochum, Germany). The purpose was to evaluate the degree of alteration of studied carbonates. For details of this screening method refer to (Fairchild, 1983; ten Have and Heijnen, 1985; Marshall, 1988; Machel and Burton, 1991; Machel et al., 1991; Bruckschen and Richter, 1994; Bruhn et al., 1995; Barbin et al., 1997).

Ultrastructure inspection of micrite samples was performed under the SEM using a LEOGemini 1530 instrument on eight freshly cut rock chips at the Centre of Scientific Instrumentation at the University of Granada and at the facilities the Institute for Geology, Mineralogy and Geophysics at Bochum, Germany.

An average of three powder subsamples was drilled from each rock slab for matrix micrite geochemical analysis. Where available, diagenetic vein material and skeletal material was also sampled in order to capture the full geochemical range of each specimen. A total of 1031 powder samples were analyzed for their major and trace elemental abundance (Ca, Mg, Mn, Fe, Sr) using inductively coupled plasma-atomic emission spectrometry (ICP-AES). Dissolution of 1.5 mg of powdered sample in 1 ml of 3M HNO_3 (over 12 hours) was followed by further dilution with 2 ml of distilled water. A small amount of insoluble residue was observed for most of the samples. This corresponds to non-carbonate materials belonging to the detrital (clay) fraction, as silicate minerals (e.g., illite and montmorillonite, commonly present in Ammonitico Rosso facies; Jenkyns et al., 1974). This fraction is not dissolved during acid treatment of bulk micrite samples. Filtering the samples is crucial for an efficient functioning of the used equipment (correct flows and absence of clogging particles at the ICP nebulizer) and to ensure that only carbonate bound elements are measured. Most of the samples were therefore filtered (ca. 90%). Maximum elemental scatter for duplicate samples was in the order of 3% for all elements. Elemental analyses were performed at the Institute for Geology, Mineralogy and Geophysics (Ruhr University Bochum, Germany). Carbon and oxygen isotope ratios presented here are from Coimbra et al. (2009) and chapter 4.

Several types of carbonate materials were analyzed (matrix micrite, carbonate cements, belemnite rostra, neomorphic ammonite shells) and compared regarding their elemental composition (presented in chapter 4). Here, the focus is on matrix micrite data only (Fig. 6.2), whilst results from other subsamples are shown in Coimbra et al. (2009) and chapter 4.

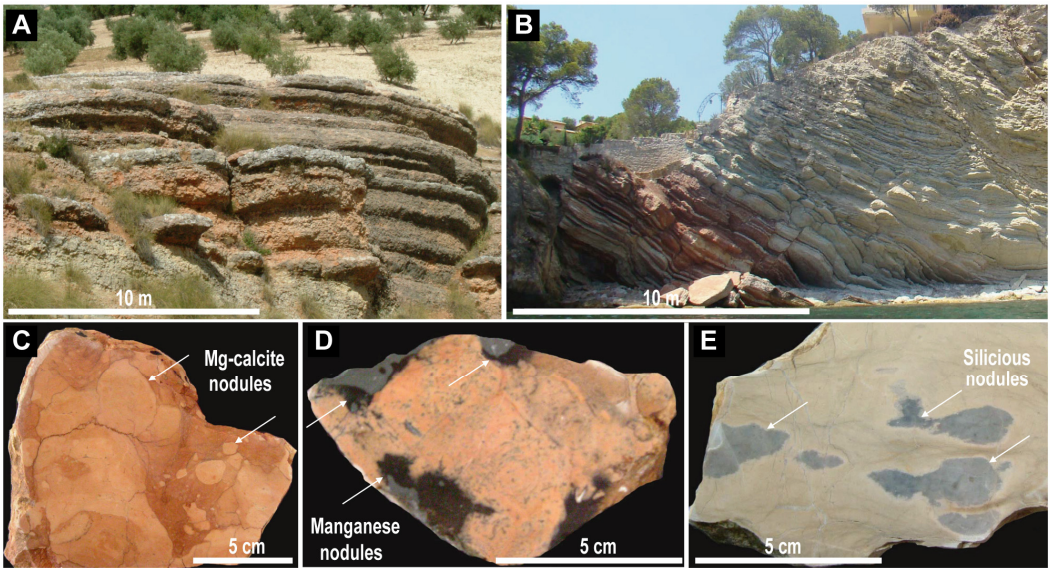

Fig. 6.2- Field views and macroscopic features of hand samples of the studied materials: A and B- Outcrop views of the Cardador and Cala Fornells sections, S Spain and Majorca Island, respectively. Note colour variations from greyish to reddish and the presence of marker beds; C to E: hand slabs evidencing the variability of lithofacies observed on the studied materials (C- Mg-calcite nodules; D- Manganese nodules present at the Salcedo section; E- Siliceous nodules from the Cuber section).

6.3.2- Statistical approach

The description of the statistical tools used is organized according to their complexity, and this applies also to the following subchapters.

6.3.2.1- Descriptive statistics

When dealing with large datasets (here, 6090 data points), the application of reduction methods is significant in order to achieve a better grip on data distribution. The following protocol has been performed: the mean value for the three sub-samples analyzed from each rock slab was calculated and subsequently used for further data evaluation (presented in

Appendix 6.1, Fig. A1). The stratigraphic trend of each proxy is indicated by a full line that connects the calculated average values.

Mean values served to compute boxplots in Fig. 6.3 (see Tukey, 1977; McGill et al., 1978 for detailed descriptions), representing the inter-quartile range (the difference between first and third quartiles). The median, mean, maximum and minimum values are shown in Fig. 6.3. The ends of the whiskers represent the limits beyond which values are considered as non-representative. Because average values of the mean and the median are available, the choice of connecting median values to interpret proximal to distal trends was based on the fact that the median is less affected by extreme values (e.g., maximum value of a stratigraphically thin level). Therefore, the median is thought to better represent background geochemical signals. Mean values were also tested for the interpretation of spatial (proximal-to-distal) trends and displayed the same relative pattern as median values.

The filtering of the samples prior to ICP-AES analysis may affect total elemental abundances in individual samples. This because the argillaceous portion of the initial bulk samples is eliminated by retaining clay minerals in the filter. In order to correct the dataset for this effect, all values were divided by measured Ca concentration (and multiplied by 100). Further statistical evaluations were then preformed using the corrected dataset (Sr/Ca, Mg/Ca, Fe/Ca, Mn/Ca) in order to avoid bias effects of sampling strategy inherent to elemental analysis.

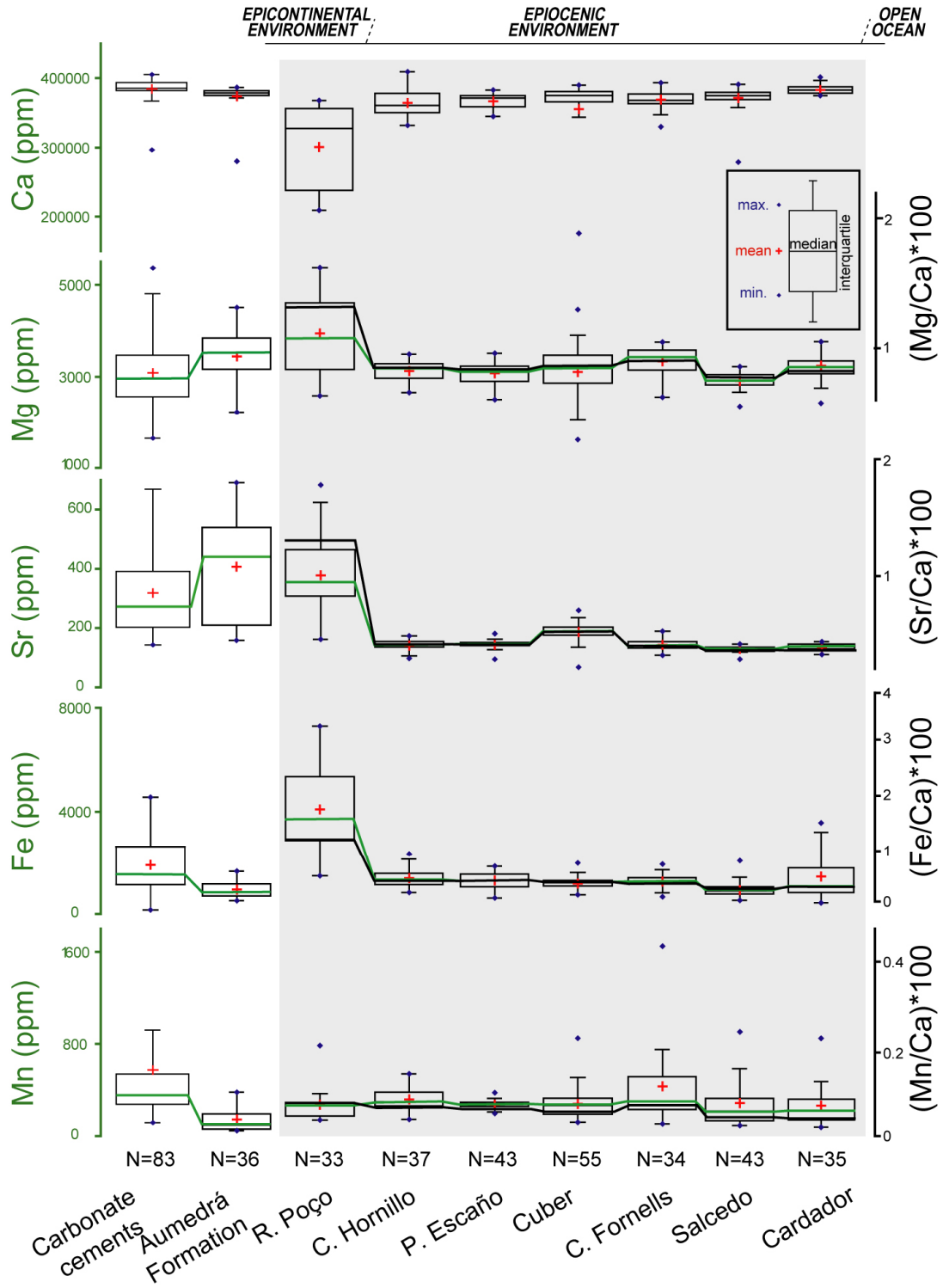

Fig. 6.3- Boxplot representation of elemental abundances for the different studied materials and their distribution along the proposed proximal to distal transect (boxplot parameters described on the legend). Absolute measured elemental concentration (in ppm) on the left and corrected values on the right. Type of material, number of samples and locations are indicated. Note connected median values throughout the epicontinental and epioceanic sections in order to allow a better assessment of spatial elemental variability.

6.3.2.2- Principal component analysis

Principal component analysis (PCA) was applied for recognition of patterns in the large dataset analyzed, providing a combination of variables that account for the observed variance (see Wold et al., 1987 for detailed description).

6.3.2.3- Cluster analysis

Cluster analysis was used to establish groups of variables within the dataset providing clustering of values into similarity classes (Danielsson et al., 1999, see also Everitt et al., 2001 for detailed description of this method). The performed hierarchical clustering joins observations with increasing levels of similarity represented by the dendrogram. The truncation level was imposed for similarity values of higher than 0.45 (horizontal dashed line in Fig. 6.7).

The agglomerative hierarchical clustering algorithm uses the dissimilar proximity type, but was converted into similarity in order to optimize the performed analysis since major differences have already been established by principal component analysis. In this case, agglomeration was performed by using the "unweighted pair-group average linkage". It represents an intermediate approach regarding to compaction and dilation of the data space produced by simple and complete linkage (respectively), allowing a fair representation of the data space properties.

6.3.2.4- Variogram computation: Geostatistical analysis of temporal variability

The concept of regionalised variable can be applied to this study concerning the analyzed geochemical parameters (and also petrographic) measured along the analysed series throughout the proximal to distal transect. Simple variogram function (see Appendix 6.2 and Fig. 6.9A) was applied for all proxies. Cross-variograms (see Appendix 6.2 and Fig. 6.9B) were performed only for those variables that showed certain similarity on their simple variograms (see Fig. 6.9A and C). For the purpose of analysis and comparison of results the simple variograms have been normalised by variance data; and in the case of the cross variograms, normalised by the covariance of the variables. Given the number of sections and variables studied, the number of the calculated simple and cross variograms is high. For this

reason, general types are summarized in Fig. 6.9C. This approach facilitates the interpretation of temporal variability within the spatial context of the studied proximal to distal transect.

6.4- Data presentation

6.4.1- Petrographic properties

A detailed description of petrographic properties of thin sections and cathodoluminescence (CL) patterns for selected samples were provided by Coimbra et al., 2009. Only the most essential information is given below. Luminescence microscopy revealed dull to patchy bright luminescence of matrix micrite. In contrast, carbonate cements showed a luminescence pattern characterized by the presence of three cement generations (Coimbra et al., 2009). These are characterized by a non-luminescent scalenohedral calcite phase (generation 1), followed by a bright orange, blocky calcite cement generation (generation 2). Generation 3, a blocky calcite phase, occludes the central parts of cement filled voids and is characterized by a dull orange luminescent pattern. Ultra-structure inspection revealed the presence of micritized biogenic structures (algae/bacterial filaments) and cocoliths (Coimbra et al., 2009).

6.4.2- Geochemical results

Elemental concentrations (in ppm) from all sections along the sampled transect are shown in Fig. 6.3. Epioceanic sections are characterized by narrow boxplots, i.e. low-variant data. Calcium content is only slightly lower than 400000 ppm, the expected stoichiometric proportion in pure calcite ($CaCO_3$). Magnesium, Sr, Fe and Mn values fluctuate around 3500, 180, 1000 and 300 ppm, respectively. In general, matrix micrites from all epioceanic sections display a similar range of elemental values (see Fig. 6.3).

Matrix micrite from the epicontinental section at Rocha Poço, carbonate cements from all settings, and the samples from the Aumedrá Formation in the epioceanic section from the Majorca Island differ in terms of their elemental abundances from epioceanic sections (Fig. 6.3), the latter showing lesser variability.

When dividing elemental concentrations by their respective calcium content (element (ppm)/Ca (ppm)*100) in order to avoid the filtering bias, no significant differences are imposed (Fig. 6.4). Measured values (in ppm) and corrected values show a very significant positive linear correlation (up to R=0.99, p<0.0001, Fig. 6.4B).

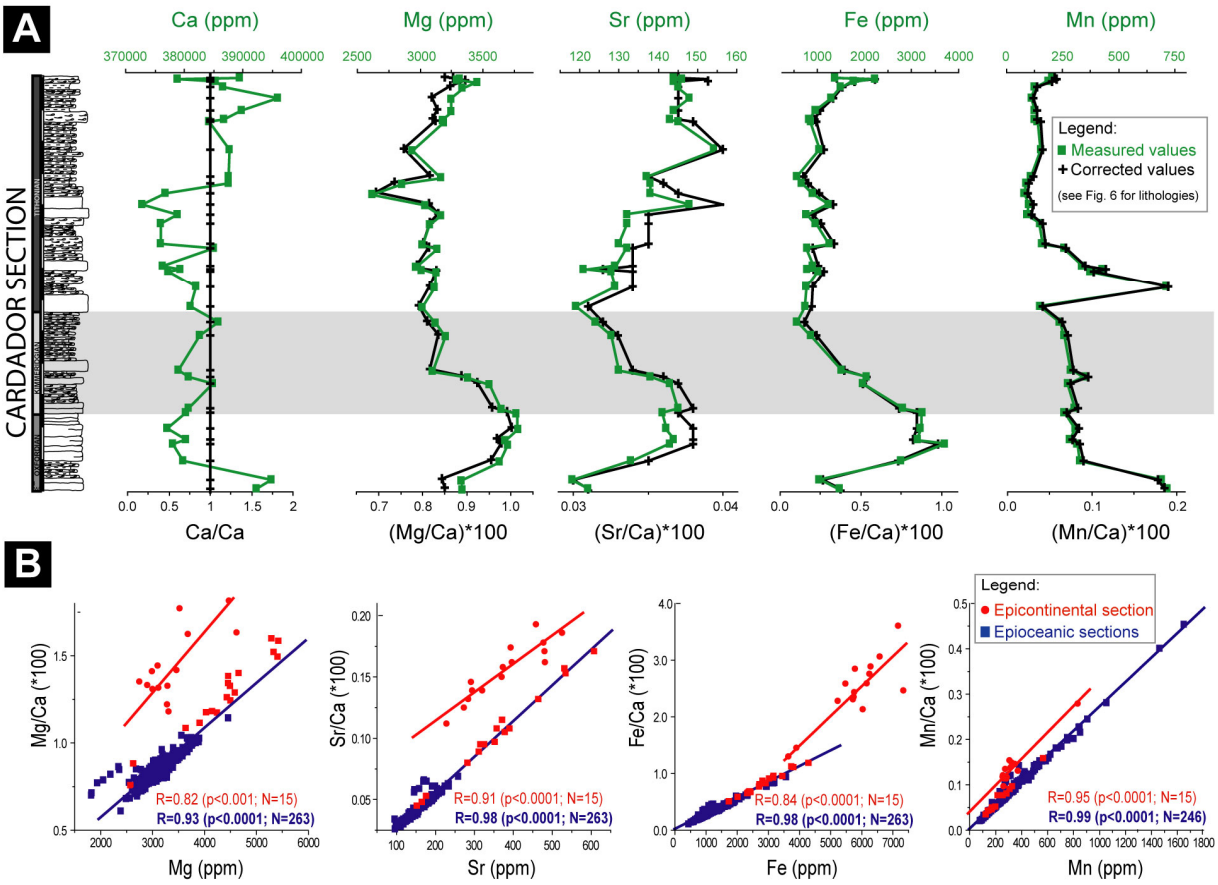

Fig. 6.4- Comparison between measured and corrected elemental values: A- Stratigraphic variation of both measured (squares) and corrected values (crosses) (upper and lower axis, respectively). Note similar stratigraphic trends on both datasets (example for the Cardador section); B- Linear correlations between measured and corrected values. Level of correlation indicated by R, p and N parameters; bold lettering for epioceanic sections). The Rocha Poço section (red) has been sub-divided into two different symbols: circles for more siliclastic horizons at the base of the section and squares for spongiolithic bioherms and overlaying limestones.

Several cross plots between elemental and isotope proxies were tested (Fig. 6.5A to F). All epioceanic sections (represented by squares in Fig. 6.5) show values within a rather narrow range. A relation between plotted variables is not obvious. In contrast, samples from the epioceanic Cuber section and the epicontinental Rocha Poço section depart from the above trend.

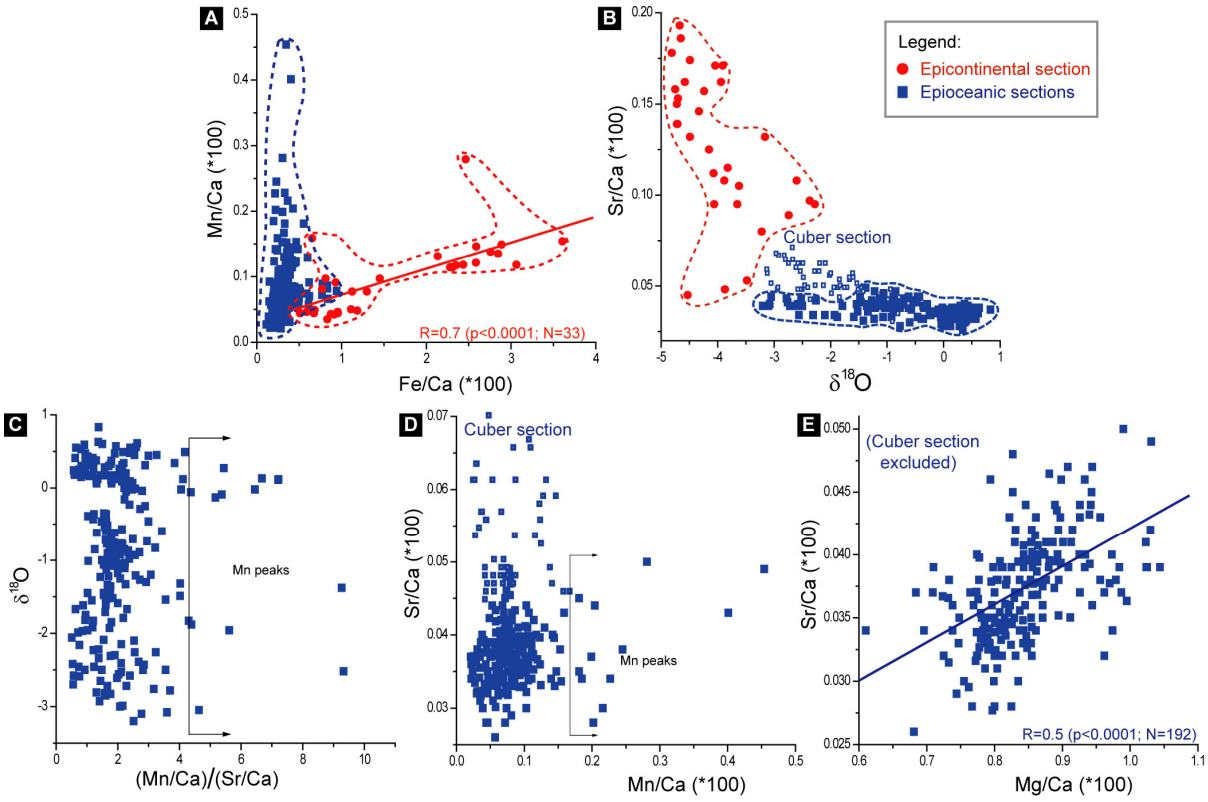

Fig. 6.5- Elemental relations between proxies often used as diagenesis indicators (see text for references). Note the differences in behavior between the epicontinental and all the remaining epioceanic sections, and the lack of relation between tested elements for epioceanic sections. Linear correlation mentioned when relevant (A and E).

Within all sections, the stratigraphic behavior of manganese seems of particular interest due to the occurrence of pronounced shifts towards higher values (up to 1500 ppm; Fig. 6.6) observed in all datasets.

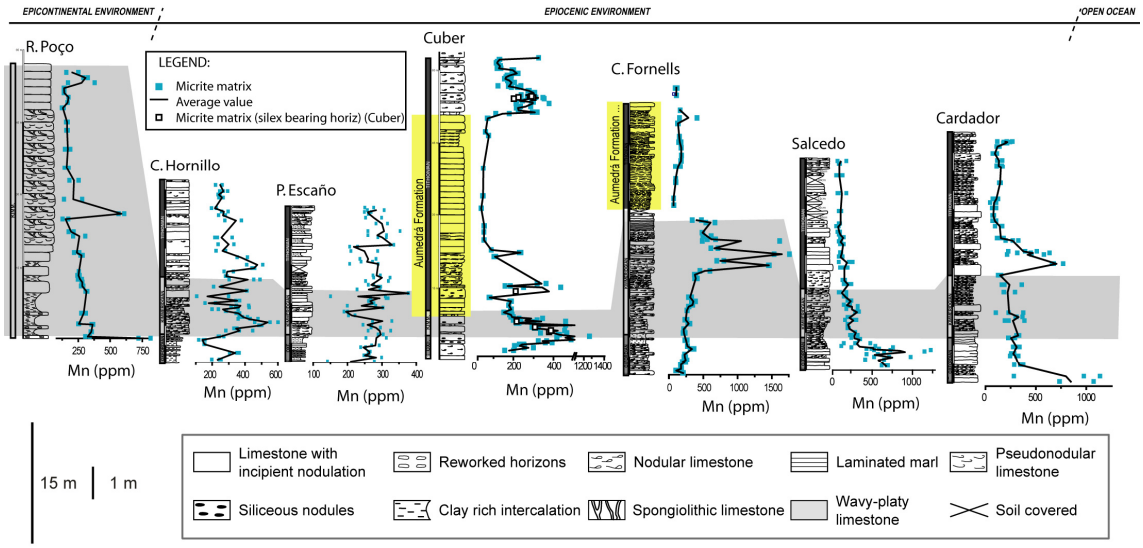

Fig. 6.6- Manganese stratigraphic variation for all sections. Shaded area correlates Kimmeridgian deposits throughout the investigated transect. Note that shaded area at Rocha Poço is mainly restricted to the Lower Kimmerdigian

6.4.3- Results of elemental abundance statistical analysis

PCA shows two principal components (PC) explaining 85% of the total variance of the analyzed dataset (PC1- 60% and PC2- 25%, Fig. 6.7A). The contribution of each proxy for the obtained components is shown in Fig. 6.7A. Principal component 1 (PC1 in Fig. 6.7) explains the variance of Mg, Fe and Sr. Manganese elemental values in micrite samples are clearly decoupled from all other geochemical proxies and are best explained by principal component 2 (PC2 in Fig. 6.7). On the basis of PCA results, data from the Aumedrá Formation horizons in the epioceanic Cuber section (Fig. 6.6 for stratigraphic distribution) and from the epicontinental record at Rocha Poço are excluded from further statistic analysis, since they departure significantly from the overall epioceanic data.

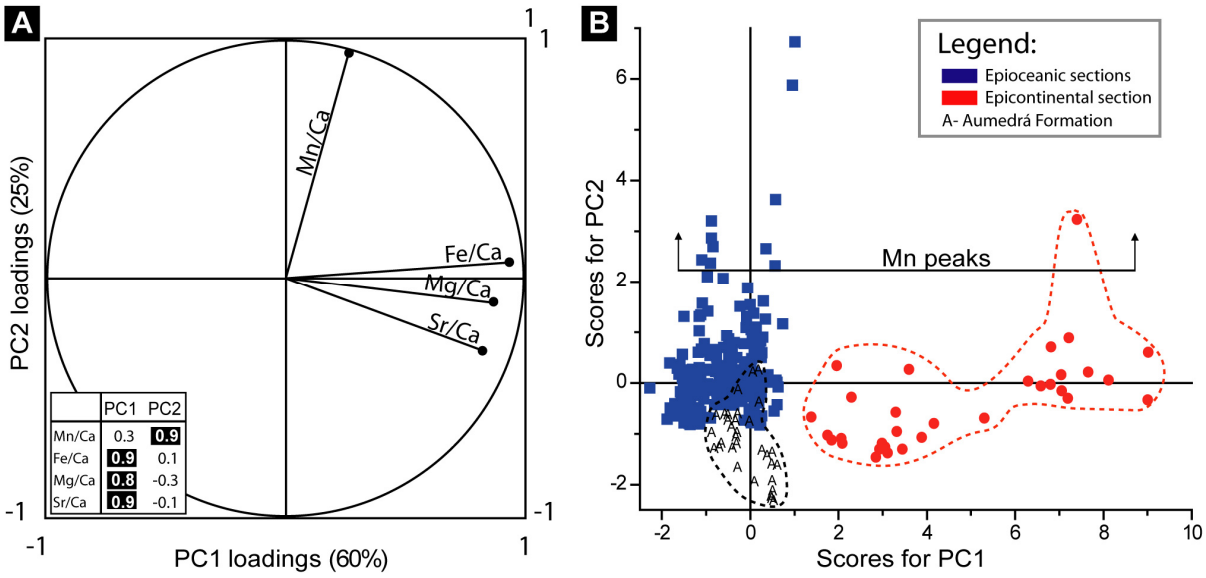

Fig. 6.7- Principal component analysis results for all studied sections and proxies: A- Principal Component loadings for PC1 and PC2 (values indicated on the inlet) indicating the contribution of each proxy on the corresponding PC axis; B: Principal component scores. Note the similitude between all epioceanic sections behavior (tightly clustered; see inlet with legend) and how the Aumedrá Formation samples and also the ones from the epicontinental section departure from the mentioned behavior.

Hierarchical cluster analysis was performed for all analyzed geochemical proxies and the resulting dendrogram is shown in Fig. 6.8. Two clusters were found: cluster 1, including Sr/Ca, Fe/Ca and Mg/Ca and cluster 2 including Mn/Ca elemental values in micrites.

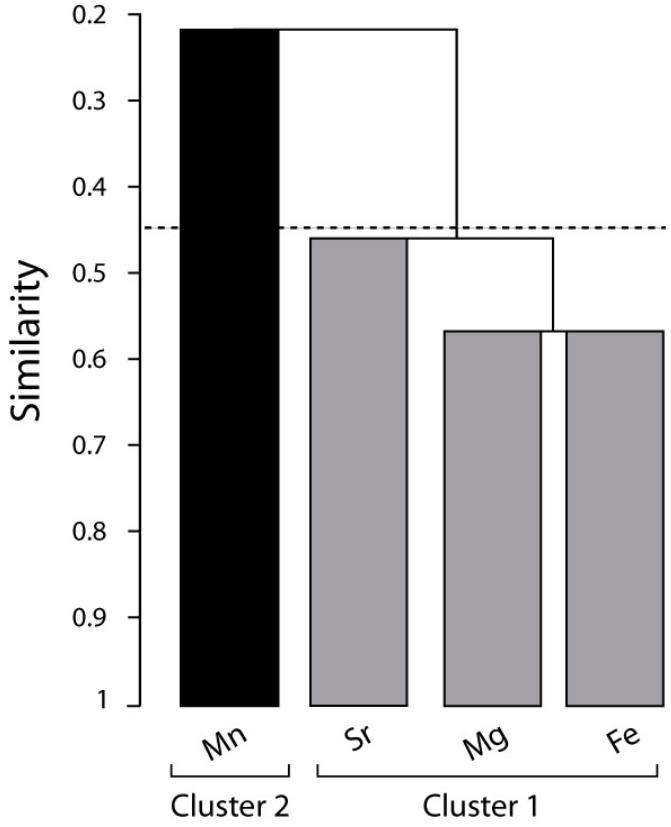

Fig. 6.8- Dendrogram for the hierarchical cluster analysis performed for all proxies from epioceanic sections. Cluster numbers correspond to those used on Figure 6.10.

The spatio-temporal variability of elemental data was investigated for epioceanic sections by means of variogram analysis, shown in Fig. 6.9. Carbon and oxygen isotope data from Coimbra et al., 2009, 2011 were included, since this approach is attempted for the first time and well known trends are useful for interpretation purposes). Simple and cross variograms (Appendix 6.2 and Fig. 6.9) are presented in Fig. 6.9A and B, respectively. The variograms of the studied variables are well structured in all the sections. In essence, variograms show low values in the random component (C_0, see Appendix 6.2) and a clear temporal variation structure that presents differential behaviour depending on the analyzed section and proxy (Fig. 6.9A and B). On the other hand, a sort of cyclicity in the distribution of data is observed in an important number of variables (e.g., Mg, Sr in Fig. 6.9A). This behaviour allows recognition of general first order trends (Figs. 6.9A and B), summarized in Fig. 6.9C. They range from cyclic behavior of shorter period with variable beats, (a and b in Fig. 6.9C) and longer period (c in Fig. 6.9C). Moreover, some variables (e.g., $\delta^{13}C$) show a

very marked regularity (d in Fig. 6.9C), even a general invariable trend (e in Fig. 6.9C) through time. Maximum and minimum variation values are systematically verified for the intervals t=10, t=20 and/or t=30 (Fig. 6.9A to C).

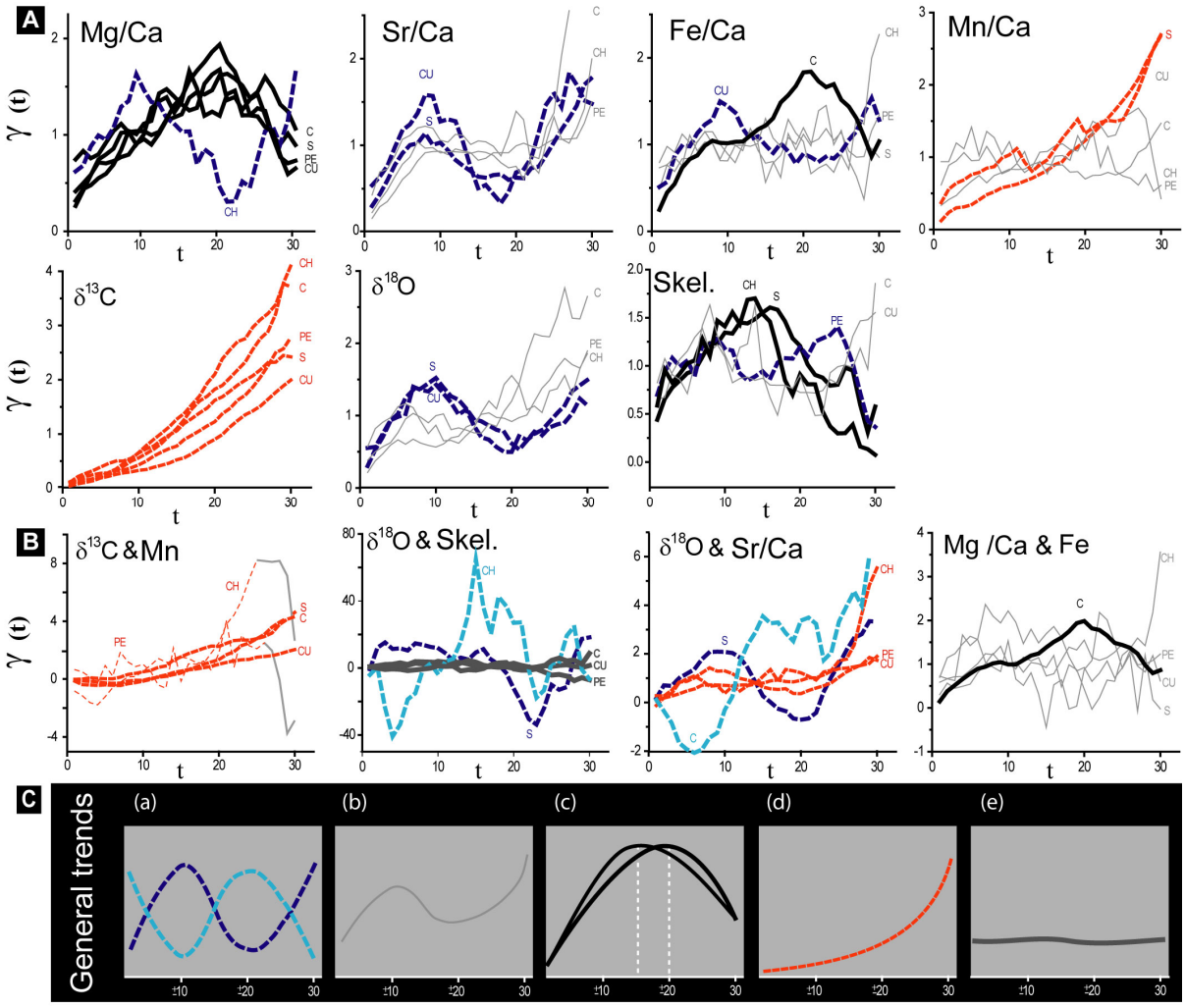

Fig. 6.9- Variograms computed for the all proxies on the epioceanic dataset (except Cala Fornells, see text for explanation). Abbreviations used are according to Fig. 1A: A- Simple variograms for the seven analyzed proxies, with indication of the correspondence between the obtained curves and the respective section (same abbreviations as used in Fig. 10.1); B: Cross variograms that compare resulting variance on sets of two proxies; C- General trends inferred from the overall shapes of the variogram curves. Representation from (a) to (e) are discussed on the text.

6.5- Interpretation

Matrix micrite samples provided the most complete record for the studied stratigraphic interval and, encouragingly, the obtained data are comparable along the proximal-to-distal transect investigated (Fig. 6.1). In order to assess the degree of similarity between all epioceanic sections, elemental datasets from all the epioceanic sections were plotted separately. Relative variations were less than 3% for all elements and, more interestingly, they are below the intra-sample maximum scattering. Whilst matrix micrite trace elemental data form the backbone of this study, the geochemistry of for example carbonate cements, or biogenic carbonate hardparts such as belemnite guards or neomorphic ammonite shells is used for assessing the diagenetic history of the limestone successions investigated (see Coimbra et al., 2009 for details on the paragenetic succession).

In short, a limited alteration of the matrix micrite is in agreement with observations resulting from cathodoluminescence (dull luminescence) and ultra-structure inspection. These observations agree with elemental concentrations similar to those expected for low-Mg calcite (see Milliman, 1974; Veizer, 1983, Banner and Hanson, 1990, Lu, 2008). Moreover, the range of geochemical data reported from coeval Ammonitico Rosso facies from Italy (Préat et al., 2006) supports an overall good degree of geochemical and petrographical preservation, at least from early diagenetic nodules. Following previous work (Veizer, 1983; Cicero and Lohman, 2001; Immenhauser et al., 2003; Azmy et al., 2006; Renard et al., 2007; van der Kooij, 2009) diagenesis-sensitive elemental ratios and oxygen-isotope values are shown in cross-plots in Fig. 6.5.The outcome is in agreement with a limited diagenetic alteration of matrix micrite proxy data (Fig. 6.5A to F) from epioceanic sections.

In contrast, the micrite proxy data from the epicontinental Rocha Poço section (circles in Fig. 6.5A to C) departs significantly from the epioceanic record (squares in Fig. 6.5A to C). These differences are indicative of a more-than-minor degree of diagenetic alteration of primary seawater values. Thus, the increase in Sr elemental abundance accompanied by depleted $\delta^{18}O$ values (Fig. 6.5C), and the significant correlation between Fe and Mn (Fig. 6.5B), attests for significant influx from continental sources in these coastal waters.

In the epioceanic Cuber section (Fig. 6.5C and E) matrix micrite Sr content is higher relative to those of all other epioceanic sections (open squares in Fig. 6.5C and E). This is especially evident for the Aumedrá Formation horizons (see Fig. A1, Appendix 6.1), characterized by very high (up 600 ppm) matrix micrite Sr concentrations. Details for atypical behavior in the Aumedrá Formation are discussed elsewhere, interpreted as the environmental

expression of local conditions forcing expected distinctions across the proximal to distal transect under scope.

A time control on the produced variograms was approached through linking range values (R in Fig. B) and the corresponding stratigraphic interval in a given section. Range values (0 to 20 in the x-axis in variograms, Fig. B see Appendix 6.2), correspond to the value for independence among compared samples from the sections under study, therefore determining particular stratigraphic intervals. Hence, a time content corresponds to each range value obtained for each section. The duration of 15.7 Myr (Gradstein et al., 2004; Ogg and Przybylski, 2006) is assumed for the Late Jurassic and the number of samples from each section was equally distributed stratigraphically, which would result in time control assuming constant sedimentation and compaction rates. This approach necessarily represents an oversimplification of the complex time-thickness distribution in ancient carbonate sections, but it is the only available if supported by precise biostratigraphy. Linking the range (R) of the variograms with the above information, a significant cycle-pattern is observed, with frequencies of 3.8 Myr (R=10), 7.6 (R=20) and 11.4 Myr (R=30) (Fig. 6.9C).

Worth of mention is that variograms present a general twofold trend. A random component characterizing local variations in time, and obviously space, and a structured component representing the general variation registered for a given variable along stratigraphic series and settings, i.e., signal variation in space and time or regionalisation across the analysed proximal to distal transect.

In summary, an overall good degree of preservation of marine matrix micrite values in epioceanic settings, as suggested in Coimbra et al. (2009), has been confirmed by the obtained elemental data. Epioceanic realm conditions are therefore well represented by the studied materials, and elemental associations registered within this environment provide information on the geochemical conditions present during sediment deposition and early diagenetic stabilization.

6.6- Discussion

An objective distinction between early marine burial vs. late diagenesis effects was desired. The application of statistical analyses was chosen through the application of PCA and hierarchical clustering. Thus, we attempt to support the recognition of coexisting processes

affecting the distribution of primary elements across the studied area and stratigraphic interval, as well as their behavior in the related time span. In fact, the behavior of Mg, Sr and Fe seems to be "frozen" in carbonate nodules early during marine diagenesis, while Mn content in matrix micrite would relate to local significant hydrothermal activity in the epioceanic realm. All these aspects will be taken into consideration below.

6.6.1- Carbonate mineralogy, early marine diagenesis and the role of Iron, Magnesium and Strontium

The formation of early diagenetic Ammonitico Rosso nodules is a significant process that deserves attention. Generally, most authors now agree that nodule formation occurs at a very early diagenetic stage, depending on a complex combination of physical, (micro)biological and chemical processes (e.g., Jenkyns, 1974; Müller and Fabricius, 1974; Mullins et al.,1980; Clari et al.,1984; Clari and Martire, 1996, Coimbra et al., 2009). Coupling of Mg, Sr and Fe in the nodular facies was consistently verified both by PCA and cluster analysis (PC1 in Fig. 6.7 and cluster 1 in Fig. 6.8). The obtained results document that the behavior of these elements are (i) significant during nodule formation, but are (ii) controlled by unrelated geochemical processes.

The significance of magnesium as indicated by PCA and cluster analysis is perhaps best explained by the parent high-Mg calcite mineralogy (Mg concentration >10000 ppm) of the nodules formed within the Ammonitico Rosso facies (Jenkyns, 1971; Préat et al., 2006). The post-depositional alteration of Mg-calcite from skeletals such as foraminiferan tests may contribute to the bulk Mg content. A significant loss of Mg commonly occurs during the stabilization of high and intermediate Mg calcite to low-Mg calcite (3500 ppm). As laid out in Coimbra et al. (2009), the early lithification (nodulation) of matrix micrites in the presence of marine pore waters prevented a subsequent geochemical alteration of the studied materials. The interplay between current energy, sedimentary input and winnowing, burrowing and water pumping provided favorable conditions for the early occurrence of carbonate nodules (see Fig. 6.10A, simplified after Coimbra et al., 2009).

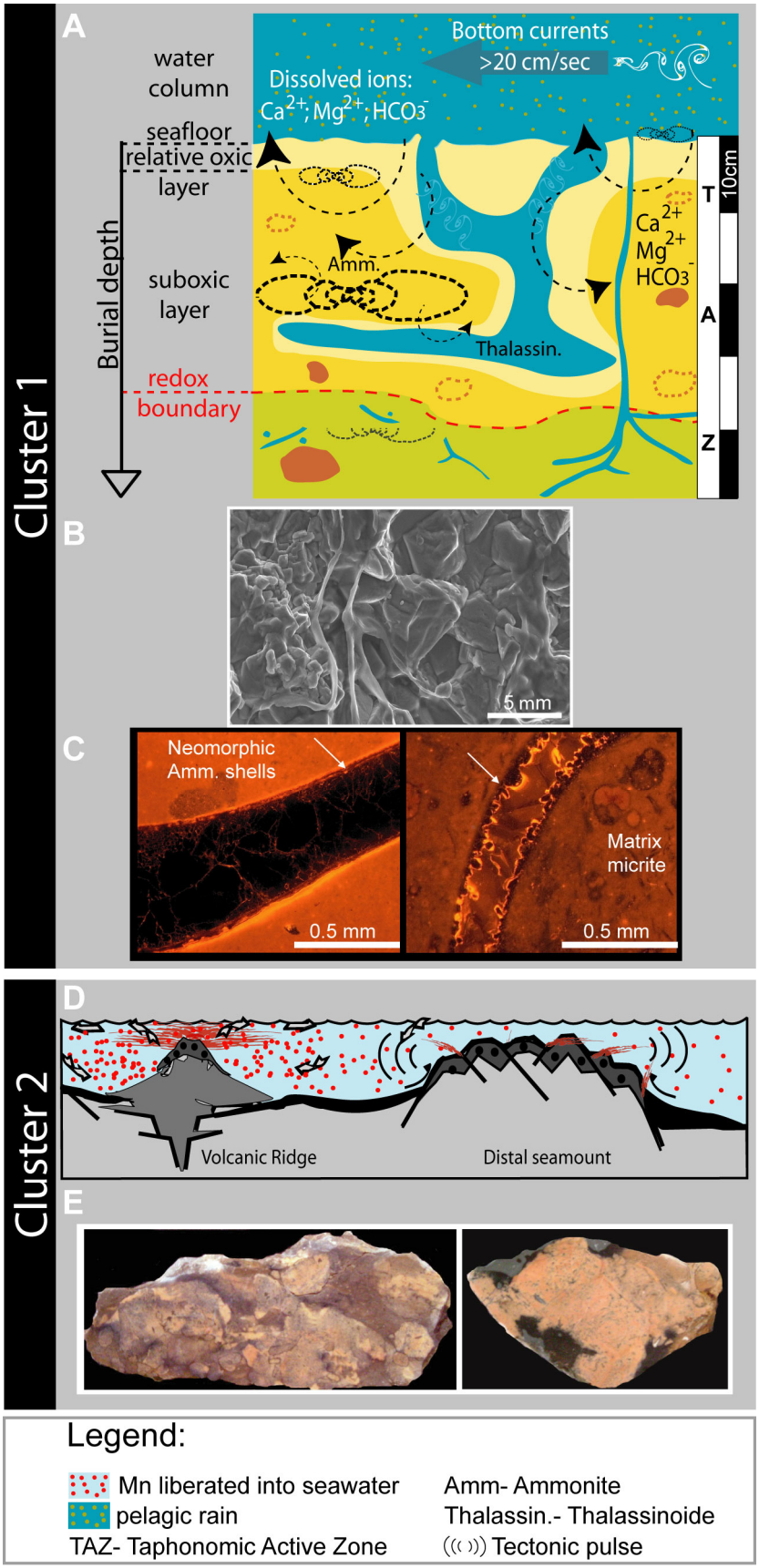
Cluster 1
A
water column
seafloor
relative oxic layer
suboxic layer
redox boundary
Burial depth
Bottom currents
>20 cm/sec
Dissolved ions:
Ca2+; Mg2+; HCO3-
Amm.
Thalassin.
Ca2+
Mg2+
HCO3-
T
A
Z
10cm
B
5 mm
C
Neomorphic Amm. shells
0.5 mm
Matrix micrite
0.5 mm
Cluster 2
D
Volcanic Ridge
Distal seamount
E
Legend:
Mn liberated into seawater
pelagic rain
TAZ- Taphonomic Active Zone
Amm- Ammonite
Thalassin.- Thalassinoide
(( )) Tectonic pulse

Fig. 6.10- Schematic representation of the significance of each cluster: A to C- Mechanisms that account for the contribution of Mg, Fe, and Sr (cluster 1) on early diagenetic nodule formation. A- Factors involved in early diagenetic nodule formation; B- Ultrastructure image showing micritized bacterial/algae filaments; C- Neomorphic ammonite shells showing variable degree of preservation (the example on the right is more affected by diagenesis, presenting orange luminescent cement generations, indicative of early marine burial stage; D- Idealized representation of the environmental context forcing the hydrothermal supply that accounts for Mn enrichment on the studied materials. Note Mn staining in hand samples. See text for explanations.

The significance of strontium and nodule formation is probably best understood by aragonitic dissolution. It occurs very early during diagenesis of ammonite shells and other aragonitic skeletals belonging to other organisms also common in the epicontinental environment such as blue-green algae, forams, briozoa, bivalves, gastropod and some brachiopods, together with less common corals and cirripeda, and potential fish otolites. Dissolution/reprecipitation mechanisms of thermodynamically instable ammonite shells commonly result in neomorphic calcite (see Fig. 6.10C) (Buchardt and Weiner, 1981; Veizer, 1983; Ditchfield et al., 1994; Lécuyer and Bucher, 2006). The occurrence of aragonite in shell materials commonly shows high Sr content (8000-10000 ppm) and during dissolution-recrystallization, Sr in released in the surrounding pore water (Fig. 6.10C). According to Jenkyns (1971) and Coimbra et al. (2009) this mechanism contributes to increased lithification rates of matrix micrite during the very early diagenesis when dissolution of aragonite (and fine grained calcite) provide the necessary supply of Ca^{2+} and HCO_3^- for incipient nodule formation.

The significance and source of iron in Ammonitico Rosso and related facies has been widely debated (Berner, 1969; Jenkyns, 1971; Mamet and Préat, 2003, 2006; Préat et al., 2006, 2008). Specifically, the oxidation state of iron (Fe^{2+} versus Fe^{3+}; Figs. 6.2 A, B and C) resulting in alternating grayish and reddish limestones and the activity of iron-reducing bacteria and fungi has been the subject of previous research (Mamet and Préat, 2003, 2006; Préat et al., 2006, 2008). Interestingly, Fe abundances in limestone samples have found to be rather invariant independent of coloration (red versus gray) throughout the investigated sections. This underscores the significance of the oxidation state and involves bacterially (microbially) mediated Fe fixation. Iron reducing microaerophilic biofilms are known to proliferate on dysoxic environments within the sediment/water interface (McClean et al.,

1996). Unequivocal evidence for microbes in Ammonitico Rosso facies is rarely preserved but microbial filaments have been identified in various samples under the scanning electron microscope (Fig. 6.10B) and reported by other authors (Jenkyns, 1971; Préat et al., 2006, 2011). Low levels of illumination, combined with low oxygen levels (Fig. 6.10A), low sedimentation rates (Coimbra et al., 2009) and the availability of Fe^{2+} (and/or Mn^{2+}) provide suitable environments for biologically induced (or controlled) precipitation of Fe/Mn oxy-hydroxides (hematite: $Fe^{3+}{}_2O_3$). Oxy-hydroxides in the matrix resulted in red pigmentation that commonly typifies Ammonitico Rosso facies (e.g., Préat et al., 2006).

6.6.2- Manganese: sources and dispersal mechanisms

PCA and cluster analysis points to a decoupling of manganese from iron, magnesium and strontium. Marine manganese sources include continental input and/or hydrothermal release of Mn into seawater (Bender et al., 1970; Kickmaier and Peters, 1990; Corbin et al., 2000; Vincent et al., 2006; Middag et al., 2011). Continental input via riverine runoff is here excluded due to lack of correlation between Fe and Mn (Fig. 6.5B) and setting seaward from epicontinental shelves for the epioceanic sections investigated.

In the context of the structured palaeomargin under study (Figs. 6.1C and D), bottom instability with or without relevant changes in bottom physiography could result on seepage of hydrothermal Mn plumes (Bender et al., 1970; Kickmaier and Peters, 1990; Corbin et al., 2000). The presence of a volcanic range (the Mid-Subbetic Volcanic Ridge, Figs. 6.1D and 10E) is likely evidence for local hydrothermal Mn source, but pulses of synsedimentary faulting also would contribute with the same effect. Field studies from present-day examples establish that seawater chemistry near sites with volcanic activity is directly linked to this influence (Rubin, 1997; Love et al., 2000). Depending on the size and distance of the submarine active-volcanic focus, marine currents and other factors, seawater masses located hundreds of kilometers away are affected (e.g., Lupton and Craig, 1981). Specifically, a considerable enrichment in Fe and Mn ratios is reported for seawater and sediments. In addition, elements such as V, B, As or Pd are enriched too (e.g., Rubin 1997).

Conversely, volcanic and hydrothermal activity acts a sink for major and minor elements such as Mg, Mo, W or Re (Rubin, 1997, Elderfield, 2010). With respect to the investigated transect, the Mn distribution in seawater – and hence sediment (Fig. 6.6) – is a

function of distance between Mn source and the section measured, as well as factors such as current patterns and sedimentation rates (e.g., Middag et al., 2011). Evidence for pulses of tectonic activity and related effects during the Late Jurassic are reported by other authors (Ziegler, 1988; Marques et al., 1991, Pena dos Reis et al., 2000; Salas et al., 2001; see Olóriz et al., 2003b for correlation of tectonic pulses among distant areas in Europe, north-west Africa, the central-north Atlantic Basin and the Mexico-Caribbean region) and correspond to the biochronostratigraphic interval corresponding to the epioceanic sections that record Mn maxima (Corbin et al., 2000; de Rafaélis, 2001; see Fig. 6.6).

6.6.3- Time control on elemental distribution patterns: significance of variograms

The behavior of geochemical data throughout time in their paleogeograhical context was approached by variogram computation, the application of which on ancient carbonates seems to have never been attempted since no literature was found on this subject.

In order to translate the observed patterns into mechanisms that relate to fluctuations of the studied proxies, the behavior of the carbon isotope record was the starting point. This proxy behaves similarly on all studied sections (Fig. 6.9A, lower left), and is comparable to other Tethyan published records (see Coimbra et al., 2009, 2011 for references) showing no identifiable recurrence in cycle patterns under applied biochronostratigraphic control and variogram resolution. Differential rates affecting equivalent curves indicate a persistent pattern (type-d general pattern in Fig. 6.9C) interpreted as resulting from control by a remote factor such as the effects of global climate (i.e., the global control on carbon cycle) on the west-Tethyan region. No element behaves according to this trend except the Mn/Ca ratio in the two distant sections at Salcedo and Cuber (Fig. 6.9A, upper right), while the other investigated sections show a rather spaghetti pattern (i.e., no inherent structure) irrespective of their relative distance to the mentioned sections. The registered behavior in the Salcedo and Cuber sections could inform about persistent closer vicinity to areas experiencing bottom instability by frequent tectonic activity and related effects during the Late Jurassic (e.g., hydrothermal seepage throughout faulting, among others, with a rather short-distance effect).

Interestingly, within the context of the considered influence of the "west-Tethyan climate", the behavior of the oxygen isotope record in the variogram offers sinuous curves (Fig. 6.9A. lower center) which agree with a slightly modified type-a general pattern (Fig.

6.9C) in the case of two distant sections (at Salcedo and Cuber), together with evidence for a more accentuated overimposition of a long-term factor in the other relatively less separate sections. Without denies a subtle longer-term factor interference over the regular type-a general trend mentioned for the Salcedo and Cuber sections, the behavior of the other analyzed sections roughly adapt to a type-b general trend (Fig. 6.9C). The latter reveals particular regions with greater potential for recognition of long-term factors influence within the wider paleogeographic area investigated. Recurrent fluctuations in the oxygen isotope record across epioceanic swells point to repetitive changes in temperature of bottom water masses on these submarine highs. The nature of the long-term factor remains obscure (climate, long-term eustasy?) but the combined effect of comparatively intricate bottom physiography and the related forcing of marine current patterns should be taken into account.

The behavior according to the type-a general pattern and slight deviations (Fig. 6.9C), also commonly identified among analyzed elements (Mg, Sr, and locally Fe), indicates a cycle pattern of ranges R=10, or ca. 4 Myr semi-period, and R=20, or ca. 8 Myr period. Cyclicity in these ranges is of lower frequency than regressive/transgressive (R/T) cycles (0.5 to 3 Myr) proposed by Stephen and Davies (1998) and roughly accords with factors controlling T/R facies cycles (3 to 10 Myr) proposed by these authors, even better with the high-range (4 to 6 Myr) assumed for third-order sequences proposed by Olóriz et al. (2003) for Upper Jurassic tectono-eustatic sequences in north-central Mexico and the northern Gulf-Rim areas, and their potential correlation with stratigraphic evolution in the north-Central Atlantic Basin and southern Europe within the context of the excessively wide and variable time duration assumed for third-order depositional sequences (see Olóriz et al., 2003b for references). All of this point to tectono-eustasy as the potential trigger factor. The local out-of-phase, lapse behaviour for the Mg/Ca ratio in the Cañada el Hornillo section (Fig. 6.9A, upper left) is of interest. This record separates from that of all the other analyzed sections, which include the very close Puerto Escaño section (Fig. 6.9A, upper left). In this case, differential setting within the same swell (top-to-wedge vs. upper and/or middle-lower slope) can relate to difference in macroscopic appearance among AR facies (degree of nodularity to its near absence) as well as could relate to relative timing of ecological response to tectono-eustasy dynamics among high- vs. low-Mg calcite biota colonizing these two sites of reference.

Type-c general patterns (Fig. 6.9C) are less common and relates to variograms showing complementary, more variable, spaghetti curves (skeletals and the Fe/Ca ratio in Fig.

6.9A, lower right and upper center-right, respectively). In these cases the range R close to 20, or semi-period of ca. 8 Myr (see above), relates to a higher range of tectono-eustasy dynamics forcing greater timing for the highest degree of dissimilarity among samples. Skeletals and Fe are known to be mainly controlled by comparatively local conditions, these being related to ecology (fertilization and productivity) and/ or transportation (reworking included). It is interpreted that the larger the tectono-eustatic effects the higher the ecologic and hydrodynamic outcomes, which would be registered as events in correspondence with their difference against background or standard for the sedimentary records investigated.

Type-e general patterns (Fig. 6.9C) showing a typical horizontal trend indicate no relationships between the combined variables in the variogram (Fig. 6.9B).

From the previous, lower frequency time variations can be related to the influence of comparatively long-term to remote factors on elemental distribution across wide areas, including selective behaviors. From all analyzed proxies, the carbon isotope record better records the longer-term trend identified and interpreted (Fig. 6.9A). Among elements, magnesium offers the recurrent fluctuations of longer period, a pattern that could relate to the dominance of Ammonitico Rosso facies, where Mg abundance is tightly related to bottom water conditions and early diagenetic nodule formation (see above).

6.6.4- Elemental versus isotope chemostratigraphy, the significance of statistical analysis and the view forward

The number of studies applying elemental chemostratigraphy to fossil carbonate sections (e.g., Vincent el al., 2006, Renard et al., 2007; Boulila et al., 2010; van der Kooij et al., 2010) is indeed unbalanced when compared with the very considerable number of previous work applying the more conventional isotope chemostratigraphy approach (Jenkyns,1980; Menegatti et al., 1998; Joachimski et al., 2002; Immenhauser et al., 2003; Jiang et al., 2007; Bodin et al., 2010; Huck et al., 2011). In fact, the interpretation of the elemental composition of carbonate skeletal material, carbonate cements or bulk rock (matrix micrite) samples is far from trivial owing to the complex array of interplaying environmental, biological and diagenetic factors (Price et al., 1998; Immenhauser et al., 2002; Niebuhr and Joachimski, 2002; Brand et al., 2003; Voigt et al., 2003; Rosales et al., 2004; Westphal, 2006; Brigaud et al., 2008; Price and Page, 2008; Warnke et al., 2010). The same, however,

accounts for isotope (mainly carbon and oxygen) data and their use as a stratigraphic tool. The application of isotope stratigraphy from hemipelagic and pelagic sections (Voigt and Hilbrecht, 1997; Immenhauser et al., 2003; Rais et al., 2007; Renard et al., 2007; Louis-Schmid et al., 2007; Coimbra et al., 2009; van der Kooij et al., 2009) is –under favourable conditions – a valuable tool due to assumed "continuous" stratigraphic records – and the lack or rarity of meteoric exposure horizons. Conversely, the interpretation of the chemical composition of neritic deposits from ancient epicontinental to epeiric settings is promising but often fraught with problems. Prominent amongst these problems are hiatal surfaces (Bhattacharya, 2011 and references therein) and potential stratigraphical gaps, the effects of meteoric diagenesis (Land, 1970; Allan and Mathews, 1982; Lohman, 1987; Immenhauser et al., 2002; Pavlović et al., 2002; Whitaker et al., 2006; Hamon and Merzeraud, 2007; Hernawati et al., 2010) and the overall high degree of continentality in coastal and epeiric water masses and related sediments (Allan and Mathews, 1982; Moore, 2000; Austin et al., 2006; Vincent et al., 2006; Cramer and Saltzman, 2007; Cage and Austin, 2008; Immenhauser et al., 2008; Kharol et al., 20111).

Following previous multi-proxy approaches –i.e., work combining biostratigraphy with carbon and strontium isotope stratigraphy (e.g., Jones and Jenkyns, 2001) – it is proposed that the combination of isotope and elemental stratigraphy is a potentially valuable strategy that deserves consideration. This approach has been applied to short stratigraphic intervals before with variable success. Important examples include elemental stratigraphy across short stratigraphic intervals representing Jurassic and Cretaceous oceanic anoxic events (Jones and Jenkyns, 2001; Jenkyns, 2010). These stratigraphic intervals, however, represent periods of globally perturbed chemical cycles and might not represent standard case examples.

Similar to isotope chemostratigraphy, one of the main problems related to elemental stratigraphy is the filtering of noising effects contained in the dataset. The presented contribution is considered encouraging and –combined with the limited number of case studies found– documents the advantage of a rigorous statistical analysis of elemental data. The statistical approach used in the case under study provides a solid, quantitative fundament for the interpretation of these data in their environmental and diagenetic context.

Nevertheless, whilst numerous case studies from basins around the globe offer reference curves for isotope stratigraphy, the lack of reference to coupled elemental

chemostratigraphy sections is evident. At present, it is envisaged that elemental stratigraphy is a correlation tool with a more-than-regional significance, if the effects of assumed teleconnections are considered. In such a context is not reproducibility of regional trends, but their inter-regional compatibility that applies. Hence, this research encourages the application of the element chemostratigraphy approach to more case studies and different time slices and foresees a significant potential for understanding paleoenvironmental dynamics as registered in the sedimentary record.

6.7- Conclusions

From the seven studied sections that comprise the proximal to distal studied transect, only the epicontinental record at Rocha Poço revealed a high degree of diagenetic overprint, along with evidences of continental influence on the geochemical record. All the remaining epioceanic sections showed a remarkable degree of preservation and a fairly homogeneous elemental behavior throughout the studied transect.

Elemental associations provided by distinct statistic tools (PCA, cluster analysis) evidenced valuable, informative relations between analyzed elements. Magnesium, Fe and Sr, relate to early nodule formation on Ammonitico Rosso facies, with each element contributing in a different way to this process, but largely revealing pre-to-very early diagenetic environmental conditions. Manganese exhibits a behavior that departures from all other analyzed proxies. The presence of Mn is attributed to hydrothermal supply, in agreement with high rates of seafloor spreading during Late Jurassic times. The occurrence of the Mid-Subbetic Volcanic Ridge could also be an example of local potential source for Mn in the region investigated, in addition to the widespread synsedimentary faulting typical in the epioceanic fringe corresponding to the structured south and eastern paleomargin of the Iberian subplate.

The first interpretation of variogram computation applied to geochemical data of ancient carbonates suggests this to be a promising statistic tool providing the most precise information available. Hence, several time-patterns of geochemical behavior were attained, not provided by any other attempted method. The temporal expression of geochemical proxies on the studied transect are so far interpreted as a superimposed effect of global, regional and

local processes. Further work may provide a better understanding of variogram significance on similar approaches.

Acknowledgements

We wish to thank Dieter Buhl, Ulrike Schulte, Beate Gehnen and Noushin Arshadi (Ruhr Universität Bochum-RUB) for their support during laboratory measurements; Rolf Neuser (RUB) for the cathodoluminescence and SEM analysis; Matthias Born (RUB) and Alberto Montes (University of Granada-UGR) for the preparation of thin sections; and Alicia González, Concepción Hernandez and Hoda Khaldy (CIC-UGR) for collaboration during SEM analysis and preparation of laboratory material. We also thank Beatriz Marques (University of Lisbon) for background information and field support in S Portugal. This research was supported by Projects CGL2005-01319 and CGL2008-05251-E (MICINN) and the Research Group RNM-178 Junta de Andalucía, Spain.

Appendix 6.1. Stratigraphic elemental abundances

The complete geochemical dataset is presented in Fig. A (and A-cont.). The elemental proxies are presented in their absolute concentration values, used to compute the boxplots presented in Fig. 6.1.

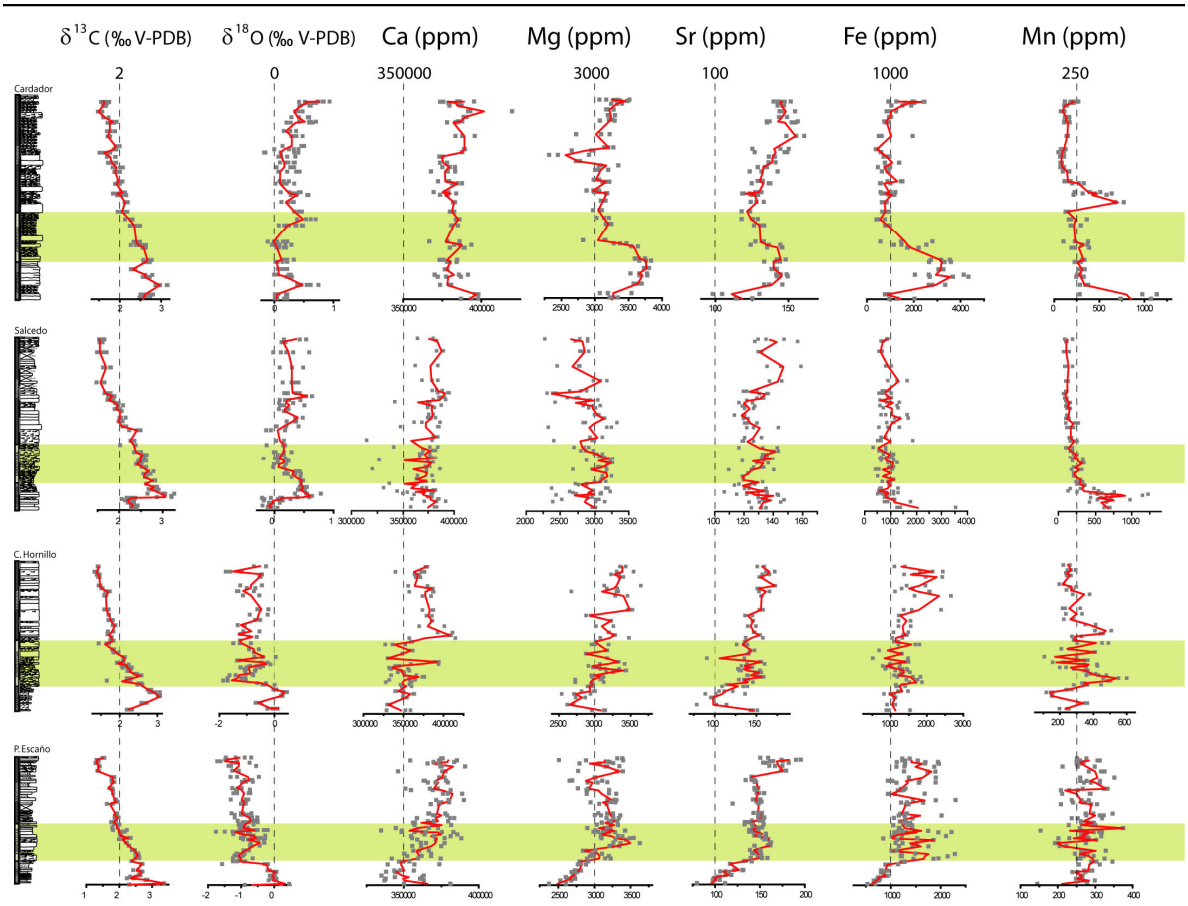

Fig. A- Stratigraphic plots of the studied geochemical proxies: C and O stable isotopes, Ca, Mg, Sr, Fe and Mn. All elemental proxies are shown in their absolute concentration values (in ppm).

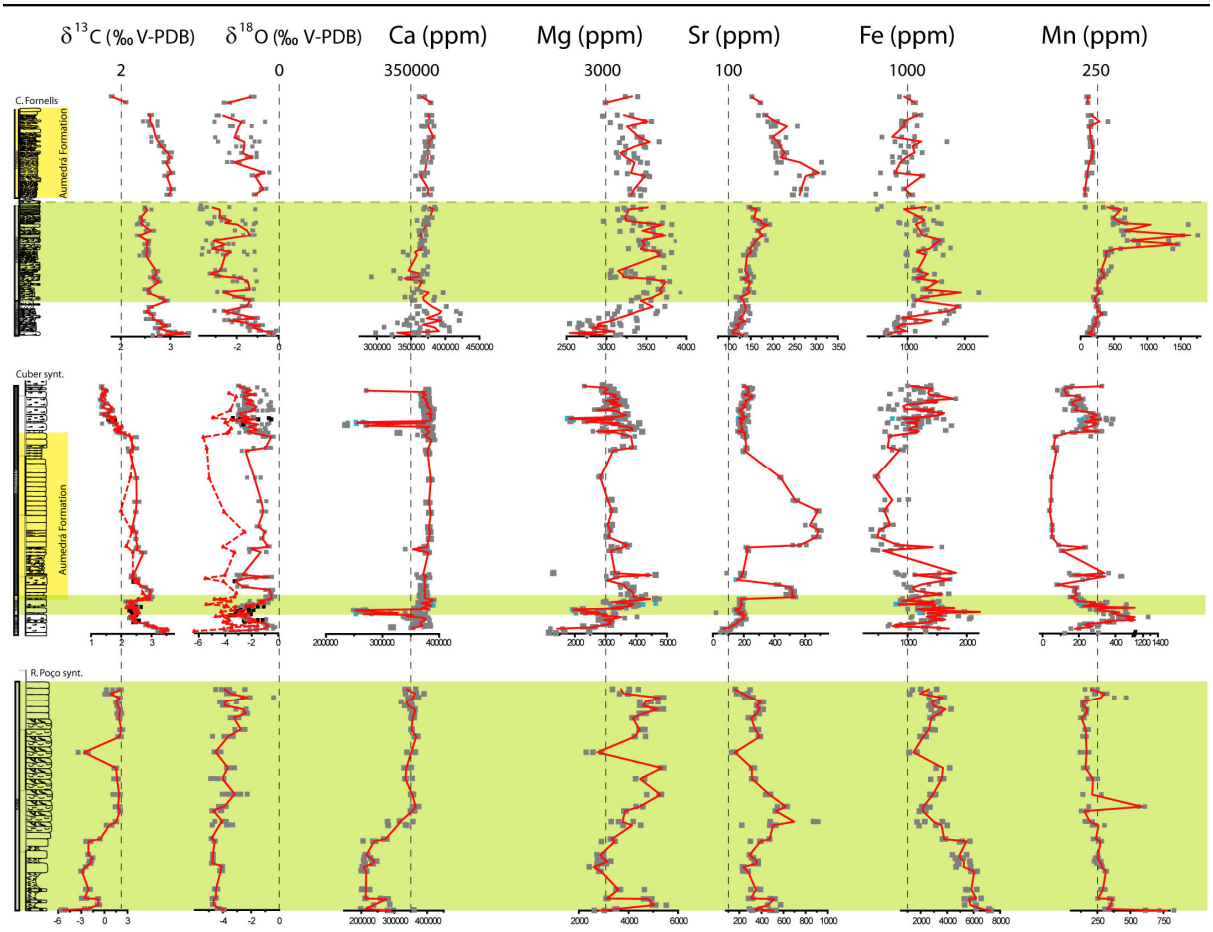

Fig. A -cont.- Stratigraphic plots of the studied geochemical proxies: C and O stable isotopes, Ca, Mg, Sr, Fe and Mn. All elemental proxies are shown in their absolute concentration values (in ppm).

Appendix 6.2. Temporal variability: Simple and cross-variogram computation

The analysis of the temporal variability is not a standard procedure in paleoenvironmental studies. In fact, to our knowledge, this is the first attempt to apply this method to carbonate major and trace elemental abundances in time series datasets. Therefore, a wider overview of the applied equations and relevant parameters is presented bellow.

From a geostatistical point of view, this aspect of temporal variability has been quantitatively analysed by means of the variogram function, expressed as:

$$\gamma_k(t) = \frac{1}{2n(t)} \sum_{i=1}^{n(t)} \{ z_k(x_i) - z_k(x_i + t) \}^2$$

where $z_k(x_i)$ and z_k (x_{i+t}) are the values of the z_k variable, observed in samples x_i and x_{i+t} of a series; n(t) is the number of pairs of distance data (here stratigraphic intervals) whose distance is the time vector t. It must be clarified in this study of the analysis of data temporal variability that vector t represents a relative time value, i.e., it corresponds to an ordinal value of separation of the experimental sample x_i and x_{i+t} in the series. It follows from the previous expression that a variogram is a vectorial function, which quantifies the variance of the first-order quadratic increments of the z_k variable. Both, its analysis and interpretation, are important to quantify the variable's temporal variability.

A diagram of a typical variogram (case of a second-order stationary variable, extracted from the Mg curve for the Cuber section) is presented as an example to illustrate relevant parameters (Fig. B).

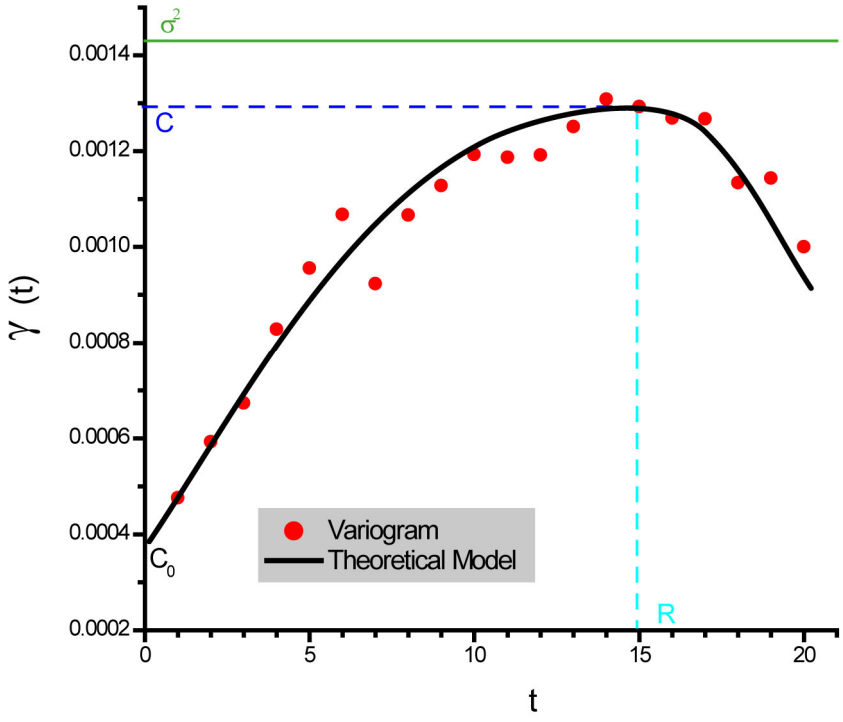

Fig. B- Diagram of a typical variogram (extracted from the magnesium curve at the Cuber section), illustrating relevant parameters used for variogram interpretation. See text for explanations.

The C_0 discontinuity value at the origin, called 'nugget effect', represents the abovementioned random component of the data; it corresponds to variability of an inferior scale to that of the data sampling (although in some cases it can also be explained by a variation caused by measure errors). The C parameter (sill) corresponds to the structured variability of the

experimental data (temporal regionalisation). The sum of both components is equivalent to the variable's total variability, quantitatively expressed by the statistical variance σ^2 (stationary case). The last parameter, R, is the range which represents in this study case the time from which the data pairs $z_k(x_i)$ and $z_k (x_i+t)$ reach their independence; i.e., they are not correlated. It is worth mentioning that this general variogram diagram can vary depending on the inherent data variation features (i.e. presence of trends, cyclicities, etc.).

In the multivariate case, the cross-variogram function has been used to analyse the variability or joint correlation (coregionalisation) between two variables z_j and z_k:

$$\gamma_{jk}(t) = \frac{1}{2n(t)} \sum_{i=1}^{n(t)} \{ z_j(x_i) - z_j(x_i + t) \} . \{ z_k(x_i) - z_k(x_i + t) \}$$

The respective results are presented in Fig. 6.9B.

7

Conclusions

7.1- Suitability of the working approach

The working approach presented in this work rendered a thorough control of the obtained results. On the field, special care was taken to choose a sample density that could be adequate for the studied time frame and the particular conditions of each section analyzed. An average of 5 samples per meter of studied section proved to be appropriate for the condensed sections under scope, allowing the construction of stratigraphic geochemical curves that were representative for each section and contrastable with coeval data reported by other authors. Also during field work, -special care was taken in order to provide the diversity of carbonate materials that are the backbone of the diagenetic and environmental interpretations presented along this research. More than picking random samples almost bed-by-bed, selective sampling applied according to a better control of representative lithologic features and extra samples were chosen exactly because they presented either skeletal components that could also be sampled, or secondary diagenetic features (veins) that had a high potential to inform on the diagenetic imprint affecting the materials under study.

In order to ensure the control of intra-sample variability, an average of 4 sampling points was chosen for each slab. This approach has the advantage of ensuring that relative changes in microstratigraphic order (time) are more significant than a mere single sampled point, since they can be compared with intra-sample variability. Aside from working with several powder samples from each slab, whenever possible other carbonate materials were also sampled, allowing the control on the differential diagenetic pathways of the distinct materials registered. This allowed a thorough comparison between distinct carbonate materials and ensured a high number of analyzed samples that allowed performing statistical methods with a high level of significance.

The petrographic analysis of the studied materials was performed in a way that it could reinforce the analytical (geochemical) results. Each thin section produced was chosen from exactly the same area that was drilled for geochemical inspection. In this way, geochemical work gained from microfacies information, and vice versa, in a more precise way.

Regarding data treatment, analytical results were plotted following standard representations (i.e., stratigraphic ordering). Once this option was exhausted, alternative methods were necessary in order to solve the complex variability of such an extended dataset. The application of statistic treatment provided the adequate tools to go further than

interpretations based on mere stratigraphic variations. In the search of alternative methods that could better apply to the obtained dataset, spatio-temporal implications became available, providing new information that had not been depicted by any other method.

7.2- Reliability of the obtained dataset

Petrographic features pointed to a fair preservation of the studied material. Overall, the carbonate ultrastructure of micritic material is well preserved, as attested by the occurrence of algal filaments and/or bacterial remains and coccoliths. Early stabilization of matrix micrite carbonate is envisaged to be able to preserve these delicate structures. The degree of preservation of coccoliths also supports a good degree of preservation. Furthermore, matrix micrite shows dull luminescence, indicative of limited diagenetic overprint and clearly in contrast with latter diagenetic feature, that show a very distinct and characteristic luminescence pattern. All the above attests for a good preservation state of the studied material and is consistent with the interpretation of near-pristine carbon and oxygen-isotope values, except for late cements.

The average value of 2‰ retrieved from matrix micrite for all epioceanic sections is in agreement with available published data from Upper Jurassic Tethyan paleomargins. In fact, all the analysed materials are also within this range, except belemnite rostra. This fact supports the notion that the carbon isotope ratio is less prone to severe diagenetic alteration, and hence, quite conservative. Belemnite rostra contrast with these observations, despite their demonstrable fair degree of preservation. Vital and ecologic effects interpreted for this fossil group, and known from their present relatives, account for the obtained depleted $\delta^{13}C$ values. The $\delta^{13}C_{micrite}$ record obtained from the epioceanic record in bulk samples is somewhat comparable, whilst the epicontinental record at Rocha Poço is far more complex. A combination of factors explain the low carbon isotope values recorded for the more siliciclastics horizons from the base of this section. Despite acknowledged uncertainties, diagenesis certainly contributed to the observed such lowered values, but probably also in addition to the effect of continental influx on this epicontinental, more proximal setting.

Overall ^{18}O-enriched Ammonitico Rosso micrite isotope ratios from the epioceanic record rule out a significant diagenetic alteration through this proxy, already supported by petrographic evidences. Significant changes in salinity can also be excluded as a forcing

factor, since surface seawater evaporation on shelves and subsequent basin-ward transport of density currents, is not consistent with the epioceanic settings analyzed, and even in such case, the ecology of benthic communities would provide information pointing in that direction, which is not the case. Therefore, porewater temperature is the sole driving factor that can account for the higher than usually reported oxygen isotope values, mainly controlled by seawater temperature, reflecting a close-to-original isotopic signal. The comparison with oxygen isotope values retrieved form other carbonate materials is again coherent with this interpretation, with $\delta^{18}O_{belemnite}$ within similar range of values as matrix micrite. The epicontinental record of a particular set of statigraphically controlled bulk samples and the carbonate cements are the only cases where diagenetic influence can not be ruled out, explaining the lower (negative) obtained dataset.

The elemental record handled during this research revealed the same patterns, i.e., well preserved materials presented values within the expected range of elemental concentrations, whilst diagenetic alteration could also be depicted through further elemental data treatment (statistical approach).

7.3- Epioceanic record and Late Jurassic paleoceanographic conditions

7.3.1- Stratigraphic patterns of stable (C and O) isotopes

The stratigraphic behaviour of both carbon and, interestingly, oxygen isotope ratios obtained for matrix micrite present comparable trends within the epioceanic record. Main shifts can be attributed to Late Jurassic paleoceanographic conditions.

As widely recognized, the major mid-Oxfordian transgression imposed an overall positive trend in seawater $\delta^{13}C_{DIC}$. The obtained $\delta^{13}C_{micrite}$ values of the epioceanic sections reflect this feature, reaching maximum values at the stratigraphic interval corresponding to this time. During the Kimmeridgian the long-term sea levels continued to globally rise, superimposed to short-term pulses. Nevertheless, no record of these events was recognized on the carbon isotope curve from the epioceanic sections that record a persistent decreasing trend during this time. Renewed growth of carbonate platforms that accompanied sea-level rise during the Kimmeridgian resulted on perching of high inorganic carbonate production on shelves that account for the obtained record. During Tithonian times, when long-term sea

level reversed to persistent fall with widespread regression effects, the stable decreasing trend is still recorded, reaching the minimum values recorded for the Late Jurassic. Towards the Jurassic-Cretaceous boundary, major climate reorganization that affected carbonate-shelves is attributed to the described $\delta^{13}C$ trend. The $\delta^{13}C$ record from all epioceanic studied sections is hence in agreement with assumed 'global' signature of seawater $\delta^{13}C_{DIC}$.

The oxygen isotope composition retrieved from all epioceanic sections is more volatile than the above commented carbon isotope record. Still, analogous behaviour can be recognized within all the studied sections, –resulting in a comparable stratigraphic curve. A significant positive shift is observed during Mid-Oxfordian times, coinciding with the timing of the major Tethyan transgression. Since the obtained oxygen isotope values are assumed to reflect changes in bottom seawater paleotemperature, this would denote that colder water masses and then paleotemperatures can be depicted during episodes of higher sea-level, as a result of a deeper and/or cooler conditions on the studied areas. The same feature (i.e., positive shift) can be identified towards the end of the Kimmeridgian, although sometimes obscured by slight differences between sections. In this way, the attributes of the oxygen isotope stratigraphic curve can be traced back to well known sea-level fluctuations, rendering to this proxy a high potential for providing reliable information about paleoenvironmental dynamics in open sea settings.

The only cases where epioceanic isotope (C and O) values registered an offset regarding Tethyan trends related to the presence of the Aumedrá carbonates (Aumedrá Fm.), already atypical macro- and microscopically for distal swell settings, and latter even more in terms of the geochemical record. An aragonitic factory determining primary mineralogy is favoured, followed by the corresponding differential diagenetic pathways coupled with sorting during transport.

7.3.2- Spatial patterns of stable (C and O) isotopes

The proximal to distal transect under scope could clearly be differentiated by the obtained dataset. At first, the epicontinental setting revealed a very particular geochemical signature, in accordance to its proximity to main emerged lands in the paleomargin. Continental influence could be depicted by the analyzed carbon and oxygen isotope ratios,

both with conspicuous lower values when compared to the epioceanic realm. The elemental record of the epicontinental record confirmed this proximal influence, being the only sections with a clear relation between the elements Fe and Mn, which are related to continental influx.

All epioceanic sections presented rather similar records, especially true for carbon isotope values. Small relative variations in oxygen isotope values could be traced back to different locations and/or depths, along the proposed paleogeographic model, in all cases in agreement with the latter. From more proximal to distal, an overall decrease in seawater paleotemperature could be depicted, with minor local variations forced by hydrothermalism, also recorded by the geochemical record (mainly oxygen isotopes and Mn concentrations).

7.3.3- Elemental behaviour (in space and time)

The elemental record provided insight on preservation potential of the studied matrix micrite samples, paleoceanographic differences among the studied sections, relative differences in depositional setting, and variations in time that could not be depicted by other proxies. The statistic treatment of such an extended dataset was favored, proving the right path towards a better understanding of the complexity of the elemental record available.

Micrite elemental data from the epicontinental record confirmed the continental influence, being the only sections with a clear relation between the elements Fe and Mn, apart from being also the only record with a clear indication of diagenetic overprint (relation Sr vs. $\delta^{18}O$). In contrast, all epioceanic sections showed persistent elemental relations: Magnesium, iron and strontium on one hand; and manganese clearly decoupled from the previous. The first group of elements contributed for the early formation of nodules typical for Ammonitico Rosso facies, and the influence (at least regional) of hydrothermalism was responsible for the differential, significant manganese contamination recognized on all epioceanic sections. The particular case of the carbonate materials encased by mafic rocks provided further key evidences.

The application of variogram analysis to the available dataset provided several time-patterns of geochemical behavior that had not been available by any other performed method. The temporal expression of geochemical variables along the studied proximal to distal transect was attributed to the combined influence of global, regional and local processes.

7.4- Claims for future research

Following the scope of the present research, further information from different settings would certainly contribute to enhance the understanding of paleoenvironmental and paleoceanographic dynamics and its potential of retrieval by means of carbonate geochemistry. Several directions can be taken to achieve this purpose. One is to gather more information on epicontinental settings, in order to obtain a more complete record. Second is the comparison between different Tethyan areas (Tunisia, Morocco) could result interesting since the already known dynamics may or may not apply along wide regional distances. Third, and since precise biochronostratigraphic control is available for coetaneous Atlantic/east-Pacific sections (Olóriz et al., 2003b; Cobiella and Olóriz, 2010) of similar age, an evaluation of similarities and differences between two ancient Oceans and their epicontinental, at times epeiric, water masses becomes attractive taken into account the potential of the available dataset.

8

Appendix- Pixel counting for percentage estimation: applications to sedimentary petrology

Rute Coimbra. [(a)], Federico Olóriz [(a)]

[(a)] Departamento de Estratigrafia y Paleontologia, Universidad de Granada, Spain

Submitted to Computers and Geosciences (May 2011)

8.1- Introduction

The analysis of thin sections under the microscope is of wide application in geology. The first, most striking characteristic will be the presence of different types of grains and matrix, as is the case in sedimentary rocks. Nevertheless, the less time consuming approach to estimate relative abundances requires a trained eye, since semi-quantitative estimations are based on visual comparison charts or shadow diagrams (e.g., Folk, 1951; Terry and Chilingar, 1955; Baccelle and Bosellini, 1965). Other methods (point, line, area or ribbon counting, see Flügel, 2004) are time consuming, since their reliability increases with the number of counts. Here we suggest a new approach that eliminates subjectivity inherent to percentage analysis. The "pixel counting" method allows the analysis of components of any shape, colour or size with automatic precision and, therefore, an invariable reliability. This method is based on a very fast procedure (around 20 samples per hour, depending of their complexity). Furthermore, precise percentage estimation may allow the recognition of trends or patterns, otherwise masked by rough estimations, constituting a new parameter comparable with other available quantitative data sets.

8.2- Material and Methods

Several sources of information were tested by means of pixel counting percentage estimation. These comprise: (i) the Baccelle and Bosellini (1965) visual comparison charts; (ii) microscope photographs of thin sections from Upper Jurassic limestones from the Betic Cordillera and lateral equivalents in the Majorca Island (see Coimbra et al., 2009 for description and microfacies analysis of the Cardador; research in progress for the Cuber section); and (iii) cathodoluminescence images of neomorphic ammonite shells (research in progress). For pixel counting purposes, image files were run on Adobe® Photoshop® software CS2 (version 9).

In used (untreated) image files, colour is the distinctive analysed parameter on the assumption that differences in colouration indicate variations in origin, composition and/or diagenetic processes. Colour selection is accomplished by using the tool "magic wand", able to discriminate different areas based on their different colours. By activating the "histogram"

tool on expanded view format, information on total pixel count is shown on the left lower corner of this tool box.

8.3- Results

In order to validate the "pixel counting" method, the starting point was the analysis of the Baccelle and Bosellini (1965) comparison charts (Fig. 8.1A to E).

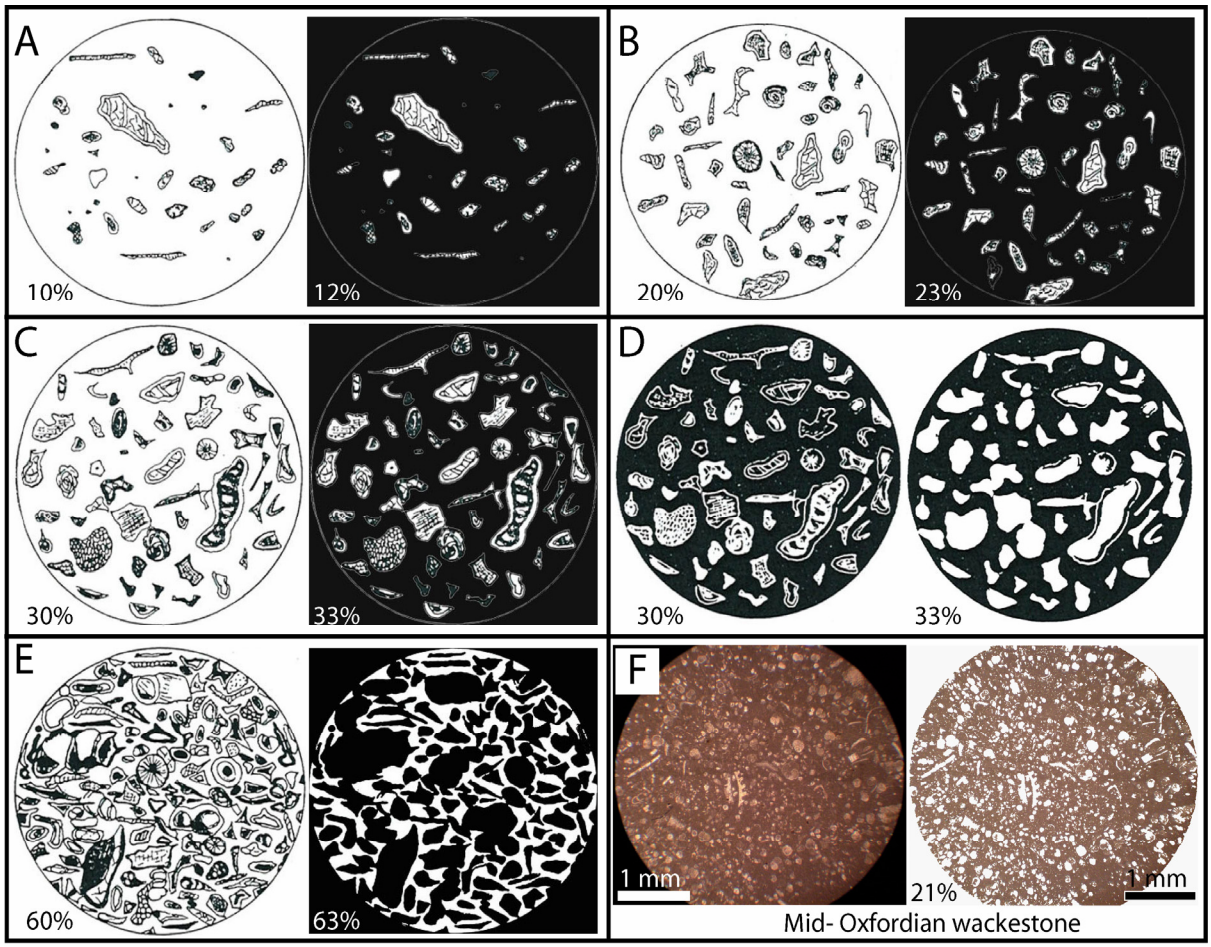

Fig. 8.1- Application of pixel counting percentage estimation to visual comparison charts. A to E) Original charts on the left and pixel counting resulting image on the right (a black background was sometimes added to enhance contrast); F) Example from an Oxfordian horizon: original image on the left; selected matrix micrite used for the pixel counting on the right (with indication of resulting skeletal relative abundance).

The chosen examples (and several other, not shown here) showed a consistent 3% increase respect to the percentages originally attributed to each visual percentage chart (e.g., compare right and left images in Fig. 8.1A to E). The isolation of the black rim that limits

each chart corresponds exactly to a 3% of the total image. Therefore, by excluding this element (not present on microscope images) the same percentage counts are obtained. This holds true regardless the selected elements (matrix micrite or grains whatever their nature, in black or white background; throughout a wide range of relative proportions as shown in Fig. 8.1A to E).

Regarding the application of this method to real examples, for the considered set of samples (procedure repeated more than 300 times for different lithofacies) it was found that matrix micrite quantification is easier to accomplish (rather than direct skeletal material abundance) due to its higher abundance, and follows recommendations about matrix counting control (e.g., Flügel 1982). In order to illustrate each step of this method, a representative example is presented (Fig. 8.1F, a Mid-Oxfordian wackestone). The total of pixels on the image is 373120, including the black areas that surround the circular microscope field in microphotography. These areas will be present in all images since photographic equipment captures rectangular areas, and the microscope field is circular (see Fig. 8.1F, on the left). By selecting the black borders of the photograph (the area surrounding the microscope field), the number of pixels of that area must can subtracted from the total area of the image, by simply inverting the selection of the "magic wand" ("selection menu"). If all the photos have been taken with the same camera and optical parameters, the total number of pixels will be the same and the areas in black also have the same number of pixels, hence, this step can be performed only once and is valid for all samples. For the presented example, the number of pixels for the circular field is 267225, corresponding to 100% abundance of matrix micrite. The selection of brownish areas corresponding to matrix in the case study with the "magic wand", as apposite to whitish skeletal materials, can be performed manually or automatically, the latter by using the "similar" option on the right button of the mouse (or using the "selection menu"). The micrite pixel count is of 211644, making a 79% of micrite matrix present on the sample and therefore, a 21% of skeletal remains. The use of the "tolerance" button allows the refining of the selection. This option controls the tone and colour of the selected areas (or particles), and the value chosen for this tool determines the range of neighbouring colours and tones that are similar enough to be included in the selection. In our case, the chosen "tolerance" value of 20 was the ideal value, providing automatic selections that required only small corrections due to misinterpretations. This procedure allows the user to correct the selection in case of automatic misassumption. A clear example of this situation

is demonstrated in Fig. 8.2, where a recristalized vein may be selected automatically when the intention is to select only white pixels corresponding to skeletal material. This feature should not be part of the count; see Fig. 8.2. Just by deselecting ("selection menu"), all the remaining selection will be active, and this non desired feature is eliminated from the final pixel count.

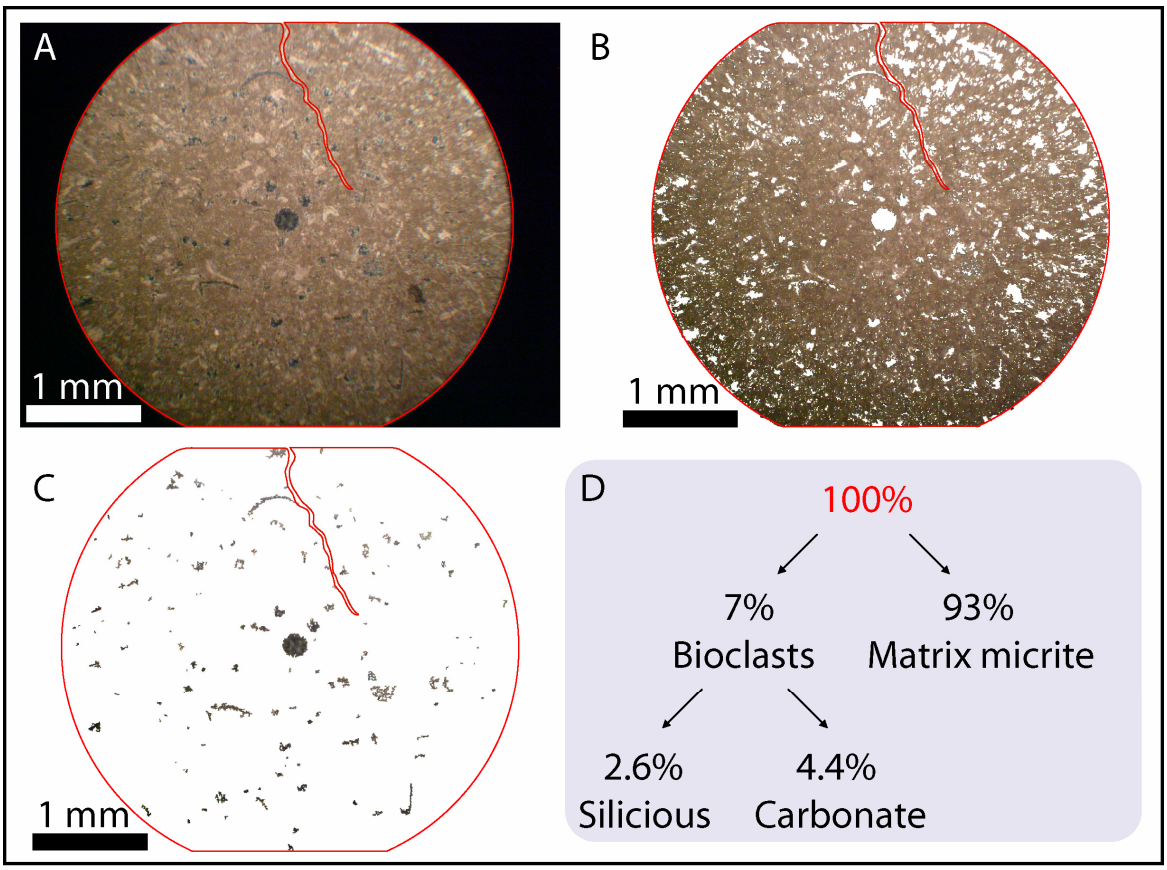

Fig. 8.2- Application of pixel counting percentage estimation to carbonate microfacies with multi-mineralogic skeletal components. A to C) Consecutive steps applied during pixel counting selection; D) Quantitative information retrieved from the performed analysis.

8.4- Applications of pixel counting percentage estimation

8.4.1- Skeletal precipitation mode

An example of a carbonate matrix micrite encasing bioclasts of distinct mineralogy (Fig. 8.2A) is presented in order to demonstrate the potential of the proposed pixel counting method. The presence of a diagenetic vein was excluded from pixel counting (see above).

Calcium carbonate bioclasts could be differentiated from siliceous ones (because they present distinct colours), allowing an estimation of first, the total skeletal abundance, and second, the relative proportion of bioclasts with carbonate and siliceous mineralogy. The possibility of distinguishing between any colour (here, whitish, grey and brownish) allows the application of this method to a wide range of materials (not exclusive to carbonate rocks). This feature marks a clear difference regarding the only pixel counting approach found on the literature (Teagle et al., 2006). The pre-requisite of image treatment prior to the percentage estimation suggested by these authors potentially limits the application of pixel counting to white and black areas With the new method here described, no image treatment is required, and true colours and shades are used, enhancing its applicability.

8.4.2- Stratigraphic approaches

The repeated pixel counting percentage estimation on a set of stratigraphically consecutive samples resulted on the establishment of a chronostratigraphic trend that accurately reflects variations in skeletal abundance throughout the Upper Jurassic section (Fig. 8.3). This parameter can by itself be interpreted on the light of changing environmental conditions. Furthermore, when combined with other analytical proxies (in this case, the oxygen isotope ratio), this method allowed to contrast optical and geochemical variables (Fig. 8.3), thus proving useful for understanding the interplay between environmental depositional conditions and their preservation in the case study.

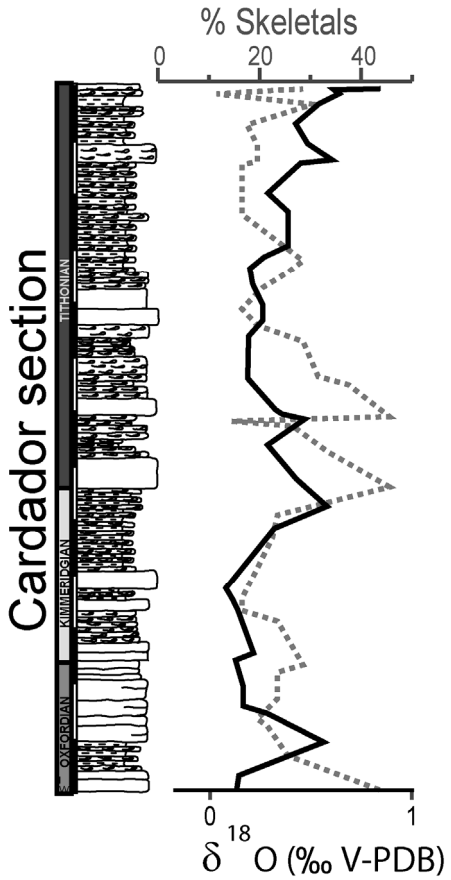

Fig. 8.3- Stratigraphic representation of consecutive pixel counting percentage estimation of skeletal abundance on carbonate facies. Note the comparable trend of the obtained curve (dashed line) and the available oxygen isotope stratigraphic trend (full line).

8.4.3- Diagenesis and cement generations

An example of diagenetically altered ammonite shells is presented on Fig. 8.4. Pixel counting on a succession of three cement generations in studied cases A and B (Fig. 8.4, numbers 1 to 3) allowed the estimation of the relative proportion (percentage) of each cement generation. This is of relevance since cement stratigraphy reflects changes occurred during distinct diagenetic phases. In this way, and together with geochemical variables, each cement generation could be attributed to a specific geochemical signature. The relative higher pixel abundance in the early phase in Fig. 8.4B relates to comparatively lower diagenetic overprint, coinciding with equivalent isotope signature with respect to matrix, and an overall geochemical signature consistent with preservation of porewater conditions early during

diagenesis. In contrast, later phases record a clear diagenetic overprint (cement generations 2 and 3 in Fig. 8.4C and D).

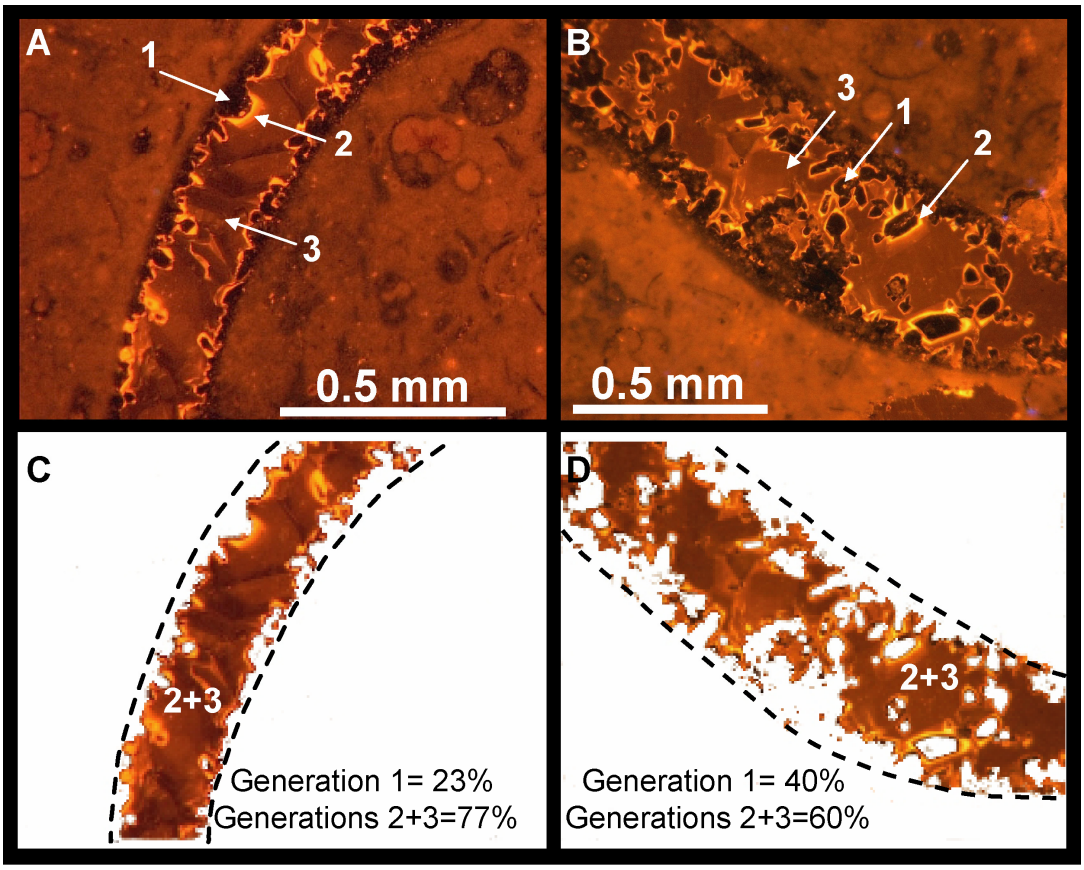

Fig. 8.4- Application of pixel counting percentage estimation to cathodoluminescence images of neomorphic ammonite shells embedded in a carbonate micrite matrix. A and B) Original images, with indication of identified cement generation (numerals 1 to 3). Note the different proportions of cement generations. C and D) The same images, with the selected pixels resulting from pixel counting, with indication of the percentage corresponding to the cement generations 1 and the sum of generations 2 and 3.

8.5- Conclusions

Abundance quantification of different types of materials present in thin sections through pixel counting percentage estimation comes as an alternative to the use of the visual comparison charts, of great help for experienced eyes, or to other time consuming quantative estimations (see above). The proposed automated, objective approach can provide a new parameter comparable and compatible with other quantitative data sets. The use of the pixel counting percentage estimation procedure grants a fast and easy way to solve the quantification issue, and its application to several different lithofacies, shapes, sizes and

colours has been demonstrated. The described approach shows several advantages regarding pixel counting proposed by other authors (Teagel et al., 2006) since it can be applied to any petrographic study (still no limitation has been identified).

9

References

Abbink, O., Targarona, J., Brinkhuis, H. and Visscher, H., 2001. Late Jurassic to earliest Cretaceous palaeoclimatic evolution of the southern North Sea. Global and Planetary Change, 30(3-4): 231-256.

Adabi, M., 2004. A re-evaluation of aragonite versus calcite seas. Carbonates and Evaporites, 19(2): 133-141.

Adabi, M.H. and Rao, C.P., 1991. Petrographic and geochemical evidence for original aragonite mineralogy of upper Jurassic carbonates (Mozduran formation), Sarakhs area, Iran. Sedimentary Geology, 72(3-4): 253-267.

Adabi, M.H. and Rao, C.P., 1996. Petrographic, elemental and isotopic criteria for the recognition of carbonate mineralogy and climates during the Jurassic (examples from Iran and England). 13th Geological Convention, Australia, p. 6.

Alaasm, I.S. and Veizer, J., 1982. Chemical stabilization of low-mg calcite - an example of brachiopods. Journal of Sedimentary Petrology, 52(4): 1101-1109.

Allan, J.R. and Matthews, R.K., 1977. Carbon and oxygen isotopes as diagenetic and stratigraphic tools: Surface and subsurface data, Barbados, West Indies. Geology 5: 16-20.

Allan, J.R. and Matthews, R.K., 1982. Isotope signatures associated with early meteoric diagenesis. Sedimentology, 29: 797-817.

Allerton, S., Lonergan, L., Platt, J.P., Platzman, E.S. and McClelland, E., 1993. Palaeomagnetic rotations in the eastern Betic Cordillera, southern Spain. Earth and Planetary Science Letters, 119(3): 225-241.

Álvaro, M., Barnolas, A., Cabra, P., Comasrengifo, M.J., Fernandezlopez, S.R., Goy, A., Delolmo, P., Delpozo, J.R., Simo, A., Ureta, S., 1989. The Jurassic of Majorca (Balearic Islands). Cuadernos De Geologica Iberica, No 13: 67-120.

Álvaro, M., Barnolas, A., Del Olmo, P., Ramírez Del Pozo, J. and Simó, A., 1984. Estratigrafía del Jurásico. Sedimentología del Jurásico de Mallorca. Grupo Español del Mesozoico e Instituto Geológico y Minero de España, 43–71.

Anderson, T.F., and Arthur, M. A., 1983. Stable isotopes of oxygen and carbon and their application to sedimentologic and paleoenvironmental problems. SEPM Short Course, 151 p.

Anderson, T.F., Popp, B.N., Williams, A.C., Ho, L.-Z. and Hudson, J.D., 1994. The stable isotopic records of fossils from the Peterborough Member, Oxford Clay Fm. (Jurassic), UK: palaeoenvironmental implications. Journal of the Geological Society of London 151, 125–138.

Arenas, C. and Pomar, L., 2010. Microbial deposits in upper Miocene carbonates, Mallorca, Spain. Palaeogeography, Palaeoclimatology, Palaeoecology, 297(2): 465-485.

Arthur, M.A., Schlanger, S.O. and Jenkyns, H.C., 1987. The Cenomanian-Turonian Oceanic Anoxic Event, II. Palaeoceanographic controls on organic-matter production and preservation. Geological Society, London, Special Publications, 26(1): 401-420.

Astall, C.M., Taylor, A.C. and Atkinson, R.J.A., 1997. Behavioural and physiological implications of a burrow-dwelling lifestyle for two species of upogebiid mud-shrimp (Crustacea: Thalassinidea). Estuarine Coastal and Shelf Science, 44(2): 155-168.

Astraldi, M., Conversano, F., Civitarese, G., Gasparini, G.P., Ribera d'Alcalà, M. and Vetrano, A., 2002. Water mass properties and chemical signatures in the central Mediterranean region. Journal of Marine Systems, 33-34: 155-177.

Auster, P., Moore, J., Heinonen, K., Watling, L., Freiwald, A., Roberts, J.M., 2005. A habitat classification scheme for seamount landscapes: assessing the functional role of deep-water corals as fish habitat. In: Freiwald, A. and Roberts, J.M. (Editors), Cold-Water Corals and Ecosystems. Erlangen Earth Conference Series. Springer Berlin Heidelberg, pp. 761-769.

Austin, W.E.N., Cage, A.G. and Scourse, J.D., 2006. Mid-latitude shelf seas: A NW European perspective on the seasonal dynamics of temperature, salinity and oxygen isotopes. The Holocene 16 (7): 937–947.

Azéma, J., Foucault, A., Fourcade, E., García- Hernández, M., González- Donoso, J.M., Linares, A., Linares, D., López- Garrido, A.C., Rivas, P. and Vera, J.A., 1979. Las microfacies del Jurásico y Cretácico de las Zonas Externas de las Cordilleras Béticas. . Secretariado Publicaciones. Universidad de Granada, Granada, 83 pp.

Azmy, K., Kaufman, A.J., Misi, A. and de Oliveira, T.F., 2006. Isotope stratigraphy of the Lapa Formation, Sao Francisco Basin, Brazil: Implications for Late Neoproterozoic glacial events in South America. Precambrian Research, 149(3-4): 231-248.

Baccelle, L., Bosellini. A., 1965. Diagrammi per la stima visiva della composizione percentuale nelle rocce sedimentarie. Annali della Universiti di Ferrara, Sezione IX, Science Geologiche e Paleontologiche 1, 59-62.

Banner, J.L. and Hanson, G.N., 1990. Calculation of simultaneous isotopic and trace-element variations during water-rock interaction with applications to carbonate diagenesis. Geochimica Et Cosmochimica Acta, 54(11): 3123-3137.

Barbin, V. and Schvoerer, M., 1997. Cathodoluminescence and geosciences. Comptes Rendus de l'Académie des Sciences, Sciences de la Terre et des Planètes, 325(3): 157-169.

Bartolini, A., Baumgartner, P.O. and Guex, J., 1999. Middle and Late Jurassic radiolarian palaeoecology versus carbon-isotope stratigraphy. Palaeogeography Palaeoclimatology Palaeoecology, 145(1-3): 43-60.

Bartolini, A., Baumgartner, P.O. and Hunziker, J., 1996. Middle and Late Jurassic carbon stable-isotope stratigraphy and radiolarite sedimentation of the Umbria-Marche basin (central Italy). Eclogae Geologicae Helvetiae, 89(2): 811–844.

Bartolini, A., Pittet, B., Mattioli, E. and Hunziker, J.C., 2003. Shallow-platform palaeoenvironmental conditions recorded in deep-shelf sediments: C and stable isotopes in Upper Jurassic sections of southern Germany (Oxfordian-Kimmeridgian). Sedimentary Geology, 160(1-3): 107-130.

Basaham, A.S., 2009. Geochemistry of Jizan shelf sediments, southern Red Sea coast of Saudi Arabia. Arabian Journal of Geosciences, 2(4): 301-310.

Bathurst, R.G.C., 1971. Carbonate sediments and their diagenesis. Developments in sedimentology., 12. Elsevier, New-York, 620 pp.

Bathurst, R.G.C., 1971. Carbonate Sediments and Their Diagenesis. Developments in Sedimentology 12. (First Edition) Elsevier, Amsterdam, 658 pp..

Beckman, A. and Mohn, C., 2002. The upper ocean circulation at Great Meteor seamount. Part II: Retention potential of the seamount-induced circulation. Ocean Dynamics 52: 194-204.

Bender, M.L., Ku, T.L. and Broecker, W.S., 1970. Accumulation rates of manganese in pelagic sediments and nodules. Earth and Planetary Science Letters, 8(2): 143-148.

Berger, W. and Vincent, E., 1986. Deep-sea carbonates: Reading the carbon-isotope signal. Geologische Rundschau, 75(1): 249-269.

Berkyová, S. and Munnecke, A., 2010. "Calcispheres" as a source of lime mud and peloids- evidence from the early Middle Devonian of the Prague Basin, the Czech Republic. Bulletin of Geosciences, 85(4): 585-602.

Berner, R.A., 1969. Migration of iron and sulfur within anaerobic sediments during early diagenesis. American Journal of Science, 267(1): 19-42.

Berner, R.A., 2005. GEOCARBSULF: A combined model for Phanerozoic atmospheric O_2 and CO_2. Geochimica et Cosmochimica Acta, 70: 5653-5664.

Bhattacharya, J.P., Practical problems in the application of the sequence stratigraphic method and key surfaces: integrating observations from ancient fluvial–deltaic wedges with Quaternary and modelling studies. Sedimentology, 58(1): 120-169.

Bickert, T., Schulz, H.D. and Zabel, M., 2006. Influence of Geochemical Processes on Stable Isotope Distribution in Marine Sediments. Marine Geochemistry. In: Schulz, H.D. and Zabel, M. (Editors), Marine Geochemistry. Springer Berlin Heidelberg, pp. 339-369.

Birgel, D., Feng, D., Roberts, H.H. and Peckmann, J., 2011. Changing redox conditions at cold seeps as revealed by authigenic carbonates from Alaminos Canyon, northern Gulf of Mexico. Chemical Geology 285, 82−96.

Blackey, N., 2010. Reconstructing the ancient Earth- Late Jurassic Paleogeography, in: http://cpgeosystems.com/paleomaps.html.

Blackwelder, B.W., Macintyre, I.G. and Pilkey, O.H., 1982. Geology of continental-shelf, Onslow Bay, North-Carolina, as revealed by submarine outcrops. Aapg Bulletin-American Association of Petroleum Geologists, 66(1): 44-56.

Bodin, S., Mattioli, E., Fröhlich, S., Marshall, J.D., Boutib, L., Lahsini, S. and Redfern, J., 2010. Toarcian carbon isotope shifts and nutrient changes from the Northern margin of Gondwana (High Atlas, Morocco, Jurassic): Palaeoenvironmental implications. Palaeogeogra phy Palaeoclimatology Palaeoecology 297: 377-390.

Boehlert, G.W., 1988. Current-topography interactions at mid-ocean seamounts and the impact on pelagic ecosystems. Geojournal, 16(1): 45-52.

Boulila, S., de Rafélis, M., Hinnov, L.A., Gardin, S., Galbrun, B. and Collin, P.-Y., 2010. Orbitally forced climate and sea-level changes in the Paleoceanic Tethyan domain (marl-limestone alternations, Lower Kimmeridgian, SE France). Palaeogeography Palaeoclimatology Palaeoecology, 292(1-2): 57-70.

Boulvain, F., De Ridder, C., Mamet, B., Preat, A. and Gillan, D., 2001. Iron microbial communities in Belgian Frasnian carbonate mounds. Facies, 44: 47-59.

Bowen, R., 1961. Palaeotemperature analyses of Mesozoic Belemnoidea from Germany and Poland. Journal of Geology, 69: 75-83.

Brachert, T.C. and Dullo, W.C., 2000. Shallow burial diagenesis of skeletal carbonates: selective loss of aragonite shell material (Miocene to Recent, Queensland Plateau and Queensland Trough, NE Australia) - implications for shallow cool-water carbonates. Sedimentary Geology, 136(3-4): 169-187.

Brand, U. and Veizer, J., 1980. Chemical diagenesis of a multicomponent carbonate system - 1: Trace elements. Journal of Sedimentary Research, 50(4): 1219-1236.

Brand, U., 2004. Carbon, oxygen and strontium isotopes in Paleozoic carbonate components: an evaluation of original seawater-chemistry proxies. Chemical Geology, 204(1-2): 23-44.

Brand, U., Logan, A., Hiller, N. and Richardson, J., 2003. Geochemistry of modern brachiopods: applications and implications for oceanography and paleoceanography. Chemical Geology, 198(3-4): 305-334.

Brett, C.E. and Baird, G.C., 1986. Comparative taphonomy a key to paleoenvironmental interpretation based on fossil preservation. Palaios, 1(3): 207-227.

Brigaud, B., Puceat, E., Pellenard, P., Vincent, B. and Joachimski, M.M., 2008. Climatic fluctuations and seasonality during the Late Jurassic (Oxfordian-Early Kimmeridgian) inferred from $\delta^{18}O$ of Paris Basin oyster shells. Earth and Planetary Science Letters 273: 58–67.

Bromley, R.G., 1996. Trace fossils: biology, taphonomy, and applications. Second edition. Trace fossils: biology, taphonomy, and applications. Second edition: i-xvi, 1-361.

Bruckschen, P. and Richter, D., 1994. Zementstratigraphische Grundmuster in marinen Karbonatablagerungen des Phanerozoikums- ein Abbild der normalen Beckenentwicklung. Zentralblatt für Geologie und Paläontologie, 7/8(Teil 1): 959-972.

Bruckschen, P., Oesmann, S. and Veizer, J., 1999. Isotope stratigraphy of the European Carboniferous: proxy signals for ocean chemistry, climate and tectonics. Chemical Geology, 161: 127-163.

Bruhn, F., Bruckschen, P., Richter, D.K., Meijer, J., Stephan, A., Veizer, J., 1995. Diagenetic history of sedimentary carbonates - constraints from combined cathodoluminescence and trace-element analysis by micro-pixe. Nuclear Instruments & Methods in Physics Research Section B-Beam Interactions with Materials and Atoms, 104(1-4): 409-414.

Buchardt, B. and Weiner, S., 1981. Diagenesis of aragonite from upper cretaceous ammonites - a geochemical case-study. Sedimentology, 28(3): 423-438.

Cacho, I., Grimalt, J.O., Sierro, F.J., Shackleton, N. and Canals, M., 2000. Evidence for enhanced Mediterranean thermohaline circulation during rapid climatic coolings. Earth and Planetary Science Letters, 183(3-4): 417-429.

Cage, A.G., Austin, W.E.N., 2008. Seasonal dynamics of coastal water masses in a Scottish fjord and their potential influence on benthic foraminiferal shell geochemistry. In: Austin, W.E.N. and James, R.H. (Editors), Biogeochemical Controls on Palaeoceanographic Proxies. Geological Society, London, Special Publications 303, pp. 155–172.

Caracuel, J., 1996. Asociaciones de megainvertebrados, evolución ecosedimentaria e interpretaciones ecoestratigráficas en umbrales epioceánicos del Tethys occidental (Jurásico superior). Univ.Granada (unpublished). Granada.

Caracuel, J.E. and Olóriz, F., 1998. Revisión estratigráfica del Jurásico Superior de la Sierra Norte (Mallorca). Revista de la Sociedad Geológica de España 11(3-4): 345-353.

Caracuel, J.E. and Olóriz, F., 1999. Recent data on the Kimmeridgian- Tithonian boundary in the Sierra Norte of Mallorca (Spain), with notes on the genus *Hybonoticeras* Breistroffer. Geobios 32 (4): 575-591.

Caracuel, J.E. and Olóriz, F., 1999a. Revisión estratigráfica del Jurásico Superior de la Sierra Norte (Mallorca). Revista de la Sociedad Geológica de España 11: 345-353.

Caracuel, J.E., El Kadiri, K. and Olóriz, F., 1995. Radiolarian facies and discontinuities around the Dogger-Malm boundary in the "Puig d'en Paré" Formation (Sierra Norte, Mallorca). Geobios 28: 675–681.

Caracuel, J.E., Monaco, P. and Oloriz, F., 2000a. Taphonomic tools to evaluate sedimentation rates and stratigraphic completeness in Rosso Ammonitico facies (epioceanic Tethyan Jurassic). Rivista Italiana Di Paleontologia E Stratigrafia, 106(3): 353-367.

Caracuel, J.E., Olóriz, F. and Rodríguez-Tovar, F.J., 2000b. Oxfordian biostratigraphy from the Lugar Section (External Subbetic, Southern Spain). GeoResearch Forum 6, 55–64.

Caracuel, J.E., Oloriz, F. and Sarti, C., 1998. Updated biostratigraphy of the Kimmeridgian and Lower Tithonian at Lavarone (Trento Plateau, Italy). Correlation for epioceanic Western Tethys. Geologica et Palaeontologica, 32: 235-251.

Cardin, V., Bensi, M. and Pacciaroni, M., 2001. Variability of water mass properties in the last two decades in the South Adriatic Sea with emphasis on the period 2006-2009. Continental Shelf Research, 31(9): 951-965.

Cariou, E., Enay, R., Atrops, F., Hantzpergue, P., Marchand, D. and Rioult, M., 1997. Oxfordien. In: Cariou, E. and Hantzpergue, P. (Coordinators). Biostratigraphy du Jurassique ouest-européen et méditerranéen: Zonations parallèles et distribution des invertébrés et microfossiles: Bulletin Centre Recherches Elf Exploration Production, Mémoire 17 : 79-86.

Carpenter, S.J. and Lohmann, K.C., 1989. $\delta^{18}O$ and $\delta^{13}C$ variations in Late Devonian marine cements from the Golden Spike and Nevis reefs, Alberta, Canada. Journal of Sedimentary Petrology, 59(5): 792-814.

Carpenter, S.J. and Lohmann, K.C., 1995. $\delta^{13}C$ and $\delta^{18}O$ values of modern brachiopod shells. Geochimica et Cosmochimica Acta, 59: 3749-3764.

Carpenter, S.J. and Lohmann, K.C., 1997. Carbon isotope ratios of Phanerozoic marine cements: Re-evaluating the global carbon and sulfur systems. Geochimica et Cosmochimica Acta, 61(22): 4831-4846.

Carpenter, S.J., Lohmann, K.C., Holden, P., Walter, L.M., Huston, T.J., Halliday, A.N., 1991. $\delta^{18}O$ values, $^{87}Sr/^{86}Sr$ and Sr/Mg ratios of Late Devonian abiotic marine calcite: Implications for the composition of ancient seawater. Geochimica et Cosmochimica Acta, 55: 1991-2010.

Cecca, F., Fourcade, E. and Azema, J., 1992. The disappearance of the ammonitico rosso. Palaeogeography Palaeoclimatology Palaeoecology, 99(1-2): 55-70.

Cecca, F., Garin, B.M., Marchand, D., Lathuiliere, B. and Bartolini, A., 2005. Paleoclimatic control of biogeographic and sedimentary events in Tethyan and peri-Tethyan areas during the Oxfordian (Late Jurassic). Palaeogeography Palaeoclimatology Palaeoecology, 222(1-2): 10-32.

Cecca, F., Savary, B., Bartolini, A., Remane, J. and Cordey, F., 2001. The Middle Jurassic-Lower Cretaceous Rosso Ammonitico succession of Monte Inici (Trapanese domain, western Sicily): sedimentology, biostratigraphy and isotope stratigraphy. Bulletin De La Societe Geologique De France, 172(5): 647-659.

Chamberlain, J.A., Ward, P.D. and Weaver, J.S., 1981. Post-mortem ascent of Nautilus shells - Implications for Cephalopod paleobiogeography. Paleobiology, 7(4): 494-509.

Chave, K.E., 1962. Factors influencing the mineralogy of carbonate sediments. Limnology and Oceanography, 7(2): 218-223.

Checa, A., Molina, J.M. and Olóriz, F., 1983. Intercalaciones calcareniticas en la facies "Ammonitico Rosso" del Jurasico superior de la Sierra del Ahillo (Subbético Externo, Cordilleras Béticas). Comunicaciones del X Congreso Nacional de Sedimentología, Menorca: 3.17-3.20.

Chen, K.P., Jiao, J.J., Huang, J.M. and Huang, R.Q., 2007. Multivariate statistical evaluation of trace elements in groundwater in a coastal area in Shenzhen, China. Environmental Pollution, 147(3): 771-780.

Chester, R., 2000. Marine geochemistry (2nd edition). Blackwell Science, United Kingdom, 506 pp.

Cicero, A.D. and Lohman, K.C., 2001. Sr/Mg variation during rock-water interaction: Implications for secular changes in the elemental chemistry of ancient seawater. Geochimica et Cosmochimica Acta, 65(5): 741-761.

Clari, P.A. and Martire, L., 1996. Interplay of cementation, mechanical compaction and chemical compaction in nodular limestones of the Rosso Ammonitico Veronese (middle - upper Jurassic, northeastern Italy). Journal of Sedimentary Research, 66(3): 447 - 458.

Clari, P.A., Marini, P., Pastorini, M. and Pavia, G., 1984. Il Rosso Ammonitico Inferiore (Baiociano-Calloviano) nei monti lessini settentrionali (Verona). Rivista Italiana Di Paleontologia E Stratigrafia, 90(1): 15-86.

Cobiella-Reguera, J.L And Olóriz, F., 2009. Oxfordian – Berriasian stratigraphy of the North American paleomargin in western Cuba: Constraints for the geological history of the proto-Caribbean and the early Gulf of Mexico, *in* Bartolini, C. and Román Ramos, J.C., eds., Petroleum systems in the southern Gulf of Mexico, American Association of Petroleum Geologists Memoir 90: 421-451.

Coggon, R.M., Teagle, D.A.H., Smith-Duque, C.E., Alt, J.C. and Cooper, M.J., 2010. Reconstructing Past Seawater Mg/Ca and Sr/Ca from Mid-Ocean Ridge Flank Calcium Carbonate Veins. Science 327: 1114−1117.

Coimbra, R., Immenhauser, A. and Oloriz, F., 2009. Matrix micrite $\delta^{13}C$ and $\delta^{18}O$ reveals synsedimentary marine lithification in Upper Jurassic Ammonitico Rosso limestones (Betic Cordillera, SE Spain). Sedimentary Geology 218: 332-348.

Colacichi, R., Bartolini, A. and Baumgartner, P.O., 2000. Silicious sedimentation in the Mediterranean Jurassic caused by volcanism, greenhouse climate and eutrophication. Georesearch Forum, 6: 417-426.

Comas, M.C. and Olóriz, F., 1986. Génesis de las capas de coquinas de la secuencia pelágica del Cenicero (Tithónico inferior, Zona Subbética). Grupo Español de Sedimentología. XI Congreso Español de Sedimentología, Barcelona, Facultad de geología, Universitat de Barcelona. Institut Jaume Almera, CSIC. Resúmenes de comunicaciones, p. 186.

Comas, M.C., 1978. Sobre la Geología de los Montes Orientales: Sedimentación y evolución paleogeográfica desde el Jurásico al Mioceno inferior (Zona Subbética, Andalucía), Universidad Bilbao, Bilbao, 1-323. pp.

Comas, M.C., Olóriz, F. and Tavera, J.M., 1981. The red nodular limestones (Ammonitico Rosso) and associated facies: a key for settling slopes or swell areas in the subbetic upper Jurassic submarine topography (southern Spain). In: Farinacci, A. and Elmi, S. (Editors), Rosso Ammonitico Symposium Proceedings. Roma, pp. 144-136.

Combé-Morel, R. and Mariotti, N., 1986. Les bélemnites de la Carrière de Serra San Quirico (province d'Ancona, Apennin Central, Italie) et la paléobiogéographie des bélemnites de la Téthys Méditerranéene au Tithonique inférieur. Geobíos, 19(3): 299-321.

Corbin, J.C., Person, A., Iatzoura, A., Ferre, B. and Renard, M., 2000. Manganese in pelagic carbonates: indication of major Tectonic events during the geodynamic evolution of a passive continental margin (the Jurassic European margin of the Tethys-Ligurian Sea). Palaeogeography Palaeoclimatology Palaeoecology, 156(1-2): 123-138.

Craig, H. and Gordon, A. 1965. Deuterium and oxygen-18 variations in the ocean and the marine atmosphere, *in* Stable Isotopes in Oceanic Studies and Palaeotemperatures, Tongiorgi, E. ed., Pisa, Italy: Consiglio Nazionale delle Richerche, p. 9–130.

Cramer, B.D. and Saltzman, M.R., 2007. Fluctuations in epeiric sea carbonate production during Silurian positive carbon isotope excursions: A review of proposed paleoceanographic models. Palaeogeography Palaeoclimatololy Palaeoecology 245: 37–45.

D'Argenio, B., 1974-76. Le piattaforme carbonatiche periadriatiche una rasegna di problema nel quadro geodinamico mesozoico dell'area mediterranea. Memoria della Societá Geologica Italiana 13 (2): 137-159.

da Silva, A.C. and Boulvain, F., 2008. Carbon isotope lateral variability in a Middle Frasnian carbonate platform (Belgium): Significance of facies, diagenesis and sea-level history. Palaeogeography Palaeoclimatology Palaeoecology, 269(3-4): 189-204.

Danielsson, A., Cato, I., Carman, R. and Rahm, L., 1999. Spatial clustering of metals in the sediments of the Skagerrak Kattegat. Applied Geochemistry, 14(6): 689-706.

Dauphin, Y., 1979. Contribution a l'etude de la formation des gisements de cephalopodes. 1. Les coquilles de spirules (Dibranchiata) de Nouvelle Caledonie. Cahiers de l'Indo-Pacifique, 1(2): 165-194.

Davies, D.J., Powell, E.N. and Stanton, R.J., 1989. Relative rates of shell dissolution and net sediment accumulation - a commentary - Can shell beds form by the gradual accumulation of biogenic debris on the sea-floor?. Lethaia, 22(2): 207-212.

de Boer, P.L., 1986. Changes in the organic carbon burial during the Early Cretaceous. In: Summerhayes, C.P. and Shackleton, N.J. (Editors), North Atlantic Palaeoceanography. Geological Society Special Publication, pp. 321-331.

de Leeuw, J.W., Frewin, N.L., Van Bergen, P.F., Sinninghe Damste, J.S. and Collinson, M.E., 1995. Organic carbon as a palaeoenvironmental indicator in the marine realm. Geological Society of London Special Publication, 83: 43-71.

de Rafélis, M., Emmanuel, L., Renard, M., Atrops, F. and Du Chene, R.J., 2001. Geochemical characterization (Mn content) of third order eustatic sequences in Upper Jurassic pelagic carbonates of the Vocontian Trough (SE France). Eclogae Geologicae Helvetiae, 94(2): 145-152.

de Schootbrugge, B., Fölmmi, K.B., Bulot, L.G. and Burns, S.J., 2000. Palaeoceanographic changes during the Early Cretaceous (Valanginian-Hauterivian): Evidence from oxygen and carbon stable isotopes. Earth and Planetary Science Letters 181: 5-31.

Dera, G., Brigaud, B., Monna, F., Laffont, R., Pucéat, E., Deconinck, J.-F., Pellenard, P., Joachimski, M.M., Durlet, C., 2011. Climatic ups and downs in a disturbed Jurassic world. Geology, 39: 215-218.

Dera, G., Pucéat, E., Pellenard, P., Neige, P., Delsate, D., Joachimski, M.M., Reisberg, L., Martinez, M., 2009. Water mass exchange and variations in seawater temperature in the NW Tethys during the Early Jurassic: Evidence from neodymium and oxygen isotopes of fish teeth and belemnites. Earth and Planetary Science Letters, 286(1-2): 198-207.

Desrochers, A., Bourque, P.-A. and Neuweiler, F., 2007. Diagenetic Versus Biotic Accretionary Mechanisms of Bryozoan-Sponge Buildups (Lower Silurian, Anticosti Island, Canada). Journal of Sedimentary Research, 77(7): 564-571.

Dias, Á.S. and Barriga, F.J.A.S., 2006. Recurrent neomorphic and cement microtextures from different diagenetic environments, Quaternary to Late Neogene carbonates, Great Bahama Bank. Marine Geology 255: 157–175.

Dias, ÁS., Früh-Green, G.L., Bernasconi, S.M. and Barriga, F.J.A.S., 2011. Geochemistry and stable isotope constraints on high-temperature activity from sediment cores of the Saldanha hydrothermal field. Marine Geology, 279(1-4): 128-140.

Dickson, J.A.D. and Coleman, M.L., 1980. Changes in carbon and oxygen isotope composition during limestone diagenesis. Sedimentology, 27(1): 107-118.

Ditchfield, P.W., 1997. High northern palaeolatitude Jurassic-Cretaceous palaeotemperature variation: New data from Kong Karls Land, Svalbard. Palaeogeography Palaeoclimatology Palaeoecology, 130(1-4): 163-175.

Ditchfield, P.W., Marshall, J.D. and Pirrie, D., 1994. High-latitude paleotemperature variation - New data from the Tithonian to Eocene of James-Ross-Island, Antarctica. Palaeogeography Palaeoclimatology Palaeoecology, 107(1-2): 79-101.

Dogan, A., Ozsan, A., Dogan, M., Karpuz, C. and Brenner, R., 2006. Classifications of hardgrounds based upon their strength properties. Carbonates and Evaporites, 21(1): 14-20.

Dopieralska, J., Belka, Z. and Haack, U., 2006. Geochemical decoupling of water masses in the Variscan oceanic system during Late Devonian times. Palaeogeography, Palaeoclimatology, Palaeoecology, 240(1-2): 108-119.

Doyle, P., 1992. A review of the biogeography of cretaceous belemnites. Palaeogeography Palaeoclimatology Palaeoecology, 92(3-4): 207-216.

Dromart, G., Garcia, J.P., Picard, S., Atrops, F., Lécuyer, C., Sheppard, S.M.F., 2003. Ice age at the Middle-Late Jurassic transition? Earth and Planetary Science Letters, 213(3-4): 205-220.

Dutton, A., Huber, B.T., Lohmann, K.C. and Zinsmeister, W.J., 2007. High-resolution stable isotope profiles of a dimitobelid belemnite: Implications for paleodepth habitat and late maastrichtian climate seasonality. Palaios, 22: 642-650.

Eggins, S., De Deckker, P., Marshall, J., 2003. Mg/Ca variation in planktonic foraminifera tests: implications for reconstructing palaeo-seawater temperature and habitat migration. Earth and Planetary Science. Letters 212: 291-306.

Ekdale, A.A. and Bromley, R.G., 2003. Paleoethologic interpretation of complex Thalassionoides in shallow-marine limestones, Lower Ordovician, southern Sweden. Palaeogeography, Palaeoclimatology, Palaeoecology, 192: 221-227.

El Kadari, K., 2002. Jurassic ferruginous hardgrounds of the "Dorsale Calcaire" and the Jbel Moussa Group (Internal Rif, Morocco); stratigraphical context and paleoceanographic consequences of mineralization processes: Geologica Romana 36: 33-69.

Elderfield, H., 2011. Seawater Chemistry and Climate. Science, 327 (5969): 1092-1093.

Emeis, K-Ch. and Weissert, H., 2009. Tethyan–Mediterranean organic carbon-rich sediments from Mesozoic black shales to sapropels. Sedimentology 56: 247-266.

Eriksen, C.C., 1998. Internal wave reflection and mixing at Fieberling Guyot. Journal of Geophysical Research-Oceans, 103(C2): 2977-2994.

Everitt B.S., Landau S. and Leese M., 2001. Cluster analysis (4th edition). Arnold, London.

Fairchild, I.J., 1983. Chemical controls of cathodoluminescence of natural dolomites and calcites - New data and review. Sedimentology, 30(4): 579-583.

Fallot, P., 1948. Les Cordillères bétiques. Estudios Geológicos, 8: 83-172.

Fanning, K.A. and Schink, D.R., 1969. Interaction of marine sediments with dissolved silica. Limnology and Oceanography, 14(1): 59-68.

Fanton, K.C., Holmden, C., Nowlan, G.S. and Haidl, F.M., 2002. $^{143}Nd/^{144}Nd$ and Sm/Nd stratigraphy of Upper Ordovician epeiric sea carbonates. Geochimica Et Cosmochimica Acta, 66: 241-255.

Farinacci, A. and Elmi, S., (eds.) 1981. Rosso Ammonitico Symposium. Tecnoscienza, Roma, 602pp.

Ferreri, V., Weissert, H., Dargenio, B. and Buonocunto, F.P., 1997. Carbon isotope stratigraphy: A tool for basin to carbonate platform correlation. Terra Nova, 9(2): 57-61.

Flügel, E., 2009. Microfacies of Carbonate Rocks: Analysis, Interpretation and Application, Berlin, Springer-Verlag, 976p.

Folk, R.L., 1951. A comparison chart for visual percentage estimation. Journal of Sedimentary Petrology 21 (1): 22-23.

Fontboté, J.M., Guimerà J., Roca E., Sàbat F., Santanach, P., Fernandez-Ortigosa F., 1990. The Cenozoic Geodynamic Evolution of the Valencia Trough (Western Mediterranean). Revista de la Sociedad Geológica de España, 3(3-4): 249-259.

Fornós, J.J., Rodríguez-Perea, A. and Sabat, F. 1988. Shelf facies of the Middle-Upper Jurassic. Artá Caves ("Serres de Llevant", Mallorca, Spain). Congreso Geológico de España 1: 75-79.

Frank, T.D. and Lohmann, K.C., 1996. Diagenesis of fibrous magnesian calcite marine cement: Implications for the interpretation of $\delta^{18}O$ and $\delta^{13}C$ values of ancient equivalents. Geochimica et Cosmochimica Acta, 60(13): 2427-2436.

Friedman, G., 1964. Early diagenesis and lithification in carbonate sediments. Journal of Sedimentary Research 34 (4): 777-813.

Froelich, P.N., Klinkhammer, G.P., Bender, M.L., Luedtke, N.A., Heath, G.R., Cullen, D., Dauphin, P., Hammond, D., Hartman, B., Maynard, V., 1979. Early oxidation of organic-matter in pelagic sediments of the eastern equatorial Atlantic - Suboxic diagenesis. Geochimica et Cosmochimica Acta, 43(7): 1075-1090.

Fürsich, F.T., Kennedy, W.J. and Palmer, T.J., 1981. Trace fossils at a regional discontinuity surface - The Austin-Taylor (Upper Cretaceous) contact in central Texas. Journal of Paleontology, 55(3): 537-551.

Fursich, F.T., Oschmann, W., Singh, I.B. and Jaitly, A.K., 1992. Hardgrounds, reworked concretion levels and condensed horizons in the jurassic of Western India- Their significance for basin analysis. Journal of the Geological Society, 149: 313-331.

Gagan, M.K., Ayliffe, L.K., Beck, J.W., Cole, J.E., Druffel, E.R.M., Dunbar, R.B., Schrag, D.P., 2000. New views of tropical paleoclimates from corals. Quaternary Science Reviews, 19: 45-64.

Garcia- Hernández, M., López- Garrido, A.C., Rivas, P., Sanz de Galdeano, C. and Vera, J.A., 1980. Mesozoic palaeogeographic evolution of the External Zones of the Betic Cordillera. Geological Mijnbouw 59: 155-168.

Gelabert, B., Sabat, F. and Rodriguez-Perea, A., 1992. A structural outline of the Serra de Tramuntana of Mallorca (Balearic Islands). Tectonophysics, 203(1-4): 167-183.

Geyssant, J., 1997. Tithonien, *in* Cariou, E., Hantzpergue, P., (coord.), Biostratigraphy du Jurassique ouest-européen et méditerranéen: Zonations parallèles et distribution des invertébrés et microfossiles. Bulletin Centre Recherches Elf Exploration Production, Mémoire 17: 97-102.

Gill, G.A., Santantonio, M. and Lathuiliere, B., 2004. The depth of pelagic deposits in the Tethyan Jurassic and the use of corals: an example from the Apennines. Sedimentary Geology, 166(3-4): 311-334.

Given, R.K. and Lohmann, K.C., 1985. Derivation of the original isotopic composition of Permian marine cements. Journal of Sedimentary Research, 55(3): 430-439.

Götte, T. and Richter, D.K., 2009. Quantitative aspects of Mn-activated cathodoluminescence of natural and synthetic aragonite. Sedimentology, 56(2): 483-492.

Gradstein, F.M., Ogg, J.G. and Smith, A.G. 2004. A Geologic Time Scale. Cambridge University Press, Cambridge, 589 pp.

Griffis, R.B. and Suchanek, T.H., 1991. A model of burrow architecture and trophic modes in Thalassinidean shrimp (Decapoda, Thalassinidea). Marine Ecology-Progress Series, 79(1-2): 171-183.

Gröcke, D.R., Price, G.D., Ruffell, A.H., Mutterlose, J. and Baraboshkin, E., 2003. Isotopic evidence for Late Jurassic-Early Cretaceous climate change. Palaeogeography, Palaeoclimatology, Palaeoecology, 202(1-2): 97-118.

Gruszczyński, M., 1998. Chemistry of Jurassic seas and its bearing on the existing organic life. Acta Geologica Polonica 48(1): 1-29.

Gutjahr, M., Hoogakker, B.A.A., Frank, M. and McCave, I.N., 2010. Changes in North Atlantic deep water strength and bottom water masses during Marine Isotope Stage 3 (45 to 35 ka BP). Quaternary Science Reviews, 29: 2451-2461.

Hallam, A., 1999. Evidence of sea-level fall in sequence stratigraphy: Examples from the Jurassic. Geology 27: 343-346.

Hallam, A., 2001. A review of the broad pattern of Jurassic sea-level changes and their possible causes in the light of current knowledge. Palaeogeography, Palaeoclimatology, Palaeoecology, 167(1-2): 23-37.

Hallam, A., Crame, J.A., Mancenido, M.O., Francis, J. and Parrish, J.T., 1993. Jurassic Climates as Inferred from the Sedimentary and Fossil Record [and Discussion]. Philosophical Transactions of the Royal Society of London. Series B: Biological Sciences, 341(1297): 287-296.

Hallock, P., 1997. Reefs and reef limestones in Earth history. In: Birkeland, C. (Editor), Life and Death of Coral Reefs. Chapman and Hall, New York, pp. 13-42.

Hamon, Y. and Merzeraud, G., 2007. C and O isotope stratigraphy in shallow-marine carbonate: a tool for sequence stratigraphy (example from the Lodève region, peritethian domain). Swiss Journal Geosciences 100: 171-84.

Handoh, I.C. and Lenton, T.M., 2003. Periodic mid-Cretaceous oceanic anoxic events linked by oscillations of the phosphorus and oxygen biogeochemical cycles. Global Biogeochemical Cycles 17, 4, 1092, 3-1 – 3-11. Jones, C. E., and H. C. Jenkyns,(2001). Seawater strontium isotopes, oceanic anoxic events, and seafloor hydrothermal activity in the Jurassic and Cretaceous. American Journal of Science 301 : 112-149.

Hantzpergue, P., Atrops, F., and Enay, R., 1997. Kimméridgien. In E. Cariou , P. Hantzpergue (coords.): Biostratigraphie du Jurasique Ouest-Européen et Méditerranéen: Zonations parallèles et distribution des invertébrés et microfossiles. Groupe Français Etude Jurassique. Bulletin du centre de recherches Elf Exploration-Production, Mémoir 17: 87-96.

Haq, B.U., Hardenbol, J. and Vail, P.R., 1988. Mesozoic and Cenozoic chronostratigraphy and cycles of sea-level change. In: Wilgus Cheryl, K., Hastings Bruce, S., Ross Charles, A., Posamentier Henry, W., Van Wagoner, J., Kendall Christopher, G.S.C. (Edsitors), Sea-level changes; an integrated approach. SEPM (Society for Sedimentary Geology), Tulsa, OK, United States, pp. 72–108.

Hardenbol, J., Thierry, J., Farley, M.B., Jacquin, T., DeGraciansky, P.-C. and Vail, P.R., 1998. Mesozoic-Cenozoic sequence chronostratigraphic framework. In: deGraciansky, P.-C., Hardenbol, J., Jacquin, T., Vail, P.R. and Farley, M.B. (Editors), Sequence stratigraphy of European Basins. SEPM Special Publication, Society for Sedimentary Geology, pp. 3-13.

Hardie, L.A., 1996. Secular variation in seawater chemistry: an explanation for the coupled secular variation in the mineralogies of marine limestones and potash evaporites over the past 600 m.y. Geology 24: 279-283.

Hendry, J.P., Ditchfield, P.W. and Marshall, J.D., 1995. Two-stage neomorphism of Jurassic aragonitic bivalves; implications for early diagenesis. Journal of Sedimentary Research 65: 214-224.

Hernández-Molina, F.J., Larter, R.D., Rebesco, M. and Maldonado, A., 2006. Miocene reversal of bottom water flow along the Pacific Margin of the Antarctic Peninsula: Stratigraphic evidence from a contourite sedimentary tail. Marine Geology 228: 93-116.

Hernawati, Y., McNeill, D., Klaus, J., Eberli, G.P.and Swart, P.K., 2010. Isotope Signature as a Tool for Meteoric Diagenesis. In: Comparative Sedimentology Laboratory, Rosenstiel School of Marine and Atmospheric Science, Univ. Miami. Ann. Rev Meeting, 2010, pp. 73–74.

Hesselbo, S.P., Grocke, D.R., Jenkyns, H.C., Bjerrum, C.J., Farrimond, P., Morgans Bell, H.S., Green, O.R., 2000. Massive dissociation of gas hydrate during a Jurassic oceanic anoxic event. Nature, 406 (6794): 392-395.

Hoefs, J., 1997. Stable Isotope Geochemistry. Springer, Berlin-Heidelberg, 201 pp.

Hoffman, A., Gruszczynski, M., Malkowski, K., Halas, S., Matyja, B.A., Wierzbowski, A., 1991. Carbon and oxygen isotope curves for the Oxfordian of central Poland. Acta Geologica Polonica, 41(3-4): 157-164.

Hollmann, R., 1962. Uber Subsolution und die "Knollen Kalke" des Calcare Ammonitico Rosso Superiore im Monte Baldo (Malm, Norditalien). Neues Jahrbuch für Geologie und Paläontologie Monatshefte, 1962: 163-179.

Hollmann, R., 1964. Subsolutions-Fragmente. (Zur Biostratinomie der Ammonoidea im Malm des Monte Baldo/Norditalien). Neues Jahrbuch für Geologie und Paläontologie Abhandlungen, 119: 22-82.

Holmden, C., Creaser, R.A., Muehlenbachs, K., Leslie, S.A. and Bergstrom, S.M., 1998. Isotopic evidence for geochemical decoupling between ancient epeiric seas and bordering oceans: Implications for secular curves. Geology, 26(6): 567-570.

Hongo, Y., Obata, H., Sotto Alibo, D. and Nozaki, Y., 2006. Spatial variations of rare earth elements in north pacific surface water. Journal of Oceanography 62: 441-455.

Huber, B.T., Hodell, D.A., Hamilton, C.P., 2005. Middle-late Cretaceous climate of the southern high latitudes: Stable isotope evidence for minimal equator-to-pole thermal gradients. Geological Society of America Bulletin 107: 1164-1191.

Huck, S., Rameil, N., Korbar, T., Heimhofer, U., Wieczorek, T.D. and Immenhauser, A., 2010. Latitudinally different responses of Tethyan shoalwater carbonate systems to Early Aptian oceanic anoxic event (OAE1a). Sedimentology 57: 1585-1614.

Hudson, J.D., 1975. Carbon isotopes and limestone cement. Geology, 3(1): 19-22.

Hudson, J.D., 1977. Stable isotopes and limestone lithification. Journal of the Geological Society of London 133 (6): 637- 660.

Immenhauser, A., 2005. High-rate sea-level change during the Mesozoic: New approaches to an old problem. Sedimentary Geology, 175: 277-296.

Immenhauser, A., 2009. Estimating palaeo-water depth from the physical rock record. Earth-Science Reviews, 96(1-2): 107-139.

Immenhauser, A., Della Porta, G., Kenter, J.A.M. and Bahamonde, J.R., 2003. An alternative model for positive shifts in shallow marine carbonate $\delta^{13}C$ and $\delta^{18}O$. Sedimentology (Letter section), 50(5): 953-959.

Immenhauser, A., Holmden, C. and Patterson, W.P., 2008. Interpreting the Carbon-Isotope Record of Ancient Shallow Epeiric Seas: Lessons from the Recent. In: Pratt, B.R. and Holmden, C. (Editors), Dynamics of Epeiric Seas. Geological Association of Canada Special Publication, pp. 135-174.

Immenhauser, A., Kenter, J.A.M., Ganssen, G., Bahamonde, J.R., van Vliet, A., Saher, M.H., 2002. Origin and significance of isotope shifts in Pennsylvanian carbonates (Asturias, NW Spain). Journal of Sedimentary Research, 72(1): 82-94.

James, N.P., Bone, Y. and Kyser, T.K., 2005. Where has all the aragonite gone? - Mineralogy of holocene neritic cool-water carbonates, southern Australia. Journal of Sedimentary Research, 75(3): 454-463.

James, R.H. and Austin, W.E.N., 2008. Biogeochemical controls on palaeoceanographic environmental proxies: a review. Geological Society, London, Special Publications, 303(1): 3-32.

James, V., Canerot, J., Meyer, A. and Biteau, J.J., 2000. Growth and destruction of Bathonian silica nodules in the Western Pyrenees (France). Sedimentary Geology, 132(1-2): 5-23.

Jenkyns, H.C. and Wilson, O.A., 1999. Stratigraphy, paleoceanography, and evolution of Cretaceous Pacific Guyots: Relicts from a Greenhouse world. American Journal of Science, 299: 341-392.

Jenkyns, H.C., 1971. Genesis of condensed sequences in Tethyan Jurassic. Lethaia, 4(3): 327-352.

Jenkyns, H.C., 1974. Origin of red nodular limestones (Ammonitico Rosso, Knollenkalke) in the Mediterranean Jurassic: A diagenetic model. In: Hsü, K.J. and Jenkyns, H.C. (Editors), Pelagic sediments: on Land and under the Sea. International Association of Sedimentologists, Special Publication, pp. 249-271.

Jenkyns, H.C., 1980. Cretaceous anoxic events: from continents to oceans. Journal of the Geological Society, London, 137: 171-188.

Jenkyns, H.C., 1988. The early Toarcian (Jurassic) anoxic event; stratigraphic, sedimentary and geochemical evidence. American Journal of Science, 288(2): 101-151.

Jenkyns, H.C., 1995. Carbon-isotope stratigraphy and paleoceanographic significance of the lower Cretaceous shallow-water carbonates of Resolution Guyot, Mid-Pacific mountains. Proceedings. Ocean Drilling Program. Scientific Results, 143: 99-104.

Jenkyns, H.C., 1996. Relative sea-level change and carbon isotopes: Data from the Upper Jurassic (Oxfordian) of central and Southern Europe. Terra Nova, 8(1): 75-85.

Jenkyns, H.C., 2010. Geochemistry of oceanic anoxic events. Geochemistry Geophysics and. Geosystems 11: 3004-3034.

Jenkyns, H.C., Jones, C.E., Grocke, D.R., Hesselbo, S.P. and Parkinson, D.N., 2002. Chemostratigraphy of the Jurassic System: applications, limitations and implications for palaeoceanography. Journal of the Geological Society, 159: 351-378.

Jiang, G., Kaufman, A.J., Christie-Blick, N., Zhang, S. and Wu, H., 2007. Carbon isotope variability across the Ediacaran Yangtze platform in South China: Implications for a large surface-to-deep ocean $\delta^{13}C$ gradient. Earth and Planetary Science Letters, 261: 303-320.

Jiménez de Cisneros, C., Mas, J.R. and Vera, J.A., 1991. Geochemistry of speleothems from Jurassic palaeokarst (Subbetic, southern Spain). Sedimentary Geology, 73(3-4): 191-208.

Jiménez de Cisneros, C., Molina, J.M., Nieto, L.M., Ruiz-Ortiz, P.A. and Vera, J.A., 1993. Calcretes from a palaeosinkhole in jurassic palaeokarst (subbetic, southern Spain). Sedimentary Geology, 87(1-2): 13-24.

Jiménez, A.P., Jiménez De Cisneros, C., Rivas, P. and Vera, J.A., 1996. The early toarcian anoxic event in the westernmost Tethys (Subbetic): Paleogeographic and paleobiogeographic significance. Journal of Geology, 104(4): 399-416.

Jiménez-Espinosa, R., Jiménez-Millan, J. and Nieto, L., 1997. Factors controlling the genesis of Fe-Mn crusts in stratigraphic breaks of the eastern Betic Cordillera (SE Spain) deduced from numerical analysis of geological data. Sedimentary Geology, 114(1-4): 97-107.

Joachimski, M.M., 1994. Subaerial exposure and deposition of shallowing upward sequences: evidence from stable isotopes of Purbeckian peritidal carbonates (basal Cretaceous), Swiss and French Jura Mountains. Sedimentology, 41: 805-824.

Joachimski, M.M., Pancost, R.D., Freeman, K.H., Ostertag-Henning, C. and Buggisch, W., 2002. Carbon isotope geochemistry of the Frasnian-Famennian transition. Palaeogeography, Palaeoclimatolog, Palaeoecology, 181: 91-109

Jolliffe, I. T., 2002. Principal Component Analysis (2nd Edition). Springer, New York.

Jones, C.E. and Jenkyns, H.C., 2001. Seawater Strontium Isotopes, Oceanic Anoxic Events, and Seafloor Hydrothermal Activity in the Jurassic and Cretaceous. American Journal of Science, 301(2): 112-149.

Katz, M.E., Wright, J.D., Miller, K.G., Cramer, B.S., Fennel, K., Falkowski, P.G., 2005. Biological overprint of the geological carbon cycle. Marine Geology, 217(3-4): 323-338.

Keeling, R.F., Kortzinger, A. and Gruber, N., 2010. Ocean Deoxygenation in a Warming World. Annual Review of Marine Science, 2 (1): 199-229.

Kendall and Alnaji, 2009. SEPM Sequence Stratigraphy Web: Carbonate Diagenesis Image Gallery, in: http://sepmstrata.org/carbonatediagenesisgallery/carbdiagenesisgallery.html.

Keim, L. and Schlager, W., 1999. Automicrite facies on steep slopes (Triassic, Dolomites, Italy). Facies, 41: 15-25.

Kester, D.R., 1975. Dissolved gases other than CO_2. In: Riley, J.P. and Skirrow, G. (Editors), Chemical Oceanography. Academic Press, London, pp. 498-556.

Kester, D.R., Crocker, K.T. and Miller Jr., G.R., 1973. Small-scale oxygen variations in the thermocline. Deep Sea Research and Oceanographic Abstracts, 20(4): 409-410, IN17-IN18, 411-412.

Keupp, H., Jenisch, A., Herrmann, R., Neuweiler, F. and Reitner, J., 1993. Microbial carbonate crusts-a key to the environmental analysis of fossil spongiolites? Facies, 29(1): 41-54.

Keupp, H., Koch, R. and Leinfelder, R.R., 1990. Controlling processes in the development of the Upper Jurassic spongiolites in Southern Germany: state of the art, problems and perspectives. Facies 23: 141-174.

Kharol, S.K., Badarinath, K.V.S., Kaskaoutis, D.G., Sharma, A.R. and Gharai, B., 2011. Influence of continental advection on aerosol characteristics over Bay of Bengal (BoB) in winter: results from W-ICARB cruise experiment. Annals Geophysics 29: 1423-1438.

Kickmaier, W., Peters, T.J., 1990. Manganese occurrences in the Al Hammah Range- Wahrah Formation, Oman Mountains. In: Robertson, A.H.F., Searle, M.P. and Ries, A.C (Editors), The Geology and Tectonics of the Oman Region. Geological Society Special Publication 49, pp. 239-249.

Kievman, C.M., 1998. Match between late Pleistocene Great Baham Bank and deep-sea oxygen isotope records of sea level. Geology, 26(7): 635-638.

Kinoshita, K., Wada, M., Kogure, K. and Furota, T., 2003. Mud shrimp burrows as dynamic traps and processors of tidal-flat materials. Marine Ecology-Progress Series, 247: 159-164.

Klein, R.T., Lohmann, K.C. and Thayer, C.W., 1996. Bivalve skeletons record sea-surface temperature and $\delta^{18}O$ via Mg/Ca and $^{18}O/^{16}O$ ratios. Geology, 24(5): 415-418.

Klompmaker, A.A., Waljaard, N.A. and Fraaije, R.H.B., 2009. Ventral bite marks in Mesozoic ammonoids. Palaeogeography Palaeoclimatology Palaeoecology, 280(1-2): 245-257.

Kristensen, E., 2000. Organic matter diagenesis at the oxic/anoxic interface in coastal marine sediments, with emphasis on the role of burrowing animals. Hydrobiologia, 426(1-3): 1-24.

Kutzbach, J.E. and Gallimore, R.G., 1989. Pangaean Climates: Megamonsoons of the Megacontinent. J. Geophys. Res., 94(D3): 3341-3357.

Land, L.S., 1970. Phreatic versus vadose meteoric diagenesis of limestones: evidence from a fossil water table. Sedimentology 14: 175-185.

Lasemi, Y., 1995. Platform carbonates of the upper Jurassic Mozduran Formation in the Kopet Dagh Basin, Ne Iran - Facies, paleoenvironments and sequences. Sedimentary Geology, 99(3-4): 151-164.

Lécuyer, C. and Bucher, H., 2006. Stable isotope compositions of a late Jurassic ammonite shell: a record of seasonal surface water temperatures in the southern hemisphere? eEarth 1(1): 1-7.

Lees, A. and Miller, J., 1985. Facies variation in Waulsortian buildups, Part 2: Mid-Dinantian buildups from Europe and North America: Geological Journal 20: 159-180.

Lees, A. and Miller, J., 1995. Waulsortian banks. In: Monty, C.L.V., Bosence, D.W.J., Bridges, P.H. and Pratt, B.R. (Editors), Carbonate Mud-Mounds. International Association of Sedimentologists, Special Publications 23, 191-271.

Lehman, U. and Kulicki, C., 1990. Double function of aptychi (Ammonoidea) as jaws and opercula. Lethaia 23: 325-331.

Leinfelder, R.R., Krautter, M., Nose, M., Ramalho, M.M. and Werner, W., 1993. Silicious sponge facies from the Upper Jurassic of Portugal. Neues Jahrbuch für Geologie und Paläontologie Abhandlungen, 189(1-3): 199 - 254.

Lewy, Z., 2009. The possible trophic control on the construction and function of the aulacocerid and belemnoid guard and phragmocone. Revue de Paleobiologie, 28(1): 131-137.

Libes, S.M., 1992. An introduction to marine biogeochemistry. Wiley, New York, pp. 928.

Lohman, K.C., 1987. Geochemical patterns of meteoric diagenetic systems and their applicationto studies of palaeokarst. In: James, N.P. and Choquette, P.W. (Editors), Palaeokarst. Springer Verlag, Berlin, pp. 58-80.

Lohmann, K.C., 1982. "Inverted J" carbon and oxygen isotopic trends: a criterion for shallow meteoric phreatic diagenesis. Geological Society of America, Abstract Programs 4: 548.

Longinelli, A., Wierzbowski, H. and Di Matteo, A., 2003. $\delta^{18}O$ (PO_4^{3-}) and $\delta^{18}O$ (CO_3^{2-}) from belemnite guards from Eastern Europe: implications for palaeoceanographic reconstructions and for the preservation of pristine isotopic values. Earth and Planetary Science Letters, 209(3-4): 337-350.

Loucks, R.G., Rodgers, S., Kerans, C. and Janson, X., 2003. Platform-Margin, Slope, and Basinal Carbonate Depositional Environments. American Geological Institute and American Association of Petroleum Geologists, Bureau of Economic Geology, online learning modules, in: http://www.beg.utexas.edu/lmod/.

Louis-Schmid, B., Rais, P., Bernasconi, S.M., Pellenard, P., Collin, P.-Y., Weissert, H., 2007. Detailed record of the mid-Oxfordian (Late Jurassic) positive carbon-isotope excursion in two hemipelagic sections (France and Switzerland): A plate tectonic trigger? Palaeogeography, Palaeoclimatology, Palaeoecology, 248(3-4): 459-472.

Love, S.P., Goff, F., Schmidt, S.C., Counce, D., Pettit, D., Christensen, B. and Siebe, C., 2000. Passive infrared spectroscopic remote sensing of volcanic gases: Ground-based studies at White Island and Ruapehu, New Zealand, and Popocatépetl, Mexico, in: Mouginis-Mark, P.J., Crisp, J.A., Fink, J.H. (Eds.), Remote sensing of active volcanism: Geophysical Monograph 116. AGU, Washington DC, pp. 117-138.

Lowenstein, T.K., Timofeeff, M.N., Brennan, S.T., Hardie, L.A. and Demicco, R.V., 2001. Oscillations in Phanerozoic seawater chemistry: Evidence from fluid Inclusions. Science, 294(5544): 1086-1088.

Lu, F., 2008. Pristine or altered: low-Mg calcite shells survived from massive dolomitization? A case study from Miocene carbonates. Geo-Marine Letters, 28(5): 339-349.

Lukeneder, A., Harzhauser, M., Müllegger, S. and Piller, W., 2008. Stable isotopes ($\delta^{18}O$ and $\delta^{13}C$) in *Spirula spirula* shells from three shells from three major oceans indicate developmental changes paralleling depth distributions. Marine Biology, 154(1): 175-182.

Lupton, J.E. and Craig, H., 1981. A Major Helium-3 Source at 15°S on the East Pacific Rise. Science 214: 13-18.

Maceachern, J.A., Raychaudhuri, I. and Pemberton, S.G., 1992. Stratigraphic applications of the Glossifungites Ichnofacies: Delineating discontinuities in the rock record. In: Pemberton, S.G. (Editor), Applications of Ichnology to Petroleum Exploration. SEPM Core Workshop 17, pp. 169-198.

Machel, H.G. and Burton, E.A., 1991. Factors governing cathodoluminescence in calcite and dolomite, and their implications for studies of carbonate diagenesis. In: Barker, C.E. and Kopp, O.C. (Editors), Luminescence Microscopy and Spectroscopy: Qualitative and Quantitative Applications. SEPM Short Course 25, pp. 37-57.

Machel**,** H.G., 2000**.** Application of cathodoluminescence to carbonate diagenesis. In: Pagel, M., Barbin, V., Blanc, P. and Ohnenstetter, D. (Editors), Cathodoluminescence in Geosciences. Springer, Berlin, pp. 271–302.

Machel, H.G., Mason, R.A., Mariano, A.N. and Mucci, A., 1991. Causes and measurements of luminescence in calcite and dolomite. In: Barker, C.E. and Kopp, O.C. (Editors), Luminescence Microscopy and Spectroscopy: Qualitative and Quantitative Applications. SEPM Short Course 25, pp. 9-25.

Macintyre, I.G. and Milliman, J.D., 1970. Physiographic features on the outer shelf and upper slope, Atlantic margin, southern United States. Geological Society of America Bulletin, 81: 2477-2598.

Mackenzie, F.T. and Pigott, J.D., 1981. Tectonic controls of Phanerozoic sedimentary rock cycling: Journal of the Geological Society of London 138: 183-196.

Maeda, H., Seilacher, A., 1996. Ammonoid taphonomy. In: H. Landman, K. Tanabe and R.A. Davis (Editors), Topics in Geobiology 13: 544-578.

Mahowald, N.K., Kohfeld, M., Hansson, Y., Balkanski, S.P., Harrison, I.C., Prentice, M., Schulz and Rodhe, H., 1999. Dust sources and deposition during the last glacial maximum and current climate: A comparison of model results with paleodata from ice cores and marine sediments. Journal of Geophysical Research 104: 15895-15916.

Malchus, N. and Steuber, T., 2002. Stable isotope records (O and C) of Jurassic aragonitic shells from England and NW Poland: palaeoecologic and environmental implications. Geobios 35: 29−39.

Maliva, R.G., 1995. Recurrent neomorphic and cement microtextures from different diagenetic environments, Quarternary to late Neogene carbonates, Great Bahama Bank. Sedimentary Geology, 97(1-2): 1-7.

Malkoč, M. and Mutterlose, J., 2010. The early Barremian warm pulse and the late Barremian cooling: A high-resolution geochemical record of the boreal realm. Palaios, 25(1-2): 14-23.

Malkoč, M., Mutterlose, J., Pauly, S., 2010. Timing of the Early Aptian $\delta^{13}C$ excursion in the Boreal Realm. Newsletters on Stratigraphy, 43: 251-273.

Mamet, B. and Préat, A., 2003. On the bacterial and fungal origin of the Ammonitico Rosso red pigmentation (Jurassic, Verone area, northern Italy). Revue de micropaléontologie, 46: 35-46.

Mamet, B. and Préat, A., 2005. Why is “Red Marble” red?. Revista Española de Micropaleontología, 31(1): 13-21.

Mamet, B. and Préat, A., 2006. Iron-bacterial mediation in Phanerozoic red limestones: State of the art. Sedimentary Geology, 185: 147-157.

Marcus, Y., 2009. Effect of ions on the structure of water: Structure making and breaking. Chemical Reviews 109: 1346-1370.

Marques, B. and Oloriz, F., 1989a, La plate-forme de l'Algarve au Jurassique supérieur: les grandes discontinuités stratigraphiques: Cuadernos de Geología Ibérica 13: 237-249.

Marques, B. and Oloriz, F., 1989b, La marge Sud-Ouest d`Ibérie pendant le Jurassique supérieur (Oxfordien-Kimmerdgien): essai de reconstruction geo-biologique: Cuadernos de Geología Ibérica 13: 251-263.

Marques, B., 1983. Oxfordiano-Kimeridgiano do Algarve Oriental: estratigrafia, paleobiologia (Ammonoidea) e paleobiogeografia., Univ. Nova Lisboa, Lisboa, 547 pp.

Marques, B., 1985. Litostratigrafia do Oxfordiano-Kimmeridgiano do Algarve. Comunicações dos Serviços Geológicos de Portugal 71 (1): 33-39.

Marques, B., Oloriz, F. and Rodriguez-Tovar, F.J., 1991. Interaction between tectonics and eustasy during the Upper Jurassic and Lowermost Cretaceous; examples from the south of Iberia. Bulletin. Société Géologique de France, 162(6): 1109-1124.

Marshal, J.D., 1992. Climatic and oceanographic isotopic signals from the carbonate record and their preservation. Geological Magazine 129 (2): 143-160.

Marshall, D. J., 1988. Cathodoluminescence of Geological Materials. Boston: Unwin Hyman. 146 pp.

Marshall, J.D. and Ashton, M., 1980. Isotopic and trace element evidence for submarine lithification of hardgrounds in the Jurassic of eastern England. Sedimentology, 27: 271-289.

Marshall, J.D., 1992. Climatic and oceanographic isotopic signals from the carbonate rock record and their preservation. Geological Magazine, 129(2): 143-160.

Martin, J.M. and Whitfield, M., 1983. The significance of the river input of chemical elements to the ocean. In: Wong, C.S., Boyle, E., Bruland, K.W., Burton, J.D. and Goldberg, E. (Editors), Trace metals in seawater. Plenum, New York, pp. 265-296.

Martin, M.A. and Pollard, J.E., 1996. The role of trace fossil (ichnofabric) analysis in the development of depositional models for the Upper Jurassic Fulmar Formation of the Kittiwake Field (Quadrant 21 UKCS). In: Hurst, A. (Editor), Geology of the Humber Group: Central Graben and Moray Firth. Geological Society, London, Special Publications 114, pp. 163-183.

Martin, R.E., 1995. Cyclic and secular variation in microfossil biomineralization - clues to the biogeochemical evolution of Phanerozoic oceans. Global and Planetary Change, 11: 1-23.

Martire, L., 1996. Stratigraphy, facies and synsedimentary tectonics in the Jurassic Rosso Ammonitico Veronese (Altopiano di Asiago, NE Italy). Facies, 35: 209-236.

Matheron, G., 1971. The theory of regionalized variables and its applications: Cahier 5. Centre de géostatistique et de Morphologie Mathématique, Fointainebleau, France.

Matyszkiewicz, J., 1996. The significance of Saccocoma-Calciturbidites for the analysis of the Polish epicontinental Late Jurassic basin: An example from the southern Cracow-Wielun upland (Poland). Facies, 34: 23-40.

McArthur, J.M., Janssen, N.M.M., Reboulet, S., Leng, M.J., Thirlwalle, M.F. and van de Schootbrugge, B., 2007. Palaeotemperatures, polar ice-volume, and isotope stratigraphy (Mg/Ca, $\delta^{18}O$, $\delta^{13}C$, $^{87}Sr/^{86}Sr$): the Early Cretaceous (Berriasian, Valanginian, Hauterivian). Palaeogeography, Palaeoclimatology, Palaeoecology 248 (3-4): 391-430.

McArthur, J.M., Mutterlose, J., Price, G.D., Rawson, P.F., Ruffell, A. and Thirlwall, M.F., 2004. Belemnites of Valanginian, Hauterivian and Barremian age: Sr-isotope stratigraphy, composition ($^{87}Sr/^{86}Sr$, $\delta^{13}C$, $\delta^{18}O$, Na, Sr, Mg), and palaeo-oceanography. Palaeogeography, Palaeoclimatology, Palaeoecology 202 (3-4): 253-272.

McCave, I.N. and Hall, I.R., 2006. Size sorting in marine muds: Processes, pitfalls, and prospects for paleoflow-speed proxies. Geochemistry, Geophysics, Geosystems 7(10): 1-37.

McCave, I.N., Manighetti, B. and Beveridge, N.A.S., 1995a. Circulation in the glacial North-Atlantic inferred from grain-size measurements. Nature, 374(6518): 149-152.

McCave, I.N., Manighetti, B. and Robinson, S.G., 1995b. Sortable silt and fine sediment size composition slicing - Parameters for paleocurrent speed and paleooceanography. Paleoceanography, 10(3): 593-610..

McCrea, J.M., 1950. On the isotopic chemistry of carbonates and a paleotemperature scale. Journal of Chemical Physics, 18(6): 849-857.

McGill, R., Tukey, J.W. and Larsen, W.A., 1978. Variations of box plots. American Statistician, 32(1): 12-16.

McLaren, P. and Bowles, D., 1985. The effects of sediment transport on grain-size distribution. Journal of Sedimentary Petrology, 55(4): 457-470.

MClaughlin, P.I., Brett, C.E., 2004. Sequence stratigraphy and stratonomy of marine hardgrounds: examples from the Middle Paleozoic of Eastern Laurentia. Geological Society of America, Abstracts with Programs, 36(5): 110.

MClaughlin, P.I., Brett, C.E., and Wilson, M.A., 2008. Hierarchy of sedimentary discontinuity surfaces and condensed beds from the Middle Paleozoic of eastern North America: Implications for cratonic sequence stratigraphy. In: Pratt, B. R. and Holmden, C. (Editors), Dynamics of Epeiric Seas: Sedimentological, Paleontological, and Geochemical Perspectives. Geological Association of Canada Special Paper 48, pp. 175-200.

McLean, R.J.C., Fortin, D. and Brown, D.A., 1996. Microbial metal-binding mechanisms and their relation to nuclear waste disposal. Canadian Journal of Microbiology, 42(4): 392-400.

Melim, L.A. and Scholle, P.A., 2002. Dolomitization of the Capitan Formation forereef facies (Permian, west Texas and New Mexico): seepage reflux revisited. Sedimentology, 49(6): 1207-1227.

Menegatti, A.P., Weissert, H., Brown, R.S., Tyson, R.V., Farrimond, P., Strasser, A. and Caron, M., 1998. High-resolution $\delta^{13}C$ stratigraphy through the Early Aptian "Livello Selli" of the Alpine Tethys. Paleoceanography 13: 530-545.

Menegatti, A.P., Weissert, H., Brown, R.S., Tyson, R.V., Farrimond, P., A., S., and Caron, M., 1998. High-resolution $\delta^{13}C$ stratigraphy through the early Aptian "Livello Selli" of the Alpine Tethys. Paleoceanography, 13(5): 530-545.

Middag, R., de Baar, H.J.W., Laan, P. and Klunder, M.B., 2011. Fluvial and hydrothermal input of manganese into the Arctic Ocean. Geochimica et Cosmochimica Acta, 75(9): 2393-2408.

Mii, H.S., Grossman, E.L. and Yancey, T.E., 1999. Carboniferous isotope stratigraphies of North America: Implications for Carboniferous paleoceanography and Mississippian glaciation. Geological Society of America Bulletin, 111(7): 960-973.

Milliken, K.L. and Pigott, J.D., 1977. Variation of oceanic Mg/Ca ratio through time: implication of the calcite sea. Geological Society of America Abstract Program 9: 64-65.

Milliman J. D., 1974. Marine Carbonates. Springer-Verlag, Berlin, pp. 375.

Milliman, J.D. and Droxler, A.W., 1995. Calcium carbonate sedimentation in the global ocean: linkages between the neritic and pelagic environments. Oceanography 8(3): 92-94.

Milliman, J.D. and Muller, J., 1973. Precipitation and lithification of magnesian calcite in deep-sea sediments of eastern Mediterranean-sea. Sedimentology, 20(1): 29-45.

Milliman, J.D., 1971. Carbonate lithification in deep sea. In: Bricker, O.P. (Editor), Carbonate cements. John Hopkins University Studies Geology 19, pp. 95-102.

Milliman, J.D., 1974. Marine Carbonates. Springer-Verlag, New York, 375 pp.

Milliman, J.D., Hook, J.A. and Golubic, S., 1985. Meaning and usage of micrite cement and matrix - Reply to discussion. Journal of Sedimentary Petrology, 55(5): 776-777.

Mitchell, S., Ball, J., Crowley, S., Marshall, J., Paul, C., Veltkamp, C., Samir, A., 1997. Isotopic data from Cretaceous chalks and foraminifera: environmental or diagenetic signals? Geology 25: 691-694.

Mitchell, S.F., 2005. Eight belemnite biohorizons in the Cenomanian of northwest Europe and their importance. Geological Journal, 40(3): 363-382.

Molina, J.M. and Vera, J.A., 2000. Isolated carbonate platforms (guyots) from the Subbetic Jurassic. Geogaceta, 27: 107-110.

Molina, J.M. and Vera, J.A., 2008. Resedimented carbonate and volcanic rocks in the Berriasian-Hauterivian of the Subbetic (Alamedilla, Betic Cordillera, southern Spain). Cretaceous Research, 29(5-6): 781-789.

Molina, J.M., 1987. Análisis de fácies del Mesozoico en el Subbético Externo (provincia de Córdoba y Sur de Jaén). Doctoral dissertation, University of Granada, Granada, 518 pp.

Molina, J.M., Ruíz-Ortiz, P. and Vera, J.A., 1986-1987. Capas de tormentas (tempestitas) en el Jurásico del Subbético Externo (Cordilleras Béticas). Acta Geológica Hispanica 21-22: 167-175.

Möller, P., Lüders, V., Schröder, J. and Luck, J., 1991. Element partitioning in calcite as a function of solution flow rate: a study on vein calcites from the Harz Mountains. Mineralium Deposita, 26(3): 175-179.

Monaco, P. and Giannetti, A., 2002. Three-dimensional burrow systems and taphofacies in shallowing-upward parasequences, Lower Jurassic carbonate platform (Calcari Grigi, Southern Alps, Italy). Facies, 47: 57-82.

Monien, D., Kuhn, G., von Eynatten, H. and Talarico, F.M., Geochemical provenance analysis of fine-grained sediment revealing Late Miocene to recent Paleo-Environmental changes in the Western Ross Sea, Antarctica. Global Planet In Press, Corrected Proof.

Moore, D.G., 1969. Reflection profiling studies of the California Continental Borderland: Structure and Quaternary turbidite basins. Geological Society of America Abstract Programs, 107: 142.

Moore, G.T., Hayashida, D.N., Ross, C.A. and Jacobson, S.R., 1992. Paleoclimate of the Kimmeridgian/Tithonian (Late Jurassic) world: I. Results using a general circulation model. Palaeogeography, Palaeoclimatology, Palaeoecology, 93(1-2): 113-150.

Moore, W.S., 2000. Determining coastal mixing rates using radium isotopes. Continental Shelf Research 20: 1993-2007.

Morse, J.W., Arvidson, R.S.and Lüttge, A., 2007. Calcium carbonate formation and dissolution. Chemical Revies 107: 342-381.

Muhs, D.R., Budahn, J., Reheis, M., Beann, J., Skipp, G.and Fisher, E., 2007. Airborne dust transport to the eastern Pacific Ocean off southern California: Evidence from San Clemente Island. Journal of Geophysical Research 12: 13203-13240.

Mukai, H. and Koike, I., 1984. Pumping rates of the mud shrimp Callianassa japonica. Journal of the Oceanographical Society of Japan, 40(4): 243-246.

Müller, J. and Fabricius, F., 1974. Magnesian-calcite nodules in the Ionian deep sea: an actualistic model for the formation of some nodular limestones. In: Hsü, K.J. and Jenkyns, H.C. (Editors), Pelagic sediments: on Land and under the Sea. Blackwell Publishing Ltd., pp. 235-247.

Müller-Stoll, H., 1936. Beiträge zur Anatomie der Belemnoidea. Nova Acta Leopoldina, 4: 159-226.

Mullins, H.T., Neumann, A.C., Wilber, R.J. and Boardman, M.R., 1980. Nodular carbonate sediment on Bahamian slopes - Possile precursors to nodular limestones. Journal of Sedimentary Petrology, 50(1): 117-131.

Munn, C.B., 2004. Marine microbiology. Ecology and application. Garland Science/Bios Scientific, Oxford, UL, 282 pp.

Munnecke, A. and Samtleben, C., 1996. The formation of micritic limestones and the development of limestone-marl alternations in the Silurian of Gotland, Sweden. Facies, 34: 159-176.

Munnecke, A. and Samtleben, C., 1996. The formation of micritic limestones and the development of limestone-marl alternations in the Silurian of Gotland, Sweden. Facies, 34(1): 159-176.

Munnecke, A. and Westphal, H., 2005. Variations in primary aragonite, calcite, and clay in fine-grained calcareous rhythmites of Cambrian to Jurassic age - an environmental archive? Facies, 51(1-4): 611-626.

Munnecke, A., Westphal, H., Elrick, M. and Reijmer, J.J.G., 2001. The mineralogical composition of precursor sediments of calcareous rhythmites: a new approach. Israel Journal of Earth Sciences, 90: 795-812.

Mutterlose, J. and Wiedenroth, K., 2008. Early Cretaceous (Valanginian - Hauterivian) belemnites from western Morocco: stratigraphy and palaeoecology. Cretaceous Research, 29(5-6): 814-829.

Mutterlose, J., Malkoč, M., Schouten, S., Damste, J.S.S. and Forster, A., 2010. TEX86 and stable delta $\delta^{18}O$ paleothermometry of early Cretaceous sediments: Implications for belemnite ecology and paleotemperature proxy application. Earth and Planetary Science Letters, 298(3-4): 286-298.

Muttoni, G., Erba, E., Kent, D.V. and Bachtadse, V., 2005. Mesozoic Alpine facies deposition as a result of past latitudinal plate motion. Nature, 434(7029): 59-63.

Myrow, P.M., 1995. Thalassinoides and the enigma of early Palaeozoic open-framework burrow systems. Palaios, 10(1): 58-74.

Naydin, D.P. and Teys, R.V., 1976. Oxygen isotope compositions of Eurasian Toarcian- Aalenian seas. Geochemistry International 13: 163-173.

Neuweiler, F., Daoust, I., Bourque, P.-A. and Burdige, D.J., 2007. Degradative Calcification of a Modern Siliceous Sponge from the Great Bahama Bank, The Bahamas: A Guide for Interpretation of Ancient Sponge-Bearing Limestones. Journal of Sedimentary Research, 77(7): 552-563.

Neuweiler, F., d'Orazio, V., Immenhauser, A., Geipel, G., Heise, K.-H., Cocozza, C. and Miano, T.M., 2003. Fulvic acid-like organic compounds control nucleation of marine calcite under suboxic conditions. Geology, 31(8): 681-684.

Niebuhr, B. and Joachimski, M.M., 2002. Stable isotope and trace element geochemistry of Upper Cretaceous carbonates and belemnite rostra (Middle Campanian, north Germany). Geobios, 35(1): 51-64.

Nieto, L.M., Ruiz-Ortiz, P.A., Rey, J. and Benito, M.I., 2008. Strontium-isotope stratigraphy as a constraint on the age of condensed levels: Examples from the Jurassic of the Subbetic Zone (southern Spain). Sedimentology, 55(1): 1-29.

Nunn, E.V. and Price, G.D., 2010. Late Jurassic (Kimmeridgian-Tithonian) stable isotopes ($\delta^{18}O$, $\delta^{13}C$) and Mg/Ca ratios: New palaeoclimate data from Helmsdale, northeast Scotland. Palaeogeography Palaeoclimatology Palaeoecology 292: 325-335.

Nunn, E.V., Price, G.D., B., H.M., Page, K.N. and Leng, M.J., 2009. Terrestrial and marine carbon isotope signals from the Callovian-Kimmeridgian (Late Jurassic) succession at Staffin Bay, Isle of Skye, Scotland. Journal of the Geological Society, 166: 633-641.

O'Dogherty, L., Sandoval, J., Bartolini, A., Bruchez, S., Bill, M. and Guex, J., 2006. Carbon-isotope stratigraphy and ammonite faunal turnover for the Middle Jurassic in the Southern Iberian palaeomargin. Palaeogeography, Palaeoclimatology, Palaeoecology, 239(3-4): 311-333.

Ogg, J.G. and Przybylski, P., 2006. Jurassic chronostratigraphic charts and a display interface. 1. Hettangian through Aalenian (J. Ogg and P. Przybylski). 2. Bajocian through Tithonian (P. Przybylski and J. Ogg), 7th International Congress on the Jurassic System, 6-18 Sept 2006,

Krakow, Poland. Volumina Jurassica 4: 199. (Upper Jurassic chart produced by James Ogg and Gabi Ogg in Feb 2006 for the International Commission on Stratigraphy).

Ogg, J.G., Steiner, M.B., Oloriz, F. and Tavera, J.M., 1984. Jurassic magnetostratigraphy, 1. Kimmeridgian-Tithonian of Sierra Gorda and Carcabuey, southern Spain. Earth and Planetary Science Letters, 71(1): 147-162.

Olivier, N. and Boyet, M., 2006. Rare earth and trace elements of microbialites in Upper Jurassic coral- and sponge-microbialite reefs. Chemical Geology, 230(1-2): 105-123.

Olivier, N., Pittet, B. and Mattioli, E., 2004. Palaeoenvironmental control on sponge-microbialite reefs and contemporaneous deep-shelf marl-limestone deposition (Late Oxfordian, southern Germany). Palaeogeography Palaeoclimatology Palaeoecology, 212(3-4): 233-263.

Olivier, N., Pittet, B., Gaillard, C. and Hantzpergue, P., 2007. High-frequency palaeoenvironmental fluctuations recorded in Jurassic coral- and sponge-microbialite bioconstructions. Comptes Rendus Palevol, 6(1-2): 21-36.

Olóriz, F. (Coord.), 1996. Facies, fossil assemblages and eco-sedimentary evolution in epicontinental shelves and epioceanic swells. Middle-Upper Jurassic (Betic Cordillera). IV International Symposium Cephalopods - Present and Past, Granada, p. 41.

Olóriz, F. and Villaseñor, A.B., 2010. Ammonite biogeography: From descriptive to dynamic, ecological interpretations. In: Tanabe, K., Shigeta,Y., Sasaki, T. and Hirano, H. (Editors), Cephalopods - Present and Past. Tokai University Press, Tokyo, pp. 253-265.

Olóriz, F., 1978. Kimmeridgiense-Tithónico inferior en el Sector Central de las Cordilleras Béticas (Zona Subbética). Paleontología. Bioestratigrafía. Ph. D. Thesis, University of Granada.

Olóriz, F., 1997. Interpretaciones ecoestratigráficas. Aplicaciones a los materiles del Jurasico Superior. In: Gámez Vintaned, J.A. and Liñan, E. (Editors), Vida y Ambientes del Jurásico. Zaragoza, pp. 33-56.

Oloriz, F., 2000. Time-averaging and long-term palaeoecology in macroinvertebrate fossil assemblages with ammonites (Upper Jurassic). Revue de Paleobiologie Volume Special (8): 123-140.

Oloriz, F., Caracuel, J.E. and Ruizheras, J.J., 1995a. Numerical-analysis of sedimentary components - A key for interpretation of macroscopic and microscopic features in Ammonitico Rosse facies (uppermost Jurassic lowermost Cretaceous). Journal of Sedimentary Research Section a-Sedimentary Petrology and Processes, 65(1): 234-243.

Olóriz, F., Caracuel, J.E., Marques, B. and Rodríguez-Tovar, F.J., 1995b. Asociaciones de Tintinnoides en facies ammonitico rosso de la Sierra Norte (Mallorca). Revista Española de Paleontología, nº Extra. Homenaje al Dr. G. Colom: 77-93.

Olóriz, F., Caracuel, J.E., Ruiz-Heras, J.J., Rodriguez-Tovar, F.J. and Marques, B., 1996. Ecostratigraphic approaches, sequence stratigraphy proposals and block tectonics: example from epioceanic swell areas in south and east Iberia. Palaeogeography, Palaeoclimatology, Palaeoecology, 121: 273-295.

Olóriz, F., Linares, A., Goy, A., Sandoval, J., Caracuel, J.E., Rodríguez-Tovar, F.J., Tavera, J.M., 2002a. The Betic Cordillera and Balearic Islands. In: Gibbons, W. and Moreno, T. (Editors), The Geology of Spain. The Geological Society of London, pp. 235-253.

Olóriz, F., Marques, B. and Caracuel, J.E., 1998. Biostratigraphic research in the Middle-Upper Oxfordian from Mallorca (Spain), a key for ecostratigraphic approach in the Western Tethys. Geobios 31: 319-336.

Olóriz, F., Molina-Morales, J.M. and Serna-Barquero, A., 1999. Revisión estratigráfica del intervalo Kimmeridgiense medio-Tithonico basal en el el perfil G10 del sector de Venta Quesada (Sierra Gorda, provincia de Granada). Geogaceta, 26: 71-74.

Olóriz, F., Palmqvist, P. and Pérez-Clarós, J.A., 1997. Shell features, main colonized environments, and fractal analysis of sutures in Late Jurassic ammonites. Lethaia, 30(3): 191-204.

Olóriz, F., Reolid, M. and Rodriguez-Tovar, F.J., 2002b. Fossil assemblages, lithofacies, taphofacies and interpreting depositional dynamics in the epicontinental Oxfordian of the Prebetic Zone, Betic Cordillera, southern Spain Palaeogeography, Palaeoclimatology, Palaeoecology 185: 53-75.

Olóriz, F., Reolid, M. and Rodriguez-Tovar, F.J., 2003a. A late Jurassic Carbonate Ramp colonized by sponges and benthic microbial communities (External Prebetic, Southern Spain). Palaios, 18: 528 - 545.

Oloriz, F., Rodriguez-Tovar, F.J. and Marques, B., 1994. Macroinvertebrate assemblages and ecostratigraphic structuration within a Highstand System Tract. An example from the Lower Kimmeridgian in southern Iberia. Geobios Memoire Special (Villeurbanne), 17(2): 605-614.

Olóriz, F., Villaseñor, A.B. and González-Arreola, C., 2003b. Major lithostratigraphic units in land-outcrops of north-central Mexico and the subsurface along the northern rim of Gulf of Mexico Basin (Upper Jurassic-lowermost Cretaceous): a proposal for correlation of tectono-eustatic sequences. Journal of South American Earth Sciences, 16(3): 119-142.

Olszewski, T.D., 2004. Modeling the influence of taphonomic destruction, reworking, and burial on time-averaging in fossil accumulations. Palaios, 19(1): 39-50.

Osete, M.L., Freeman, R. and Vegas, R., 1988. Preliminary palaeomagnetic results from the Subbetic Zone (Betic Cordillera, southern Spain): kinematic and structural implications. Physics of the Earth and Planetary Interiors, 52(3-4): 283-300.

Osete, M.-L., Gómez, J.J., Pavón-Carrasco, F.J., Villalaín, J.J., Palencia-Ortas, A., Ruiz-Martínez, V.C., Heller, F., 2011. The evolution of Iberia during the Jurassic from palaeomagnetic data. Tectonophysics, 502(1-2): 105-120.

Palmer, T.J. and Wilson, M.A., 2004. Calcite precipitation and dissolution of biogenic aragonite in shallow Ordovician calcite seas. Lethaia, 37(4): 417-427.

Panchuk, K.M., Holmden, C. and Kump, L.R., 2005. Sensitivity of the epeiric sea carbon isotope record to local-scale carbon cycle processes: Tales from the Mohawkian Sea. Palaeogeography, Palaeoclimatology, Palaeoecology, 228(3-4): 320-337.

Panchuk, K.M., Holmden, C.E. and Leslie, S.A., 2006. Local Controls on Carbon Cycling in the Ordovician Midcontinent Region of North America, with Implications for Carbon Isotope Secular Curves. Journal of Sedimentary Research, 76(2): 200-211.

Parente, M., Frijia, G. and Di Lucia, M., 2007. Carbon-isotope stratigraphy of Cenomanian-Turonian platform carbonates from the southern Apennines (Italy): a chemostratigraphic approach to the problem of correlation between shallow-water and deep-water successions. Journal of the Geological Society, 164: 609-620.

Paul, C.R.C., Allison, P.A. and Brett, C.E., 2008. The occurrence and preservation of ammonites in the Blue Lias Formation (lower Jurassic) of Devon and Dorset, England and their palaeoecological, sedimentological and diagenetic significance. Palaeogeography Palaeoclimatology Palaeoecology, 270(3-4): 258-272.

Pavlović, G., Prohić, E., Miko, S. and Tibljaš, D., 2002. Geochemical and petrographic evidence of meteoric diagenesis in tufa deposits in Northern Dalmatia (Zrmanja and Krupa Rivers, Croatia). Facies 46: 27-34.

Pearce, C.R., Hesselbo, S.P. and Coe, A.L., 2005. The mid-Oxfordian (Late Jurassic) positive carbon-isotope excursion recognised from fossil wood in the British Isles. Palaeogeography Palaeoclimatology Palaeoecology, 221(3-4): 343-357.

Pemberton, G.S., Risk, M.J. and Buckley, D.E., 1976. Supershrimp: deep bioturbation in the Strait of Canso, Nova Scotia. Science, N.Y., No. 4241: 790-791.

Pena dos Reis, R.P.B., Proença Cunha, P., Dinis, J.L. and Trincão, P.R., 2000. Geologic Evolution of the Lusitanian Basin (Portugal) during the Late Jurassic. GeoResearch Forum 6: 345–356.

Pisera, A., Satir, M., Gruszczyński, M., Hoffman, A. and Małkowski, K., 1992. Variation in $\delta^{13}C$ and $\delta^{18}O$ in Late Jurassic carbonates, submediterranean province, Europe. Annales Societatis Geologorum Poloniae 62: 141-147.

Plunkett, J.M., 1997. Early Diagenesis of Shallow Platform Carbonates in the Oxfordian of the Swiss Jura Mountains: Unpublished Ph.D. Thesis, Université de Fribourg, Fribourg, Switzerland, 166 p.

Podlaha, O.G., Muterlose, J. and Veizer, J., 1998. Preservation of delta O-18 and delta C-13 in belemnite rostra from the Jurassic Early Cretaceous successions. American Journal of Science, 298(6): 534-534.

Pomar, L. and Hallock, P., 2008. Carbonate factories: A conundrum in sedimentary geology. Earth-Science Reviews, 87(3-4): 134-169.

Pope, M. and Read, J.F., 1997. High-resolution surface and subsurface sequence stratigraphy of late middle to late Ordovician (late Mohawkian-Cincinnatian) foreland basin rocks, Kentucky and Virginia. Aapg Bulletin-American Association of Petroleum Geologists, 81(11): 1866-1893.

Porter, S.M., 2007. Seawater Chemistry and Early Carbonate Biomineralization. Science, 316(5829): 1302.

Porter, S.M., 2010. Calcite and aragonite seas and the de novo acquisition of carbonate skeletons. Geobiology, 8(4): 256-277.

Pratt, L.M., Force, E.R. and Pomerol, B., 1991. Coupled manganese and carbon-isotopic events in marine carbonates at the Cenomonian-Turonian boundary. Journal of Sedimentary Petrology, 61(3): 370-383.

Préat, A., de Jong, J.T.M., Mamet, B. and Mattielli, N., 2008. Stable Iron Isotopes and Microbial Mediation in Red Pigmentation of the Rosso Ammonitico (Mid-Late Jurassic, Verona Area, Italy). Astrobiology, 8(4): 1-17.

Préat, A., Mamet, B., Di Stefano, P., Martire, L. and Kolo, K., 2011. Microbially-induced Fe and Mn oxides in condensed pelagic sediments (Middle-Upper Jurassic, Western Sicily). Sedimentary Geology, 237(3-4): 179-188.

Préat, A., Morano, S., Loreau, J.-P., Durlet, C. and Mamet, B., 2006. Petrography and biosedimentology of the Rosso Ammonitico Veronese (middle-upper Jurassic, north-eastern Italy). Facies, 52: 265 - 278.

Price, G.D. and Page, K.N., 2008. A carbon and oxygen isotopic analysis of molluscan faunas from the Callovian-Oxfordian boundary at Redcliff Point, Weymouth, Dorset: implications for belemnite behaviour. Proceedings of the Geologists Association, 119: 153-160.

Price, G.D. and Sellwood, B.W., 1994. Paleotemperature indicated by upper Jurassic (Kimmeridgian Tithonian) fossils from Mallorca determined by oxygen-isotope composition. Palaeogeography Palaeoclimatology Palaeoecology, 110(1-2): 1-10.

Price, G.D. and Sellwood, B.W., 1997. "Warm" palaeotemperatures from high Late Jurassic palaeolatitudes (Falkland Plateau): Ecological, environmental or diagenetic controls? Palaeogeography, Palaeoclimatology, Palaeoecology, 129: 315-327.

Price, G.D. and Teece, C., 2010. Reconstruction of Jurassic (Bathonian) palaeosalinity using stable isotopes and faunal associations. Journal of the Geological Society, 167(6): 1199-1208.

Price, G.D., 1999. The evidence and implications of polar ice during the Mesozoic. Earth-Science Reviews, 48(3): 183-210.

Price, G.D., 2010. Carbon-isotope stratigraphy and temperature change during the Early-Middle Jurassic (Toarcian-Aalenian), Raasay, Scotland, UK. Palaeogeography Palaeoclimatology Palaeoecology, 285(3-4): 255-263.

Price, G.D., Sellwood, B.W., Corfield, R.M., Clarke, L. and Cartlidge, J.E., 1998. Isotopic evidence for palaeotemperatures and depth stratification of Middle Cretaceous planktonic Foraminifera from the Pacific Ocean. Geological Magazine, 135(2): 183-191.

Price, G.D., Twitchett, R.J., Smale, C. and Marks, V., 2009. Isotopic analysis of the life history of the enigmatic squid Spirula spirula, with implications for studies of fossil Cephalopods. Palaios, 24(5-6): 273-279.

Pufahl, P.K., James, N.P., Kyser, T.K., Lukasik, J.J. and Bone, Y., 2006. Brachiopods in epeiric seas as monitors of secular changes in ocean chemistry: A Miocene Example from the Murry Basin, South Australia. Journal of Sedimentary Research, 76: 926-941.

Rais, P., Louis-Schmid, B., Bernasconi, S. and Weissert, H., 2007. Palaeoceanographic and palaeoclimatic reorganization around the Middle-Late Jurassic transition. . Palaeogeography, Palaeoclimatology, Palaeoecology 251: 527-546.

Ramalho, M., 1988. Sur la découverte de biohermes stromatolithiques à spongiaires siliceux dans le Kimméridgien de l'Algarve, Portugal: Comunicações dos Serviços Geológicos de Portugal 74: 41-55.

Rao, C.P. and Adabi, M.H., 1992. Carbonate minerals, major and minor elements and oxygen and carbon isotopes and their variation with water depth in cool, temperate carbonates, western Tasmania, Australia. Marine Geology, 103(1-3): 249-272.

Rao, C.P. and Jayawardane, M.P.J., 1994. Major minerals, elemental and isotopic composition in modern temperate shelf carbonates, Eastern Tasmania, Australia: Implications for the occurrence of extensive ancient non-tropical carbonates. Palaeogeography, Palaeoclimatology, Palaeoecology, 107(1-2): 49-63.

Reid, R.P., Macintyre, I.G. and James, N.P., 1990. Internal precipitation of microcristalline carbonate-A fundamental problem for sedimentologists Sedimentary Geology, 68(3): 163-170.

Renard, M., 1985. Géochimie des carbonates pélagiques: mises en evidence des fluctuations de la composition des eaux océaniques depuis 140 m.a. Doc.B.R.G.M, 85: 650.

Renard, M., de Rafélis, M., Emmanuel, L., Beltran, C., Moullade, M. and Tronchetti, G., 2007. Fluctuations of sea-water chemistry during Gargasian (Middle Aptian) time. Data from trace-element content (Mg, Sr, Mn, Fe) in hemipelagic carbonates from La Marcouline Quarry (Cassis, SE france). Carnets de Geologie: 1-38.

Reolid, M. and Benito, M., 2011. Belemnite taphonomy and lithofacies in an epicontinental shelf of the upper Oxfordian – lower Kimmeridgian (Prebetic, Betic Cordillera). In: Bádenas, B., Aurell, M. and Alonso-Zarza, A.M. (Editors), Abstracts of the 28th IAS Meeting of Sedimentology, Zaragoza, Spain, p. 379.

Reolid, M. and Luis, M.N., 2010. Jurassic Fe-Mn macro-oncoids from pelagic swells of the External Subbetic (Spain): Evidences of microbial origin. Geologica Acta, 8(2): 151-168.

Revsbech, N.P., Sorensen, J., Blackburn, T.H. and Lomholt, J.P., 1980. Distribution of oxygen in marine-sediments measured with microelectrodes. Limnology and Oceanography, 25(3): 403-411.

Rexfort, A. and Mutterlose, J., 2006. Oxygen isotope of Sepia officinalis - a key to unterstanding the ecology of belemnites?. Earth and Planetary Science Letters, 247: 212-221.

Rexfort, A. and Mutterlose, J., 2009. The role of biogeography and ecology on the isotope signature of cuttlefishes (Cephalopoda, Sepiidae) and the impact on belemnite studies. Palaeogeography Palaeoclimatology Palaeoecology, 284(3-4): 153-163.

Rey, J. and Delgado, A., 2002. Carbon and oxygen isotopes: a tool for Jurassic and early Cretaceous pelagic correlation (southern Spain). Geological Journal, 37(4): 337-345.

Rey, J. and Delgado, A., 2005. Chemostratigraphic signals and sea-level changes from the Jurassic and Early Cretaceous in the Sierra de Quípar: Betic Cordilleras, southern Spain. GFF-Geologiska Foreningens i Stockholm Forhandlingar 127(1): 25-32.

Rey, J., 1993. Análisis de la cuenca subbética durante el Jurásico y Cretácico en la transversal Caravaca Vélez-Rubio, University of Granada, Granada, 460 pp.

Richter, D.K., Neuser, R.D., Schreuer, J., Gies, H. and Immenhauser, A., 2011. Radiaxial-fibrous calcites: a new look at an old problem. Sedimentary Geology, DOI: 10.1016/j.sedgeo.2011.06.003.

Ries, J.B., 2004. Effect of ambient Mg/Ca ratio on Mg fractionation in calcareous marine invertebrates: A record of the oceanic Mg/Ca ratio over the Phanerozoic. Geology 32: 981-984.

Rodrigo-Gámiz, M., Martínez-Ruiz, F., Jiménez-Espejo, F.J., Gallego-Torres, D., Nieto-Moreno, V., Romero, O. and Ariztegui, D., 2011. Impact of climate variability in the western Mediterranean during the last 20,000 years: oceanic and atmospheric responses. Quaternary Science Review 30: 2018–2034.

Rodriguez-Tovar, F.J., Reolid, M. and Abad, I., 2010. Geochemical analysis at the Lower Toarcian in the Fuente de la Vidriera section, Betic Cordillera, Spain: approaching the T-OAE. In: Abstract book, STRATI2010- 4th "French" Congress on Stratigraphy.

Rohling, E.J. and Bigg, G.R., 1998. Paleosalinity and $\delta^{18}O$: A critical assessment. Journal of Geophysical Research-Oceans, 103(C1): 1307-1318.

Romanek, C.S., Grossman, E.L. and Morse, J.W., 1992. Carbon isotopic fractionation in synthetic aragonite and calcite: effects of temperature and precipitation rate. Geochimica et Cosmochimica Acta, 56: 419-430.

Rosales, I., Quesada, S. and Robles, S., 2001. Primary and diagenetic isotopic signals in fossils and hemipelagic carbonates: the Lower Jurassic of northern Spain. Sedimentology, 48: 1149-1169.

Rosales, I., Robles, S. and Quesada, S., 2004. Elemental and oxygen isotope composition of early Jurassic belemnites: Salinity vs. temperature signals. Journal of Sedimentary Research, 74(3): 342-354.

Rosenfeld, M., Yam, R., Shemesh, A. and Loya, Y., 2003. Implication of water depth on stable isotope composition and skeletal density banding patterns in a Porites lutea colony: results from a long-term translocation experiment. Coral Reefs, 22(4): 337-345.

Ross, D.J. and Skelton, P.W., 1993. Rudist formation of the Cretaceous: a palaeoecological, sedimentological and stratigraphical review. In: Wright, V.P. (Editor), Sedimentology Review/1. Blackwell, pp. 73-91.

Rowley, D.B. and Marwick, P.J., 1992. Haq et al. Eustatic sea level curve: implications for sequestered water volumes: Journal of Geology 100: 703– 715.

Rubin, K., 1997. Degassing of metals and metalloids from erupting seamount and mid-ocean ridge volcanoes: Observations and predictions. Geochimica et Cosmochimica Acta. 61: 3525-3542.

Rubinson, M. and Clayton, R.N., 1969. Carbon-13 fractionation between aragonite and calcite. Geochimica et Cosmochimica Acta, 33(8): 997-1002.

Sabat, F., Gelabert, B., Rodríguez-Perea, A. and Giménez, J., 2011. Geological structure and evolution of Majorca: Implications for the origin of the Western Mediterranean. *Tectonophysics*, doi:10.1016/j.tecto.2011.07.005.

Sabatino, N., Neri, R., Bellanca, A., Jenkyns, H.C., Masetti, D., Scopelliti, G., 2011. Petrography and high-resolution geochemical records of Lower Jurassic manganese-rich deposits from Monte Mangart, Julian Alps. Palaeogeography Palaeoclimatology Palaeoecology, 299(1-2): 97-109.

Sadler, P.M., 1993. Models of time-averaging As a maturation Process: How Soon Do Sedimentary Sections Escape Reworking?. In: Kidwell, S.M. and Behrensmeyer, A.K. (Editors), Taphomomic Aproaches to time resolution in fossil assemblages. Short Courses in Paleontology 6, pp. 188-209.

Saelen, G., 1989. Diagenesis and construction of the belemnite rostrum. Palaeontology, 32(4): 765-798.

Saelen, G., Doyle, P. and Talbot, M.R., 1996. Stable-isotope analyses of belemnite rostra from the Whitby Mudstone Fm., England: Surface water conditions during deposition of a marine black shale. Palaios, 11: 97-117.

Salas, R., Guimerá, J., Mas, R., Martín-Closas, C., Meléndez, A. and Alonso, A., 2001. Evolution of the Mesozoic central Iberian Rift System and its Cainozoic inversion (Iberian chain). In: Ziegler, P.A., Cavazza, W., Robertson, A.H.F. and Crasquin-Soleau, S. (Editors), Peri-Tethys Memoir 6: Peri-Tethyan Rift/Wrench Basins and Passive Margins. Mémoires du Muséum National d'Histoire Naturelle 186, pp. 145-185.

Sandberg, P.A., 1983. An ascillation trend in Phanerozoic non-skeletal carbonate mineralogy. Nature, 305(5929): 19-22.

Sandberg, P.A., 1985. Aragonite cements and their occurence in ancient limestones. In: Schneidermann, N. and Harris, P.M. (Editors), Carbonate cements. SEPM 36, pp. 33-57.

Sanders, D., 2003. Syndepositional dissolution of calcium carbonate in neritic carbonate environments: geological recognition, processes, potential significance. Journal of African Earth Sciences, 36: 99-134.

Savari, B., Cecca, F. and Bartolini, A., 2003. Étude stratigraphique du Rosso Ammonitico du Monte Inici (domaine Trapanais, Sicile occidentale) : événements biosédimentaires au Jurassique moyen-Crétacé inférieur. Geodiversitas, 25(2): 217- 235.

Savin, S.M., 1977. The history of the earth surface temperature during the past 100 my. Annual Review of Earth and Planetary Sciences, 5: 319-355.

Schidlowski, M., 1987. Applications of stable carbon isotopes to early biochemical evolution on earth. Annual Review of Earth and Planetary Sciences, 15: 47-72.

Schlager, W., 2003. Benthic carbonate factories of the Phanerozoic. International Journal of Earth Sciences, 92: 445-464.

Schlirf, M., 2000. Upper Jurassic trace fossils from the Bulonnais (northern France). Geologica et palaeontologica 34: 145-213.

Schmid, D.U., Leinfelder, R.R. and Nose, M., 2001. Growth dynamics and ecology of Upper Jurassic mounds, with comparisons to Mid-Palaeozoic mounds. Sedimentary Geology, 145(3-4): 343-376.

Schneider, J., Bakker, R.J., Bechstadt, T. and Littke, R., 2008. Fluid Evolution During Burial Diagenesis and Subsequent Orogenetic Uplift: The La Vid Group (Cantabrian Zone, Northern Spain). Journal of Sedimentary Research, 78(4): 282-300.

Schneider, S., Fursich, F.T. and Werner, W., 2009. Sr-isotope stratigraphy of the Upper Jurassic of central Portugal (Lusitanian Basin) based on oyster shells. International Journal of Earth Sciences, 98(8): 1949-1970.

Seilacher, A., 1971. Preservational history of ceratite shells. Palaeontology, 14: 16-21.

Sellwood, B.W. and Valdes, P.J., 2006. Mesozoic climates: General circulation models and the rock record. Sedimentary Geology, 190(1-4): 269-287.

Shackelton, N.J. and Opdyke, N.D., 1973. Oxygen isotope and paleomagnetic stratigraphy of equatorial Pacific core V28-238. Oxygen isotope temperatures on a 10*5 and 10*6 year time scale. Quaternary Research, 3: 39-55.

Shackleton, N.J. and Kennett, D.J., 1975. Palaeotemperature history of the Cenozoic and iniciation of Antarctic glaciation: oxygen and carbon isotope analysis in DSDP sites 277, 279 and 289. Initial Reports Deep Sea Drilling Project 29: 743- 755.

Shanmugam, G. and Benedict, G.L., 1983. Manganese distribution in the carbonate fraction of shallow and deep marine Lithofacies, Middle Ordovician, Eastern Tennessee. Sedimentary Geology, 35(3): 159-175.

Spaeth, C., Hoefs, J. and Vetter, U., 1971. Some aspects of isotopic composition of belemnites and related paleotemperatures. Geological Society of America, Bulletin 82: 3139-3150.

Spencer, R.J. and Hardie, L.A., 1990. Control of seawater composition by mixing of river waters and mid-ocean ridge hydrothermal brines. In: Spencer, R.J. and Chou, I.M. (Editors), Fluid-Mineral Interactions: A tribute to H. P. Eugster, pp. 409-419.

Spero, H.J., Bijma, J., Lea, D.W. and Bemis, B.E., 1997. Effect of seawater carbonate concentration on foraminiferal carbon and oxygen isotopes. Nature, 390: 497-500.

Stampfli, G.M. and Borel, G.D., 2002. A plate tectonic model for the Paleozoic and Mesozoic constrained by dynamic plate boundaries and restored synthetic oceanic isochrons. Earth and Planetary Science Letters, 196(1-2): 17-33.

Stanley, S. M and. Hardie, L. A., 1999. Hypercalcification: paleontology links plate tectonics and geochemistry to sedimentology. Geological Society of America Today 9: 1-7.

Stanley, S.M. and Hardie, L.A., 1998. Secular oscillations in the carbonate mineralogy of reef-building and sediment-producing organisms driven by tectonically forced shifts in seawater chemistry. Palaeogeography, Palaeoclimatology, Palaeoecology, 144(1-2): 3-19.

Stanley, S.M., 2006. Influence of seawater chemistry on biomineralization throughout phanerozoic time: Paleontological and experimental evidence. Palaeogeography, Palaeoclimatology, Palaeoecology, 232(2-4): 214-236.

Steinen, R.P., 1982. SEM observations on the replacement of Bahaman aragonitic mud by calcite. Geology, 10: 471-475.

Steph, S., Tidemann, R., Groeneveld, J., Sturm, A., and Nürnberg, D., 2006. Pliocene changes in tropical east Pacific upper ocean stratification: response to tropical gateways?. In: Tiedemann, R., Mix, A.C., Richter, C. and Ruddiman, W.F. (Editors), Proceedings of the Ocean Drilling Program - Scientific Results, 202: College Station, TX (Ocean Drilling Program), pp. 1-51.

Stephen, K.J. and Davies, R.J., 1998. Documentation of Jurassic sedimentary cycles from the Moray Firth basin, United Kingdom North Sea. In: de Graciansky, P.C., Hardenbol, J., Jacquin, T. and

Vail, P.R. (Editors), Mesozoic and Cenozoic Sequence Stratigraphy of European Basins. SEPM Special Publications 60, pp. 481-506.

Steuber, T. and Veizer, J., 2002. Phanerozoic record of plate tectonic control of seawater chemistry and carbonate sedimentation. Geology, 30(12): 1123-1126.

Steuber, T., 1996. Stable isotope sclerochronology of rudist bivalves: Growth rates and Late Cretaceous seasonality. Geology, 24(4): 315-318.

Stevens, G.R. and Clayton, R.N., 1971. Oxygen isotope studies on Jurassic and Cretaceous belemnites from New-Zealnad and their biogeographic significance. New Zealand Journal of Geology and Geophysics, 14(4): 829-897.

Stevens, G.R., 1965. The Jurassic and Cretaceous belemnites of New Zealand and a review of the Jurassic and Cretaceous belemnites of the Indo-Pacific region. New Zeal Dep Sci Ind Res Geol Surv Paleontol Bull, 36: 1-283.

Stoll, H.M. and Schrag, D.P., 2000. High-resolution stable isotope records from the Upper Cretaceous rocks of Italy and Spain: Glacial episodes in a greenhouse planet? Geological Society of America Bulletin, 112(2): 308-319.

Stolp, H., 1988. Microbial ecology: organisms, habitats, activities. Cambridge studies in ecology. Cambridge University Press, Cambridge, UK, 308 pp.

Swart, P.K. and Eberli, G., 2005. The nature of the $\delta^{13}C$ of periplatform sediments: Implications for stratigraphy and the global carbon cycle. Sedimentary Geology, 175(1-4): 115-129.

Swart, P.K., 2008. Global synchronous changes in the carbon isotopic composition of carbonate sediments unrelated to changes in the global carbon cycle. Proceedings of the National Academy of Sciences of the United States of America, 105(37): 13741-13745.

Swart, P.K., Reijmer, J.J. and Otto R., 2009. A reevaluation of facies on Great Bahama Bank II: variations in the $\delta^{13}C$, $\delta^{18}O$ and mineralogy of surface sediments. In: Swart, P.K., Eberli, G.P. and McKenzie, J.A. (Editors), Perspectives in Carbonate Geology: A Tribute to the Career of Robert Nathan Ginsburg. International Association of Sedimentologists Special Publication 41, pp. 47-59.

Swart, P.K., Reijmer, J.J. and Otto, R., 2009. A reevaluation of facies on Great Bahama Bank II: variations in the $\delta^{13}C$, $\delta^{18}O$ and mineralogy of surface sediments. Perspectives in Carbonate Geology: A Tribute to the Career of Robert Nathan Ginsburg, 41. International Association of Sedimentologists Special Publication, Blackwell, Oxford, 47-59 pp.

Teagle, D. A. H., Alt, J. C., Umino, S., Miyashita, S., Banerjee, N. R., Wilson, D. S., and the Expedition 309/312 Scientists, 2006. Proceedings of the Integrated Ocean Drilling Program, Volume 309/312.

ten Have, T. and Heijnen, W., 1985. Cathodoluminescence activation and zonation in carbonate rocks: an experimental approach. Geologic en Mijnbouw 64: 297-310.

Terry, R. D., Chilingar, C. V., 1955. Summary of "Concerning some additional aids in studying sedimentary formations" by M. S. Shvetsov. Journal of Sedimentary Petrology 25: 229-214.

Thierry, J., Abbate, E., Alekseev, A.S., Ait, O.R., Ait, S.H., Bouaziz, S., Canerot, J., Georgiev, G., Guiraud, R., Hirsch, F., Ivanik, M., Le, M.J., Le, N.Y.M., Medina, F., Mouty, M., Nazarevich, B., Nikishin, A.M., Page, K., Panov, D.L., Pique, A., Poisson, A., Sandulescu, M., Sapunov, I.G., Seghedi, A., Soussi, M., Tchoumatchenko, P.V., Vaslet, D., Vishnevskaya, V., Volozh, Y.A., Voznezenski, A., Walley, C.D., Wong, T.E., Ziegler, M., Barrier, E., Bergerat, F., Bracene, R., Brunet, M.F., Cadet, J.P., Guezou, J.C., Jabaloy, A., Lepvrier, C., Rimmele,G., de,W.P., Baudin, F., Belaid, A., Bonneau, M., Coutelle, A., Fekirine, B., Guillocheau, F., Hantzpergue, M., Julien, M., Kokel, F., Lamarche, J., Mami, L., Mansy, J.L., Mascle, G., Pascal, C., Robin, C., Stephenson, R., Sihamdi, N., Vera, J.A., Vuks, V.J., 2000a. Early Kimmeridgian (146–144 Ma). In: Dercourt, J., Gaetani, M., Vrielynck, B., Barrier, E., Biju Duval, B., Brunet, M.F., Cadet, J.P., Crasquin, S. and Sandulescu, M. (Editors), Peri-Tethys atlas; palaeogeographical maps; explanatory notes.

Thierry, J., Barrier, E., Abbate, E., Ait, O.R., Ait, S.H., Bouaziz, S., Canerot, J., Elmi, S., Georgiev, G., Guiraud, R., Hirsch, F., Ivanik, M., Le, M.J., Le, N.Y.M., Medina, F., Mouty, M., Nazarevitch, V., Nikishin, A.M., Page, K., Panov, D.L., Pique, A., Poisson, A., Sandulescu, M., Sapunov, I.G., Seghedi, A., Soussi, M., Tarkowski, R.A., Tchoumatchenko, P.V., Vaslet, D., Vishnevskaya, V., Volozh, Y.A., Voznezenski, A.,Walley, C.D.,Wong, T.E., Ziegler, M., Ait, B.L., Bergerat, F., Bracene, R., Brunet, M.F., Cadet, J.P., Guezou, J.C., Jabaloy, A., Lepvrier, C., Rimmele, G., de, W.P., Belaid, A., Bonneau, M., Coutelle, A., Fekirine, B., Guillocheau, F., Julien, M., Kokel, F., Lamarche, J.,Mami, L.,Mansy, J.L., Mascle,G., Meister, C., Pascal, C., Robin, C., Sihamdi, N., Stephenson, R., Vera, J.A., Vuks, V.J., 2000b. Middle Callovian (157–155Ma). In: Dercourt, J., Gaetani, M., Vrielynck, B., Barrier, E., Biju Duval, B., Brunet, M.F., Cadet, J.P., Crasquin, S. and Sandulescu, M. (Editors), Peri-Tethys atlas; palaeogeographical maps; explanatory notes.

Tintant, H., 1980. Les épizoaires intrathalames, indice d'allochtonie des coquilles de Céphalopodes. 8th Reunion Annuel des Sciences de la Terre, Marseille, pp. 384.

Tintant, H., 1983. Autochtonie ou allochtonie chez les cephalopodes. Extrait Mémoires Geologiques de l'Université de Dijon "Livre Jubilaire Gabriel Lucas", Géologie Sedimentaire 7: 257-271.

Tipper, E.T., Galy, A., and Bickle, M.J., 2006. Riverine evidence for a fractionated reservoir of Ca and Mg on the continents: Implications for the oceanic Ca cycle. Earth and Planetary Science Letters 247: 267−279.

Tobin, K.J. and Walker, K.R., 1996. Ordovician low- to intermediate-Mg calcite marine cements from Sweden: marine alteration and implications for oxygen isotopes in Ordovician seawater. Sedimentology, 43: 719-735.

Tobin, K.J., Walker, K.R., Steinhauff, D.M. and Mora, C.I., 1996. Fibrous calcite from the Ordovician of Tennessee: preservation of marine oxygen isotopic composition and its implications. Sedimentology, 43: 235-251.

Tomašových, A., Schlög, J., 2008. Analyzing variations in cephalopod abundances in shell concentration: The combined effects of production and density-dependent cementation rates. Palaios, 23(9-10): 648-666.

Tucker, M.E. and Wright, V.P., 1990. Carbonate Sedimentology. Blackwell Science, Oxford, 482 p. pp.

Tukey, J.W., 1977. Exploratory Data Analysis. Addison-Wesley, Massachusetts.

Turpin, M., Emmanuel, L. and Renard, M., 2008. Nature and origin of carbonate particles along a transect the western margin of Great Bahama Bank (Middle Miocene): Sedimentary processes and depositional model. Bulletin de la Societe Geologique de France, 179(3): 231-244.

Tynan, S. and Opdyke, B.N., 2011. Effects of lower surface ocean pH upon the stability of shallow water carbonate sediments. Science of the Total Environment, 409(6): 1082-1086.

Valdes, P.J., Sellwood, B.W. and Price, G.D., 1995. Modelling Late Jurassic Milankovitch climate variations. Geological Society, London, Special Publications, 85(1): 115-132.

van de Schootbrugge, B., Föllmi, K.B., Bulot, L.G. and Burns, S.J., 2000. Paleoceanographic changes during the early Cretaceous (Valanginian-Hauterivian): evidence from oxygen and carbon stable isotopes. Earth and Planetary Science Letters, 181(1-2): 15-31.

van der Kooij, B., Immenhauser, A., Csoma, A., Bahamonde, J. and Steuber, T., 2009. Spatial geochemistry of a Carboniferous platform-margin-to-basin transect: Balancing environmental and diagenetic factors. Sedimentary Geology, 219(1-4): 136-150.

van der Kooij, B., Immenhauser, A., Steuber, T., Bahamonde Rionda, J.R. and Meríno Tomé, O., 2010. Controlling factors of volumetrically important marine carbonate cementation in deep slope settings. Sedimentology, 57(6): 1491-1525.

van der Kooij, B., Immenhauser, A., Steuber, T., Hagmaier, M., Bahamonde, J.R., Samankassou, E. and Meríno Tomé, O., 2007. Marine Red Staining of a Pennsylvanian Carbonate Slope: Environmental and Oceanographic Significance. Journal of Sedimentary Research, 77(12): 1026-1045.

van der Putten, E., Dehairs, F., Keppens, E. and Bayens, W., 2000. High resolution distribution of tracce elements in the calcite shell layer of modern Mytilus edulis: Environmental and biological controls. Geochimica et Cosmochimica Acta, 64(4): 997-1011.

Veizer, J., 1974. Chemical diagenesis of belemnite shells and possible consequences for paleotemperature determination. Neues Jahrbuch für Geologie und Paläontologie Abhandlungen, 147: 91-111.

Veizer, J., 1983. Chemical analysis of carbonates: theory and application of trace element technique. In: Arthur, M.A., Anderson, T.F., Kaplan, I.R., Veizer, J. and Land, L.S. (Editors), Stable isotopes in sedimentary geology. SEPM Short Course 10, pp. 3-100.

Veizer, J., Ala, D., Azmy, K., Bruckschen, P., Buhl, D., Bruhn, F., Carden, G.A.F., Diener, A., Ebneth, S., Godderis, Y., Jasper, T., Korte, C., Pawellek, S., Podlaha, O.G., Strauss, H., 1999. ^{87}Sr, $\delta^{13}C$ and $\delta^{18}O$ evolution of Phanerozoic seawater. Chemical Geology, 161: 59-88.

Vera, J.A. and Molina, J.M., 1998. Shallowing-upward cycles in pelagic troughs (Upper Jurassic, Subbetic, Southern Spain). Sedimentary Geology, 119(1-2): 103-121.

Vera, J.A. and Molina, J.M., 1998. Shallowing-upward cycles in pelagic troughs (Upper Jurassic, Subbetic, Southern Spain). Sedimentary Geology 119: 103–121.

Vera, J.A., 1988. Evolución de los sistemas de depósito en el margen ibérico de la Cordillera Bética. Revista de la Sociedad Geológica de España 1: 373-391.

Vera, J.A., 1998. El Jurásico de la Cordillera Bética: estado actual de conocimientos y problemas pendientes ("The Jurassic of the Betic Range: State of the art and open questions). Cuadernos de Geología Ibérica 24: 17-42.

Vera, J.A., Martín-Algarra, A., Sánchez-Gómez, M., Fornós, J.J. and Gelabert, B.C., 2004. Cordillera Bética y Baleares. In: Vera, J.A. (Editor), Geología de España. Sociedad Geológica de España-IGME 4, pp. 347-464.

Vera, J.A., Molina, J.M., Montero, P. and Bea, F., 1997. Jurassic guyots on the Southern Iberian continental margin: a model of isolated carbonate platforms on volcanic submarine edifices. Terra Nova, 9(4): 163-166.

Vincent, B., Rambeau, C., Emmanuel, L. and Loreau, J.P., 2006. Sedimentology and trace element geochemistry of shallow-marine carbonates: an approach to paleoenvironmental analysis along the Pagny-sur-Meuse Section (Upper Jurassic, France). Facies, 52(1): 69-84.

Voelker, A.H.L., Rodrigues, T., Billups, K., Oppo, D., McManus, J., Stein, R., Hefter, J. and Grimalt, J.O., 2010. Variations in mid-latitude North Atlantic surface water properties during the mid-Brunhes (MIS 9-14) and their implications for the thermohaline circulation. Climate of the Past 6: 531-552.

Wadleigh, M.A. and Veizer, J., 1992. $^{18}O/^{16}O$ and $^{13}C/^{12}C$ in lower Paleozoic articulate brachiopods: Implications for the isotopic composition of seawater. Geochimica et Cosmochimica Acta 56: 431-443.

Walls, R.A., Mountjoy, E.W. and Fritz, P., 1979. Isotopic composition and diagenetic history of carbonate cements in Devonian Golden Spike reef, Alberta, Canada. Geological Society of America Bulletin, 90: 963-982.

Warnke, K., Oppelt, A. and Hoffmann, R., 2010. Stable isotopes during ontogeny of Spirula and derived hatching temperatures. Ferrantia, 59: 191-201.

Wefer, G. and Berger, W.H., 1991. Isotope Paleontology: growth and composition of extant calcareous species. Marine Geology, 100: 207-248.

Weiss, R.F., 1970. Solubility of nitrogen, oxygen and argon in water and seawater. Deep-Sea Research, 17(4): 721-35.

Weissert, H. and Erba, E., 2004. Volcanism, CO2 and palaeoclimate: a Late Jurassic–Early Cretaceous carbon and oxygen isotope record. Journal of the Geological Society, 161(4): 695-702.

Weissert, H. and Mohr, H., 1996. Late Jurassic climate and its impact on carbon cycling. Palaeogeography Palaeoclimatology Palaeoecology, 122(1-4): 27-43.

Westermann, G.E.G., 1996. Ammonoid life and habitat. In: Landman, H., Tanabe, K. and Davis, R.A. (Editors), Topics in Geobiology 13, pp. 607-707.

Westphal, H., 2006. Limestone-marl alternations as environmental archives and the role of early diagenesis: a critical review. International Journal of Earth Science 95: 947-961.

Wetzel, A. and Allia, V., 2000. The Significance of Hiatus Beds in Shallow-Water Mudstones: An Example from the Middle Jurassic of Switzerland. Journal of Sedimentary Research, 70(1): 170-180.

Whitaker, F.F., Paterson, R.J. and Johnston, V.E., 2006. Meteoric diagenesis during sea-level lowstands: Evidence from modern hydrochemical studies on northern Guam. Journal of Geochemical Exploration 89: 420-423.

Wierzbowski, H. and Joachimski, M., 2007. Reconstruction of late Bajocian-Bathonian marine palaeoenvironments using carbon and oxygen isotope ratios of calcareous fossils from the Polish Jura Chain (central Poland). Palaeogeography Palaeoclimatology Palaeoecology, 254: 523-540.

Wierzbowski, H. and Joachimski, M.M., 2009. Stable isotypes, elemental distribution, and growth rings of belemnopsid belemnite rostra: Proxies for life habitat. Palaios, 24(5-6): 377-386.

Wierzbowski, H., 2002. Detailed oxygen and carbon isotope stratigraphy of the Oxfordian in Central Poland. International Journal of Earth Sciences, 91(2): 304-314.

Wilkinson, B.H., Buczynski, C. and Owen, R.M., 1984. Chemical control of carbonate phases; implications from Upper Pennsylvanian calcite-aragonite ooids of southeastern Kansas. Journal of Sedimentary Research, 54(3): 932-947.

Williamson, T., 2006. Systematics and biostratigraphy of Australian early Cretaceous belemnites with contributions to timescale and palaeonvironmental assessment of the early Australian early Cretaceous system derived from stable isotope proxies. PhD thesis, James Cook University.

Wold, S., Esbensen, K. and Geladi, P., 1987. Principal component analysis. Chemometrics and Intelligent Laboratory Systems, 2(1-3): 37-52.

Woodfine, R., Jenkyns, H.C., Sarti, M., Baroncini, F and Violante, C., 2008. The response of two Tethyan carbonate platforms to the early Toarcian (Jurassic) oceanic anoxic event: environmental change and differential subsidence. Sedimentology 55: 1011-1028.

Wu, Y. and Chafetz, H.S., 2002. Stable isotopic signature of a palaeoaquifer, Mississippian Alamogordo Member limestones, Sacramento Mountains, New Mexico, USA. Sedimentology, 49: 227-235.

Yasutaka, T., Mami, T., 2006. A new method for the study of trace element partitioning between calcium carbonate and aqueous solution: A test case for Sr and Ba incorporation into calcite. Geochemical Journal 40 (2): 161-170.

Zhuravlev, A. Y. and Wood, R. A., 2009. Controls on carbonate skeletal mineralogy: Global CO_2 evolution and mass extinctions. Geology 37: 1123-1126.

Ziegler, A., Eshel, G., Rees, P.M., Rothfus, T., Rowley, D., Sunderlin, D., 2003. Tracing the tropics across land and sea: Permian to present. Lethaia, 36(3): 227-254.

Ziegler, P.A., 1988. Evolution of the Arctic-North Atlantic and the Western Tethys. American Association of Petroleum Geologists Memoir 43, pp. 164-196.

Ziegler, P.A., 1988. Evolution of the Arctic-North-Atlantic and the western Tethys. American Association of Petroleum Geologists, OK, United States.

10

Contributions to journals and scientific meetings

International journals

Published articles

Coimbra, R., Olóriz, F., 2010. Epioceanic depositional setting and skeletals from a cephalopod limestone (Betic Cordillera, SE Spain): a geochemical approach. Earth and Science Frontiers (Special Issue) 17, 297-299.

Coimbra, R., Immenhauser, A., Olóriz, F., 2009. Matrix micrite $\delta^{13}C$ and $\delta^{18}O$ reveals synsedimentary marine lithification of Upper Jurassic Ammonitico Rosso limestones (Betic Cordillera, SE Spain). Sedimentary Geology 209, 332-348.

Contributions under review

Coimbra, R., Olóriz, F.---- Contrast comparison of differential diagenetic pathways of Lower Tithonian carbonate materials from the Betic Cordillera (S Spain): Evidence for physico-chemical palaeo-seawater properties. Submitted to Palaeogeography, Palaeoclimatology, Palaeoecology (April 2011).

Coimbra, R., Olóriz, F.---- Pixel counting for percentage estimation: applications to sedimentary petrology. Submitted to Computers and Geosciences (May 2011).

Coimbra, R., Olóriz, F.---- Sediment provenance supported by geochemical evidence (Upper Jurassic, Majorca Island). Enviado a: Terra Nova (August 2011).

Coimbra, R., Immenhauser, A., Olóriz, F.--- Spatial geochemistry of Upper Jurassic marine carbonates (Iberian Subplate). Submitted to Journal of Sedimentary Geology (August 2011).

Coimbra, R., Immenhauser, A., Olóriz, F.---- Statistical analysis of elemental chemostratigraphy in Upper Jurassic Ammonitico Rosso. Submitted to Chemical Geology (September 2011).

International Scientific Meetings

Coimbra, R., Immenhauser, A., Olóriz, F.- Spatial geochemistry across the Late Jurassic S-E Iberian paleomargins (oral). 28th IAS Meeting of Sedimentology, Zaragoza- España, July 2011.

Coimbra, R., Moliner, L., Olóriz, F.- Geochemical evidences for short-term sedimentary contributions into an Early Kimmeridgian epicontinental sea (E Iberia) (poster). 28th IAS Meeting of Sedimentology, Zaragoza- España, July 2011.

Coimbra, R., Immenhauser, A., Olóriz, F.- Isotope stratigraphy of Upper Jurassic limestones: Early marine lithification and differential diagenesis of epioceanic and epicontinental deposits (Iberian subplate) (poster). 18th IAS International Sedimentological Congress, Mendoza- Argentina, September 2010.

Coimbra, R., Immenhauser, A., Olóriz, F.- Significance of nodule formation for the interpretation of matrix micrite C and O isotope ratios in Upper Jurassic Ammonitico Rosso limestones (Betic Cordillera, SE Spain) (poster). EGU General Assembly, Viena- Austria, April 2009.

Coimbra, R., Immenhauser, A., Olóriz, F.- Stable-isotope data from an epioceanic setting (Upper Jurassic, SE Spain) - preliminary data from the Internal Subbetic (poster). 26th IAS Meeting of Sedimentology, Bochum- Germany, September, 2008.